V.S.YAMAN

SYNTHESIS, CHARACTERIZATION AND INVESTIGATIONS OF THERMAL BEHAVIOR OF THE NITRO-IMIDAZOLE-BASED ENERGETIC COORDINATION COMPOUNDS

THE GRADUATE SCHOOL OF NATURAL AND APPLIED SCIENCES
OF
ATILIM UNIVERSITY

VAHİDE SELEN YAMAN

A MASTER OF SCIENCE THESIS
IN
CHEMICAL ENGINEERING

JUNE 2022

ATILIM UNIVERSITY 2022

SYNTHESIS, CHARACTERIZATION AND INVESTIGATIONS OF THERMAL BEHAVIOR OF THE NITRO-IMIDAZOLE-BASED ENERGETIC COORDINATION COMPOUNDS

A THESIS SUBMITTED TO
THE GRADUATE SCHOOL OF NATURAL AND APPLIED SCIENCES
OF
ATILIM UNIVERSITY

BY

VAHİDE SELEN YAMAN

IN PARTIAL FULFILLMENT OF THE REQUIREMENTS FOR
THE DEGREE OF MASTER OF SCIENCE IN CHEMICAL ENGINEERING

JUNE 2022

Approval of the Graduate School of Natural and Applied Sciences, Atilim University.

_____

Prof. Dr. Ender Keskinkılıç
Director

I certify that this thesis satisfies all the requirements as a thesis for the degree of **Master of Science in Chemical Engineering and Applied Chemistry, Atilim University**.

_____

Prof. Dr. Şeniz Özalp-Yaman
Head of Department

This is to certify that we have read the thesis SYNTHESIS, CHARACTERIZATION AND INVESTIGATIONS OF THERMAL BEHAVIOR OF THE NITRO-IMIDAZOLE-BASED ENERGETIC COORDINATION COMPOUNDS and that in our opinion it is fully adequate, in scope and quality, as a thesis for the degree of Master of Science- Engineering.

_____	_____
Prof.Dr. Nesrin Ekinci Machin Co-Supervisor	Prof. Dr. Şeniz Özalp-Yaman Supervisor

Examining Committee Members:

Prof. Dr. Nezire Saygılı
Faculty of Pharmacy, Hacettepe University _____

Prof. Dr. Şeniz Özalp-Yaman
Chemical Eng. Department, Atilim University _____

Prof. Dr. Nesrin Ekinci Machin
Chemical Eng. Department, Atilim University _____

Assoc. Prof. Dr. Hakan Kayı
Chemical Eng. Department, Ankara University _____

Asst. Prof. Dr. Enver Güler
Chemical Eng. Department, Atilim University _____

Date: 10.06.2022

I hereby declare that all information in this document has been obtained and presented in accordance with academic rules and ethical conduct. I also declare that, as required by these rules and conduct, I have fully cited and referenced all material and results that are not original to this work.

Name, Last Name: Vahide Selen Yaman

Signature:

ABSTRACT

SYNTHESIS, CHARACTERIZATION AND INVESTIGATIONS OF THERMAL BEHAVIOR OF THE NITRO-IMIDAZOLE-BASED ENERGETIC COORDINATION COMPOUNDS

Yaman, Vahide Selen

Master, Department of Chemical Engineering

Supervisor: Prof. Dr. Şeniz Özalp-Yaman

Co-Supervisor: Prof. Dr. Nesrin Ekinci Machin

Jun 2022, #172

Energetic materials produced in various structures have different applications both in the military as explosives and in the civilian field as propellant and pyrotechnics. However, due to the adverse effects of these materials on the environment and health as well as their high sensitivity to light and friction, it is desired to replace them with environmentally friendly, toxic metal-free and easy-handling alternatives. The main aim of this study is to synthesize and explore the performance of novel energetic organic and coordination compounds. In this scope, 5-(chloro(nitro)methyl)-4-nitro-1H-imizadole (HL) and its sodium (NaL) and ammonium (NH_4L) salts were designed and synthesized as a first time. Next, totally 34 cobalt(II/III), copper(II), iron(II/III) and zinc(II) complexes containing 5-(chloro(nitro)methyl)-4-nitro-1H-imizadole were designed in octahedral and tetrahedral structures, $[M(NH_3)_x(L)_y]^n$ [x:0, 2-4; y:1, 2, 4 or 6; n:(+1)-(-4)]. However, only 26 of these complexes could be synthesized successfully and characterized via various spectroscopic techniques (HRMS, NMR, FTIR). Especially, 6 L^- coordinated cobalt(II)/III) and iron(II)/III) complexes were found to be unstable due to the steric effect as it was also indicated by their optimized geometry calculations carried out as a part of the TUBITAK Project 117Z391 [1].

Thermo-gravimetric and differential thermal analyses (TGA-DSC) of these newly generated energetic coordination compounds were achieved and their thermal stability, thermal decomposition characteristics and kinetic parameters were determined to explore their potential to be used as an energetic material.

The simultaneous TGA-DSC curves pointed out the similar decomposition processes with the high thermal stability within the range of 25-1200 ^{o}C for all the studied complexes. Among all these compounds; HL, NaL, NH_4L and only five of the metal complexes showed exothermic behavior at around 800-1100 ^{o}C. It was observed that the exothermic decomposition temperature of the HL and its salts moved from 800 ^{o}C to 1100 ^{o}C upon coordination to the metal ions. It was very suprising that solely Co(II), Fe(II) and Cu(II) complexes including one or two L^- showed an exothermic character. Impact and friction sensitivity tests applied to the most promising two energetic compounds, $[Co(NH_3)_4(L)_2]$ and $[Fe(NH_3)_4(L)_2]$, revealed that these complexes were very resistant to impact and insensitive to friction.

The agreement between the desired energy and sensitivity results indicated that our complexes can be applied as propellants in rocket systems and as additives in small amounts to modify the ballistic properties of propellants.

Keywords: New generation explosives, metal based explosives, propellants, explosion kinetics, DFT calculations.

ÖZ

NİTRO İMİDAZOL İÇEREN ENERJİK KOORDİNASYON BİLEŞİKLERİNİN SENTEZİ, KARAKTERİZASYONU VE TERMAL ÖZELLİKLERİNİN İNCELENMESİ

Yaman, Vahide Selen
Yüksek Lisans, Kimya Mühendisliği Bölümü
Tez Yöneticisi: Prof. Dr. Şeniz Özalp-Yaman
Ortak Tez Yöneticisi: Prof. Dr. Nesrin Ekinci Machin

Haziran 2022, #172

Çeşitli yapılarda üretilen enerjik malzemeler, hem patlayıcı olarak askeri alanda hem de itici güç ve piroteknik olarak sivil alanda farklı uygulamalara sahiptir. Ancak bu malzemelerin çevre ve sağlık üzerindeki olumsuz etkileri; ışık ve sürtünmeye karşı yüksek hassasiyetleri nedeniyle çevre dostu, toksik metal içermeyen ve taşınabilir alternatifleri ile değiştirilmesi önem arz etmektedir. Bu çalışmanın temel amacı, daha önce hiç sentezlenmemiş organik ve organometalik enerjik malzemelerin sentezi ve patlayıcı olarak özelliklerinin incelenmesidir. Bu kapsamda, 5-(kloro(nitro)metil)-4-nitro-1H-imizadol ile sodyum ve amonyum tuzları tasarlanmış ve ilk defa sentezlenmiştir. Daha sonra 5-(kloro(nitro)metil)-4-nitro-1H-imizadol içeren toplam 34 adet kobalt(II/III), bakır(II), demir(II/III) ve çinko(II) kompleksi farklı şekillerde tasarlanmıştır. Ancak bu komplekslerden 26 tanesi başarılı bir şekilde sentezlenebilmiş ve çeşitli spektroskopik tekniklerle (HRMS, NMR, FTIR) karakterize edilmiştir. TÜBİTAK Projesi 117Z391 kapsamında gerçekleştirilen geometri optimizasyonu hesaplarından da anlaşılacağı üzere özellikle 6 adet L^- içeren kobalt(II)/III) ve demir(II)/III) komplekslerinin sterik etki nedeniyle kararsız olduğu tespit edilmiştir [1].

Ayrıca elde edilen malzemelerin termo-gravimetrik ve diferansiyel termal analizleri (TGA-DSC) gerçekleştirilmiş; enerjik bir malzeme olarak kullanılma potansiyellerini keşfetmek amacıyla termal kararlılığı, termal bozunma karakteristiği ve kinetik parametreleri incelenmiştir.

Eşzamanlı TGA-DSC eğrilerinden incelenen tüm komplekslerin 25-1200 ºC sıcaklık aralığında yüksek bir kararlılığa ve benzer bozunma özelliklerine sahip olduğu gözlenmiştir. Bu bileşikler arasında, HL, NaL, NH_4L ve beş adet koordinasyon bileşiği, yüksek sıcaklıklarda yüksek enerji açığa çıkararak ekzotermik davranış göstermektedir. HL ve tuzlarına ait ekzotermik bozunma sıcaklığının, metal iyonlarıyla koordine olduğunda 800 ºC'den 1100 ºC'ye taşındığı gözlenmiştir. Şaşırtıcı bir şekilde, bir veya iki L^- içeren yalnızca Co(II), Fe(II) ve Cu(II) kompleksleri ekzotermik bir karakter göstermektedir.

Ek olarak, bu potansiyel enerjik bileşiklerden ikisi, $[Co(NH_3)_4(L)_2]$ ve $[Fe(NH_3)_4(L)_2]$, için darbe ve sürtünme duyarlılık testleri yapılmıştır. Bu bileşikler darbeye karşı çok dayanıklı ve sürtünmeye karşı duyarsız olarak tanımlanmıştır.

Elde edilen sonuçlar bileşiklerin roket sistemlerinde itici güç (propellant) olarak ve iticilere ait balistik özellikleri değiştirmek için küçük miktarlarda katkı maddesi olarak uygulanabileceğini göstermektedir.

Anahtar Kelimeler: Yeni nesil patlayıcı, metal patlayıcılar, patlama kinetiği, DFT hesaplamaları.

To my family...

ACKNOWLEDGEMENTS

Firstly and foremost, I would like to express my deepest appreciation to Prof. Dr. Şeniz Özalp-Yaman, my supervisor, for her invaluable advice, continuous support, and patience. Her immense knowledge and plentiful experience have encouraged me in all the time of my academic and personal life. I would like to thank her for the opportunity to be a part of her scientific research. I always feel lucky to be her student.

I would like to express my very gratitude to Prof. Dr. Nesrin Ekinci Machin, my co-supervisor, for providing guidance and feedback throughout this study. Her perspective and contributions have great importance in enriching the quality of my thesis.

I would like to offer my sincere thanks to the members of my dissertation committee, including Prof. Dr. Nezire Saygılı, Assoc. Prof. Dr. Hakan Kayı and Asst. Prof. Dr. Enver Güler, for their insightful comments and valuable suggestions. I am very thankful for the assistance given by Assoc. Prof. Dr. Hakan Kayı. In this study, I used the valuable data obtained by his theoretical calculations. Also, I would like to thank to Prof. Dr. Zuhal Gerçek for the shaping procedure of the ligand synthesizing within this study.

I wish to thank to my colleagues, Mert Topcuoğlu, Tuğçe Gültan Gürbüz, Zuhal Selvi Vanlı Güler, Fırat Ayan and Mücahit Cihan Terzi for their friendship, help and sharing experiences with me during my study.

I am deeply grateful to my parents, Ayşegül Ünver and Erol Ünver, and my brother, Eray Ünver, for their unconditional support and endless love. I cannot forget to thank my grandmother, Kadriye İpek, and my grandfather, Osman İpek. They are the invisible heroes behind my success by their precious sacrifices over years. I would like to express my special thanks to my husband, Kaan Yaman. His love and tremendous understanding have kept me happy and motivated in every stage of my life. Without my family, it would be impossible for me to complete my study.

I acknowledge that this research is supported by TUBITAK, The Scientific and Technological Research Council of Turkey, with project number 117Z391.

TABLE OF CONTENTS

LIST OF TABLES

LIST OF FIGURES

CHAPTER 1

1. INTRODUCTION

Materials that can store and release large quantities of energy are a high precedence in the modern world. Currently, a new term that high energetic material (HEM) is used for the class of materials that known as primary and secondary explosives, propellants and pyrotechnics. In other words, the term high energetic material is generally used for any material that can attain a highly energetic state by chemical reactions.

An explosive is simply defined as a pure substance or mixture of substances that is capable of producing an explosion by its own energy. The term explosion refers to chemical detonations produced as a consequence of a chemical reaction or change of state which occurs over an exceedingly short space of time. During a chemical explosion an extremely rapid (one-hundredth of a second) exothermic transformation takes place resulting in the generation of large amount of heat and large volume of expanding gas.

Energetic materials have crucial role in industrial explosive devices for both military and civil applications such as rockets, satellites, weapons, mining and tunneling. Considering their wide applicability and increased demand, numerous energetic materials are developed over the years with targeted properties according to the application. Generally, it is expected that the high energetic materials exhibit the following features; (1) high energetic performance, (2) high chemical stability for long shelf life, (3) appropriate sensitivity to mechanical stimulu for safety handling and transport, (4) non-sensitivity to moisture and light, (5) thermal stability to at least 200 °C, (6) a lack of toxic metals, perchlorate, and nitrophenols for environmental and health issues, (7) low cost and easy preparation. According to these main criterions, research efforts on finding novel energetic materials are still continue in comparison to currently known benchmark materials/compositions.

1.1. Historical aspects of explosives

The earliest known explosive is black powder that was discovered by the Chinese in the seventh century [2]. Black powder, also known as gunpowder, is a intimate mixture of 15% charcoal, 10% sulfur and 75% potassium nitrate. In this powdered mixture, charcoal and sulfur serve a function as fuels while potassium nitrate as an oxidizer. In the revulation of the war all around the world, black powder played an important role. Chinese utilized black powder both as a gun propellant for stone projectiles and arrows, and as bombs for military purposes [3, 4]. The first modern explosive that is called nitroglycerine (NG) was invented by Ascanio Sobrero 1847 [5, 6]. Due to the unstability of NG, the handling was difficult and dangerous. Then, Swedish inventor Alfred Nobel explored a safe way to package nitroglycerin. Further, dynamite was invented by Alfred Nobel in 1866 [5, 6]. In the same decade with NG, nitration of cellulose to produce nitrocellulose (NC) was reported by Schonbein and Bottger in 1846 [5, 6]. Black powder was replaced in the late 1800s by smokeless gunpowder and picric acid because it has a low energy, leaves a substantial amount of corrosive solids after explosion, and absorbs moisture rapidly. Smokeless powder can be produce from a gelatinized nitrocellulose or a mixture of NC and NG with a small quantity of petroleum jelly added as a stabilizer. On the other hand, picric acid was defined as good substitute for black powder on military purposes.

Gunpowder was the only known explosive until the discovery of fulminating compounds in around 1600s. Mercury fulminate was introduced as first primary explosive for use in blasting caps [7]. In the early 1900's, lead azide and lead styphnate were replaced with mercury fulminate due to their high thermal stability (320-340 ^{o}C), easy synthesis method and cheap cost [8]. By the way, the toxic properties of the mercury were eliminated while the shelf life of explosives was extended. Enhanced lead-containing primary explosives in different structures were used in many application areas for both military and civilian population. However, long-term usage of lead-based explosives caused environmental pollution and negative effects on health. In addition to toxic properties of lead azide, it has degradation to CO_2, high sensitivity to impact (1-4 J) and friction (0.1-1 N). These results indicate requirement for new generation explosives. In that point, silver azide was used as an alternative

that represents less toxicity and better explosive property than lead-containing compounds [9]. However, its high sensitivity to light and friction restricted the usage of silver azide.

During the twentieth century, trinitrotoluene (TNT) was the most widely used traditional military explosive. Even though it was applied in the dye industry in the late 1800s, German army used it instead of picric acid. After a cost-effective technology for nitration of toluene was found, TNT became most popular ammunition in World War I [10]. It was preferred due to the safely melting and casting alone or with other explosives. Pentaerythritol tetranitrate (PETN) and cyclotrimethylene trinitramine (RDX) were eventually developed for use in hand and anti-tank grenades, respectively. Bombs were exploded with a mixture of TNT, RDX, and wax. Torpedo warheads were frequently made of cast RDX, TNT, and aluminum powder combinations [6].

1.2. Classifications of explosives

When discussing explosives, different criteria are considered, resulting several classifications. The classification based on detonation velocity, which is traditionally utilized in the military, is perhaps the most commonly encountered in literature [11-18]. The classification of explosives based on their source or use/application is becoming more common in the forensic profession [13]. In addition, classification according to nature and chemical structure of the explosive materials is useful to discuss the status of current and future explosives.

1.2.1. Based on the detonation velocity

The term detonation usually refers to a chemical process in which the chemical energy of a substance is rapidly released, culminating in an expansive shock wave of air. The detonation velocity is called the speed at which the shock wave front travels through the detonating explosive [11, 12]. The speed of combustion at which the detonation occurs is greater than the speed of sound in the surrounding environment [6, 14]. It should be noted that the speed of sound in a medium of ambient air is approximately 340 m/s [15-18]. The speed of sound rises when it travels through liquid

or solid media due to the closer proximity of atoms in the liquid and solid state. For instance; it can reach to 1500 m/s in water, 3000 m/s in wood or 6400 m/s in aluminum [19, 20]. The speed of sound of most explosives (usually manufactured in powdered form) is estimated to range from 1000 to 3000 m/s. To distinguish between high and low velocity detonation explosives, a preliminary velocity of detonation range of 1000–3000 m/s is commonly developed [15, 16].

Classification of explosives based on their velocity of detonation is important especially in particular industries, such as the military, mining, and demolition, where knowing the destructive force of explosives in relation to their velocity of detonation is required. The explosives usually classified into two categories: high and low explosives.

The classification of explosives is depicted in Figure 1.1 and their brief description is outlined below:

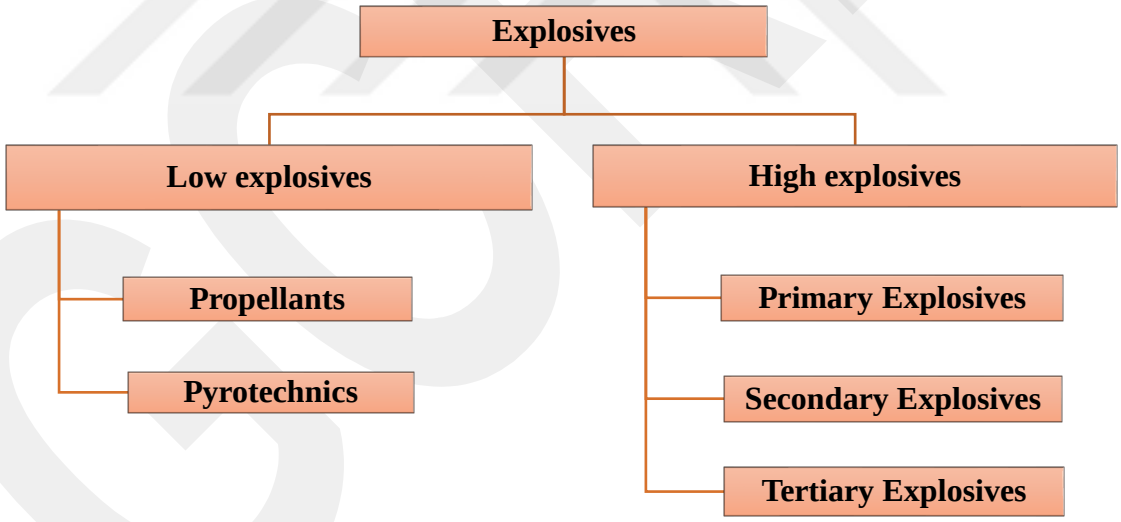

Figure 1.1. Classification of explosives based on detonation velocity

1.2.1.1. High energy explosives

High energy explosives are characterized by very high rates of reaction and generation of high pressures on explosion. They are typically subdivided according to their explosive sensitivity: (i) primary, (ii) secondary and (iii) tertiary explosives [21-24].

(i) **Primary high explosives** are energetic chemical compounds which are designed to create a shock wave to start the detonation reaction in a secondary explosive. They often are referred to as initiating explosives because they can be used to ignite secondary explosives. Primary explosives are extremely sensitive materials to different weak stimuli that can be a relatively small amount of heat, pressure, spark, electrostatic, mechanical impact or friction. The ability to rapidly deflagration to detonation transition (DDT) is the most critical attribute of a primary explosive. The explosive has the faster DDT is a better explosive assuming all other parameters are equal. As a fact, fast DDT is both strength and weakness of a primary explosive due to unintentional detonation. They are dangerous to handle and are used in comparatively small quantities. They are widely used in both military and civil applications such as for rockets, satellites and weapons. Some typical primary explosives are mercury fulminate, silver fulminate, lead azide and lead styphnate [24, 25].

(ii) **Secondary high explosives** are insensitive to weak stimuli and they necessaite using a detonator and frequently a booster. Secondary explosives comprise the most common explosives in the military such as RDX, PETN, HMX, TNT, and CL-20 [25-30]. PETN is generally used as a reference explosive, with explosives that are more sensitive than PETN are considered as primary explosives. The fact that primary explosives detonate by burning while secondary explosives detonate by shock waves is a significant difference between the two types of explosives. Secondary explosives are exceptionally powerful materials. The rate of detonation of a high explosive is one of its important properties. TNT detonates in around 7000 m/s, which is many times faster than the speed of sound, whereas the initiator lead azide detonates in about 3800 m/s. The explosion of high explosives (TNT) is distributed by a supersonic detonation which is caused by the breakdown of the molecular structure of explosives.

(iii) **Tertiary high explosives,** also called blasting agents, are insensitive to shock caused by fire, impact and friction. They can not be detonated by practical quantities of primary explosive. Instead of this, they require a secondary explosive as intermediate explosive booster. Ammonium nitrate (NH_4NO_3) and ammonium perchlorate (NH_4ClO_4) are the basic examples of tertiary explosives and categorized as oxidizer for commercial transportation and storage. These explosives have low explosion energies, around a third of TNT, when used in its pure form without any fuel components. Large-scale mining and construction industries are the main consumers. Due to some of precursors are sometimes easily accessible, they have also been used in terrorist attacks.

1.2.1.2. Low energy explosives

Low-energy explosives, unlike high-energy explosives, detonate with a subsonic wave front that does not travel faster than the speed of sound. Accumulative gases from deflagration of low explosives create overpressure inside a container. The mode of decomposition of low explosives differs from high explosives. They burn slowly and steadily. As a result, the action is less destroying. Low explosives provide progressive production of gases during combustion in a controlled manner. They are mostly used as propellants for space rockets or ammunition for firearms. Due to the thrust they generate, they are useful as rocket fuel. These materials actually produce a low-efficiency explosion. However, high amount of rocket fuel releases enough kinetic energy to propel rockets tons of miles away or even into space. Smokeless powder, black powder and flash powder are basic examples of low explosives [10-18, 25]. They are typically categorized in two parts: (i) propellants, (ii) pyrotechnics

(i) **Propellants** are combustible materials that contain all of the oxygen required for burning that supply a motion in a projectile or missile. Propellants typically burn rather than explode or detonate. A flame or spark ignites the propellant, which cause conversion from a solid to a gaseous state slowly. The high material density of these materials results in the high energy density to produce the desired thrust.

Based on their chemical composition and physical structure, propellants are described as homogeneous or heterogeneous. Homogeneous propellants contain fuels and oxidizers that are chemically bonded at the molecular level. Heterogeneous

propellants include mixing of fuel and oxidizers physically. The components of homogeneous propellants are in a wide range of chemical compounds, all of which can be grouped into four categories: nitramines, azides, nitrate esters or nitrates [31]. Composite propellants (heterogeneous propellants) generally combine of various chemical components such as inorganic oxidizer, fuel, binder, plasticizer, hardener, stabilizer and crosslinking agent. For instance, a solid propellant consists of ammonium perchlorate (AP) or ammonium dinitramide (ADN) as oxidizer; a metal fuel such as aluminum (Al); polymeric binder fuel similar to hydroxyl-terminated polybutadiene (HTPB) or glycidyl azide [32-35]. The energy is generated by the interaction of the oxidizer and fuel, while the ballistic modifiers alter combustion behavior to achieve the desired combustion rate characteristics. As a result, the physical and chemical properties of the various chemical components utilized in the fuel formulation, as well as their ratios, are critical in obtaining combustion characteristics and performance [31].

(ii) **Pyrotechnics** are substances that release heat, light, gas, fog, or sound when exposed to a chemical reaction. Although the origin of pyrotechnic materials is not known exactly, it is said that it first appeared in China in many sources. Pyrotechnics are one of the oldest types of explosives known to man. The employment of pyrotechnics can be seen in the friction lighting of a match, and the launch of fireworks into the sky. In terms of utilization, the amount of material is crucial. For example, a firework sample used in a certain amount can make a visual impact at various kinds of celebrations but activating a tankful of fireworks at the same time with a trigger can lead to big explosions and disasters.

1.2.2. Based on the usage area

Another way to classify explosives is based on their usage area. Explosives are used in both military and civilian applications for both constructive and destructive purposes. Forensic and intelligence investigations interest categorization of explosives according to the easy/complicate, legal/illegal obtaining to solve and prevent the criminal use of explosives [17-18]. Therefore, they are classified according to their source, end-use or application as military and commercial explosives.

1.2.2.1. Military explosives

Military explosives comprehend explosive compositions or formulations that are used in military munitions (bombs, shells, torpedoes, grenades, missile or rocket warheads). The bulk charges in these munitions are insensitive to a certain extent, hence they are safe for handling, storage and transportation. Military explosives have high physical and chemical stability over a wide range of temperature and humidity for a long period of time. The raw materials necessary to production in bulk such explosives must keep readily available for a possible wartime. Military explosives are strictly controlled in most countries, with only military personnel allowing access to them. Common military explosives are RDX, PETN, HMX and TNT.

Military explosives are generally organic molecules containing only carbon, hydrogen, oxygen and nitrogen atoms. In these molecules, oxygen and nitrogen atoms are commonly present as nitro-groups ($-NO_2$). Due to those nitro-groups, military explosives are called as nitro-explosives [12–20, 27]. Nowadays, most military explosives are plasticized using inert flexible binders in order to make moldable and easy to handle explosive compositions. Since plasticizers are non-energetic compounds, addition of them reduce the explosive power of the mixture. For this reason, the mass proportion of plasticizers in plastic explosives does not usually exceed 10%. For instance, PG-2 (common plastic explosive) is composed of 91% RDX (explosive), 5.3% bis(2-ethylhexyl) phthalate (plasticizer), 2.1% polyisobutylene (binder) and 1.6% motor oil [6, 15-18].

1.2.2.2. Commercial explosives

Commercial explosives include those explosives that are used in mining and quarrying (coal, metal ores, rock salt). Another key application field of these explosives is civil engineering such as road building, tunnel driving, land reclamation, canal construction, changing river courses and even for fire fighting in conflagrations of oil wells. Dynamite and ANFO (Ammonium nitrate-fuel oil) compositions are the most prevalent commercial explosives. They are high explosives with low detonation velocities (compared to military explosives), allowing for more precise control over the required power to move and fragment rocks and buildings. Also, large quantities of explosives have also been used in seismographic prospecting for new oil reserves

in recent years. The demand for explosives is increasing every year, with an annual growth rate of roughly 8-9%. The typical process for all of these applications is to drill a hole into solid rock or coal, insert an explosive cartridge with a detonator, and then fire the explosive to shatter the rock or coal bed.

1.2.3. Based on the chemical composition

The classification of explosives according to their chemical structure is necessary in terms of chemical identification. The knowledge about the chemical composition of explosives is useful to predict the chemical reaction that causes a detonation. Also it is important to select the appropriate methodology and analytical instrumentation on the analysis of explosives. For instance, gas/liquid chromatography is proper to determine organic explosives such as TNT despite that entirely ineffective for black powder. Likewise, ion chromatography or capillary electrophoresis is suitable to determine the ionic components of black powder, but very useless for TNT.

Energetic materials generally include nitro, azide and hydrazino groups in the molecules [25]. The $–NO_2$ and $–ONO_2$ groups are the major source of oxygen in the energetic molecules, which contribute notably to release the energy through combustion processes. Nevertheless, oxygen is not required for decomposition; for instance, the decomposition energy of lead azide is derived from the breaking of weak linkages between nitrogen atoms.

The first significant approach for a chemical classification of explosives, which was proposed by Van’t Hoff in 1909, was based on the seven types of chemical bonds that usually provide explosive properties to molecules, including: N=O (nitro-compounds, nitric esters and salts), N=N (diazo-compounds), O-Cl (chlorates and perchlorates), N=C (fulminates), N-Cl (nitrogen chloride), O-O (peroxides and ozonides) and C≡C (acetylene and acetylides) [14, 25]. Then the classification was extended by Plets, who specified the chemical groups containing the previously described bonds and added an eighth class for organometallic explosives with M-C bonds [6, 14, 28]. The explosive characteristics of any particular substance, according to Plets' hypothesis, are dependent on the presence of definite structural groups [12]. In the literature, there are present more chemical groups of explosives. Therefore, the

research still continues to revise previous information and find a more practical and comprehensive chemical classification of explosives. Some of important categories that were reported in the literature are determined as azides, nitrate esters, nitramines, chlorates and perchlorates, furazans and furoxans, tetrazoles, imidazoles.

1.2.3.1. Azide based explosives

Organic explosive azides are defined by the presence of at least one carbon atom and one azide group in their structure ($-N_3$). Common organic triazides are cyanuric triazide (C_3N_{12}) and ammonium azidotetrazolate (NH_4CN_7) [6, 24, 36]. It is well known that azides decompose rapidly if exposure to heat, mechanical shock or spesific chemical reagents. With the formation of a nitrogen molecule, the decomposition of azides is usually accompanied by the release of high quantities of energy. Organic azides have high positive heat of formation, good thermal and hydrolytic stability, high density and burning rate. However, risks of handling azides are important with considering the toxic and explosive nature of hydrazoic acid. Due to high sensitivity of these materials, they are synthesized in place in the solvent and used instantly in the production of high-energy compounds. In this regard, it is stated that the ratio of (C+O)/N represents a threshold value. If the ratio is less than 3:1, a severe decomposition of azide may occur. Furthermore, more caution must be exercised while handling low molecular weight azide molecules. These compounds are extremely dangerous because of explosions can happen for a variety of causes while handling.

Energetic organic azides have been extensively investigated not only as explosives but also as solid propellants. The incorporation of energetic azides into propellant formulations minimizes the amount of flame and smoke in exhaust gases, making the propellant compositions more environmentally friendly. Also, energetic azido plasticizers and polymers is formed by the substitution of hydrogen by energetic azido ($–N_3$) group in organic molecules. A great number of organic azides is reported in the literature over the last two decades. Compounds from this category include azidopolyethers, azidonitramines, azidonitro compounds, azidoalkanes and azidoesters [37].

1.2.3.2. Nitrate ester based explosives

Nitro-group is bonded to an oxygen atom (O-NO_2) in the molecular structure of nitrate esters. Organic nitrate esters such as nitrocellulose (NC), nitroglycerine (NG), and penerythritol tetranitrate (PETN) have explosive abilities and have been utilized in shell and demolition charges by the military for many years. The esterification/O-nitration of cellulose with a combination of HNO_3 and H_2SO_4 produces nitrocellulose. The nitrogen concentration of nitrocellulose which is used as propellant is varies in the range from 12.2 to 13.4%. The heat of the explosion, the amount of gases released, and the temperature of the explosion are all affected by the nitrogen content of nitrocellulose. The nitrate ester of glycerol is called as nitroglycerine (glycerol). Nitroglycerine is an extremely sensitive and energetic substance. It boils at 180°C, then decomposes exothermically and explodes at 215–218°C [37].

1.2.3.3. Nitramine based explosives

Nitramines are a type of organic nitrate explosive and has the high energy density potential. In their structure, nitro-group is bonded to a nitrogen atom (N-NO_2). The most well-known members of this group are RDX (research department explosive; hexahydro-1,3,5-trinitro-1,3,5-triazine) and HMX (hexahydro-1,3,5-trinitro-1,3,5-triazine) (high melting explosive; octahydro-1,3,5,7-tetranitro-1,3,5,7-tetrazocine). RDX was extremely important during World War II; it was used in conjunction with TNT (2,4,6-trinitrotoluene) and wax to enable handling easier and to decrease sensitivity. The molecular structure of HMX is similar to RDX, but it has a greater melting point, density, and detonation velocity. However, HMX is more expensive and sensitive than RDX.

TNAZ (1,3,3-Trinitroazetidine) is a highly nitrated four-member nitrogen heterocyclic ring with better performance when compared to melt castable explosive TNT [40–43]. The strained ring structure is projected to provide an additional source of energy [38–41]. Efforts are also made to decrease volatility of TNAZ by integrating some additional components into TNAZ energetic formulations.

CL-20 (2,4,6,8,10,12-hexanitrohexaazaisowurtzitane) is a novel nitramine explosive possessing 20% more energy than HMX. It has high density (2 g/cm^3) and

detonation velocity (9400 m/s) [42]. Also, hazard characteristics of these energetic materials are reduced. CL-20 is synthesized by debenzylation, acetylation and nitration of hexabenzyl isowurtizitane. One of the stages in the CL-20 synthesis requires the use of a high-priced palladium catalyst. There is a search in order to find another catalytic material to minimize the cost of CL-20.

1.2.3.4. Chlorate and perchlorate based explosives

An inorganic chlorate salt (oxidizer) is blended with one or more chemicals that act as a fuel in chlorate-based explosives. A chlorine atom is evenly bound to three oxygen atoms in the chlorate anion (ClO_3^-). As it is known, chlorate anion is the conjugate base of chloric acid. It configures stable chlorate salts with the combination with metals. Chlorates might be seperated as ammonium chlorate and metal-chlorates. Ammonium chlorate is exceedingly unstable; hence ammonium chlorate-based explosives are not manufactured. Actually, the majority of chlorate-based explosives are some pyrotechnic powders which are prepared mixing of potassium/sodium chlorate and black powder [43–45].

A chlorine atom is equally bound to four oxygen atoms in the perchlorate anion (ClO_4^-). It is the conjugate base of perchloric acid. Unlike ammonium chlorate, ammonium perchlorate (AP) is relatively stable and can cause an explosion on its own through unimolecular decomposition. As a consequence, AP is frequently combined with aluminum powder and plasticizers in AP-containing propellants. Besides, metal-perchlorates are used to form flash powder which is mainly produced with the combination potassium perchlorate and aluminum/magnesium powder [43-45].

1.2.3.5. Furazan and furoxan based explosives

As an alternative in the heterocycles, furazan and N-oxide derivative furoxan are explosophoric units which are used as building blocks in the synthesis of advanced energetic materials. They play an important role on the basis of compact scaffolds, high positive heats of formation (196.8 and 198.5 kJ/mol), rich combination modes and variable synthetic methods [46]. Also, they contain high nitrogen and oxygen contents which are 62.8% and 69.7% respectively [46]. When exposed to nucleophiles, furazan is much more stable than furoxan. Although, a wide range of mono-furazan or

furoxan structures are developed, the majority of these structures have weak stabilities and limited varieties. Despite this, energetic compounds based on poly furazan and furoxan structures show low mechanical sensitivity and detonation performance.

In general, macromolecular structures have linkages through C-C bonds, azo/azoxy bridges to create larger heterocycles that definitely enlarge conjugated systems. This supplies additional stabilization effect, especially on thermal stabilities of molecules. Similarly, macrocyclic polyfurazan structures have potential as new heat resistant energetic materials with their excellent thermal stabilities. Likewise, low melting points of tri-furazan/furoxan derivatives make them ideal for melt-cast technologies.

1.2.3.6. Tetrazole based explosives

Among the common five-membered azoles, tetrazole compounds have promising nitrogen-rich backbone with the high nitrogen content. In this group, especially amino tetrazoles that have high nitrogen percentage are the most studied heterocyclic structures. For example, 5-amino-1H-tetrazole (N=82.33%), 3-hydrazino-4-amino-1,2,4-triazole (N=73.65%), 4-amino-1,2,4-triazole (N=66.63%) have surprisingly high thermal stability, even though they have high endothermic formation enthalpy [47].

Moreover, the main decomposition product, dinitrogen gas, complies with green chemistry approach. The tetrazole ring provides a good balancing of stability and energetic performance along with two functionalization sites. For instance, if two energetic nitramino groups are added to tetrazole, potassium 1,5-di(nitramino)tetrazolate compound is designed. It outperforms any of the previous potassium salts in terms of detonation parameters (Detonation velocity (D_v): 10011 m/s, detonation pressure (P): 52.2 GPa) [48]. After 50 mg 1,5-di(nitramino)tetrazolate is ignited with a typical pyrotechnical igniter, it successfully detonates 500 mg of secondary explosive (RDX). As a result, it is a strong primary explosive candidate instead of lead azide and lead styphnate.

The N-N functionality, ring strain, and high density of tetrazoles all contribute to their high temperatures of formation and thermodynamic stability. However, their great sensitivity limits them as primary explosives. On the other hand, introducing an

N-O functionality in the tetrazole structure is a better method for obtaining low-sensitive secondary explosives. Additionally, N-Hydroxyl-substituted such as N-$NHNO_2$, N-OH, N-CH_2ONO_2 groups are other alternatives for new energetic tetrazoles [49].

1.2.3.7. Imidazole based explosives

Imidazole derivatives with two or more than two nitro groups are predicted as suitable energetic components in the explosive formulations [50–56]. In this regard, several nitroimidazole derivatives are designed and investigated such as 2,4-dinitroimidazole, 4,5-dinitroimidazole, 2,4,5-trinitroimidazole, 1,2,4,5-tetranitroimidazole [52-56]. Among these examples, 2,4-dinitroimidazole is reported as less sensitive than RDX and HMX and more energetic than 1,3,5-triamino-2,4,6-trinitrobenzene (TATB) [37]. Furtermore, it is seen that the cost of production of 2,4-dinitroimidazole is less expensive. Also 1-methyl-2,4,5-trinitroimidazole is suggested as another potential insensitive imidazole based explosive.

Although imidazole is an isomer of pyrazole, its density and thermal stabilities are generally better than pyrazole. As example, the density of 1H-pyrazole (1.12 g/cm^3) is slightly lower than that of 1H-imidazole (1.23 g/cm^3). Based on some previous studies, it is concluded that the detonation properties of trinitroimidazolates are higher than those of their pyrazole analogs [49].

Regarding the complexity of energetic materials, determination of functional groups and backbones give a shortcut to maximizing performance while minimizing stability losses. N-trinitroethylamination of imidazoles offers a new design for developing high-performance energetic materials. N-trinitroethylaminoimidazoles exhibit high densities (1.909 g/cm^3), positive oxygen balances (14.29%) which indicate high-dense energetic oxidizers [57].

N-nitramino functionality into imizadole structure is different way to obtain high energetic materials. For instance, the density of hydrazinium 1-amino 2,4-dinitroimidazolate surpasses density of HMX (d, 1.90 g/cm^3). It is an energetic material candidate having with not only detonation performance (P: 40.5 GPa, D_v: 9209 m/s) but also low impact sensitivity (IS, 12 J). Research efforts in searching for

bisimidazole-based high energy density materials are focused on the utilization of the N-nitramino functionality. For instance, 4,4’,5,5’-tetranitro-2,2’-bi(imidazole) can be modified with nitration using concentrated sulfuric acid and fuming nitric acid. The resulting compound could be classified as a high explosive by exhibition excellent detonation performance and crystal density of 2.007 g/cm^3. Additionally, energetic salts derived from 4,4',5,5'-tetranitro-2,2'-biimidazole have good densities and attractive detonation properties (P: 29.5-38.2 Gpa, D_v: 8409-9169 m/s), as well as moderate impact and friction sensitivity (IS, 5-30 J; FS, 60-240 N) [49].

Due to the creation of C-N bonds, nucleophilic aromatic substitution is critical for the development of advanced energetic materials. Chloro-substituted polynitrobenzenes have high reaction activity with nucleophilic reagents. Novel energetic benzene-imidazoles are synthesized by combining dinitroimidazole with a variety of chloro-substituted polynitrobenzenes to obtain better energetic performance.

Chemical stability is one of the problems related with imidazole compounds. The hydrogen linked to first position in the ring is quite acidic and it may inhibit the chemicals in the explosive or propellant formulations [58]. The nitration of the first position in imidazole yields 1,4-dinitroimidazole. Isomerization of the compound under heat describes synthesis of 2,4-dinitroimidazole which is a highly energetic material for energetic applications [51, 59, 60]. Another sutiable candidates are N-methyl, N-esters, and N-picryl derivatives of 2,4,5-trinitroimidazole according to literature. The integration of a picryl group into an organic compound enhances density, whilst the addition of a hydrocarbon chain promotes thermal stability [56]. In spite of their importance, detailed investigations on the thermodynamic characteristic of the imidazole derivatives are insufficient in the literature.

1.3. Solid Propellants

As discussed in section 1.2.1.1, propellant is a part of low explosives, which may be defined as combustible materials that includes required oxygen for adiabatic combustion. Their basic function is to provide propulsion to a bullet or rocket. Propellants have energetic properties to produce high temperatures, pressures and propulsive force for a particular mission. High specific impulse, consistent and repeatable burning rate and ignition characteristics, high density, ease of production,

cheap cost, and acceptable ageing properties are all desirable features for a propellant [61]. In addition, propellants should produce low-smoke exhaust; have sufficient thermophysical and qualities mechanical to safe operating and storage. Solid propellants are widely used in airspace and military industries. The most common commercial application of solid propellant is automobile airbags.

In a solid propellant, main chemical ingredients are present such as oxidizer, binder and fuel.

1.3.1. Oxidizers

An oxidizer is a substance with a high oxidation potential as well as that contains a high electronegative atom or functional group. Atoms on the right side of the periodic table show high electronegativity that correspond oxidizing property, while atoms on the left side show low electronegativity that corresponds fuel property. Thus, fluorine is the most efficient oxidizer and the F_2/H_2 propellant system has the maximum specific impulse of any chemical propulsion system [37]. Composite propellants are a heterogeneuos mixture that generally based on powder inorganic oxidizer and fuel. The oxidizer is a key component that has at least 70% weight in composite propellants. Solid propellants are preferred due to their combustion resulting completely gaseous products that have low molecular weight. Integration with other ingredients, high oxygen concentration, low heat of formation and low hygroscopicity are necessary requirements for an oxidizer. Besides, long shelf-life without modifications such as phase transition is a significant factor to select a good oxidizer. Ammonium perchlorate (AP) is the most common oxidizer due to fulfil most of the requirements. In spite this, it is harmful to the environment in terms of acid rain and ozone depletion. For instance, AP/Aluminum (Al) solid rocket generates hydrogen chloride, aluminum oxide, and aluminum chloride. Additionally, the exhaust trail causes problems in the detection and tracking of rockets or missiles [6]. Nitronium perchlorate (NP) which has advantageous heat of formation and oxygen balance is considered as another propellant alternative, but it was eliminated because of its instability in the presence of moisture. However inorganic nitrates have worse oxidation effectiveness than perchlorates, they are used due to their low cost and smokeless, non-toxic emissions [62, 63]. The usage of a few energetic ingredients such as NC, NG, PETN, RDX and

HMX in rocket motors is limited on the ground of their shock, friction and temperature sensitivity [6]. The shape and size of the solid oxidizer or metal fuel particles have a significant impact on composite propellant properties. The particles should have a spherical shape since this facilitates easy mixing and improved performance.

Ammonium dinitramide (ADN) and hydrazinium nitroformate (HNF) seem as new eco-friendly oxidizers candidate in propellant formulations with superior heat of formation values (−71 and −151 kJ/mol, respectively) [64, 65]. ADN has less impact sensitivity, high burning rates of nitramines and low melting point (90 ^{o}C). ADN is synthesized by nitration of aliphatic monoisocyanate using nitronium tetrafluoborate and nitric acid. The NH_4^+ or K^+ salts of dinitramide are more stable compared to dinitramines [37]. The use of ADN in place of AP enhances the energetic performance of the propellants. In line with literature, utilizing ammonium dinitramide instead of ammonium perchlorate allows the spacecraft to carry 8% more mass into orbit [37].

HNF is another possible oxidizer that is produced by the reaction of anhydrous hydrazine with trinitromethane in ethylene dichloride. It is a non-hygroscopic together with having high friction sensitivity. The purity of the hydrazinium nitroformate produced plays a major role in its stability. As addition to the challenges with purity and crystal structure, using HNF in practical compositions has the drawback about the inconsistences with the standard binder (hydroxy terminated polybutadiene). Glycidyl azide polymer (GAP) is identified as suitable binder for hydrazinium nitroformate based propellants [66].

1.3.2. Binders

Binders constitute a structural matrix to facilitate better consolidation between the solid components in composite propellants or plastic bonded explosives. They influence both mechanical and chemical properties of propellant such as processing and aging. Moreover, they protect metalic or non-metallic fuels from moisture and oxygen. The binders should have acceptable viscosity, high tensile strength and elongation in order to keep integrity of rocket propellant grains during flight. Hydroxy terminated polybutadiene (HTPB), carboxy-terminated polybutadiene (CTPB) are exceedingly used common binders in the last decades. They lead to higher solid fractions (total 88–90% of AP and Al) and better physical characteristics [67].

The binders form from liquid monomers or polymers. There are several inert binders such as polyester, epoxy, polysulfide, polyurethane. Energetic polymers are investigated to develop novel propellants which have distinctive combination of high energy and low vulnerability [68-72]. Propellant formulations consist of azido groups or nitro/nitrato groups. Glycidyl azide polymer (GAP), poly bis azidomethyl oxetane (P-BAMO) and poly azidomethyl methyl oxetane (P-AMMO) are the examples for azido polymers that decompose exotermically. Polyglycidyl nitrate (PGN) and nitratomethyl methyl oxetane (NIMMO) are examples for nitrato polymers that are oxygen rich compounds [37].

On the other hand, polynitropolyphenylene (PNP) is described as a binder for some pyrotechnic formulations. PNP respresents the aromatic compounds with $C–NO_2$ groups in a chain of benzene. PNP is considered as high temperature resistant binder with the deflagration temperature at 286-294 °C and explosion energy as 3300 $J.g^{-1}$ [6]. Further, it is insensitive to impact and friction.

Research polybutadiene with terminal functional groups is the most recent advances in the field of binders. Poly(butadiene-acrylic acid) (PBAA) is the simplest copolymer in this category of polybutadiene wherein the functional -COOH groups are randomly distributed along the backbone. PBAA-based composites have poor mechanical strenght because of random location of carboxyl groups. Therefore, acrylonitrite is introduced (PBAN) to improve these properties. However, CTPB has better performance than PBAN by providing high specific impulse.

A different approach is to placing metal elements into the polymer structure. Accordingly, light metals such as Li, Be, Mg and Al are used to enhance energy.

1.3.3. Fuels

In propellant mixtures, addition of metal fuels is used to achieve high combustion temperature and specific impulse. Propellants contain metal fuels by 14-20% [73]. Actually, fuels have a wide range from from metallic to non-metallic elements. For instance, aluminum (Al), magnesium (Mg), beryllium (Be), chromium (Cr), boron (B), iron (Fe), titanium (Ti), tungsten (W) and zirconium (Zr) is listed in the literature as known metal fuels. In case non-metalic fuels, carbon (C), silicon (Si), antimony (Sb),

sulfur (S) and phosphorus (P) is listed mainly. Especially, the small spherical particles (5–60 μm) of aluminum and magnesium powders are frequently used as metal additives [73]. In comparison, while Mg powder generates more light, Al powder supply more stability and storage life. As another alternative, Be has higher potential energy value than Al. Nevertheless, powdered Be is rarely employed because of its extreme toxicity and high expense. B is one of the well-known high energy density materials with high heat of oxidation and low atomic weight. But it is very difficult to ignite it due to formation of boron oxide on its surface. Some coating additives are necessary to keep the surface without boron oxide [6].

Zr can provide higher density-impulse with the ratio 20% than other metals which used in rocket or ballistic missile defense system. Zr has extreme sensitivity to electrostatic discharge that causes serious safety concerns. Therefore, a safer process is developed using aluminum for coating of zirconium to use in energetic formulations.

Usage of energetic additives insetad of non-energetic additives definitely increases the performance level of solid propellant and gun propellant formulations.

1.4. Metal Based Explosives

Coordination compounds are desirable primary explosive candidates for numerous propulsive and energy converter operations. Primary explosives were first manufactured materials with moderate explosion capabilities and good sensitivity [74]. For more than a century, the most typically used primary explosives were mercury fulminate (MF), lead azid (LA), and lead styphnate (LS) [75]. Mercury fulminate, the first primary explosive, is made with a simple procedure from mercury, ethanol, and nitric acid. However, the high expense and toxicity of mercury are significant disadvantages [76]. Mercury compounds are found to be hazardous to the kidneys and neurological system. Many enzymes involved in metabolic processes in biological systems can be inhibited by mercury cations. Moreover, MF is extremely responsive to external stimulation and is incapable of performing at high-pressure conditions [77].

After that, lead azide and lead styphnate were used to replace MF. They are frequently employed in primer combinations to initiate burning. Whereas these

compounds are less risky for handling than MF, they do not eliminate the environmental dangers that toxic heavy metals create. Lead has negative effects on tissues and organs such as bones and heart when ingested or inhaled [78]. Also the usage of LA and LS in military products is resulted in intolerable levels of pollution. In addition to health and environmental concerns, LA generates highly toxic hydrazoic acid (HN_3) when react with water and carbondioxide at room temperature. HN_3 interacts with copper cables and coatings and form copper azide ($Cu(N_3)_2$). Several military incidents are caused by the product that is very sensitive and dangerous [79].

Hence, a comprehensive research effort to discover environmentally benign energetic materials as substitutes for heavy metal based compounds. Thus, many novel chemical substances are developed as "green" primary explosives. One of the alternative substances is silver containing compounds. Silver azide (SA) provides many benefits that are improved explosive property, high stability, and good compliancy in microscale explosion equipments [80]. In spite this, silver salts have some problems represent light sensitivity, expensive cost and the toxic effect on microorganisms and aquatic life [81].

Other groups of metal explosive candidates contain the alkali metals (cesium, potassium etc.) and transition metals (copper, iron etc.). A wide range of new explosives is investigated such as calcium nitrimino-tetrazolate [8], copper chlorotetrazolate [82] and copper(II) coordination complexes of the 5-nitrotetrazolate anion [83], but they have drawbacks that restrict their extensive usage. For instance, copper(I) 5-nitrotetrazolate [84, 85] is among the most attractive lead azide alternative with similar safety and initiation characteristics, but its transportation and storage are challenging due to inherent sensitivity to impact (IS: 0.04 J) and friction (FS: 0.1 N) [86].

In addition, micron sized inorganic complexes have various disadvantages because of their high ignition temperatures and higher aggregation rates that cause limited energy release. On the contrary, nano sized inorganic complexes supply high specific surface area and excess energy of surface atoms. Therefore, there is a rising attention in usage of metal nanoparticles for energetic purposes [87].

Several energetic metal-based compounds are expected to be capable of self-sustained combustion and behave as a burning catalyst. As explosive, coordination compounds comprise molecular fragments having oxidizing characteristics. Cr, Mn, Fe, Ni, and Co are transition metals that play an essential role in coordination chemistry. Salts of the bivalent metals form stable complexes. Furthermore, group I and II metals such as Cu, Ag, Zn, and Cd can form stable combinations. A total of oxidizing groups is defined by the valence of the central metal atom, whereas the coordination number of the metal determines the fuel content in an energetic molecule. Changes in the valence of metal atoms allow the regulation of fuel-oxidizer ratio [88].

In recent years, metal salt and coordination compounds are designed as new energetic material candidates. In addition, five-member nitrogen-rich heterocyclic structures are used as a source of energetic material for a long time [75]. In this manner, many studies represent potential structures that can be expressed with the general formula $(M)_X(L)_Y(An)_Z$ [76]. In this formula, 'M' corresponds to transition metal, 'L' corresponds to a nitrogen-rich ligand molecule while 'An' corresponds to an oxygen-rich anion. The transition metal constitutes the general molecular structure and coordinates the other molecules (ligands) to ensure the desired level stability level of the compound.

For an extended period, several scientific attempts have been made to obtaine an environmental friendly and more efficient energetic coordination compound. One of the example for such kind of coordination compounds are Mn(II), Co(II), Ni(II), Cu(II) and Zn(II) complexes of tetrazole oxide, 1H,1'H-[5,5'-bitetrazole]-1,1'-diol (H_2BTO) [89]. In this study, tetrazole oxide is selected as a suitable energetic linker due to its high-energy density and good stability. Indeed, these metal complexes demonstrate good thermal stability (all beyond 200 ^oC), mechanical insensitivity and high detonation capability [89].

In another study, thermally stable cobalt(III) complexes, penta(ammine)(5-cyanotetrazolate-N^2)cobalt(III) perchlorate [83] and tetra(ammine)di(5-nitrotetrazolate- N^2)cobalt(III) perchlorate [83], are found to have desirable explosive properties. Similar to these Co(III) perchlorate complexes, manganese(II), iron(II), zinc(II) and copper(II) perchlorate complexes containing 1-amino-5-methyltetrazole

are examined for being primary explosives. Although all compounds indicate good thermal stabilities up to 199 °C and possess sensitivities in the range of primary explosives, their usage as energetic compounds are restricted due to their health risks caused by perchlorate counter ion. On the other hand, among these compounds, iron(II)-(1-amino-5-methyltetrazole) complexes shows primary explosive properties successfully and its performance tested with asecondary high explosive PETN [90].

First-row transition metal complexes coordinated by oxygen-rich bidentate ligands such as 5,5'-dinitro-3,3'-azo-1,2,4-triazolate ($DNAT^{2-}$) [91] and 4,4',5,5'-tetranitro-2,2'-biimmidazolate (N4BIM) exhibit insensitivity to spark, friction, and impact [58]. In that study, $(NH_4)_2[Cu^{II}_2(DNAT)_3]$, $(NH_4)_2[Fe^{II}_2(DNAT)_3]$, $(NH_4)_2[Co^{II}_2(DNAT)_3]$, $(NH_4)_4[Fe^{II}(N4BIM)_3]$, and $(NH_4)_4[Co^{II}(N4BIM)_3]$ reveal high explosive performance, but the chelation effect of the bidentate $DNAT^{2-}$ and $N4BIM^{2-}$ ligands makes their complexes too insensitive to be considered as primary explosives [74].

As green primary explosives, four Fe(II) and Cu(II) complexes including 5-nitrotetrazolato-N^2 (NT) with NH_4^+ or Na^+ counter ions are prepared according to the general structure of $(cat)_2[M^{II}(NT)_4(H_2O)_2]$ [76]. The complexes have safer preparation and transportation and comparable initiation efficiency than lead azide and lead styphnate. In an complamentary following study, new primary explosives are prepared by systematically varying the number of coordinated NT around Fe(II) to customize explosive performance. In these iron complexes, $cat[Fe^{II}(NT)_3(H_2O)_3]$, $cat_2[Fe^{II}(NT)_4(H_2O)_2]$, $cat_3[Fe^{II}(NT)_5(H_2O)]$, and $cat_4[Fe^{II}(NT)_6$, different cations are used as counter ions such as monocations sodium (Na^+), nitrosocyanaminium (NCAm), ammonium (NH_4^+), hydrazonium (Hyzm), 1,2,5-triamino-1,2,3-triazolium (TATm) and 5-amino-1-nitroso-1,2,3,4-tetrazolium (ANTm) inorder to control the sensitivity [74]. All these iron complexes exhibit high resistance to decomposition upon exposure to moisture, light, or heat.

One can conclude that upon the light of all these studies mentioned here, there has been still a need for green energetic compounds which have high energetic performance, high chemical and thermal stability as well as appropriate sensitivity to

mechanical stimulu, moisture and light in order to achieve economical, social and technological developments for homeland security and civilization purposes.

1.5. The Aim of the Study

The aim of this study is to design and synthesize novel energetic organic and coordination compounds that have never been reported before in the literature. For this purpose, 5-(chloronitromethyl)-4-nitro-1H-imidazole (HL) (Figure 1.2) and its cobalt(II/III), copper(II), iron(II/III) and zinc(II) complexes in different geometries (Figure 1.3) were synthesized and characterized via various spectroscopic techniques such as HRMS, NMR and FTIR.

Quantum chemical studies of HL and the synthesized complexes were achieved to obtained optimized geometries and investigate the activity and structure relationship of the complexes theoretically as a part of the research project (117Z391) funded by the Scientific and Technological Research Council of Turkey [1].

These newly generated compounds were also subjected to thermo-gravimetric and differential thermal analyses (TGA-DSC) to evaluate their thermal stability, thermal decomposition characteristics and kinetic behaviours.

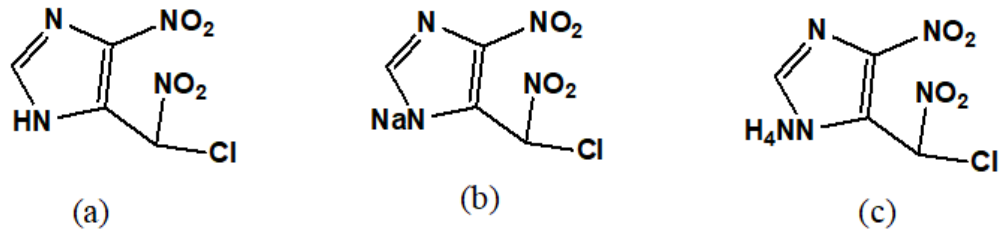

Figure 1.2. Molecular structures of 5-(chloronitromethyl)-4-nitro-1H-imidazole ligand and derivatives

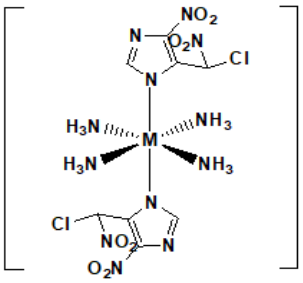

M = Co^{II}, Fe^{II}

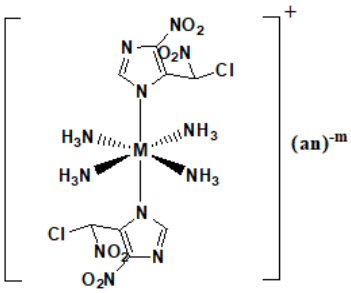

M = Co^{III}, Fe^{III}; an: PF_6^-, CO_3^{2-}

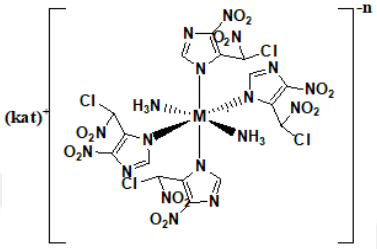

M = $Co^{II/III}$, $Fe^{II/III}$; kat: NH_4^+, Na^+

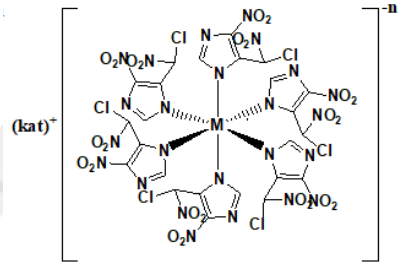

M = $Co^{II/III}$, $Fe^{II/III}$; kat: NH_4^+, Na^+

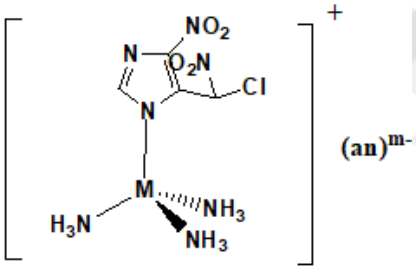

M = Cu^{II}, Zn^{II}; an: PF_6^-, CO_3^{2-}

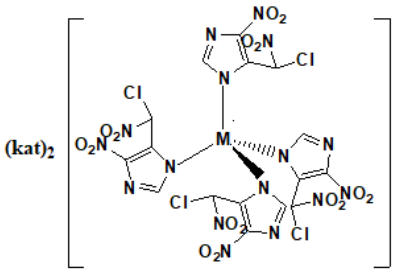

M = Cu^{II}, Zn^{II}; kat: NH_4^+, Na^+

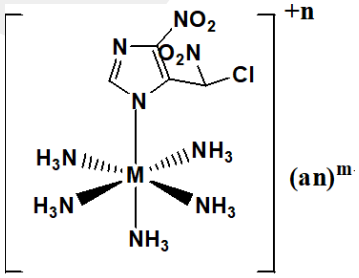

M = $Co^{II/III}$, $Fe^{II/III}$, an: CO_3^{2-}

Figure 1.3. General molecular structures of metal complexes containing 5-(chloronitromethyl)-4-nitro-1H-imidazole ligand

In this study, the numbering system presented in Table 1.1 was used to facilitate the identification of the studied complexes.

Table 1.1. Identification and numeration of metal complexes containing 5-(chloronitromethyl)-4-nitro-1H-imidazole ligand

#	Complex	#	Complex
1	$[Co(NH_3)_4(L)_2]$	**18**	$Na_3[Co(L)_6]$
2	$[Fe(NH_3)_4(L)_2]$	**19**	$(NH_4)_4[Fe(L)_6]$
3	$[Co(NH_3)_4(L)_2]PF_6$	**20**	$Na_4[Fe(L)_6]$
4	$[Co(NH_3)_4(L)_2]_2CO_3$	**21**	$(NH_4)_3[Fe(L)_6]$
5	$[Fe(NH_3)_4(L)_2]PF_6$	**22**	$Na_3[Fe(L)_6]$
6	$[Fe(NH_3)_4(L)_2]_2CO_3$	**23**	$[Cu(NH_3)_3(L)]PF_6$
7	$(NH_4)_2[Co(NH_3)_2(L)_4]$	**24**	$[Cu(NH_3)_3(L)]_2CO_3$
8	$Na_2[Co(NH_3)_2(L)_4]$	**25**	$[Zn(NH_3)_3(L)]PF_6$
9	$NH_4[Co(NH_3)_4(L)_4]$	**26**	$[Zn(NH_3)_3(L)]_2CO_3$
10	$Na[Co(NH_3)_4(L)_4]$	**27**	$(NH_4)_2[Cu(L)_4]$
11	$(NH_4)_2[Fe(NH_3)_2(L)_4]$	**28**	$Na_2[Cu(L)_4]$
12	$Na_2[Fe(NH_3)_2(L)_4]$	**29**	$(NH_4)_2[Zn(L)_4]$
13	$NH_4[Fe(NH_3)_2(L)_4]$	**30**	$Na_2[Zn(L)_4]$
14	$Na[Fe(NH_3)_4(L)_4]$	**31**	$[Co(NH_3)_5(L)]_2CO_3$
15	$(NH_4)_4[Co(L)_6]$	**32**	$[Fe(NH_3)_5(L)]_2CO_3$
16	$Na_4[Co(L)_6]$	**33**	$[Co(NH_3)_5(L)]CO_3$
17	$(NH_4)_3[Co(L)_6]$	**34**	$[Fe(NH_3)_5(L)]CO_3$

CHAPTER 2

2. EXPERIMENTAL

2.1. Materials

To synthesize the designed ligand and complexes, 4-Nitro-1H-imidazole, cobalt(II) nitrate hexahydrate (98%), iron(II) chloride tetrahydrate (98%) were supplied from Sigma-Aldrich Chemicals Co. Inc. In addition to these chemicals; iron(III) chloride hexahydrate (Merck), copper(II) chloride (99%) (Acros), zinc(II) chloride (pure) (Carlo Erba) were used. Methanol (CH_3OH), ethanol (C_2H_5OH), dimethylformamide (C_3H_7NO), acetonitrile (CH_3CN), isopropanol (C_3H_7OH) were used as solvents supplied from Merck Chemicals. The details of the experimental methods regarding the ligand and metal complexes synthesis were explained below.

2.2. Synthesis of 4-nitro-5-(dinitromethyl)-1H-imidazole Ligand (HL)

2.2.1. The synthesis of 1,4-dinitro-1H-imidazole [92]

0.4 mL of 100 % nitric acid was added dropwise to a solution of 4-nitro-1H-imidazole (0.55 g) in glacial acetic acid (1.25 mL) at ~17°C. At this temperature, 1.0 mL acetic anhydride was added drop wise to the solution. The final solution was kept at 17°C for another 2 h. After this period, the solution was stirred overnight at room temperature. Then reaction mixture was poured over 20 g of crushed ice. The white precipitate was filtered out (Figure 2.1). The obtained solid was washed with water and dried under vacuum. The white crystals were obtained in 75 % yield. The product gave molecular ion in the mass spectrum at m/z 157 M^+. ^{1}H NMR (DMSO-d_6, 600 MHz) δ(ppm) 8.962 (s, 1H, 5-H), 9.392 (s,1H, 2-H). ^{13}C-NMR (600 MHz, DMSO-d_6): δ(ppm) 119.391 (5-C), 136.254 (4-C), 147.99 (2-C).

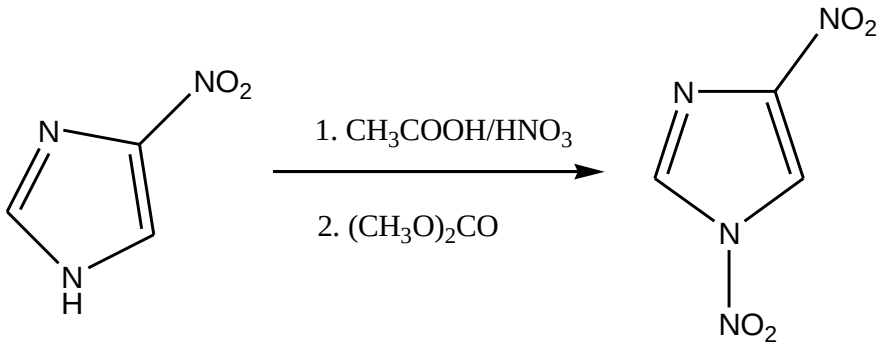

Figure 2.1. The synthesis of 1,4-dinitro-1H-imidazole

2.2.2. The synthesis of 1,4-dinitro-5-cyano-1H-imidazole [93]

1.37 mmol 1,4-dinitro-1H-imidazole was dissolved to aqueous methanol (1:1 v/v, 5 mL) at room temperature. While stirring, 1.51 mmol potassium cyanide and 1.37 mmol sodium bicarbonate were added to this solution. The reaction mixture left overnight in darkness at ambient temperature. Then the pH of the solution was adjusted to 6 by the addition of concentrated hydrochloric acid. Evaporation of solvents gave the yellow solid (Figure 2.2). After drying under vacuum, the desired product was obtained with 55 % yield. The product gave molecular ion in the mass spectrum at m/z 139 M^+. ^{1}H NMR (DMSO-d_6, 600 MHz): δ(ppm) 8.163 (2-H). ^{13}C-NMR (600 MHz, DMSO-d_6): δ(ppm) 110.501 (5-C), 139.251 (4-C), 150.377 (2-C), 102.433 (6-C).

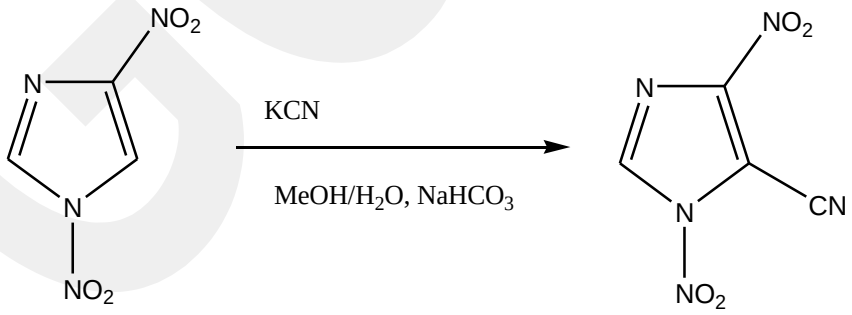

Figure 2.2. The synthesis of 1,4-dinitro-5-cyano-1H-imidazole

2.2.3. The synthesis of N'-hydroxy-4-nitro-1H-imidazole-5-carboxamidine

20 mmol 1,4-dinitro-5-cyano-1H-imidazole was dissolved in 55 mL water and 25 mL isopropanol mixture at ambient temperature. 21 mmol Na_2CO_3 was added to the solution, and the temperature was raised to 50°C. At this temperature 42 mmol $NH_2OH.HCl$ was also added to that solution mixture, and the resultant mixture was stirred at this temperature for 2 hours (Figure 2.3). The white precipitate was collected, washed with water and dried under vacuum. The crude product was recrystallized in methanol. The yield of the reaction was 82 %. The molecular ion peak was seen at m/z 172 M^+. ^1H NMR (DMSO-d_6, 600 mHz) δ(ppm) 13.597 (s, 1H, NH), 9.944 (s,1H, CH), 6.066 (s, 2H, NH_2). ^{13}C NMR (600 MHz, DMSO-d_6): δ(ppm) 124.263 (5-C), 134.203 (4-C), 143.763 (2-C), 159.479 (6-C).

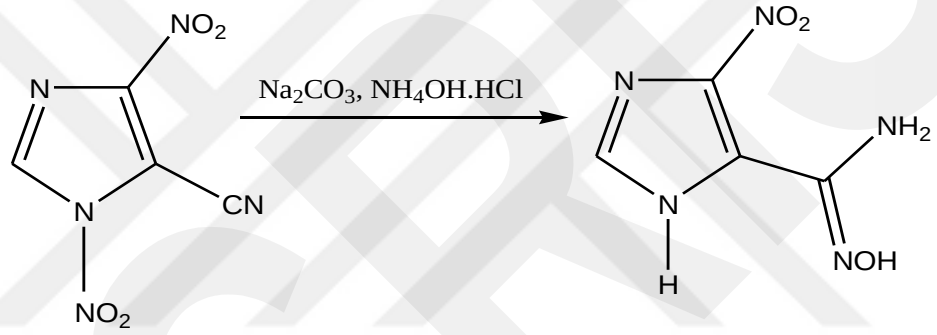

Figure 2.3. The synthesis of N'-hydroxy-4-nitro-1H-imidazole-5-carboxamidine

2.2.4. The synthesis of 4-nitro-1H-imidazole-5-carbonyl chloride oxime

15 mmol N'-hydroxy-4-nitro-1H-imidazole-5-carboxamidine was dissolved in 55 mL concentrated HCl and 30 mL water. Saturated $NaNO_2$ solution (12 mL) was added dropwise to this solution at 0°C. The mixture was stirred for additional 2 hours. The resultant solution was heated to 20°C to remove all N_2. The precipitate was filtered out, after washing with water dried under vacuum (Figure 2.4). The crude product was recrystallized in methanol. 4-nitro-1H-imidazole-5-carbonyl chloride oxime was obtained as white solid with 71 % yield. m/z: 190 M^+. ^1H NMR (600 MHz, DMSO-d_6): δ(ppm) 13.038 (s, 1H, NH), 7.955 (s, 1H, CH). ^{13}C NMR (600 MHz, DMSO-d_6): δ(ppm) 159.119 (6-C), 144.211 (2-C), 135,871 (4-C), 124.141 (5-C).

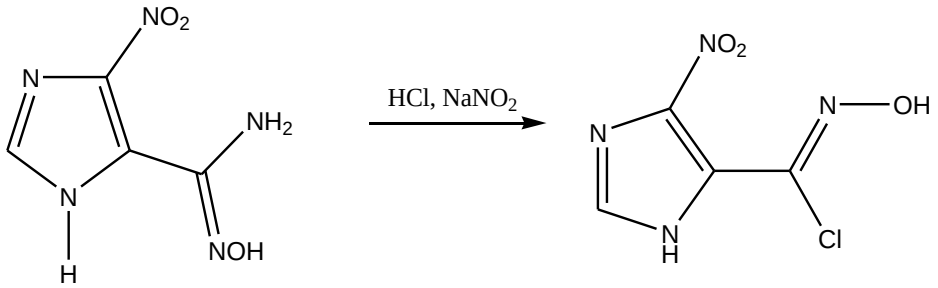

Figure 2.4. The synthesis of 4-nitro-1H-imidazole-5-carbonyl chloride oxime

2.2.5. The synthesis of 5-(chloro(nitro)methyl)-4-nitro-1H-imidazole (HL)

1 mmol 4-nitro-1H-imidazole-5-carbonyl chloride oxime was dissolved in 50 mL CH_3CN at 40°C. 0.5 mmol oxodiperoxo complex was synthesized according to the literature method [94]. Then, oxodiperoxo complex in 5 mL CH_3CN was addedinto the oxime solution dropwise (Figure 2.5). The progress of the reaction was screened by TLC. The purification of the crude product was performed by column chromatography (silica gel, pentane-chloroform 4:1). The yellow solid was obtained with 45% yield. m/z 206.81 M^+**.** ^{1}H NMR (600 MHz, DMSO-d_6): δ (ppm) 7.924 (s, 1H, 2-H), 7.555 (s, 1H, CH). ^{13}C NMR (600 MHz, DMSO-d_6): δ (ppm) 131.588 (2-C), 129.198 (4-C, 5-C).

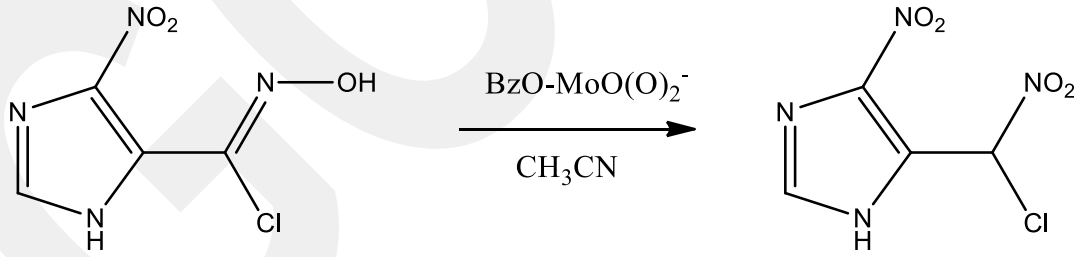

Figure 2.5. The synthesis of 5-(chloro(nitro)methyl)-4-nitro-1H-imidazole (HL)

2.2.6. The synthesis of ammonium salt of 5-(chloro(nitro)methyl)-4-nitro-1H imidazole (NH_4L)

2.5 mmol 5-(chloro(nitro)methyl)-4-nitro-1H-imidazole was dissolved in 18 mL methanol at room temperature and stirred continuously during 4 hours. 22 mL

methanolic solution of 12 mmol NH_4Cl in was added to that solution (Figure 2.6). In order to precipitate the desired product, the solution was triturated with diethyl ether. After that, the precipitated yellow solid was collected. Yellow crystals were washed with ice-water and diethyl ether. 75 % yield. m/z: 223 M^+.

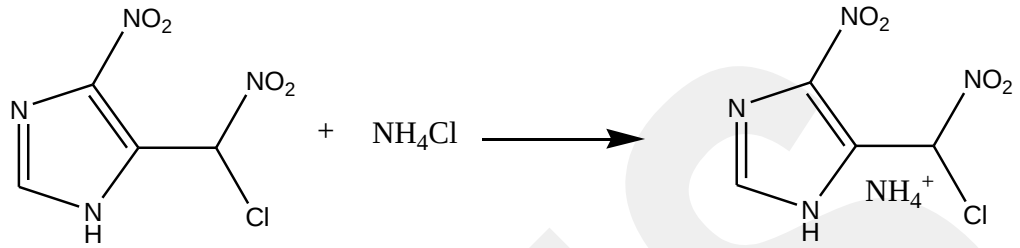

Figure 2.6. The synthesis of ammonium salt of 5-(chloro(nitro)methyl)-4-nitro-1H-imidazole (NH_4L)

2.2.7. The synthesis of sodium salt of 5-(chloro(nitro)methyl)-4-nitro-1H imidazole (NaL)

5-(chloro(nitro)methyl)-4-nitro-1H-imidazole (2.5 mmol) was dissolved in 18 mL methanol. To prepare the sodium salt of our imidazole, 22 mL methanol solution of 12 mmol NaI was added to the imidazol solution. The solution was stirred for four hours at room temperature. At ambient temperature 12 mmol NaI in 22 mL methanol was added to the solution (Figure 2.7). After that, the resultant solution was treated with diethyl ether to precipitate the desired solid. Then, the obtained yellow solid was washed with ice-water and diethyl ether. 75 % yield. m/z: 228 M^+.

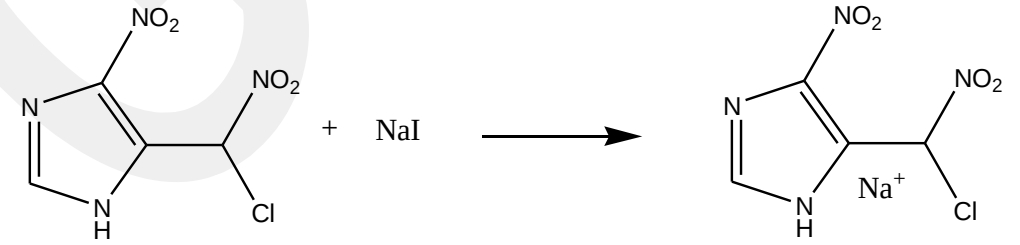

Figure 2.7. The synthesis of sodium salt of 5-(chloro(nitro)methyl)-4-nitro-1H imidazole (NaL)

2.3. Synthesis of metal complexes

2.3.1. Tetraamminebis(5-(chloro(nitro)methyl)-4-nitro-1H imizadole)cobalt(II) $[Co(NH_3)_4(L)_2]$ (1)

To the 1 mL aqueous solution of 0.875 mmol cobalt(II)nitrate hexahydrate $[Co(NO_3)_2.6H_2O]$, 1.75 mmol sodium salt of 5-(chloro(nitro)methyl)-4-nitro-1H imidazole (NaL) dissolved in aqueous dimethylformamide (C_3H_7NO) (1:1 v/v, 15 mL) was added drop wise and refluxed at around 70-80 ^oC for 70-75 hours. After, 3.50 mmol NH_3 (aq: 26%) was added to that solution at room temperature, the resultant solution was refluxed at 40 ^oC for another 3-4 hours. Then, that solution of **1** was kept in the refrigerator over night. The obtained green precipitate was filtrated and dried under vacuum. Yield: 20.2%

2.3.2. Tetraamminebis(5-(chloro(nitro)methyl)-4-nitro-1H imizadole)iron(II), $[Fe(NH_3)_4(L)_2]$ (2)

The synthesis of **2** followed exactly the same procedure of **1** described above by using 0.875 mmol iron(II)chloride tetrahydrate $[FeCl_2.4H_2O]$ and 1.75 mmol sodium salt of 5-(chloro(nitro)methyl)-4-nitro-1H imidazole. The obtained brown precipitate was collected and dried under vacuum. Yield: 18.3%

2.3.3. [Tetraamminebis(5-(chloro(nitro)methyl)-4-nitro-1H imizadole)cobalt(III)] hexafluorophosphate, $[Co(NH_3)_4(L)_2]PF_6$ (3)

The similar procedure was applied to prepare **3** by using appropriate amounts of the reagents according to their stoichiometric ratio, where 0.656 mmol 1 mL aqueous $Co(NO_3)_2.6H_2O$ was reacted with 1.312 mmol 15 mL methanolic solution of NaL. The reason of using methanol instead of water in this step was to oxidize Co(II) to Co(III). After the second reflux process carried out with 2.624 mmol NH_3 aqueous solution, the aqueous saturated tetrabutylammonium hexafluorophosphate (NBu_4PF_6) solution was added to precipitate **3**. The solution was kept in the refrigerator. The obtained dark green precipitate was filtrated and dried under vacuum. Yield: 10.5%

2.3.4. [Tetraamminebis(5-(chloro(nitro)methyl)-4-nitro-1H imizadole)cobalt(III)] carbonate, $[Co(NH_3)_4(L)_2]_2CO_3$ (4)

In order to synthesize **4**, 0.894 mmol 1 mL aqueous solution of $Co(NO_3)_2.6H_2O$ and 1.789 mmol ammonium salt of 5-(chloro(nitro)methyl)-4-nitro-1H imidazole (NH_4L) dissolved in 15 mL methanol (CH_3OH) was reacted following to the procedure of **3**. However, 3.578 mmol NH_3 solution was added prior to the second reflux in this case and the complex **4** was precipitated using saturated aqueous solution of sodium carbonate (Na_2CO_3). After maintaining the resultant solution in the refrigerator over night, the pink precipitate was collected and dried under vacuum. Yield: 11.4%.

2.3.5. [Tetraamminebis(5-(chloro(nitro)methyl)-4-nitro-1H imizadole)iron(III)] hexafluorophosphate, $[Fe(NH_3)_4(L)_2]PF_6$ (5)

Complex **5** was prepared using the methods explained for **3** by replacing the metal salt with 0.656 mmol iron(III)chloride hexahydrate [$FeCl_3.6H_2O$]. For the synthesis, 1.312 mmol NaL dissolved in aqueous DMF and 2.624 mmol NH_3 solutions were also used stoichiometrically. Yield: 13.9%

2.3.6. [Tetraamminebis(5-(chloro(nitro)methyl)-4-nitro-1H imizadole)iron(III)] carbonate, $[Fe(NH_3)_4(L)_2]_2CO_3$ (6)

The same methodology with **4** was applied to obtaine **6** using 0.671 mmol $FeCl_3.6H_2O$, 1.341 mmol NH_4L in aqueous DMF and 2.683 mmol NH_3 solutions. Yield: 30.1%.

2.3.7. Ammonium[(diamminetetrakis(5-(chloro(nitro)methyl)-4-nitro-1H imizadole)cobaltate(II)], $[NH_4]_2[Co(NH_3)_2(L)_4]$ (7)

The reaction of 0.391 mmol 1 mL aqueous $Co(NO_3)_2.6H_2O$ and 1.565 mmol 15 mL aqueous DMF solution of NH_4L was carried out as explained as previously for other complexes. Following the second reflux stage of procedure with 0.782 mmol NH_3 solution, the green precipitate was obtained with a yield of 8.73%.

2.3.8. Sodium[(diamminetetrakis(5-(chloro(nitro)methyl)-4-nitro-1H imizadole)cobaltate(II)], $Na_2[Co(NH_3)_2(L)_4]$ (8)

Complex **8** was also prepared in the same manner, in which 0.384 mmol aqueous $Co(NO_3)_2.6H_2O$, 1.538 mmol of aqueous dimethylformamide NaL and 0.769 mmol aqueous NH_3 solutions were involved. Yield: 12.2 %

2.3.9. Ammonium[(diamminetetrakis(5-(chloro(nitro)methyl)-4-nitro-1H imizadole)cobaltate(III)], $NH_4[Co(NH_3)_2(L)_4]$ (9)

In this synthesis the same procedure and the amounts of the reagents explained for preparing **7** were used. Here, NH_4L was dissolved in methanol in order to oxidize Co(II). The yield was 9.69%.

2.3.10. Sodium[(diamminetetrakis(5-(chloro(nitro)methyl)-4-nitro-1H imizadole)cobaltate(III)], $Na[Co(NH_3)_2(L)_4]$ (10)

Complex **10** was prepared by using methanolic solution of 1.452 mmol NaL and aqueous solutions of 0.363 mmol $Co(NO_3)_2.6H_2O$ and 0.726 mmol NH_3 alike to the procedure of **9**. Yield: 32.5%.

2.3.11. Ammonium[(diamminetetrakis(5-(chloro(nitro)methyl)-4-nitro-1H imizadole)ferrate(II)], $(NH_4)_2[Fe(NH_3)_2(L)_4]$ (11)

The same preparation procedure of **7** was applied in this synthesis in which 0.223 mmol $FeCl_2.4H_2O$, 0.894 mmol NH_4L and 0.447 mmol NH_3 was used. The dark brown precipitate of the compound was obtained with a yield of 5.6%.

2.3.12. Sodium[(diamminetetrakis(5-(chloro(nitro)methyl)-4-nitro-1H imizadole)ferrate(II)], $(Na)_2[Fe(NH_3)_2(L)_4]$ (12)

The procedure given for **8** was followed using 0.328 mmol $FeCl_2.4H_2O$, 0.328 mmol NaL and 0.656 mmol NH_3 in this synthesis. (Brown precipitate, yield: 9.9%)

2.3.13. Ammonium[(diamminetetrakis(5-(chloro(nitro)methyl)-4-nitro-1H imizadole)ferrate(III)], $NH_4[Fe(NH_3)_2(L)_4]$ (13)

The synthesis of **13** is similar to **9.** In this case 0.391 mmol aqueous $Fe(Cl_3).6H_2O$ and 1.565 mmol NH_4L in aqueous dimethylformamide were reacted firstly and 0.782 mmol NH_3 was added in the second step. Yield of **13** was 17.3%.

2.3.14. Sodium[(diamminetetrakis(5-(chloro(nitro)methyl)-4-nitro-1H imizadole)ferrate(III)], $Na[Fe(NH_3)_2(L)_4]$ (14)

0.328 mmol aqueous $[Fe(Cl_2).6H_2O]$ and 1.312 mmol of aqueous dimethylformamide solution of NaL was refluxed as in the procedure for **10** and 0.656 mmol NH_3 solution was added before the second reflux process. The yield was 21.8%.

2.3.15. [Triammine(5-(chloro(nitro)methyl)-4-nitro-1H imizadole)copper(II)] hexafluorophosphate, $[Cu(NH_3)_3(L)]PF_6$ (23)

23 was synthesized according the procedures provided for **5**. In this experiment, 1 mL 1.341 mmol copper(II)chloride ($CuCl_2$) was reacted with 1.341 mmol NH_4L dissolved in aqueous dimethylformamide and refluxed. 4.025 mmol NH_3 solution was added and refluxed at 40 ^oC for 3-4 hours one more time. To precipitate complex copper cation, saturated NBu_4PF_6 solution was added to precipitate **23** (Yield: 16.8%).

2.3.16. [Triammine(5-(chloro(nitro)methyl)-4-nitro-1H imizadole)copper(II)], carbonate $[Cu(NH_3)_3(L)]_2CO_3$ (24)

The procedure for **23** was repeated with 1.341 mmol $CuCl_2$, 1.341 mmol NH_4L and 4.025 mmol NH_3. Then, the saturated sodium carbonate (Na_2CO_3) solution was added to precipitate **24** (Yield: 28.3%).

2.3.17. [Triammine(5-(chloro(nitro)methyl)-4-nitro-1H imizadole)zinc(II)], hexafluorophosphate, $[Zn(NH_3)_3(L)]PF_6$ (25)

Since **23** and **25** were the counterparts of each others, the procedure defined for **23** was also applied for the preparation of **25** with the stoichiometric amounts of 1.341 mmol zinc(II)chloride ($ZnCl_2$), 1.341 mmol NH_4L and 4.025 mmol NH_3. Yield for white precipitate of **25** was calculated as 4.7%.

2.3.18. [Triammine(5-(chloro(nitro)methyl)-4-nitro-1H imizadole)zinc(II)], carbonate, $[Zn(NH_3)_3(L)]_2CO_3$ (26)

In order to synthesize **26**, the similar the procedure given for **24** was repeated by using exactly the same amount of metal salt, $ZnCl_2$, and ligands. The green precipitate was filtrated and dried under vacuum. Yield: 13.7%

2.3.19. Ammonium[(tetrakis(5-(chloro(nitro)methyl)-4-nitro-1H imizadole)cuprate(II)], $(NH_4)_2[Cu(L)_4]$ (27)

1.74 mmol NH_4L was dissolved in 15 mL aqueous dimethylformamide (C_3H_7NO) (1:1 v/v) and added to the 1 mL aqueous solution of 0.437 mmol $CuCl_2$ drop wise. The reaction mixture was refluxed at around 70-80 ^oC for 3 days. The solution was kept in the refrigerator to initiate the precipitation. Then the obtained turquoise green precipitate was collected and dried under vacuum. Yield: 6.9%

2.3.20. Sodium[(tetrakis(5-(chloro(nitro)methyl)-4-nitro-1H imizadole)cuprate(II)], $Na_2[Cu(L)_4]$ (28)

The same procedure was followed for the preparation of **27**, where 0.437 mmol $CuCl_2$ and 1.74 mmol NaL was used to obtain turquoise green precipitate of **28** was filtrated and dried under vacuum. Yield:10.4%

2.3.21. Ammonium[(tetrakis(5-(chloro(nitro)methyl)-4-nitro-1H imizadole)zincate(II)], $(NH_4)_2[Zn(L)_4]$ (29)

29 was obtained by applying the methods given for **27**. The reagents and their amounts involved in this step were 0.224 mmol $ZnCl_2$, 0.894 mmol NH_4L. The yield of white precipitates of **29** was 93.8%.

2.3.22. Sodium[(tetrakis(5-(chloro(nitro)methyl)-4-nitro-1H imizadole)zincate(II)], $(Na)_2[Zn(L)_4]$ (30)

30 was synthesized according to the procedure given for **28**, in which 0.218 mmol $ZnCl_2$, 0.875 mmol NaL were reacted to obtain white precipitates of **30** with the yield of 81.7%.

2.3.23. [Pentaammine(5-(chloro(nitro)methyl)-4-nitro-1H imizadole)cobalt(II)], carbonate, $[Co(NH_3)_5L]_2CO_3$ (31)

The parallel techniques were used to synthesize **31** with that for **4**. In that procedure 1.312 mmol $Co(NO_3)_2.6H_2O$, 1.312 mmol NaL in aqueous dimethylformamide and 6.56 mmol NH_3 solution were used. The green precipitate of **31** was obtained with the yield of 32.4%.

2.3.24. [Pentaammine(5-(chloro(nitro)methyl)-4-nitro-1H imizadole)iron(II)] carbonate, $[Fe(NH_3)_5L]_2CO_3$ (32)

The previous procedure explained for **31** was repeated using the same stoichiometric amounts of the reagents but substituting the metal salt with $FeCl_2.4H_2O$. The dark brown precipitate of **32** was collected (Yield: 25.9%).

2.3.25. [Pentaammine(5-(chloro(nitro)methyl)-4-nitro-1H imizadole)cobalt(III)], $[Co(NH_3)_5L]CO_3$ (33)

31 and **33** were prepared in the same techniques; 1.382 mmol $Co(NO_3)_2.6H_2O$, methanolic solution of 1.382 mmol NH_4L and 6.91 mmol were involved for this case. The green precipitate of **33** was obtained at the end of the reaction (Yield: 31.9%).

2.3.26. [Pentaammine(5-(chloro(nitro)methyl)-4-nitro-1H imizadole)iron(III)], $[Fe(NH_3)_5L]CO_3$ (34)

Since **32** and **34** are alike, thus the only change made in the synthesis procedure was replacement of the Fe(II) salt with 1.458 mmol $FeCl_3.6H_2O$. In this procedure, 1.458 mmol NH_4L and 7.29 mmol NH_3 was subjected. The yield for the dark brown precipitate of 34 was 37.1%.

2.4. Analytical Methods for Characterization

2.4.1. Elemental Analysis

An elemental analysis can be performed for the carbon (C), hydrogen (H), nitrogen (N) and sulfur (S) elements simultaneously. The basic operating principle of this method is based on the burning of the sample at high temperature (≥1100º C). The gaseous sample is sent to the chromatography column with an inert gas (helium, He) used as the carrier. Here, the gaseous sample is combusted with oxygen (O_2) gas and passed through the oxidation zone followed by oxidation with suitable catalysts to fully perform the quantitative combustion process. After the process, C, H, N, S elements are converted to CO_2, H_2O, N_2 and SO_2 gases and sent to the thermal conductivity detector to record the electrical signal proportional to the amount of each gas. This electrical signal then gives the percentage of elemental composition in proportion to the curve areas obtained in the spectrum [95-97].

Elemental analyses give valuable complementary information for other analytical techniques such as mass spectrometry. In our study, elemental analyses of the compounds were performed using LECO, CHNS-932 device at Middle East Technical University (METU) Central Laboratory to find the C, N, O percentages within the compounds.

2.4.2. Mass Analysis

Mass spectrometry (MS) is an analytical technique that used to determine relative molecular masses and the fragmentation of molecules for identifying the elemental composition of an unknown sample. In addition, it can be used for comparison of mass spectra with theoretical molecular weight of a compound [95-97].

This technique involves the generation of gas-phase analyte ions from either inorganic or organic compounds, and measurements of their mass-to-charge ratio (m/z). As a first step, the sample is converted to rapidly moving positive ions by electron bombardment and charged particles are separated according to their masses. Removal of one electron from the molecule (M) results into generation of parent ion (M^+ or molecular ion). This parent ion or molecular ion normally undergoes fragmentations (fragment ions or daughter ions). Second step of this method is based

on the separation of these ions according to their mass-to-charge ratio (m/z). The separation chamber of the mass spectrometer is kept under a high vacuum and all samples must be ionized to give a charge in the gas phase. These ions are detected in magnetic field by using the variety of techniques and resulting mass spectrum is a plot of relative abundance against the ratio of mass/charge.

Volatile solvents such as water, ethanol, methanol, acetonitrile, dichloromethane and acetone are used in mass analysis. In our study, the samples were prepared in a mixture of methanol and acetonitrile (1:1, v/v) and their mass measurements were completed by using high resonance mass spectroscopy (HRMS) system which is called Waters SYNAPT (G1-MS) at METU Central Laboratory as service procurement.

2.4.3. FTIR Analysis

Infrared (IR) spectroscopy is used in identification of functional groups, distinction between intermolecular and intra-molecular hydrogen bonding, determination of purity and of geometrical isomerization (cis-trans) of both organic and organometallic compounds [95-97].

When molecule absorbed electromagnetic radiation in IR region (4000-400 cm^{-1}), undergoes vibrational or rotational transitions which cause net change in the dipole moment in the molecule (IR active). If dipole moment does not change in molecules, they are defined as IR inactive that means they do not absorb IR radiation. The frequency modes of vibration depending on atom size, bond length and bond strength. Accordingly, there are two different types of vibrational modes, namely streching and bending. Stretching vibration is a rhythmical movement along the bond axis, such the interatomic distance is increasing or decreasing. Bending vibration may consist of a change in bond angle between bonds with a common atom or the movement of a group of atoms with respect to the remainder of the molecule without movement of the atoms in the group with respect to one another.

The interpretation of IR spectra involves the correlation of absorption bands in the spectrum of unknown compound with the known absorption frequencies for different types of bonds. Intensity (weak, medium or strong), shape (broad or sharp) and

position (cm^{-1}) in the spectrum are significant for the identification of the source of an absorption band.

Fourier transform infrared spectroscopy (FTIR) is the most common and fastest type of infrared spectroscopy, where Fourier transform is used to transform the signal from the time domain to its representation in the frequency domain. This technique shines a beam containing many frequencies of light at once and measures how much of that beam is absorbed by the sample.

In this study, FTIR spectrum of our compounds was measured using a Bruker FTIR spectrophotometer in the Metal Forming Center of Exellence of Atılım University.

2.4.4. NMR Analysis

Nuclear magnetic resonance (NMR) is a powerful spectroscopic method that detects the energy absorbed by changes in the nuclear spin state. This method is especially used for the characterization of organic molecules [95-97].

In this analytical technique, the sample is placed in a magnetic field and the NMR signal is produced by excitation of the nuclei sample with radio waves into nuclear magnetic resonance. Nuclear magnetic resonance is detected with sensitive radio receivers. The intramolecular magnetic field around an atom in a molecule changes the resonance frequency, thus gives an access to details of the electronic structure of a molecule and its individual functional groups. As the fields are unique or highly characteristic to individual compounds, in modern organic chemistry practice, NMR spectroscopy is the definitive method to identify monomolecular organic compounds.

^{1}H-NMR and ^{13}C-NMR are the common types of NMR spectroscopy which are used to determine the type and number of hydrogen and carbon atoms in an organic molecule, respectively. For instance, when hydrogen nuclei (protons) are studied, one can determine the number of each of the distinct types of hydrogen nuclei as well as obtain information regarding the nature of the immediate environment of each type. Protons in different environments absorb at slightly different frequencies, therefore they are distinguishable by NMR. The frequency at which a particular proton absorbs is determined by its electronic environment and the size of the magnetic field generated

by the electrons around a proton. ^{1}H-NMR absorptions generally appear as sharp signal between 0-10 ppm. The area under an NMR signal is proportional to the number of absorbing protons. NMR spectrometers automatically integrate the area under the peaks, and print out a stepped curve (integral) on the spectrum. The height of each step is proportional to the area under the peak, which in turn is proportional to the number of absorbing protons.

The combination of IR and NMR data is often sufficient to determine completely the structure of an unknown molecule.

In this study, ^{1}H-NMR measurements of studied compounds were completed by using Bruker AVANCE (300 MHz) device at METU Central Laboratory as service procurement.

2.5. Theoretical Calculations

DFT calculations were performed by Assoc. Prof Dr. Hakan Kayı and details of the theoretical studies were given in the final report of project TUBITAK-117Z391 [1].

2.6. Thermal Stability Studies

Thermal stability of the synthesized materials was studied by using thermogravimetric analysis and differential scanning calorimetry (TGA-DSC) methods under N_2 gas atmosphere in the range of 25-1200 ^{o}C for approximately 5-15 mg samples. TGA-DSC measurements of compounds were performed at different heating rates of 2.5, 5, 10, 15, 20 ^{o}C/min. Using Kissinger method [98], kinetic parameters of the complexes (apparent activation energy E and pre-exponential factor A) were calculated. These parameters reflect both the activation energies of the chemical reactions and the physical processes such as heat and mass transfer effects on the thermal decomposition process.

In differential thermal analysis, the temperature at which the maximum deflection is observed varies with heating rate for certain types of reactions. An expression can be derived relating this variation with the kinetics of the reaction. By making several differential thermal patterns at different heating rates, the kinetic constants can be

obtained directly from the differential thermal data [98]. Thus, it is possible to estimate the degradation behavior of the compounds under the non-isothermal conditions by the Kissinger method with an overall first-order reaction assumption at constant temperature.

$$\left(\frac{\partial x}{\partial t}\right)_T = k_T\,(1 - x) \tag{1}$$

Here x is the fraction of material decomposed. The magnitude of the rate constant, k_T, is determined by the temperature and is given by the Arrhenius equation.

$$k_T = A\, e^{\frac{-E}{RT}} \tag{2}$$

Herein, R is the gas constant, T is the temperature in Kelvin, and A and E_a are constants that are properties of the material. The constant E_a, called the activation energy, is often interpreted as the energy barrier opposing the reaction. The constant A, most often called the frequency factor, is a measure of the probability that a molecule having energy E_a will participate in a reaction.

When the temperature is changing with time, the reaction rate is:

$$\left(\frac{dx}{dt}\right)_T = \left(\frac{\partial x}{\partial t}\right)_T + \left(\frac{\partial x}{\partial T}\right)_t \frac{dT}{dt} \tag{3}$$

The rate of change of x with temperature, with the time coordinate fixed, $(\partial x / \partial t)_t$ is zero, because fixing the time also fixes the number and position of the particles constituting the system. The only effect of an instantaneous change in temperature is in the velocity of thermal motion of the particles. The total rate of reaction may then be expressed:

$$\frac{dx}{dt} = A\,(1 - x)\, e^{\frac{-E_a}{RT}} \tag{4}$$

This expression holds for any value of T, whether constant or variable, so long as x and T are measured at the same instant. When the reaction rate is a maximum, its derivative with respect to time is zero. Solving eq (4) for (d/dt) (dx/dt):

$$\frac{d}{dt}\left(\frac{dx}{dt}\right) = \frac{dx}{dt}\left(\frac{E}{RT^2}\right)\left(\frac{dT}{dt}\right) = A\, e^{\frac{-E_a}{RT}} \tag{5}$$

The maximum value of dx/dt occurs at temperature T_p, defined by:

$$A\, e^{\frac{-E}{RTp}} = \frac{E_a}{RT_P{}^2}\,\frac{dT}{dt} \quad (6)$$

$$\frac{d\left(\ln\frac{\beta}{T_P{}^2}\right)}{d\left(\frac{1}{T_P}\right)} = -\frac{E_a}{R} \quad (7)$$

where $\beta = dT/dt$, heating rate.

Kissinger equation gives the relationship between the heating rate and the thermal decomposition peak temperature, and is expressed as:

$$Ln(\beta/T^2_p) = - E_a/RT_p + LnA \quad (8)$$

In this equation, β indicates the heating rate ($K.min^{-1}$ or $^oC.min^{-1}$), T_p is the decay temperature (K), E_a is the apparent activation energy ($kJ.mol^{-1}$) and R is the general gas constant.

Kinetic parameters were also used to calculate the self-accelerating decomposition temperature (T_{SADT}) and the critical temperature of thermal explosion (T_b) with the following equations below.

$$T_p = T_{po}+b\beta_i+c\beta_i{}^2 \quad (9)$$

$$T_{SADT} = T_{po} \quad (10)$$

$$T_b = [(E_a-(E_a{}^2-4E_aRT_{po})^{0.5}]/2R \quad (11)$$

Here, b and c are coefficients that can be found by using the peak temperatures obtained in differential scanning calorimetry curves at varying temperature ramps. In addition, using these experimental data, activation entropy (ΔS), enthalpy (ΔH), and Gibbs free energy changes (ΔG) were calculated using the thermochemical equations given below.

$$\Delta H = E_a-RT_b \quad (12)$$

$$A = \frac{k_BT}{h}e^{\frac{\Delta S}{R}} \quad (13)$$

$$\Delta G = \Delta H-T_b\Delta S \quad (14)$$

k_B represents Boltzman constant and h is the Planck constant.

2.7. Caloriferic Value Test

The caloriferic value test was performed at Tübitak Sage Chemical Quality Control Laboratory as service procurement. During the measurements, the Parr 6200 calorimeter and semi-micro oxygen bomb that are shown in the Figure 2.8 were used.

Figure 2.8. Parr 600 calorimeter (left) and Semi-micro oxygen bomb (right) [1]

2.8. Impact and Friction Sensitivity Tests

The impact and friction sensitivity tests were carried out using the test devices shown in Figure 2.9 and Figure 2.10 and methods defined in the standarts EN-13631-3 and EN-13631-4.

Figure 2.9. BAM Impact Sensitivity Test Device [1]

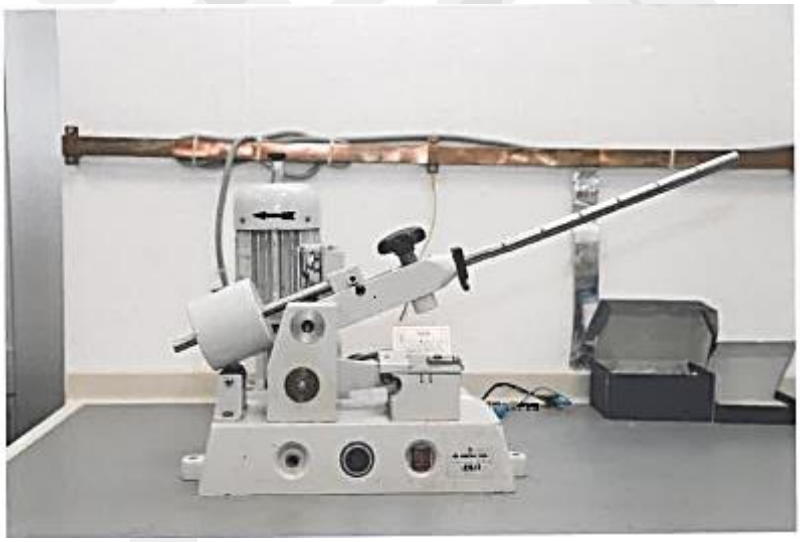

Figure 2.10. BAM Friction Sensitivity Test Device [1]

CHAPTER 3

3. RESULTS AND DISCUSSION

3.1. Molecular Modeling Study

Quantum chemical studies were performed to investigate the optimized geometries and the activity - structure relationship of the complexes theoretically. Their geometric and explosive properties were calculated in the gas phase by using density functional theory (DFT) and PM7 semi-empirical quantum mechanical method as explained in the final report of the Tubitak Project-117Z391 [1] and the results were tabulated once more in Tables 3.1 - 3.3.

The formation and decomposition enthalpy values of all complexes given in Table 3.2 and 3.3 were calculated by considering lead styphnate as a model energetic material. A good agreement between the theoretical and experimental formation enthalpies of lead styphnate proved the accuracy of the methodology applied during this project. As clearly perceived, the formation and decomposition enthalpies cannot be calculated for **15, 16, 19, 20, 21** and **22**. The careful inspection of the Table 3.1 revealed that one of L^- molecule cannot bind to the metal ion and is pushed away due to the steric hindrance observed in the design of $[M(L)_6]^n$ structures of **15, 16, 19, 20, 21** and **22.** Despite of having the similar structures, **17** and **18** indicated a possible weak interaction between the metal center and the sixth L^- with a distance of about 4Å to form $[M(L)_6]^n$.

Table 3.1. Optimized geometries of the complexes (1-34) derived PM7 method [1]

1 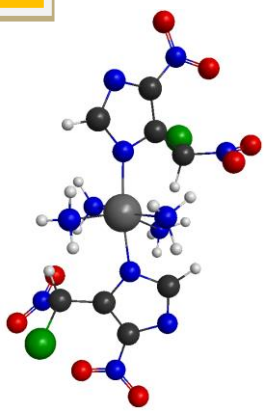	**2** 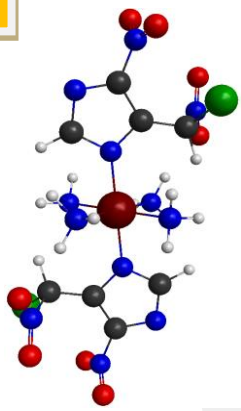	**3 or 4** 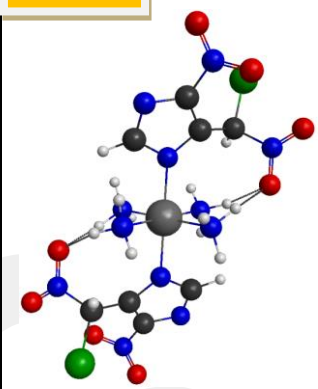
5 or 6 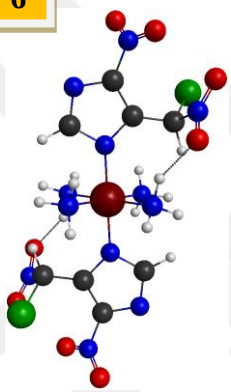	**7 or 8** 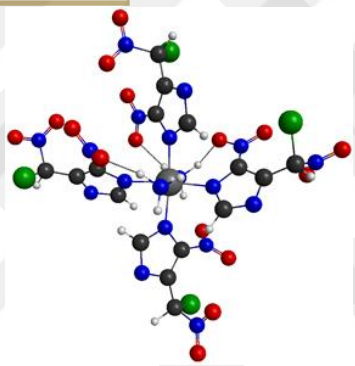	**9 or 10** 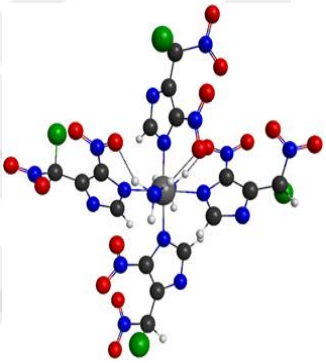
11 or 12 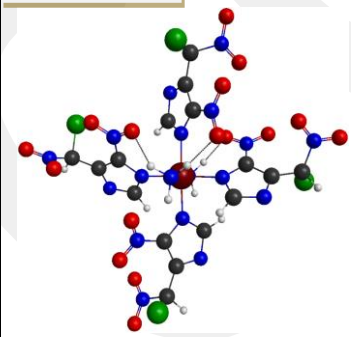	**13 or 14** 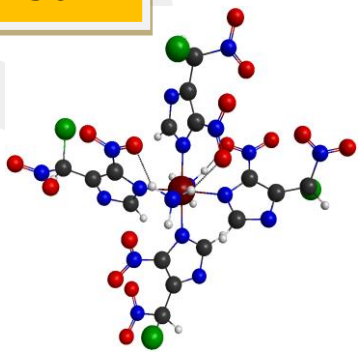	**15 or 16** 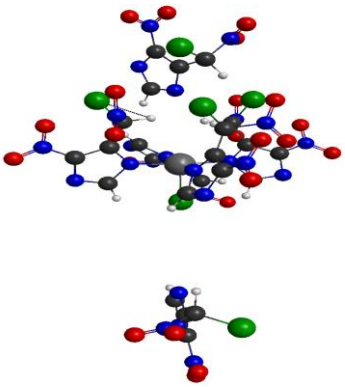

17 or 18 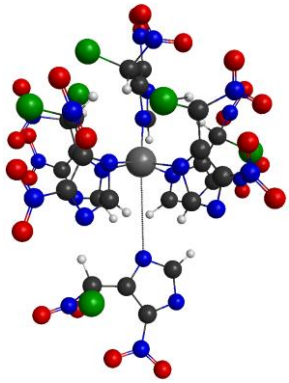	**19 or 20** 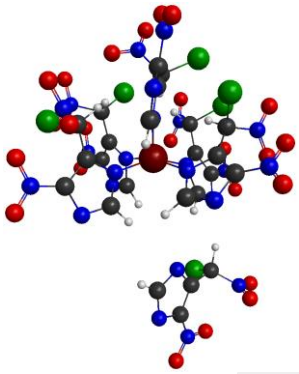	**21 or 22** 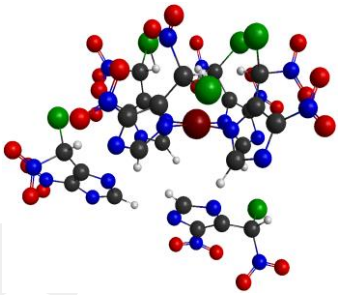
23 or 24 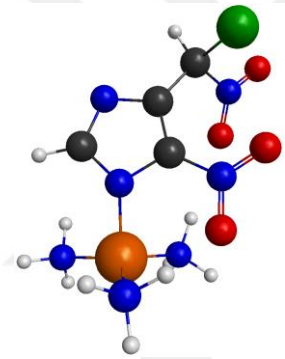	**25 or 26** 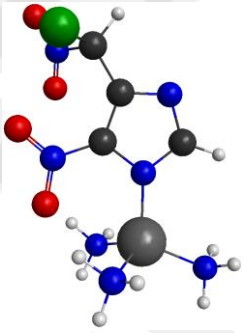	**27 or 28** 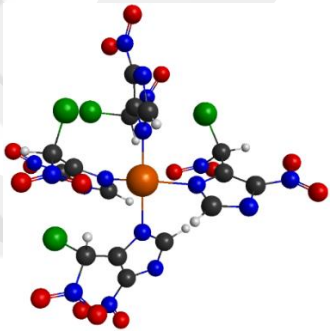
29 or 30 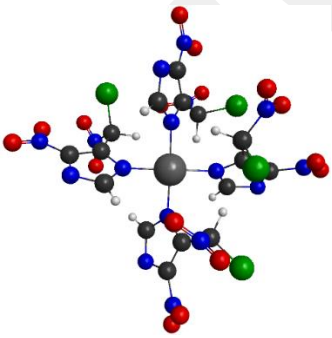	**31** 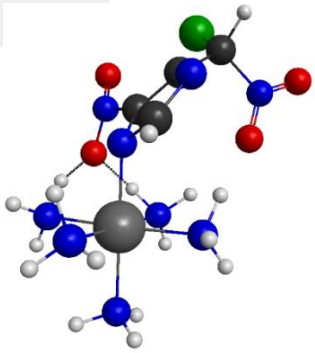	**32** 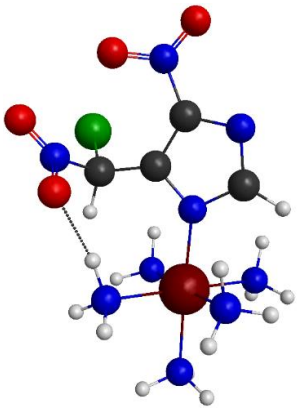

33 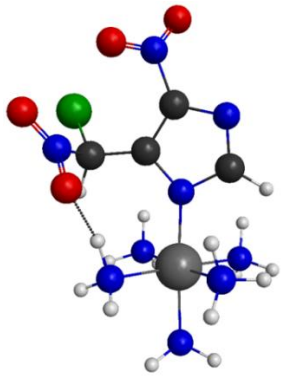	**34** 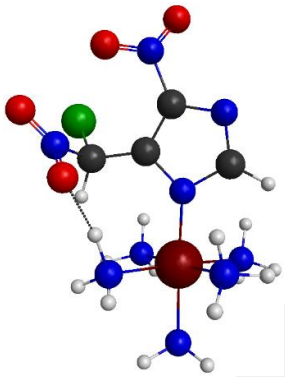	**L^-** 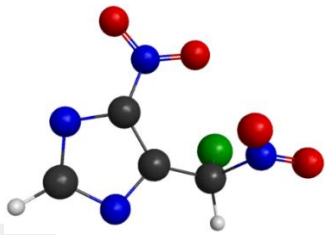
HL 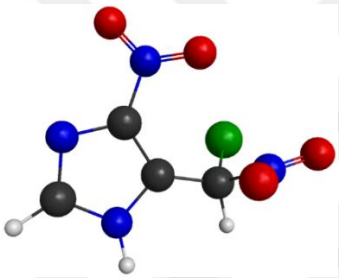	**NaL** 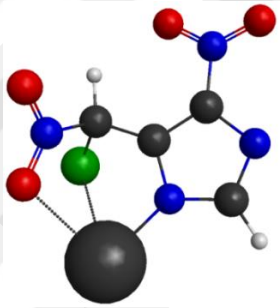	**NH_4L** 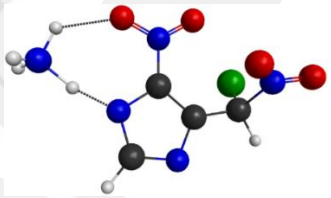
	Lead Styhpnate 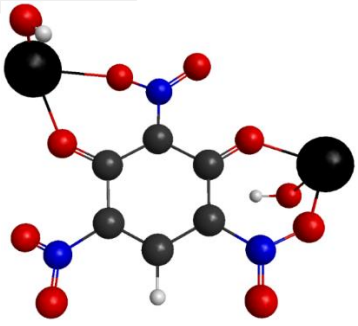	

Table 3.2. Formation enthalpy of metal complexes with PM7 method [1]

Metal Complex	**Formation Enthalpy (kJ/mol)**
Complex 1	-30.57
Complex 2	-366.53
Complex 3 or 4	449.22
Complex 5 or 6	270.99
Complex 7 or 8	-431.18
Complex 9 or 10	-370.34
Complex 11 or 12	-784.08
Complex 13 or 14	-694.43
Complex 15 or 16	Unstable Structure
Complex 17 or 18	-154.53
Complex 19 or 20	Unstable Structure
Complex 21 or 22	Unstable Structure
Complex 23 or 24	379.61
Complex 25 or 26	394.89
Complex 27 or 28	-301.74
Complex 29 or 30	-481.01
Complex 31	308.18
Complex 32	186.44
Complex 33	1244.38
Complex 34	1131.68
Lead Styhpnate	-869.26
$Ligand^-$	-162.33
$Ligand\text{-}H^+$	113.57
$Ligand\text{-}Na^+$	-113.63
$Ligand\text{-}NH_4^+$	32.07

Table 3.3. Decomposition enthalpy of metal complexes with PM7 method [1]

Metal Complex	**Decomposition Enthalpy (kJ/mol)**
Complex 1	2757.25
Complex 2	3094.06
Complex 3 or 4	2277.47
Complex 5 or 6	2456.53
Complex 7 or 8	2988.83
Complex 9 or 10	2927.99
Complex 11 or 12	3442.58
Complex 13 or 14	3252.93
Complex 15 or 16	Unstable Structure
Complex 17 or 18	2543.15
Complex 19 or 20	Unstable Structure
Complex 21 or 22	Unstable Structure
Complex 23 or 24	1457.10
Complex 25 or 26	1687.52
Complex 27 or 28	1884.91
Complex 29 or 30	2309.88
Complex 31	2503.01
Complex 32	2625.60
Complex 33	1566.82
Complex 34	1680.36
Lead Styhpnate	1413.47
Ligand-H^+	415.80
Ligand-Na^+	532.33
Ligand-NH_4^+	495.34

On the other hand, the high positive formation enthalpy is generally considered an advantage for the energetic materials as it leads to an increase in the amount of heat released during the decomposition. Thus, **11** or **12** (-784.08 kJ/mol) has the closest formation enthalpy to lead styphnate (-869.26 kJ/mol), while the complex with the highest positive formation enthalpy is complex **33** (1244.38 kJ/mol) as indicated in Table 3.2.

The enthalpy of decomposition reaction of the the complexes into ionic radicals are listed in Table 3.3. It is well known that the high enthalpy of decomposition indicates the higher stability of the compounds. All of our complexes have higher decomposition enthalpies compared to lead styphnate and the closest value to lead styphnate (1413.47 kJ/mol) was obtained for complexes **23** or **24** (1457.10 kJ/mol).

3.2. Characterization of 5-(chloro(nitro)methyl)-4-nitro-1H-imidazole (HL)

In this study, HL and salts of this ligand were designed and synthesized for the first time. The following steps are shown in Scheme 3.1 and the methods explained in the Section 2.2 were used for these syntheses.

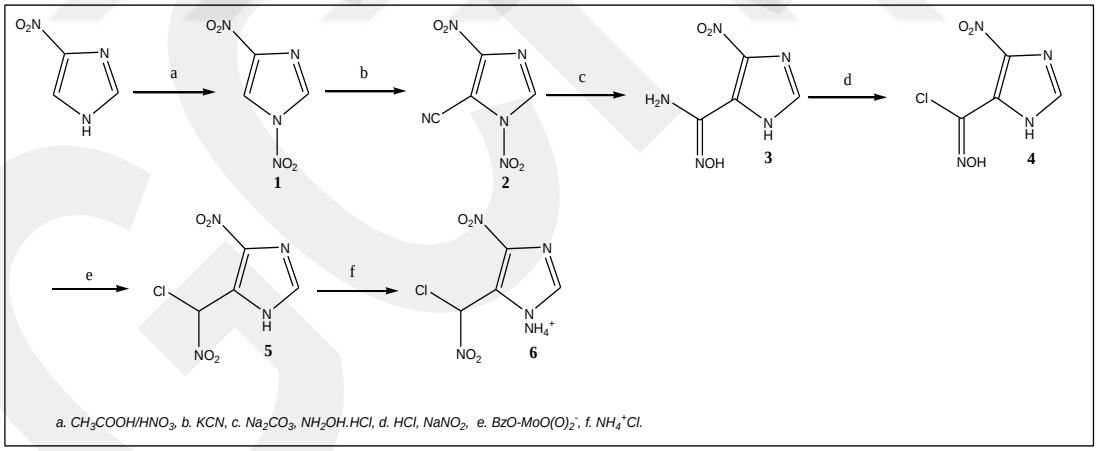

Scheme 3.1. Synthesis steps of ligand

Existence of the product obtained at each step in the ligand synthesis was verified by mass analysis, ^{1}H and ^{13}C NMR and FTIR spectrometry.

The synthesis of 1,4-dinitro-1H-imidazole, which is the initial step of ligand synthesis, was carried out according to the procedure in the literature [92] and mass

analysis results (Fig A1.1) indicated the formation of the compound. (Theoretical mass m/z: 158 g/mol; analysis result m/z: 157).

The results of ^{1}H and ^{13}C-NMR spectra of 1,4-dinitro-1H-imidazole also support the mass spectrum results. The ^{1}H-NMR (300 MHz) spectrum of the compound measured in DMSO-d_6 is presented in Figure 3.1. The singlets observed at δ(ppm) 8.962 (s, 1H, 5-H) and 9.392 (s, 1H, 2-H) of the aromatic ring are consistent with the structure. It is seen that the N-H signal of the ring at δ(ppm) 13 is dissappread. The signals of δ(ppm) 119.391 (5-C), 136.254 (4-C), 147.99 (2-C) in ^{13}C-NMR (300 MHz) measured in DMSO-d_6 belongs to the carbon atoms of the aromatic ring (Figure 3.2). In addition, the melting point of the obtained compound was measured as 246-248 °C. The literature value (241-244°C) is in compliance with the experimental measurement [93]. In addition, N-O vibrational frequencies at 1555 and 1378 cm^{-1} in the FTIR spectrum of 1,4-dinitro-1H-imidazole given in Figure 3.3 also support the accuracy of the structure.

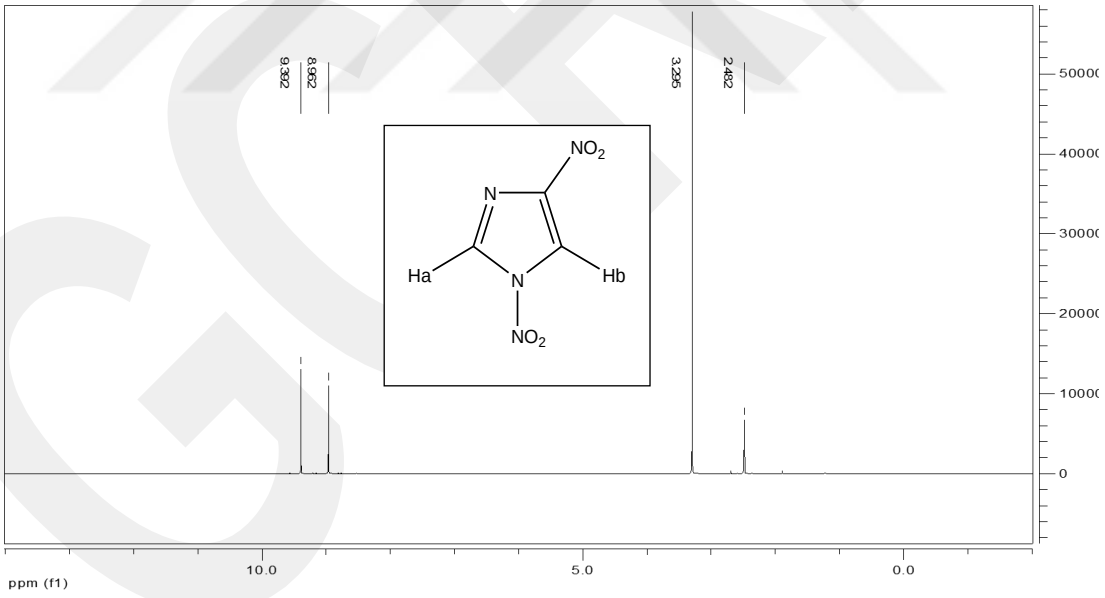

Figure 3.1. ^{1}H-NMR spectrum of 1,4-dinitro-1H-imidazole

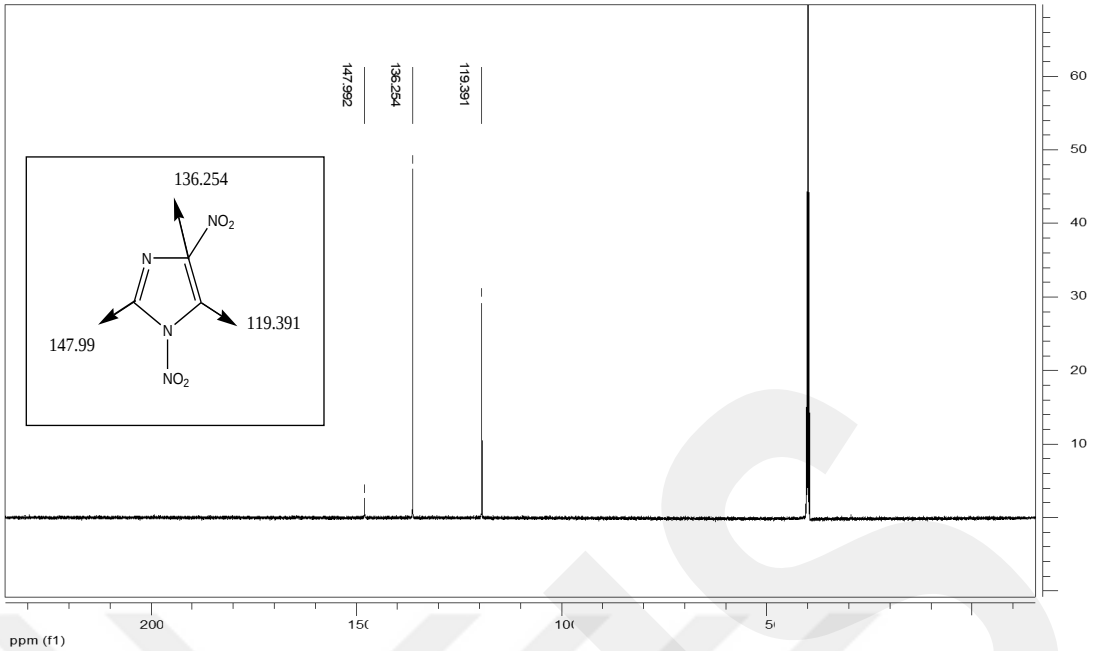

Figure 3.2. ^{13}C-NMR spectrum of 1,4-dinitro-1H-imidazole

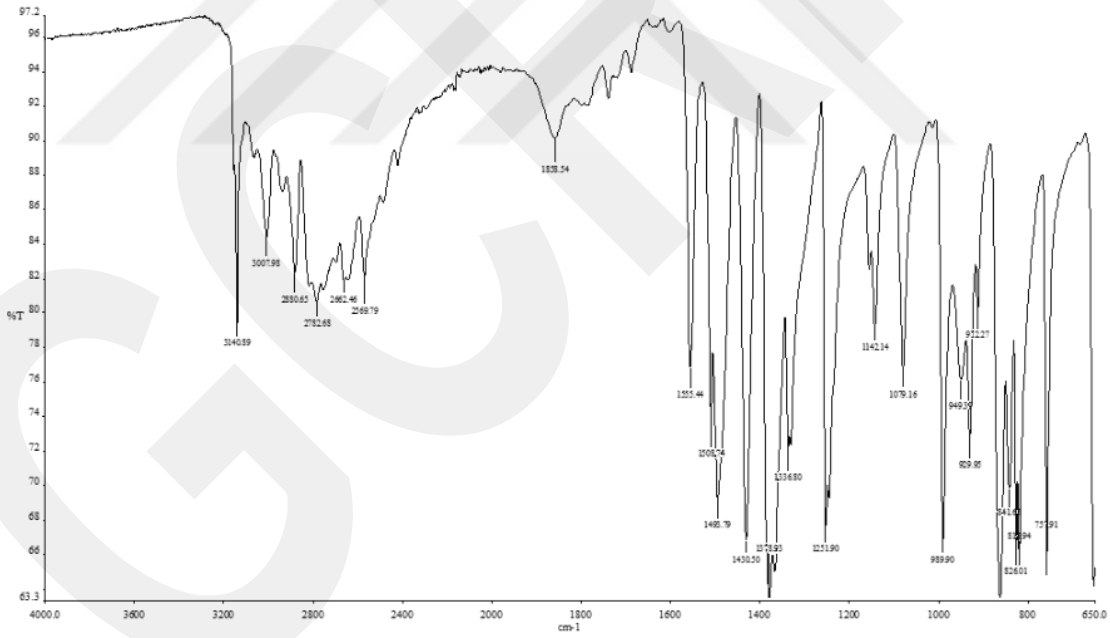

Figure 3.3. FTIR spectrum of 1,4-dinitro-1H-imidazole

1,4-dinitro-5-cyano-1H-imidazole gives molecular mass (138 g/mol) at (m/z) 139 in mass spectrum. 113 (M-CN) and 97 (M-CN-O) values are consistent with the structure (Figure A1.2). In the ^{1}H-NMR (300 MHz, DMSO-d_6) spectrum of the compound, δ(ppm) 8.163 (2-H) is consistent with the observed (Figure A3.1) singlet structure. The signals obtained at δ(ppm) 110.501 (5-C), 139.251 (4-C), 150.377 (2-C), 102.433 (6-C) in the ^{13}C-NMR (300 MHz, DMSO-d_6) spectrum and the corresponding carbon atoms are shown in Figure 3.4. The signal observed at 102.433 (6-C) ppm in the ^{13}C-NMR spectrum proves that the -CN group is attached to the molecule. Additionally, the peak observed at 2248.26 cm^{-1} in the FTIR spectrum (Figure 3.5) is the characteristic signal of the CN group and clearly shows the presence of CN in the structure.

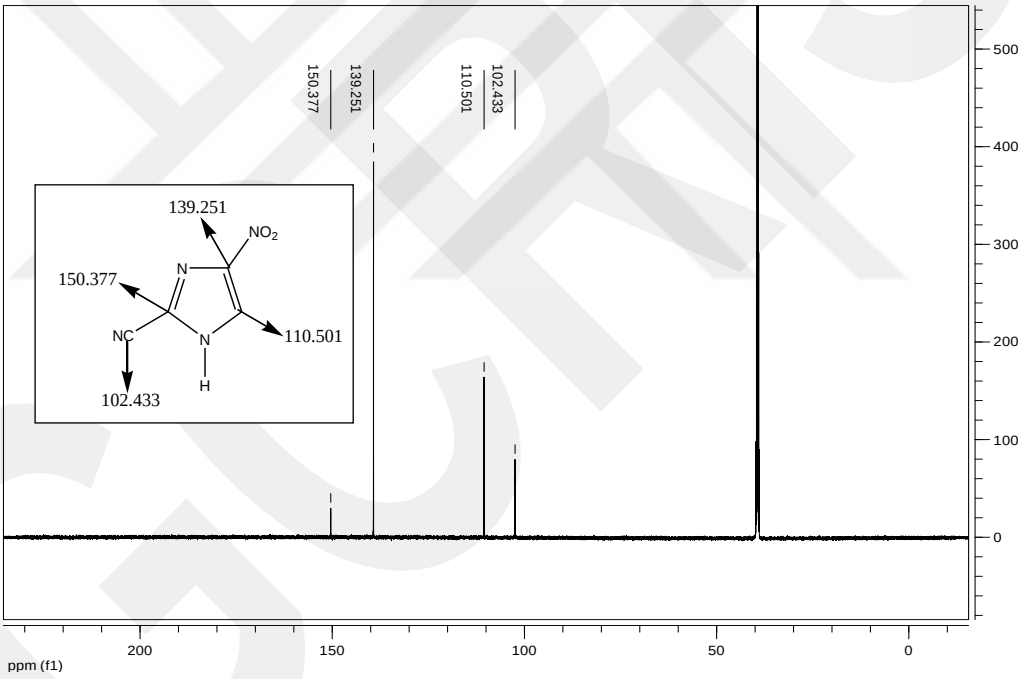

Figure 3.4. ^{13}C-NMR spectrum of 1,4-dinitro-5-cyano-1H-imidazole

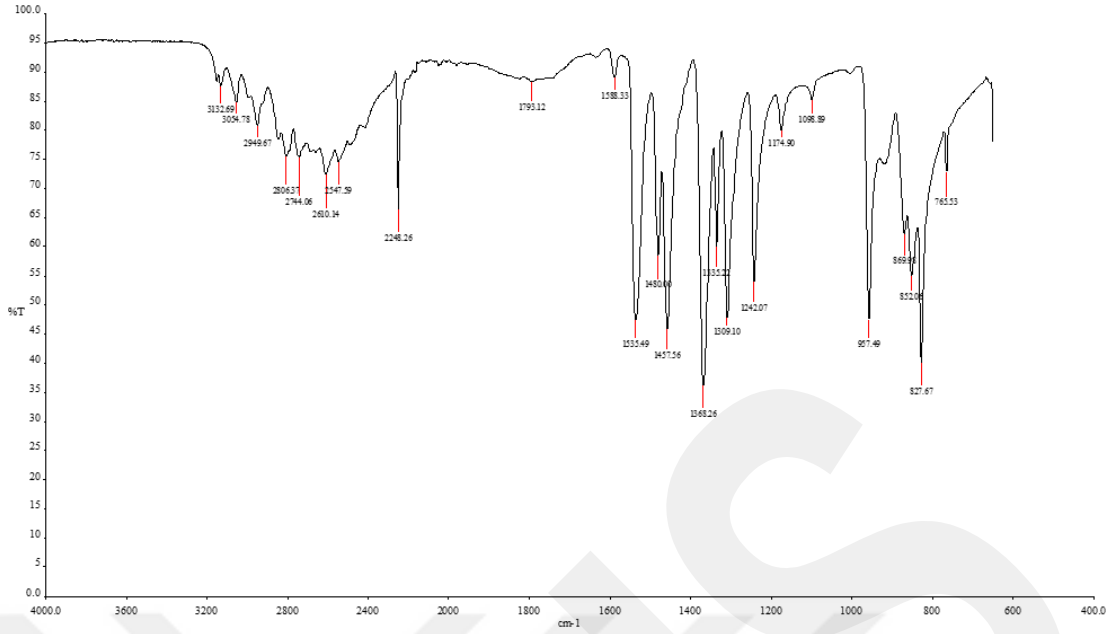

Figure 3.5. FTIR spectrum of 1,4-dinitro-5-cyano-1H-imidazole

The mass spectrum of N'-Hydroxy-4-nitro-1H-imidazole-5-carboxamide obtained in the third step is presented in Figure A1.3. Theoretically calculated mass of N'-Hydroxy-4-nitro-1H-imidazole-5-carboxamide is 171.04 g/mol and the obtained main fractions at m/z 156 (M-NH_2) and 172 (M^+) are consistent with the structure of the molucule. Furthermore, the vibrational frequencies observed at around 3393 and 1638 cm^{-1} due to the ν(N-OH) and ν(C-N) strechings, respectively, supports the formation of the desired compound (Figure A2.1). Proton-NMR spectrum of N'-Hydroxy-4-nitro-1H-imidazole-5-carboxamide (Figure A3.2) consists of three clear signals at δ(ppm) 6.066 (s, 2H, NH_2), 9.944 (s, 1H, CH), 13.597 (s, 1H, NH). However, ^{13}C-NMR spectrum of the compound yields 4 signals at δ(ppm): 124.263 (5-C), 134.203 (4-C), 143.763 (2-C), 159.479 (6-C) for 4 carbons having different chemical environment as shown in Figure 3.6. The signal at δ(ppm) 159.479 was assigned to oxime group and indicated the formation of the group successfully. One can say that, both ^{13}C-NMR and ^{1}H-NMR results confirm the molecular structure of the N'-Hydroxy-4-nitro-1H-imidazole-5-carboxamide in that stage.

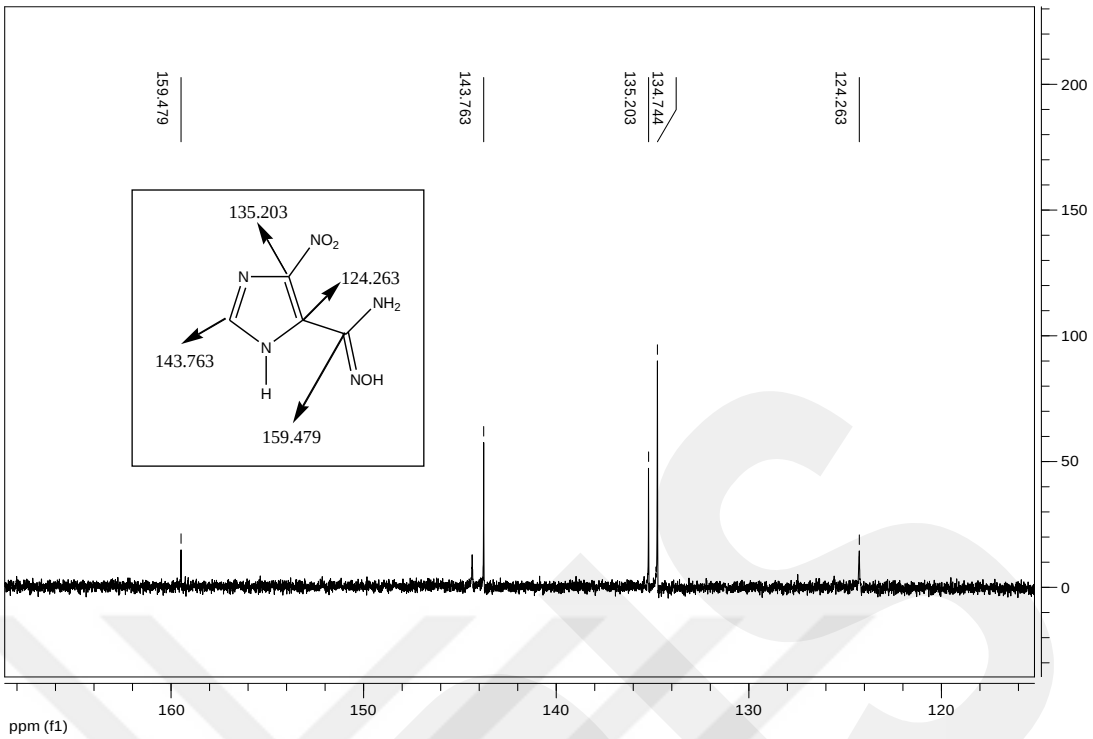

Figure 3.6. ^{13}C-NMR spectrum of N'-hydroxy-4-nitro-1H-imidazole-5 carboxamidine

4-nitro-1H-imidazole-5-carbonyl chloride was produced with 71% yield in the fourth step and its mass spectrum is presented in Figure A1.4 indicating the molecular mass at m/z 190. The results are consistent with its molecular structure (theoretical mass: 189.99 g/mole). The proton spectrum of 4-nitro-1H-imidazole-5-carbonyl chloride (Figure A3.3) shows the expected signals at δ(ppm): 13.038 (s, 1H, NH) and 7.955 (s, 1H, CH). ^{13}C-NMR of the compound given in Figure 3.7 is also confirms the structure of the compound having four signals at δ(ppm): 159,119 (6-C), 144.211 (2-C), 135,871 (4-C), 124.141 (5-C) for the C-atom in oxime group as well as for the 3 C-atoms in the aromatic ring, respectively. The presence of two oxime group the molecular structure of 4-nitro-1H-imidazole-5-carbonyl chloride is also supported by ν(N-OH) streching obtained at around 3432 cm^{-1} in the FTIR spectrum of the compound (Figure A2.2).

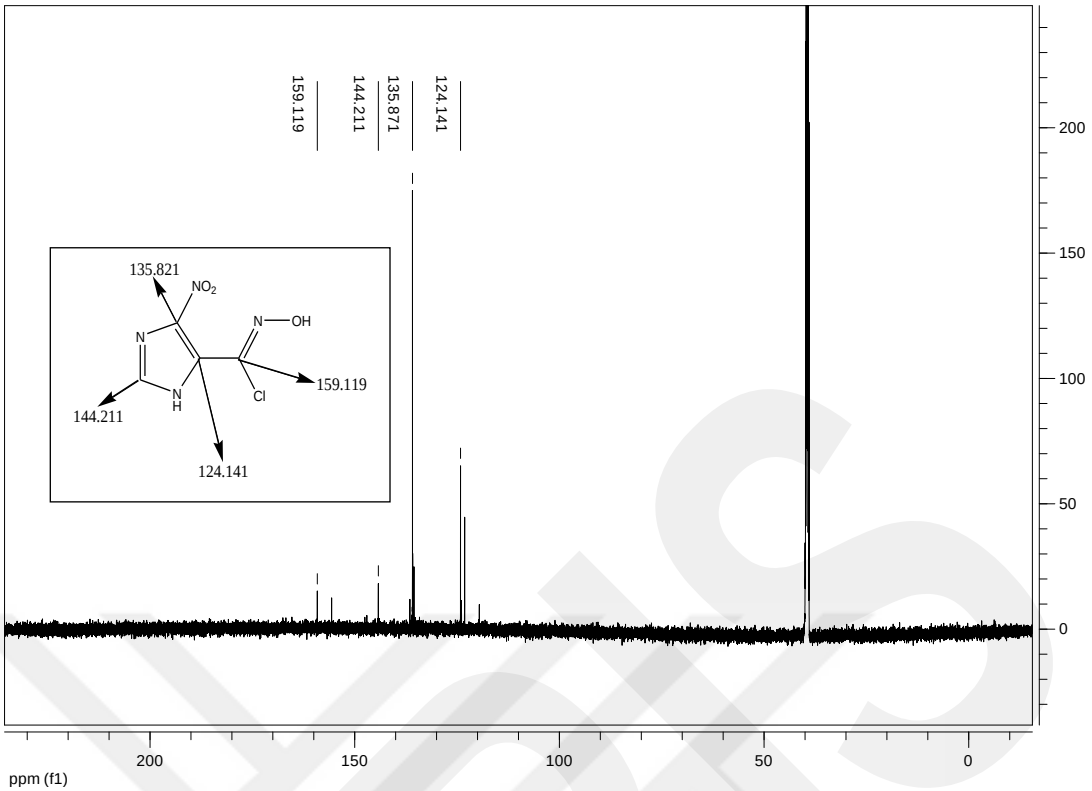

Figure 3.7. ^{13}C-NMR spectrum of 4-nitro-1H-imidazole-5-carbonyl chloride

In the last step of the procedure, 5-(chloronitromethyl)-4-nitro-1H-imidazole (HL) was synthesized successfully. The chemical analyses pointed out that HL have desired structure with two -NO_2 group. Mass fractions (m/z) obtained at 142 (M^+-Cl-NO_2), 173 (M^+-Cl) and 207 (M^+) are in line with the molecular structure. The ^{1}H-NMR and ^{13}C-NMR spectra of the compound were taken in DMSO-d_6 and are presented in Figures 3.8 and 3.9, respectively. Signals observed in δ(ppm): 7,924 (s, 1H, CH, 2-H), 7,555 (s, 1H, CH, CH) in the proton NMR spectrum and δ(ppm): 131.588 (2-C), 129,198 (4-C, 5-C) in the ^{13}C-NMR spectrum are in agreement with the structure of HL. Moreover, any absorption peak was observed for ν(-NH_2) vibrations in the IR spectrum (Figure 3.10), which also strongly supported the formation of our final product HL.

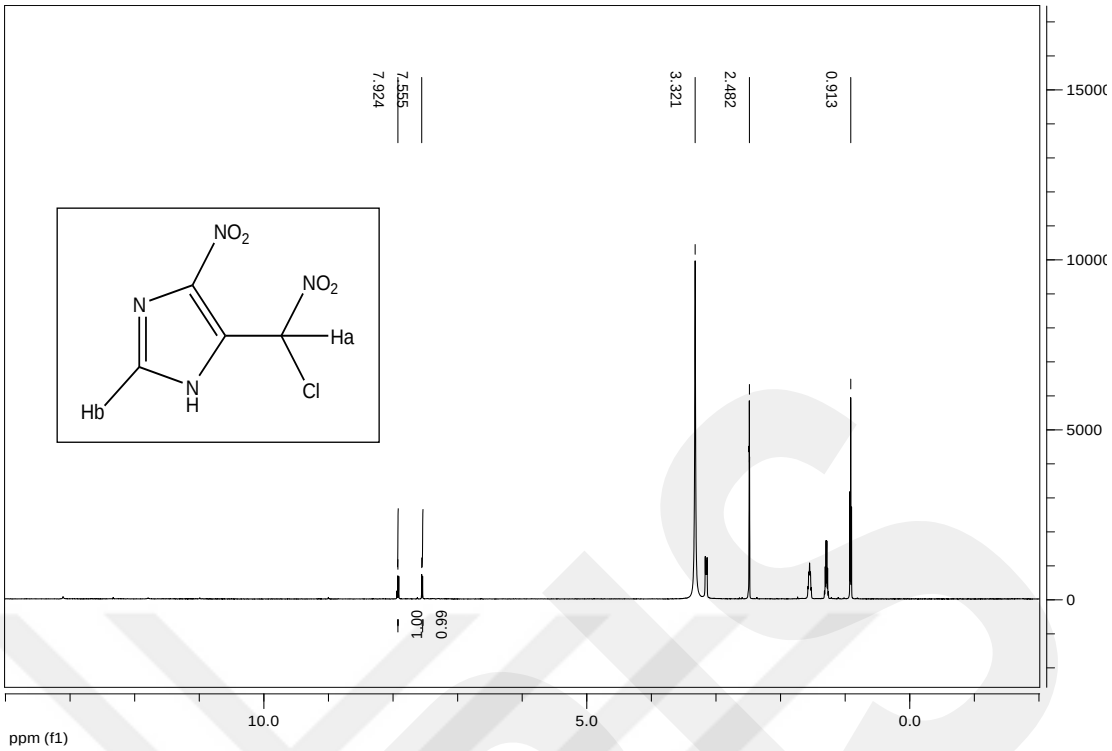

Figure 3.8. ^{1}H-NMR spectrum of 5-(chloronitromethyl)-4-nitro-1H-imidazole (HL)

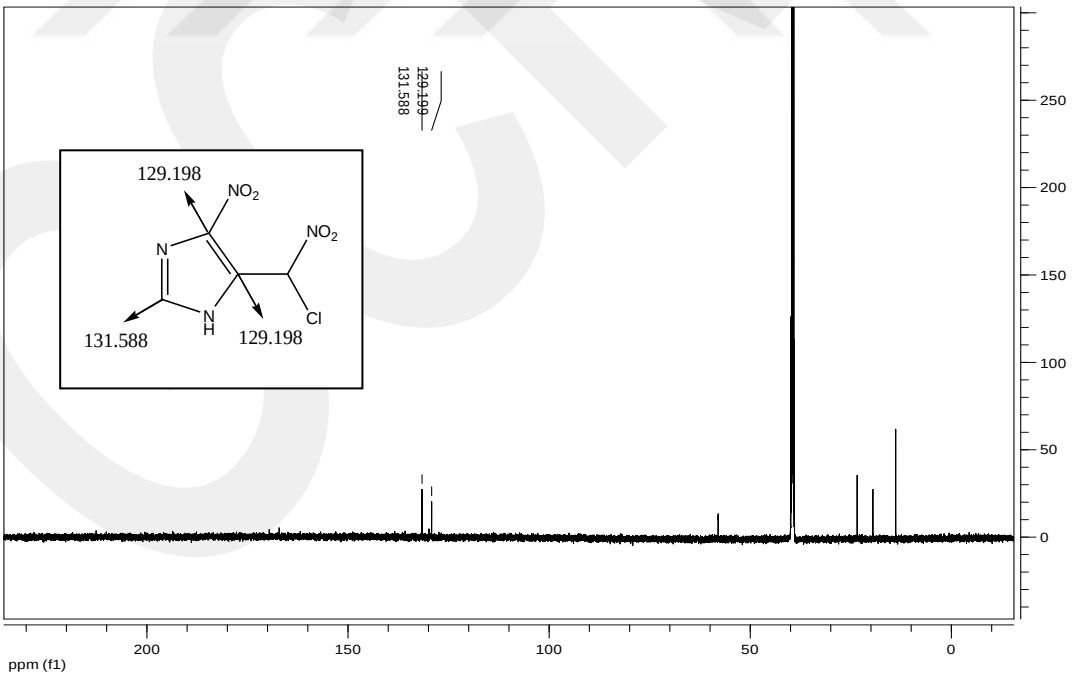

Figure 3.9. ^{13}C-NMR spektrum of 5-(chloronitromethyl)-4-nitro-1H-imidazole (HL)

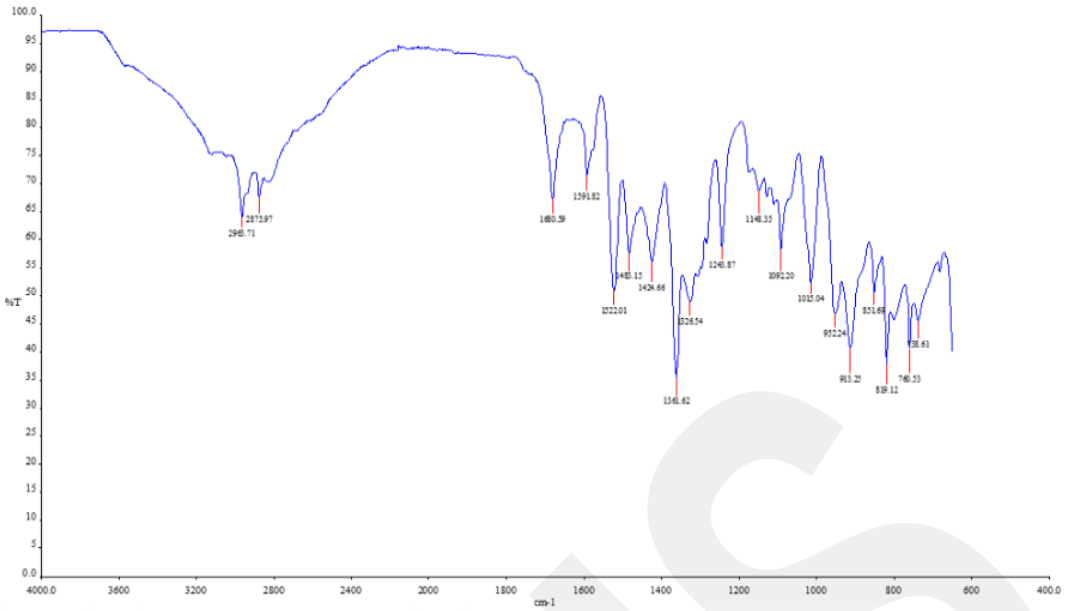

Figure 3.10. FTIR spectrum of 5-(chloronitromethyl)-4-nitro-1H-imidazole (HL)

Similarly, mass analysis (Figures A1.6 and A1.7) and FTIR spectra (A2.3) and A2.4) of the ammonium (NH_4L) and sodium (NaL) salts of the HL molecule are coherent with their structures and prove successful synthesis of all ligands.

3.3. Characterization of Metal Complexes

As can be understood from the results of the theoretical calculation, all of the 6 L^- containing Co(II/III) and Fe(II/III) complexes are unstable. According to the results of the theoretical calculations, many attempts were made to prepare complexes **17** and **18**, which have a low possibility to be synthesized, however the results of the analyses showed that these complexes could not be synthesized due to the steric effect. Thus, the characterization of successfully synthesized 26 complexes (except the ones having 6 L^-) was completed using spectroscopic techniques such as HRMS, NMR, FTIR and elemental analysis.

3.3.1. ESI-MS Analysis

The main molecular ion peak and main peak fractions of the complexes are listed in Table 3.4. As example, ESI-MS spectra of complexes **1** and **3** are shown in Figures 3.11 and 3.12, respectively and that for all other complexes are presented in Figures A1.8-A1.31. The careful inspection of the Table 3.4 indicated that molecular ion peaks were all obtained with the ionic mass fragments which were compatible with the

complex structure without any doubt. These results revealed the formation of our complexes in the desired structures successfully.

Observation of more than one ESI-MS peak in the spectra of the complexes was attributed to the formation of their different ionic species in the solvent medium. As seen in the Table 3.4, the complexes generally formed $[M^+]$, $[M+H]^+$, $[M+2H]^+$, $[M+Na]^+$ and $[M+MeOH]^+$ types molecular ions during the measurements. On the other hand, the main mass fractions are generally composed of complex anions and/or cations, without the counter ion such as Na^+, NH_4^+, PF_6^- and CO_3^{2-} which were added to obtain a neutral compound during synthesis. It was observed that the percent abundances of the main ion peaks varied between 100% and 20%.

Table 3.4. Mass spectra results (m/z) of Co(II, III), Fe(II, III), Cu(II) ve Zn(II) complexes containing 5-(chloronitromethyl)-4-nitro-1H-imidazole (*Estimated ion fractions are given in parentheses*)

Complex	**Theoretical Mass**	**Main Ion Peak *(m/z)***	**Mass Fractions *(m/z)***
1	538.1290	537.5380 (M^+)	540.4288 $(M+2H)^+$
2	535.0408	536.3344 $(M+H)^+$	582.5874 $(M+2Na)^+$, 554.5540 $[(M+H)^+ + H_2O]$
3	683.0933	685.4363 $(M+2H)^+$	701.4167 $(M+H_2O)^+$
4	1136.2670	1136.2015 (M^+)	1132.2042 $(M-4H^+)$, 1076.2418 $(M-CO_3^{(-2)})$, 1074.2435 $(M-CO_3^{(-2)}-2H^+)$
5	680.0051	679.4468 (M^+)	701.4116 $(M+Na^+-H^+)$
6	1130.0900	1131.9602 $(M+H)^+$	1134.4431 $(M+4H^+)$
7	951.2191	975.8697 $(M+Na)^+$	1004.1317 $(M+CH_3OH+H_2O)^+$, 945.6783 $(M-NH_3+CH_3CN)$, 917.1583 $(M-2NH_3)^+$, 871.5374 $(M-2NH_4-NO_2)^+$, 813.2686 $(M-3NO_2)^+$
8	961.1219 (M), 915.1425 $(M-2Na^+)$	959.6292 $(M-2H)^+$, 915.5825 $(M-2Na)^+$	1087.6841 $(M+2K+Na)^+$, 1045.7435 $(M+K+2Na)^+$
9	933.1808 (M), 915.1425 $(M-NH_4^+)$	935.5016 $(M+2H)^+$, 914.9827 $(M-NH_4)^+$	974.3422 $(M+CH_3CN)^+$, 887.5222 $(M-NO_2)^+$
10	938.1323 (M), 915.1426 $(M-Na^+)$	936.8014 $(M-2H)^+$, 914.7766 $(M-Na)^+$	1005.7617$(M+3Na)^+$
11	948.1306	949.7993 $(M+H)^+$	951.3026 $(M+2H)^+$
12	958.0337 (M),	944.0903 $(M-2Na^+ + CH_3OH)$	932.4296 $(M-Na^+-3H^+)$, 773.5397 $(M-4NO_2)$, 666.0623 $(M-4NO_2-3Cl^-)$

13	930.0926 (M),	963.3046 (M^++CH_3OH)	931.6782 $(M+H)^+$, 894.6470 ($M-Cl^-$), 822.5811 ($M-3Cl^-$)
14	935.0440	934.7501 $(M)^+$	958.6524 ($M+Na^+$), 851.4045 ($M-2Na^+-Cl^-$), 883.3308 ($M-2Na^+-2H^-$)
23	465.1380	465.1852 $(M)^+$	469.4377 ($M+4H^+$)
24	700.357	702.5308 $(M+2H)^+$	703.0320 ($M+3H^+$)
25	466.982	467.8047 $(M+H)^+$	469.4385 ($M+3H^+$)
26	704.045	704.0035 $(M)^+$	708.5324 ($M+4H^+$)
27	921.771	921.7726 $(M)^+$	922.7751 $(M+H)^+$
28	931.6739	932.7403 $(M+H)^+$	944.7349 ($M+K^+$+$2Na^+$), 930.6982 ($M-H^+$)
29	923.6151	923.2789 $(M)^+$	1005.8848 ($M+3Na^+$), 977.8515 ($M+2Na^+$), 949.8162 ($M+Na^+$)
30	933.5179	933.6688 $(M)^+$	794.4594 ($M-2Na^+-2NO_2$)
31	759.2535 (M), 349.6234 [$(M-CO_3)/2$]	349.6209 [$(M-CO_3)/2$]	149.9605 ([$(M-CO_3)/2$]-L^-)
32	753.0771 (M)	796.7905 ($M+CH_3CN+2H)^+$	312.22271([$(M-CO_3)/2$]-$2NH_3$), 295.8741 ([$(M-CO_3)/2$]-$3NH_3$)
33	409.6312	409.1793 $(M)^+$	349 ($M-CO_3^{-2}$), 437.19337 ($M+Na^+$)
34	406.5430	406.2895 $(M)^+$	439.2049 ($M+CH_3OH$), 424.2849 ($M+H_2O$), 408.3096 ($M+2H^+$)

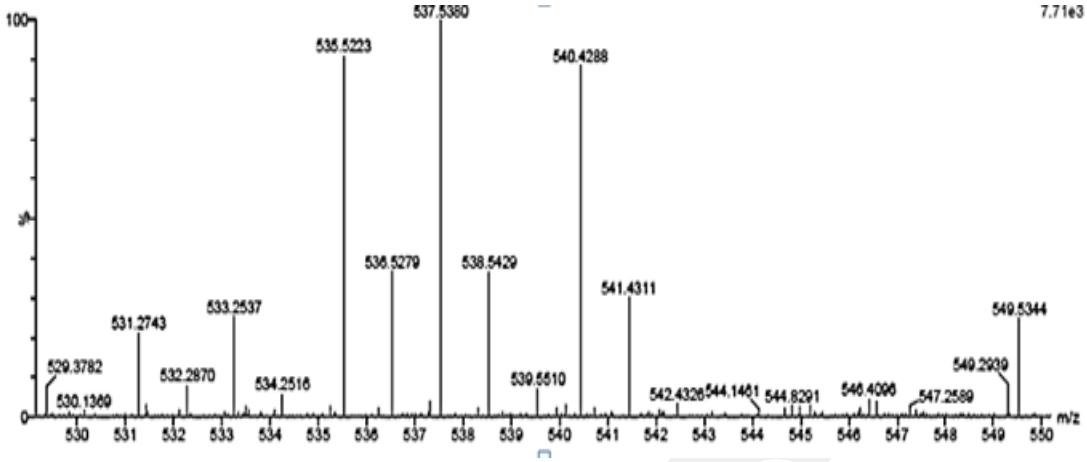

Figure 3.11. Mass spectrum of complex **1**

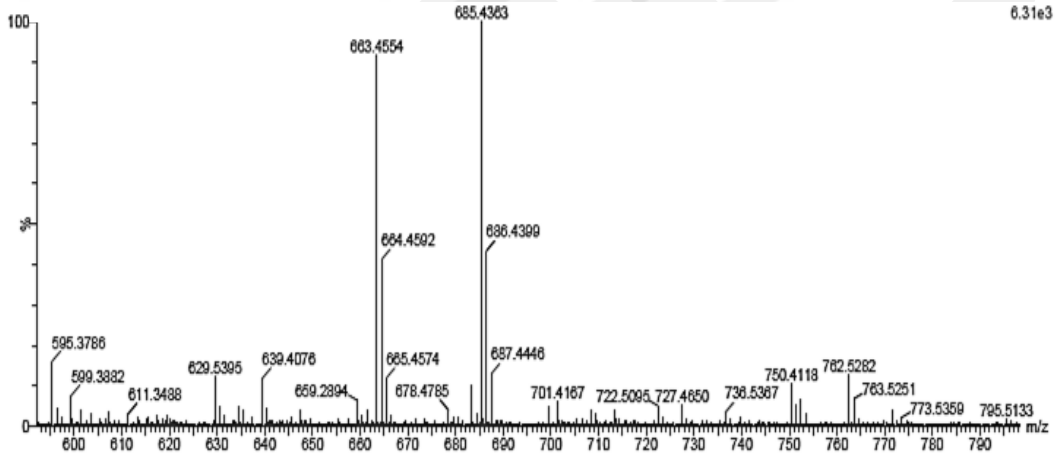

Figure 3.12. Mass spectrum of complex **3**

3.3.2. Elemental Analysis Measurements

Elemental analyses of the synthesized 26 complexes were completed and the percentages of C, H, N elements in their structures were compared with the calculated percentages. The elemental analysis results of the complexes given in Table 3.5 indicate that one, two or four L^- ligands are attached to the metal in accordance with their complex structure.

Table 3.5. Elemental analysis results of Co(II, III), Fe(II, III), Cu(II) ve Zn(II) complexes containing 5-(chloronitromethyl)-4-nitro-1H-imidazole

	Experimental			**Theoretical**		
Complex	**C%**	**N%**	**H%**	**C%**	**N%**	**H%**
1	18,02	31,41	2,89	17,86	31,23	2,99
2	17,83	30,49	2,9	17,96	31,41	3,01
3	13,28	23,99	2,71	14,07	24,60	2,36
4	20,48	31,33	2,53	17,97	29,58	2,84
5	14,78	24,34	2,23	14,13	24,71	2,37
6	18,98	24,38	2,53	18,06	24,00	2,85
7	19,10	28,95	2,29	20,20	29,45	2,33
8	21,00	26,50	1,37	19,99	26,23	1,46
9	21,79	28,2	2,03	20,59	28,52	1,99
10	19,28	26,12	1,60	20,48	26,87	1,50
11	18,94	26,47	2,06	20,27	29,55	2,34
12	20,39	25,01	1,84	20,05	26,31	1,72
13	20,73	29,14	2,05	20,66	28,61	1,95
14	19,52	26,17	1,78	20,55	26,96	1,50
23	10,22	26,05	2,48	10,32	26,31	2,38
24	14,75	28,69	3,03	15,43	29,74	3,16
25	10,91	20,40	2,44	10,88	20,99	2,37
26	16,60	26,61	3,35	15,35	27,99	3,14
27	20,22	27,13	1,63	20,84	25,66	1,74
28	20,46	24,96	0,67	21,70	25,3	0,86
29	19,92	26,44	1,75	20,80	27,35	1,74
30	20,03	28,20	0,69	20,58	27,29	0,86
31	14,45	33,87	4,45	14,24	33,20	4,51
32	14,44	33,76	4,50	14,35	33,48	4,55
33	14,52	30,01	4,22	14,66	30,77	4,18
34	14,78	30,99	4,27	14,77	31,00	4,21

3.3.3. FTIR Analysis

The characteristic FTIR absorption peaks of cobalt(II, III), iron(II, III), copper(II) and zinc(II) complexes containing 5-(chloronitromethyl)-4-nitro-1H-imidazole (HL) are shown in Table 3.6. Spectra of selected complexes obtained using platinum ATR are presented in Figures 3.13 and 3.14 and FTIR spectra of the other complexes are presented in A2.5-A2.28.

Aromatic and aliphatic –CH stretching vibrations of the ligand were observed in the range of 3067-2963 cm^{-1}. Aromatic C=N and C-C vibrations appeared at 1685 and 1591 cm^{-1}, respectively. Symmetrical and asymmetrical ν(N-O) stretchings formed within the nitro-groups in the structure were obtained between 1522 and 1326 cm^{-1}. ν(C-N) aromatic and aliphatic bond stretching was observed at 1243 and 1148 cm^{-1}. The vibrations of the ν(C-NO_2) group at 851 cm^{-1} and the ν(C-Cl) vibrations at 839 cm^{-1} were obtained [99].

When the FTIR spectra of the synthesized complexes were examined, a shift was observed almost in all absorption peaks positions of the ligand due to the coordination of the ligand to the metal ion. The vibrations of the -NH_3^- ligand in the structure of all complexes were observed in the range of 3300-3600 cm^{-1}. ν(C-N) aromatic vibrations shifted to the range of 1617-1685 cm^{-1}. Aromatic ν(C-N) bond stretchs appeared at about 1125-1175 cm^{-1}, while aliphatic ν(C-N) vibrations were obtained between the ranges of 1217-1236 cm^{-1}. Aromatic C-C vibrations have absorbtion in the band range between 1575 and 1603 cm^{-1}. The presence of nitro groups in the structures is evidenced by symmetrical and asymmetrical ν(N-O) vibrations observed at around 1500-1563 cm^{-1} and 1303-1388 cm^{-1}, respectively. Additionally, the vibrations belong to the ν(C-NO_2) streching were obtained at around 841-898 cm^{-1} and that for ν(C-Cl) vibrations were at 807-839 cm^{-1} in the spectrum of comlexes. The absorption peaks observed in the FTIR spectrum of all complexes and assigned corresponding bond vibrations in their molecular structured are presented in Table 3.6.

The occurrence and deviations in the absorption peak positions of the HL through coordination and the presence of the vibratioal frequencies attributed to -NH_3 streching demontrates obviously the existence of the ligand in the molecular structure of the complexes.

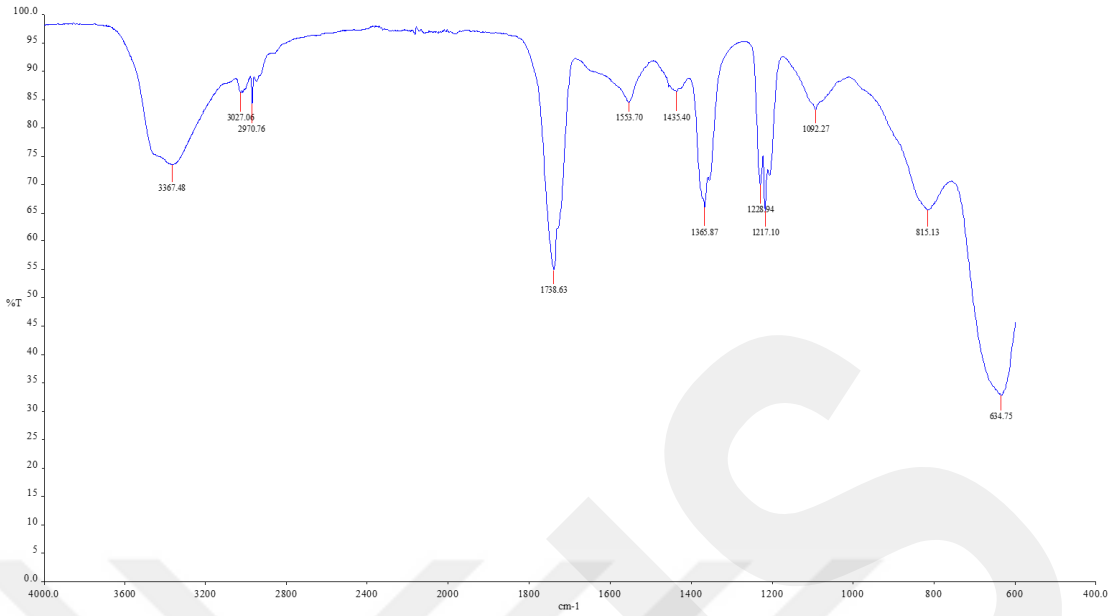

Figure 3.13. FTIR spectrum of complex **5**

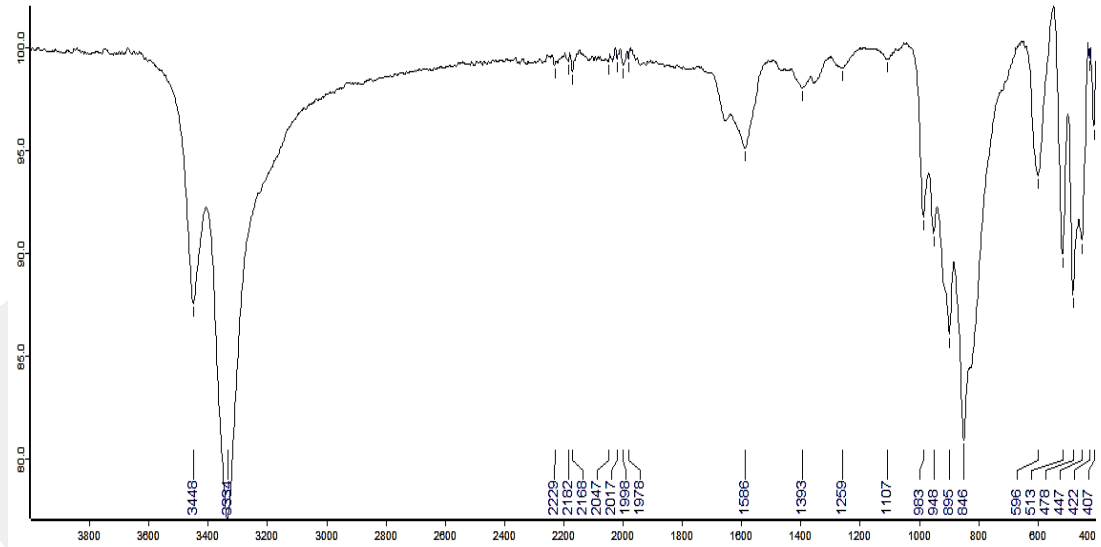

Figure 3.14. FTIR spectrum of complex **24**

Table 3.6. Characteristic FTIR absorption vibrational frequencies of Co(II,III), Fe(II,III), Cu(II) ve Zn(II) complexes containing 5-(chloronitromethyl)-4-nitro-1H-imidazole (cm^{-1})

Compound	ν(N-H)	ν(C-H) (aro)	ν(C-H) (alkyl)	ν(C=N)	ν(C-C) (aro)	ν(N-O) (asym)	ν(C-H) bend (sciss)	ν(N-O) (sym)	ν(C-N) (alyph)	ν(C-N) (aro)	ν(C-H) bend (wag)	ν(C-H) (om)	ν(C-NO_2)	ν(C-Cl)	ν(C-H) (rock)
HL	3581	3145	2963	1685	1591	1522	1433 1424	1326	1243	1148	1092 1015	952 913	851	839	760 738
NaL	-	3105	2902 2820	1636 1647	1560	1527	1440 1420	1340	1235	1146 1106	1026	973	866	826	766
NH_4L	-	3132 3044	2812	1762	1559	1507	1443	1401	-	1120	1043	958 908	853	-	797
1	3419	-	2950	-	1610	1492	1467	1402	-	1141	1086 1050	983	-	831	-
2	-	3151	-	-	1585	-	-	1348	1216	1167	1091	-	884	-	790
3	3334		2965 2879	1625	1584	-	1472	1386	1217	-	1046	975	879	831	-
4	3279	3180	2932	1637	-	-	1457	1367	1232	1102	1050	990	-	826	-
5	3367	3027	2970	1683	-	1553	1435	1365	1228 1217	-	1092	966	-	815	-
6	3345	-	2932	1649	1569	-	1437	1388 1347	1254	1100	1062 1023	925	-	824	703
7	3551	3109	-	-	1588	-	-	1347	-	1163	1090	922	-	818	748
8	3550	-	2924	1658	1583	-	1433	1357	1233 1217	1150	1114	933	-	835	725
9	3212	-	-	1629	-	-	1412	1337	1272	-	1101	982 928	863	-	-

10	3604	3095	2970	1677	1591 1575	1558 1525	1491	1320 1304	1281 1236	1175 1128	1110 1090 1014	972 926	851	807	759 712
11	-	3170	-	1648	1570	-	1494	1386	1253	1103	1062	942	851	829	757
12	-	3154	-	1642	-	-	-	1339	-	-	1084	-	887	-	790
13	3554	3163	2975	1684 1647	1570	1559	1457	-	1290	-	1082 1041	938	861	-	734
14	3349	-	-	-	-	1552	-	1350	-	-	1093	-	841	-	-
23	3427 3332	-	-	1658 1650	1580	-	1414	1303	1272	-	1103	984 915	892 842	818	785
24	3448 3334	-	-	1678	1586	-	1496	1393	1259	-	1107	983 948	895 846	-	739
25	3327	3175	2963	1605	-	-	1412	-	1278	1158	1085	983 948	884	812	746
26	3331	-	-	1689 1650	1587	1563	-	1382	1278	1109	1044	946	-	832	738
27	-	-	2988	1630	-	-	1407	-	1287 1218	1221	1024	915	-	-	786
28	3466	3016	2970	-	-	1541	1435	1365 1346	1228 1217	-	1100	-	898	816	-
29	3450	3192	2971	1617	-	-	-	-	1229 1217	-	1091 1000	934	-	-	760
30	3213	3006	2800	1654	-	-	-	1390		-	1078	-	875	-	-
31	3410	-	-	1654	1594	1559	1490	1356	-	1101	1048	-	841	-	728
32	3355	3182	-	-	1590	1503	-	1384 1350	-	1101	1082	-	889	-	795
33	3264	3175	-	1602	-	1500	-	1346	1279	-	1064	-	883	-	764
34	3350	-	2932	1650	1587	1515	1469 1439	1388 1345	1254	1101	1062 1203	921	-	830	-

3.3.4. NMR Analysis

Proton NMR measurements of 26 complexes containing single, double and four L^- were completed in DMSO-d_6. Due to the low solubility of complexes in DMSO-d_6 and no oppourtinity to extend the spinning time interval up to 8-10 h during the measurements, the signals of protons in the aromatic ring were obtained very weakly. When the obtained spectra were examined carefully, it is seen that the signals of the ligand, which were observed at 7.55 and 7.92 ppm (Figure 3.15) were shifted to the range of 7.38-8.52 ppm (Table 3.7) in metal complexes because of the direct coordination of the L- to the metal ions. Figures 3.16 and 3.17 depict the ^{1}H-NMR spectra of complexes **8** and **26** are given as example and the ^{1}H-NMR spectra of other complexes are shown in Figures A3.4-A3.15. The shifts observed in the protons of the aromatic ring in the ^{1}H-NMR spectrum indicate that the ligand is coordinated to the metal. These results support the mass, FTIR and elemental analysis results, as well.

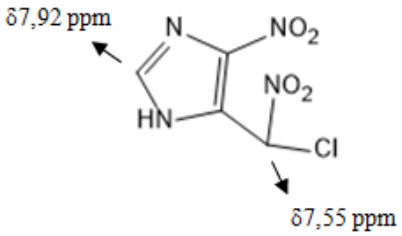

Figure 3.15. 5-(chloronitromethyl)-4-nitro-1H-imidazole ligand

It is well known NMR measurements mostly give clear results for diamagnetic compounds. Paramagnetic samples are also suitable for analysis; however, their signals are not visible on the ^{1}H-NMR region (0-14 ppm) due to effect of the strong chemical shift range of up to 120 ppm [99]. Therefore, all of our paramagnetic complexes were ^{1}H-NMR silent. As can be noticeably observed from Table 3.7, ^{1}H-NMR spectrum could not be obtained for complexes **1-4, 9, 12, 23, 24, 27, 28, 31 and 33**.

Table 3.7. ^{1}H-NMR results of Co(II,III), Fe(II,III), Cu(II) ve Zn(II) complexes containing 5-(chloronitromethyl)-4-nitro-1H-imidazole

Complex	**^{1}H-NMR (400 MHz, DMSO-$_{d6}$, δ, ppm)**
Ligand-H	7.55-7.92
1	HS-paramagnetic
2	HS-paramagnetic
3	HS-paramagnetic
4	HS-paramagnetic
5	7.97-8.24
6	7.95-8.25
7	7.28
8	7.96
9	HS-paramagnetic
10	7.38-8.36
11	7.95-8.16
12	HS-paramagnetic
13	7.94
14	7.96-8.21
23	paramagnetic
24	paramagnetic
25	7.50-8.02
26	7.96-8.33
27	paramagnetic
28	paramagnetic
29	7.58-7.95
30	7.57-7.94
31	paramagnetic
32	7.95-8.52
33	HS-paramagnetic
34	7.38-8.41

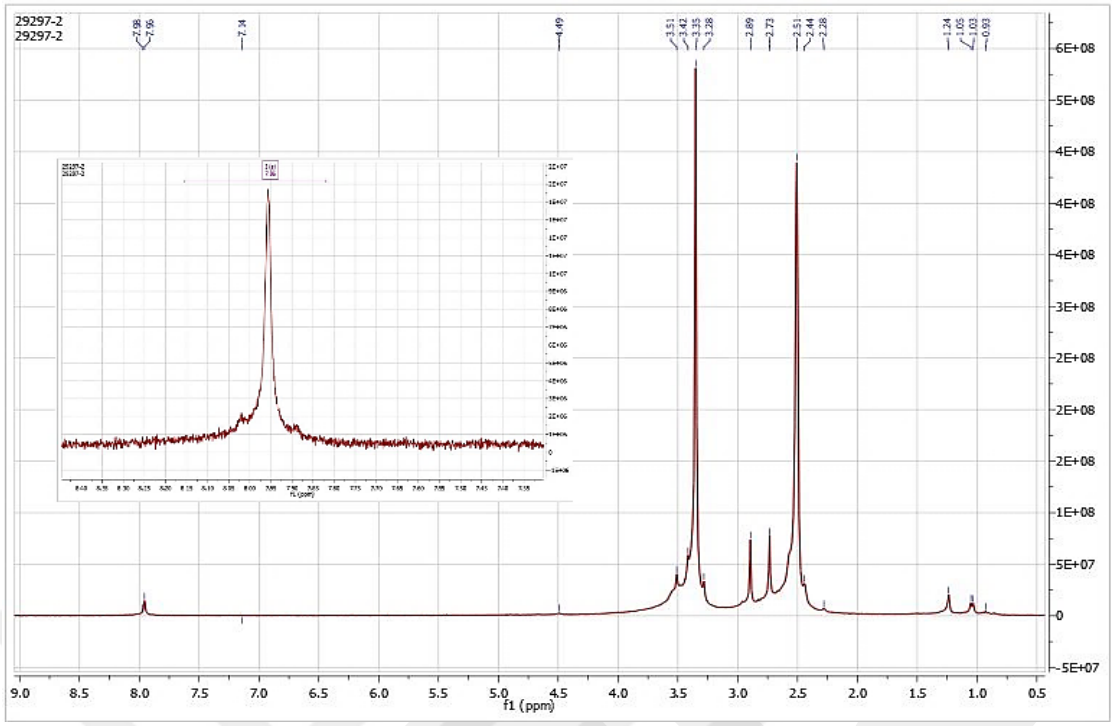

Figure 3.16. ^{1}H-NMR spectrum of complex **8**

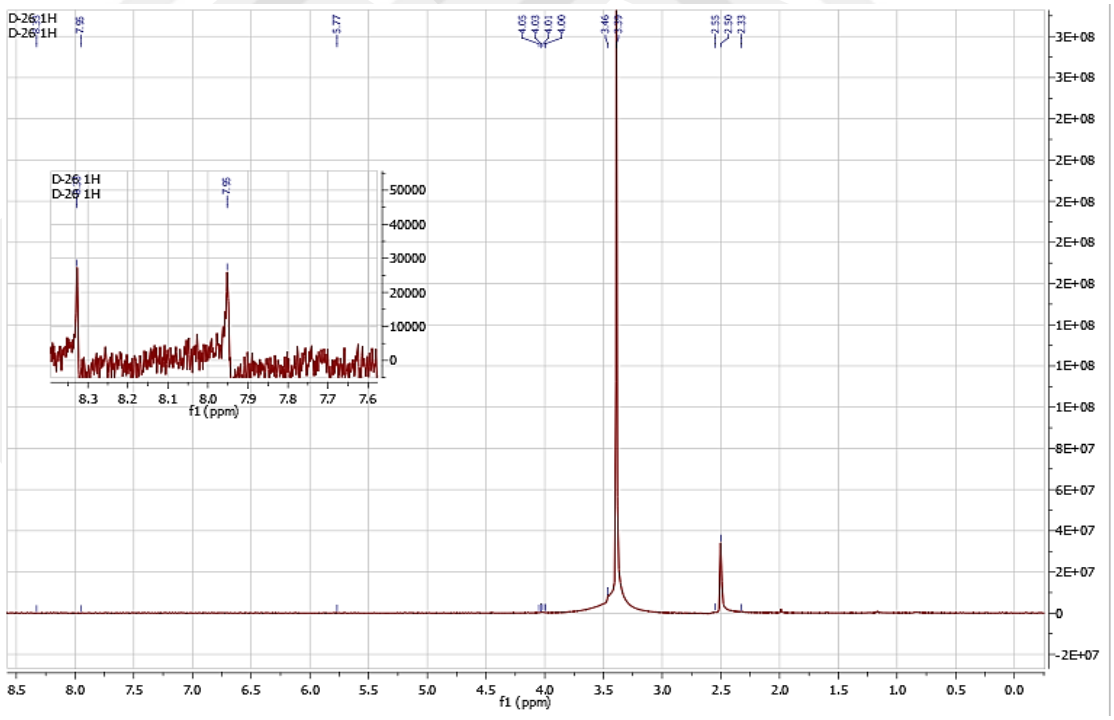

Figure 3.17. ^{1}H-NMR spectrum of complex **26**

Among them, Co(II) complexes numbered as **1** and **31** have the d^7–electronic configuration and are paramagnetic in both high and low spin electronic states. Co(III) complexes **3, 4, 9, 33** and Fe(II) complexes **2, 12** should have d^6-high spin electronic configuration. Cu(II) complexes **23, 24, 27** and **28** are in tetrahedral d^9-structure and all are paramagnetic.

It is very interesting that the existence of coordinated imidazole ligand (L^-) causes variation in the magnetic properties of the molecule in such a way that; as the number of the coordinated L^- increases, the electron density on the central atom increases simultaneously and the compound behaves like a diamagnetic compound by generating weak proton signals in ^{1}H-NMR. Hence, our paramagnetic Fe(III) complexes in their low spin d^5-electronic configuration gave weak NMR signals at around 7.30-8.45 ppm. It is possible to encounter similar cases in the literature [100].

As it's known the magnetic moment of an unpaired electron is 658 times greater than the magnetic moment of a proton and hence, unpaired electron(s)-nucleus coupling broadens the NMR signals with the consequence that the signal is not detectable or, if detected, its relaxation properties increase the threshold for detecting nucleus-nucleus interactions by generating a broad signal [101, 102]. The same situation was observed in the NMR spectrum of complexes **5**, **6**, **7**, **8**, **13**, **14** and **34** despites of their paramagnetic properties (Figures A3.1-A3.18).

An unidentified strong signal was observed at around 7.36-7.45 ppm (Figures A3.15-A3.16) in the ^{1}H-NMR of the zinc complexes was attributed to the presence of an impurity in the deutorated DMSO. In measurements made in ^{1}H-NMR, only benzene can give such a signal [103]. On the other hand, benzene was not used in the none of synthesis steps of these complexes. Furthermore, FTIR spectrum of these two zinc(II) complexes also did not contains any absorption peaks benzene ring. Therefore, this impurity may result from the use of dirty syringes during the measurement.

Among the synthesized complexes, ^{13}C-NMR analysis of the diamagnetic ones were alsotried to be performed, but no signal was obtained. The reason behind this situation is the low abundance percentage (1.1%) of C-13 isotope in nature and 50 times less sensitivity of the C-13 nucleus than the proton in NMR measurements. Considering that very weak signals were obtained in the ^{1}H-NMR spectra during 4-

hour long measurements for the complexes, not seeing a signal in ^{13}C-NMR is an expected result.

3.4. Thermogravimetric Studies

Simultaneous thermogravimetric (TG) and differential scanning calorimetry (DSC) are powerful analysis methods in gathering insight on the thermal decomposition behavior of the materials. Thermal decomposition properties of the ligand and its sodium ammonium salts as well as its metal complexes are explained in detail below.

3.4.1. Thermal decomposition behavior of HL, NaL ve NH_4L compounds

The thermal decomposition temperatures and the corresponding mass losses of HL and its salts, NaL and NH_4L, are listed in Table 3.8 and shown in Figure 3.18.

TG-DSC curves of HL, NaL and NH_4L presented similar degradation properties exhibiting two major mass losses. In the gravimetric analysis, the onset temperature is defined as the temperature at which the decomposition begins. The onset temperatures of mass losses slightly shift to higher degrees as the ramping rate increases for all compounds. However, all compounds were stable until the temperature reaches approximately 200 ^oC for the first decomposition step.

Table 3.8. Thermal decomposition temperatures and % mass losses of ligands

Compound	**DSC (^oC)**			**TGA (^oC)**			
	$T_{p,1(Endo)}$	$T_{p,1(exo)}$	$T_{p,2(exo)}$	$T_{on,1}$	% loss	$T_{on,2}$	% loss
HL	194.03	805.12	873.16	159.5	63.5	805.12	99.74
NaL	171.32	806.46	933.91	151.91	10.62	804.82	97.99
NH_4L	238.79	806.60	911.42	192.78	42.0	809.32	98.00

The first decomposition process was endothermic and accompanied with a 63.5% weight loss for HL. The peak temperature of the endotherm coincides with the completion of the first mass loss. Similarly, endothermic degradation for NH_4L was completed with a 42% mass loss. An additional endothermic change is observed in the

DSC curve of the NaL and NH_4L at 806.46 and 586.83 °C without a mass loss (as shown in Figure 3.18), most probably was associated with the phase changes and occured due to the melting of the remaining portion of the sample. The higher onset temperature and the enthalpy required for the thermal degradation of NH_4L suggested the higher stability of NH_4L compared to the NaL and HL. Since it is well known that NH_4^+ salts of high nitrogen content materials with their high lattice energy have high density and high stability due to the potential hydrogen bond network, which lowers the sensitivity, increases the heat of formation, and ultimately increases the energetic performance [15]. As can be seen in Table 3.8, HL, NaL and NH_4L are almost completely degraded in the temperature range studied.

Broad exothermic peaks in the DSC profiles of the compounds accompanied the second phase of the mass losses started at around 805 °C. These results indicated that the degradation of HL and its salts took place in two steps. During the thermo-gravimetric analyses, HL, NaL and NH_4L underwent a strong thermolysis reaction with the release of NO_2 gas, which damaged to the sample holder. The possible molecular fractions obtained after the first and the second weight losses during the thermal decomposition processes are proposed in scheme 3.2.

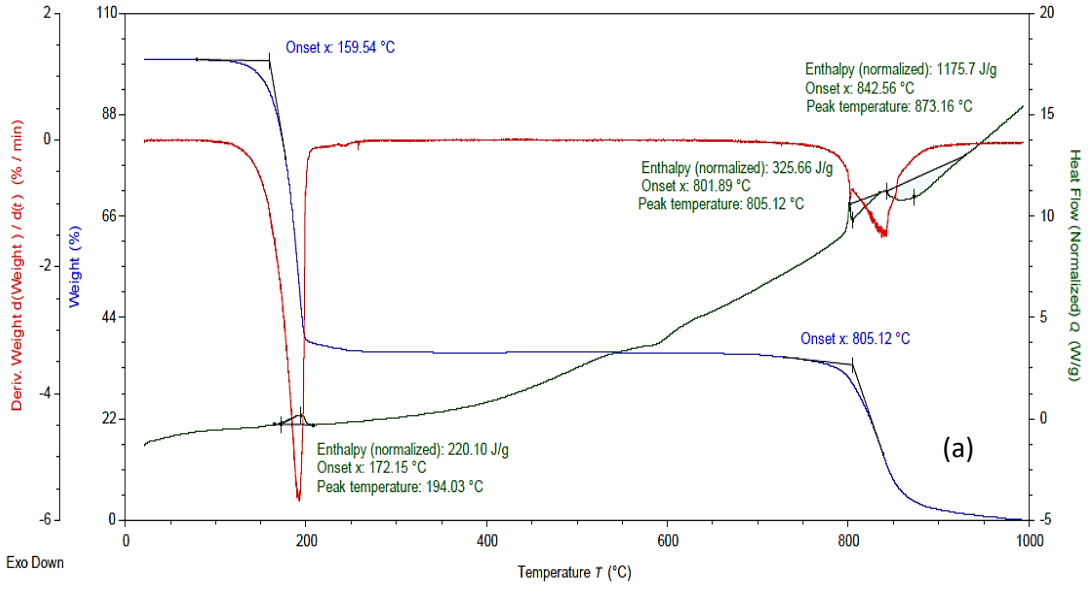

Figure 3.18. Thermal decomposition curves of (a) HL at 2.5 °C/min rate

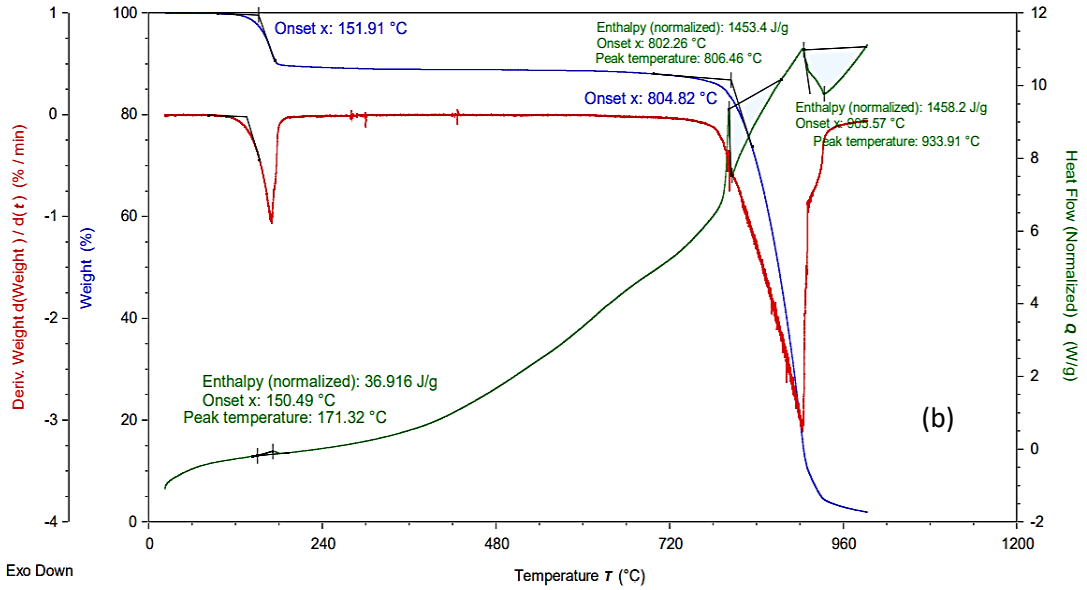

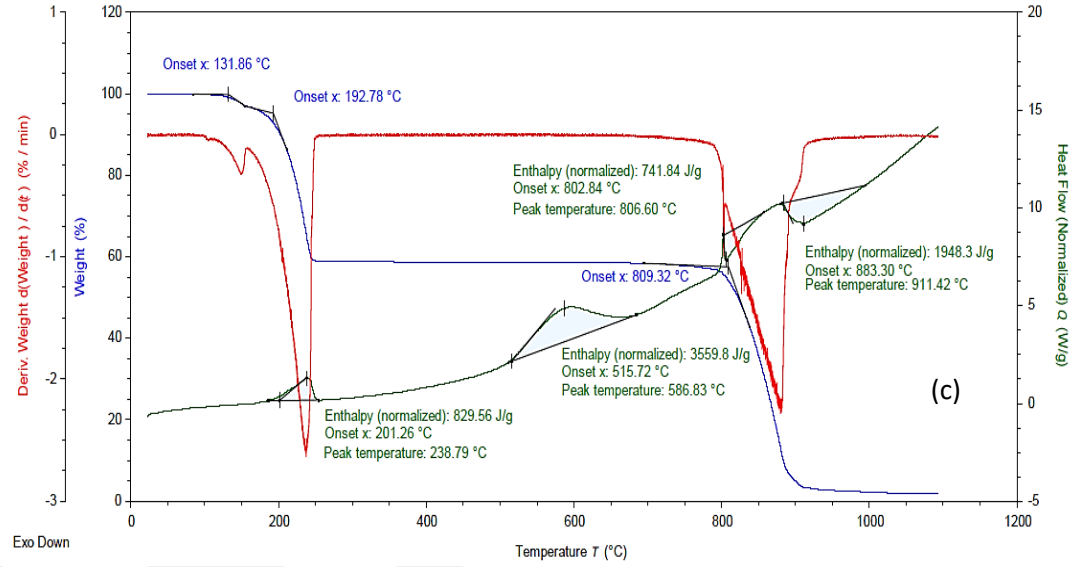

Figure 3.18. *(Continue)* Thermal decomposition curves of and (b) NaL and (c) NH_4L at 2.5 ºC/min rate

HL :

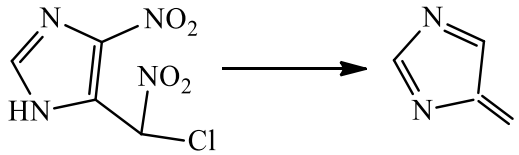

+ $(NO_2)_2Cl$ (1)

38.29% 61.71%

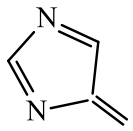

decomposes completely (2)

NaL :

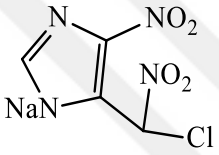

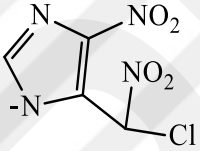

+ Na^+ (1)

89.94% 10.06%

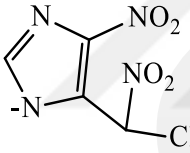

decomposes completely (2)

NH_4L :

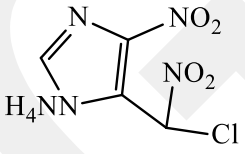

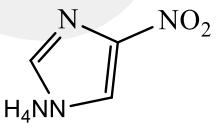

+ $CH(NO_2)Cl$ (1)

57.74% 42.26%

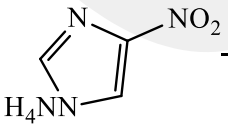

decomposes completely (2)

Scheme 3.2. Suggested thermolysis products of synthesized ligands

The temperature data required to determine kinetic parameters of HL, NaL and NH_4L for the Kissinger equation were obtained from the calorimetric curves given in Figure 3.19 for the heating rates between 2.5 to 20 ^oC/min. The Kissinger plot of Ln (β/T_p^2) vs 1/RT depicted in Figures 3.20 and 3.21.

The apparent activation energies (E_a) and the pre-exponential factors, A, of HL and NH_4L both for the 1st and 2nd mass losses, were calculated using the Kissinger plot and results are tabulated in Table 3.9. According to the Kissinger equation, the slope and intercept of the Ln(β/T_p^2) vs 1/RT graph gives the apparent activation energy (E_a) and ln(A) values respectively. Thermal gravimetric data obtained for NaL at different scanning temperatures was not precise and showed a dispersed distribution. Therefore, 1/RT versus Ln (β/T_p^2) plot could not be drawn and the kinetic parameters could not be calculated for NaL. The reason behind the fluctuations in results is the inconsistent analysis done by the analyst (different sample sizes, inhomogeneous distribution of the sample on the sample holder causing different mass and heat transfer resistances, starting the analysis at different initial temperatures, using unclean sample holder after each analysis etc.).

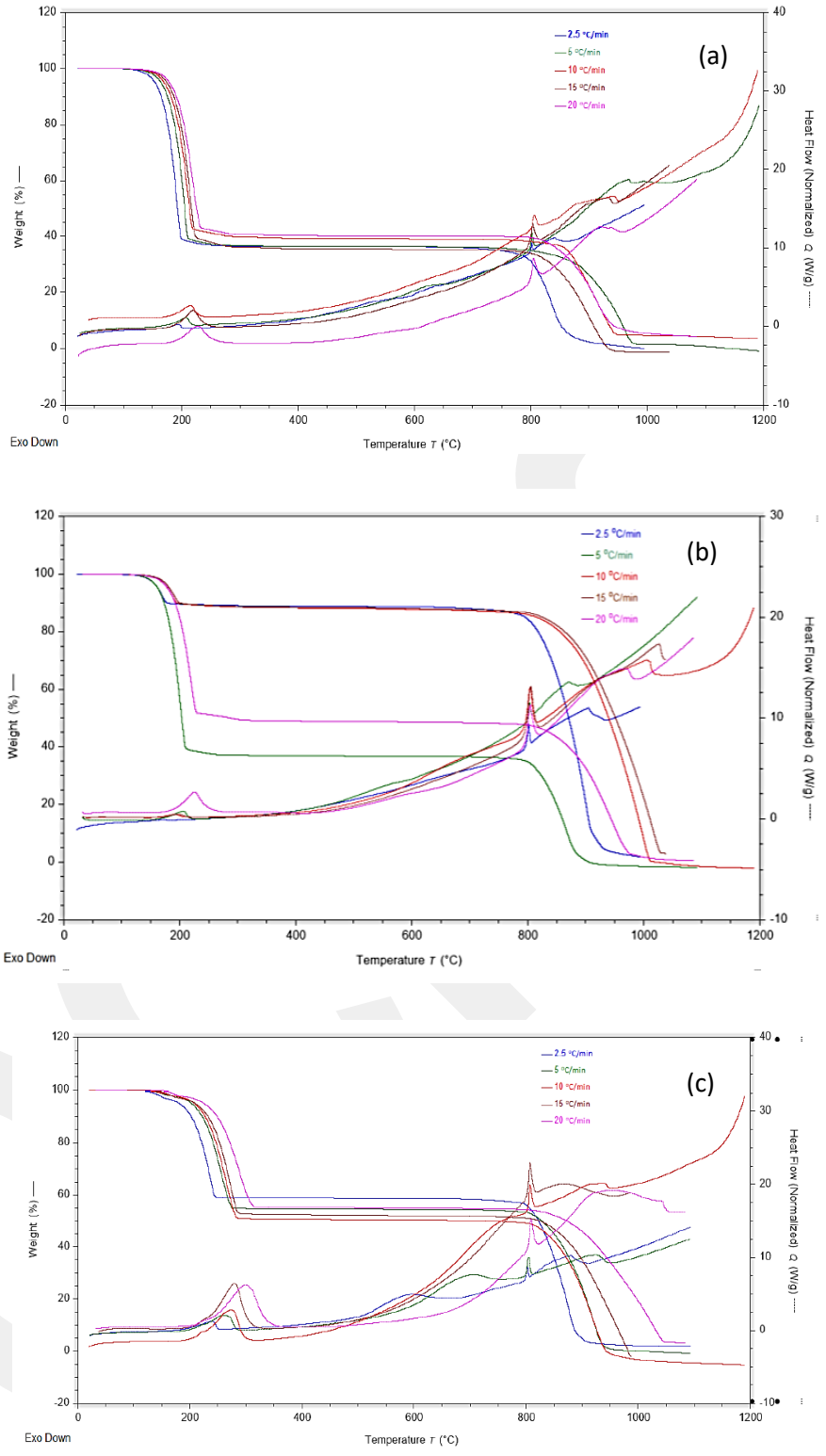

Figure 3.19. Simultaneous TG and DSC profiles of (a) HL (b) NaL (c) NH_4

(— 2.5 °C/min, — 5 °C/min, — 10 °C/min, — 15 °C/min, — 20 °C/min)

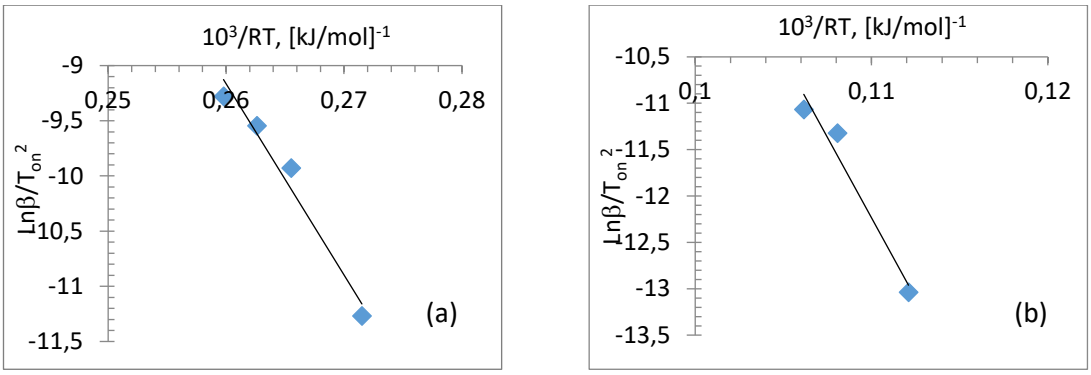

Figure 3.20. The Kissinger plot of Ln (β/T^2) vs 1/RT for HL (a) 1st mass loss and (b) 2nd mass loss

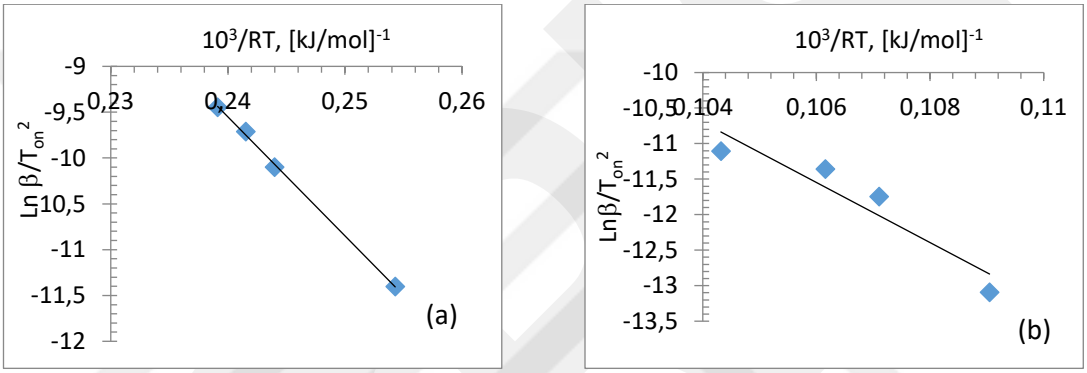

Figure 3.21. The Kissinger plot of Ln (β/T^2) vs 1/RT for NH_4L (a) 1st mass loss and (b) 2nd mass loss

Kissinger method (see section 2.6) was used to determine the apparent activation energies, E_a, and the pre-exponential factors, A, of HL and NH_4L for both 1st and 2nd mass losses, and the results are listed in Table 3.9. Activation energy of HL corresponding to its first mass loss was calculated to be higher than that of the NH_4L. However, the spesific reaction rate of both compounds for the second decomposition step at high temperatures where the second mass loss takes place was found to be similar.

Table 3.9. Activation energy (Ea) and pre-exponential factor (A) calculated from DSC profiles

Compounds	**E_{a1}, kJ/mol**	**E_{a2}, kJ/mol**	**A_1, min^{-1}**	**A_2, min^{-1}**
HL	116.73	1087	$1.24x10^{8}$	$1.17x10^{47}$
NH_4L	79.65	1178	$1.30x10^{3}$	$2.48x10^{51}$

A self-accelerating decomposition temperature (T_{SADT}) is the lowest ambient air temperature at which a self-reactive substance of specified stability (contaminant level, inhibitor content, etc.) undergoes an exothermic reaction in a specified commercial package in a period of seven days or less. The value of the critical temperature (T_b), below which the thermal explosion of a chemical cannot occur, is indispensable to prevent such a chemical from exploding. T_{SADT} and T_b are two significant parameters required to insure safe storage and process operations for the energetic materials. DSC profiles can also be used to calculate the self-accelerating decomposition temperature (T_{SADT}), the critical temperature of thermal explosion (T_b) and thermodynamic parameters such as ΔH (the change in enthalpy), ΔS (the change in entropy) and ΔG (the change in Gibbs free energy) as an indication for the compound's thermal stability. The high T_{SADT} and T_b values indicate good thermal stability of our compounds HL and NH_4L. For this purpose, exothermic peaks obtained during the second mass loss in the thermogram of the compounds were used for the calculations of these thermodynamic parameters and results are represented in Table 3.10.

Table 3.10. Self–accelerating decomposition temperature (T_{SADT}), critical temperature of thermal explosion (T_b) and thermodynamic parameters at T_b.

	Exotermic Second Mass Loss	
Ligand	**HL**	**NH_4L**
T_{SADT}, (^oC)	798.9	803.3
T_b, (^oC)	807.9	811.7
ΔH ($kJ.mol^{-1}$)	1078	1169
ΔS (kJ/mol.K)	$9.34\ x10^{3}$	$1.05\ x10^{4}$
ΔG (kJ/mol)	$-1.01\ x10^{7}$	$-1.14\ x10^{7}$

As can be seen in Table 3.10, the self-accelerating decomposition temperature and the critical temperature of explosion for HL and NH_4L are similar for the second mass loss, which is exothermic in nature. These results showed that both studied compounds are stable up to 1100-1200 ^oC, indicating their potential use in propulsion systems as an additive material [34, 37, 104].

3.4.2. Thermal decomposition behavior of metal complexes

In the scope of this study, thermal decomposition properties of Co(II/III), Fe(II/III), Cu(II) and Zn(II) complexes of L^- were investigated by thermal gravimetric measurements, as well. Thermograms of **5** and **23** are presented in Figures 3.22 and 3.23. TGA/DSC curves of all other complexes are given in Appendix 4.1-4.21.

Careful inspection of the TG-DSC curves revealed that all complexes have similar decomposition processes during close percent mass losses. The thermal decomposition temperatures and the corresponding mass losses with the possible molecular fractions of the complexes are listed in Table 3.11. Possible molecular fractions obtained after successive weight losses during thermal decomposition processes are proposed in scheme 3.3 for selected complexes **(1** and **10**) and for all other complexes in Appendix 5.

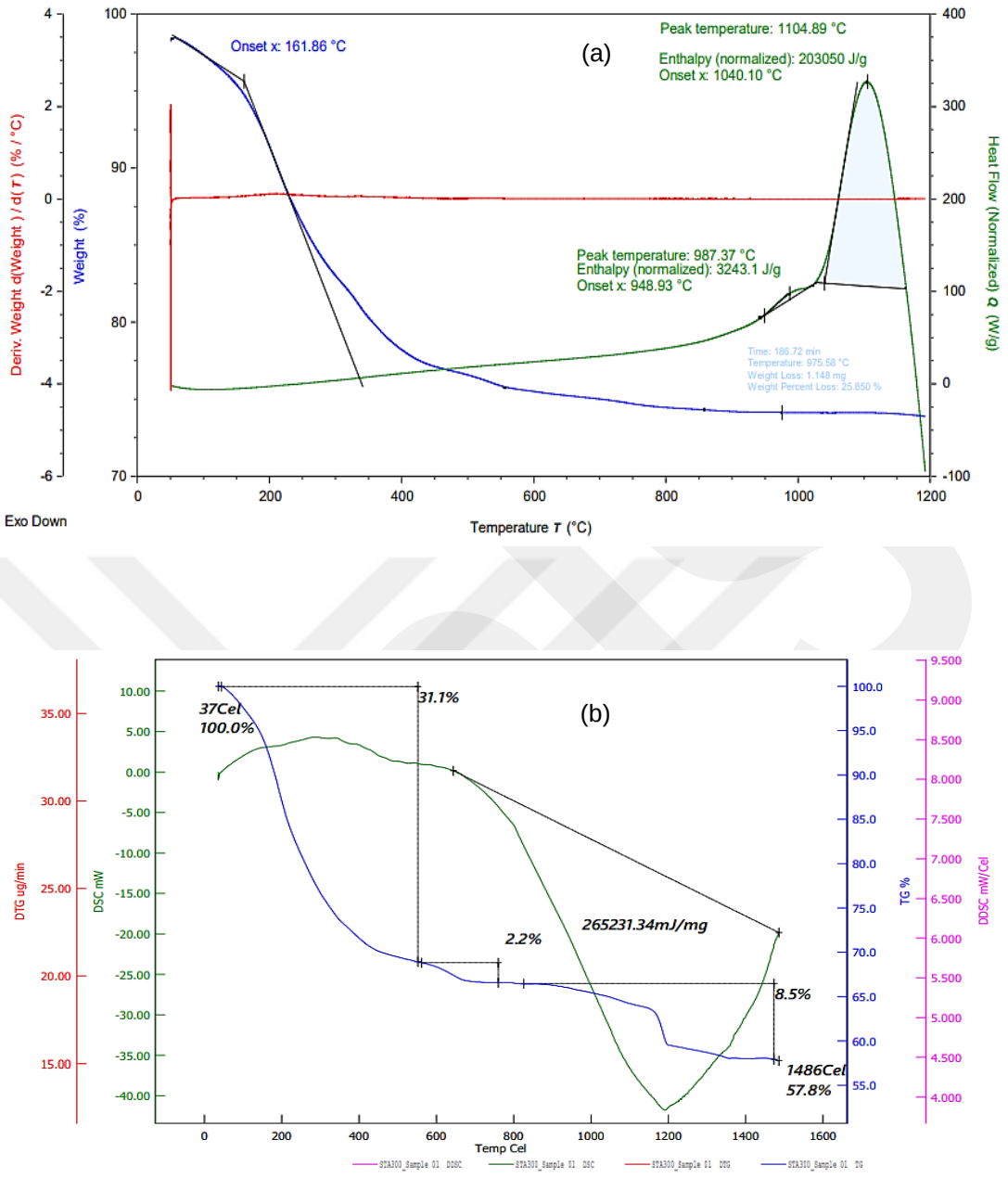

Figure 3.22. Thermal decomposition curves of **5** at 5 °C/min rate in (a) the range of 50-1200 °C and (b) the range of 50-2000 °C

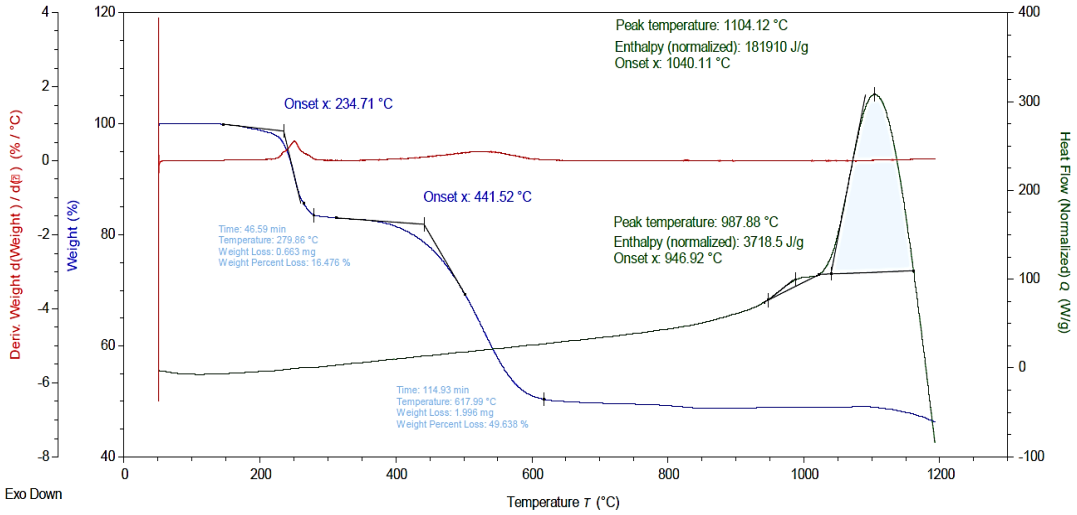

Figure 3.23. Thermal decomposition curve of **23** at 5 °C/min rate in the range of 50-1200 °C

Complex 1 :

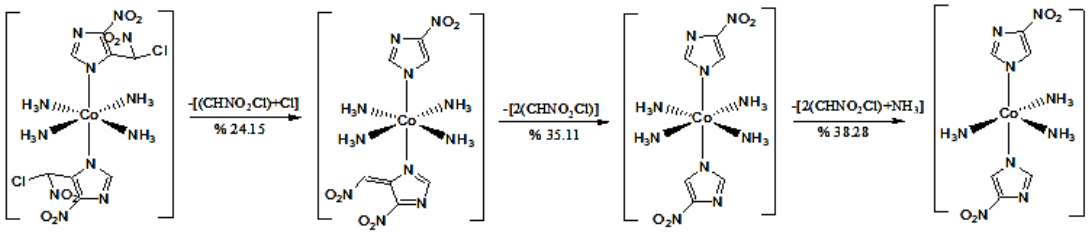

Complex 10 :

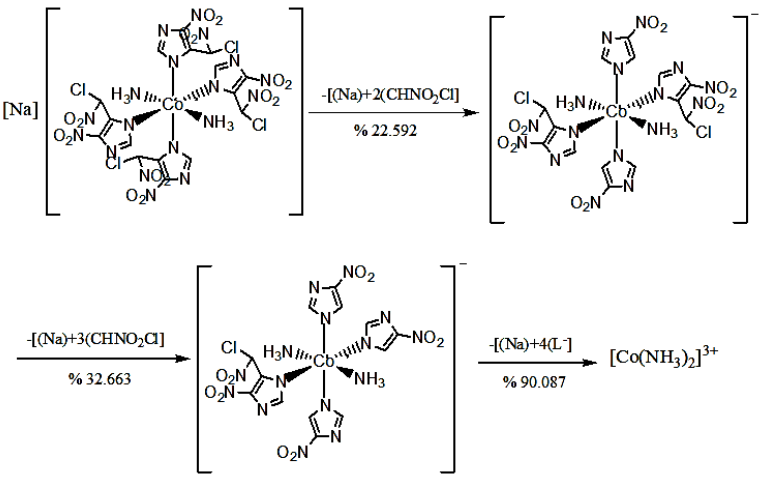

Scheme 3.3. Suggested thermolysis products for **1** and **10** in the range of 50-1200 °C

Table 3.11. Percent mass losses obtained from the TGA curves of the complexes and their corresponding estimated molecular fractions

Complex	Onset Temperature	Mass Loss	Estimated Molecular Fractions	
1	I. 219.33 °C II. 478.56 °C III. 748.85 °C	I. %23.204 II. %34.683 III. %39.331	I. M-[(CH(NO_2)Cl)+Cl] II. M-[2(CH(NO_2)Cl)] III. M-[2(CH(NO_2)Cl)+NH_3]	(%24.15) (%35.11) (%38.28)
2	I. 191.59 °C II. 494.73 °C	I. %17.113 II. %19.970	I. M-[(CH(NO_2)Cl)] II. M-[(CH(NO_2)Cl)+NH_3]	(%17.66) (%20.84)
3	I. 277.82 °C	I. %85.197	I. M-[2(L^-)+NH_3+PF_6]	(%83.89)
4	I. 273.88 °C II. 335.72 °C III. 432.11 °C IV. 542.15 °C	I. %35.471 II. % 45.308 III. %51.983 IV. %54.401	I. M-[2(CH(NO_2)Cl)] II. M-[2(CH(NO_2)Cl)+NO_2] III. M-[2(CH(NO_2)Cl)+2NO_2] IV. M-[2(CH(NO_2)Cl)+2NO_2+NH_3]	(%35.11) (%46.74) (%52.11) (%55.38)
5	I. 161.86 °C	I. %24.280	I. M-[(Cl)+PF_6]	(%26.53)
6	I. 145.79 °C II. 620.38 °C	I. %24.575 II. %27.117	I. M-[Cl+2NO_2] II. M-[2(Cl)+2NO_2]	(%23.82) (%30.45)
7	I. 272.69 °C II. 400.43 °C III. 520.91 °C	I. %8.955 II. %10.838 III. %13.350	I. M-[2(NH_4^+)+NO_2] II. M-[2(NH_4^+)+NO_2+NH_3] III. M-[2(NH_4^+)+NO_2+2NH_3]	(%8.70) (%10.42) (%12.21)
8	I. 226.84 °C II. 456.10 °C III. 753.51 °C	I. %19.731 II. %23.963 III. %44.403	I. M-[2Na^++(CH(NO_2)Cl)+NO_2] II. M-[2Na^++(2(CH(NO_2)Cl)] III. M-[2Na^++(4(CH(NO_2)Cl)]	(%19.40) (%24.44) (%44.10)
9	I. 230.16 °C II. 517.22 °C	I. %20.116 II. %27.259	I. M-[NH_4^++(2(CH(NO_2)Cl)] II. M-[NH_4^++(2(CH(NO_2)Cl)+NO_2]	(%22.18) (%27.11)
10	I. 152.49 °C II. 330.64 °C III. 796.02 °C	I. %22.439 II. %32.631 III. %89.285	I. M-[Na^++(2(CH(NO_2)Cl)] II. M-[Na^++(3(CH(NO_2)Cl)] III. M-[Na^++(4(L^-)]	(%22.59) (%32.66) (%90.07)
11	I. 162.26 °C II. 503.51 °C	I. %17.417 II. %21.169	I. M-[2(NH_4^+)+(CH(NO_2)Cl)+NO_2] II. M-[2(NH_4^+)+2(CH(NO_2)Cl)+NO_2]	(%18.62) (%23.77)
12	I. 182.11 °C II. 500.51 °C III. 574.59 °C	I. %6.897 II. %9.355 III. %10.96	I. M-[2(Na^+)] II. M-[2(Na^+)+NO_2] III. M-[2(Na^+)+NO_2+Cl]	(%4.80) (%9.60) (%13.30)
13	I. 191.88 °C II. 429.06 °C	I. %12.802 II. %17.137	I. M-[NH_4^++(CH(NO_2)Cl)] II. M-[NH_4^++(CH(NO_2)Cl)+NO_2]	(%12.10) (%17.04)
14	I. 169.16 °C II. 371.83 °C III. 630.33 °C	I. %13.013 II. %17.327 III. %20.959	I. M-[Na^++(CH(NO_2)Cl)] II. M-[Na^++(CH(NO_2)Cl)+NO_2] III. M-[Na^++(CH(NO_2)Cl)+NO_2+Cl]	(%12.56) (%17.48) (%21.27)
23	I. 234.71 °C II. 441.52 °C	I. %16.476 II. %49.638	I. [M-DMF] II. M-[(CH(NO_2)Cl)+PF_6]	(%15.71) (%51.49)
24	I. 159.53 °C II. 457.17 °C	I. %18.346 II. %54.949	I. M-[NO_2+(NH_3)] II. M-[(CH(NO_2)Cl)+NO_2+2NH_3]	(%19.69) (%54.52)
25	I. 125.10 °C	I. %75.429	I. M-[(L^-)+PF_6]	(%75.06)

26	I. 173.94 °C II. 465.12 °C III. 694.82 °C	I. % 20.783 II. %26.591 III. %28.408	I. M-[(CO_3^{2-})+Cl+NO_2] II. M-[(CO_3^{2-})+Cl+2NO_2] III. M-[(CO_3^{2-})+(CH(NO_2)Cl)+NO_2]	(%20,09) (%26,63) (%28,48)
27	I. 124.01 °C II. 244.99 °C III. 292.68 °C IV. 362.81 °C	I. %16.663 II. %24.803 III. %28.497 IV. %32.639	I. M-[2(NH_4^+)+(CH(NO_2)Cl)] II. M-[2(NH_4^+)+2(CH(NO_2)Cl)] III. M-[2(NH_4^+)+2(CH(NO_2)Cl)+NO_2] IV. M-[2(NH_4^+)+2(CH(NO_2)Cl)+NO_2+Cl]	(%14.16) (%24.41) (%29.40) (%33.25)
28	I. 201.13 °C II. 418.69 °C III. 736.17 °C	I. %20.109 II. %66.581 III. %69.004	I. M-[2(Na^+)+(CH(NO_2)Cl)+NO_2] II. M-[2(Na^+)+2(L^-)+(CH(NO_2)Cl)+NO_2] II. M-[2(Na^+)+2(L^-)+2(CH(NO_2)Cl)]	(%20.01) (%64.14) (%69.34)
29	I. 173.53 °C II. 435.42 °C III. 784.94 °C	I. %29.334 II. %39.281 III. %80.621	I. M-[2(NH_4^+)+2(CH(NO_2)Cl)+NO_2] II. M-[2(NH_4^+)+3(CH(NO_2)Cl)+NO_2] III. M-[2(NH_4^+)+3(L^-)+(CH(NO_2)Cl)]	(%29.34) (%39.57) (%80.90)
30	I. 181.19 °C II. 381.29 °C III. 790.05 °C	I. %7.680 II. %12.942 III. %92.709	I. M-[2(Na^+)] II. M-[2(Na^+)+NO_2+Cl] III. M-[2(Na^+)+4(L^-)]	(%4,93) (%13.65) (%92.99)
31	I. 165.72 °C II. 251.01 °C III. 736.60 °C	I. %14.334 II. %18.534 III. %27.072	I. M-[NO_2] II. M-[NO_2+Cl] III. M-[(CH(NO_2)Cl)]	(%13.16) (%18.03) (%27.07)
32	I. 170.23 °C II. 782.80 °C	I. %7.963 II. %9.972	I. M-[CO_3^{2-}] II. M-[(CO_3^{2-})+NH_3]	(%7,97) (%10.23)
33	I. 162.61 °C II. 250.61 °C III. 468.64 °C IV. 791.43 °C	I. %14.058 II. %18.900 III. %28.643 IV. %80.171	I. M-[CO_3^{2-}] II. M-[(CO_3^{2-})+NH_3] III. M-[(CO_3^{2-})+NH_3+NO_2] III. M-[(CO_3^{2-})+4NH_3+(L^-)]	(%14.65) (%18,81) (%30.04) (%80.17)
34	I. 408.47 °C II. 720.96 °C	I. %27.123 II. %37.490	I. M-[(CO_3^{2-})+NO_2] II. M-[(CO_3^{2-})+(CH(NO_2)Cl)]	(%26.08) (%38.00)

*M represents the molecular mass of the complexes. The percent weights of the estimated molecules or ions leaving the structure in the complexes are given in parentheses.

When the TGA results of the metal complexes were evaluated (Table 3.11), it is observed that most of the complexes are stable within the temperature range of 50-1200 ^oC with mass losses lower than 30%. Complexes which have 75% or more percent mass loss within the same temperature range are **3, 10, 25, 28, 29 and 30**. This result designated that the tetrahedral Zn(II) and Cu(II) complexes (**25, 28, 29** and **30**) are more easily decomposes thermally compared to the other complexes. On the other hand, **3** and **10** are PF_6^- and Na^+ salts of Co(II) and Co(III) complexes, respectively and found to be less stable than their equivalents containing CO_3^{2-} and NH_4^+ ions.

Thermograms of the complexes pointed out that the mass loss of the complexes started at around 150-270 ^oC (Table 3.11 and Figures A4.1-A4.21). Moreover, all Fe(II) and Fe(III) complexes exhibited a special stability towards thermal decompositon, surprisingly. Indeed, $4L^-$ containing Fe(III) complexes have unusual thermal stability with mass losses lower than 20% within the studied temperature

range. In order to observe further possible decomposition process that may occur between 1200 and 2000 ºC, 7 complexes (which brought less than 30% mass losses) were selected and subjected to another laboratory test for thermogravimetric measurement. However, only an endothermic decomposition process was observed for these selected complexes. Among them, Fe(III) complexes namely **6**, **12** and **13** were still quite stable in this temperature range and their percent degredation amount was obtained between 23% and 30% (Figures A4.3b, A4.9b and A4.10b). In that group of Fe(III) complexes, **12** induced higher stability with $4L^-$ and a counter ion of sodium. Contrary to the Fe(III) complexes, Co(II) and Co(III) ammonium complexes (**7** and **9**) containing $4L^-$ almost completely decomposed at around 1250 ºC (Figure A4.4b and A4.6b). The results obtained for these 7 complexes are briefly summarized in Table 3.12.

Table 3.12. Mass losses from the TGA curves of some complexes and their corresponding estimated molecular fractions and enthalpy values

Complex	**Onset Temperature**	**Mass Loss**	**Estimated Molecular Fractions**		**Enthalpy (J/g)**
5	I. 1193 °C	%42.2	M-[PF_6^-+($CH(NO_2)Cl$)+NO_2]	(%41.98)	265231
6	I. 1220 °C II. 1267 °C	%30.0	M-[($CH(NO_2)Cl$)+2NH_3+Cl]	(%30.65)	97395
7	I. 1236 °C II. 1273 °C	%106.1	Totally decompose		241181
9	I. 1236 °C II. 1290 °C	%71.8	M-[NH_4^++2($CH(NO_2)Cl$)+2L^-+NO_2]	(%71.16)	96040
11	I. 1200 °C	%54.0	M-[2NH_4^++3($CH(NO_2)Cl$)+L^-]	(%55.40)	168284
12	I. 1200 °C II. 1387 °C	%23.2	M-[2Na^++($CH(NO_2)Cl$)+Cl+NO_2]	(%23.16)	125662
13	I. 1200 °C	%27.5	M-[NH_4^++2($CH(NO_2)Cl$)+NO_2]	(%27.20)	90363

It is thought that the endothermic transitions observed around 988 ^{o}C and 1100 ^{o}C (Table 3.13) without a mass loss for all complexes except 1, 2, 28, 31 and 32 were attributed to a phase change process. As it is understood from the data given in Table 3.11, all these decomposition processes began with small energy outputs gained via breakage of the branches of the ligand L^- and continued with the removal of the whole ligand L^- from the molecular structure of the metal complexes.

As it is inspected from Table 3.13, only 5 of our metal compounds, **1, 2, 28, 31** and **32**, indicated exothermic character in their thermograms obtained in the range of 50-1200 ^{o}C. Interestingly, only Co(II) and Fe(II) complexes containing one (**31** and **32**) or two L^- (**1** and **2**) generated exothermic peaks around 1100 ^{o}C (Figure 3.25-3.26) during their thermolysis process, unlike their +3 charged and/or $4L^-$ containing counterparts. **28** is a sodium salt of copper(II) complex including $4L^-$ and yielded high exothermic energy at about 1122 ^{o}C (Figure 3.27). Its ammonium derivative may also achieve an exothermic thermal degradation at a temperature higher than 1200 ^{o}C, however any exothermic change could not be observed within our studying range limits. All five complexes have very high exothermic energy at around 1100 ^{o}C (Figure 3.25-3.27). Moreover, we must underline that, the exothermic energy release of HL was observed at 805 ^{o}C was shifted towards the higher temperatures (1100 ^{o}C) through its coordination to the metal ions. In the same way, the gathered amount of exothermic energy also increased from 1175 J/g to about $7.6x10^5$ J/g upon coordination of L^-.

Under the light of these findings, one can say that **1, 2, 28, 31** and **32** have high potential to be applied as additives in propellant formulations of rocket fuels [34, 37, 104]

Table 3.13. Peak maximum temperature and corresponding enthalpy values in DSC curves of complexes

Complex	Endothermic Changes			Exothermic Changes		
	Maximum Peak Temperature (°C)	**Onset Temp. (°C)**	**Enthalpy (J/g)**	**Maximum Peak Temperature (°C)**	**Onset Temp. (°C)**	**Enthalpy (J/g)**
1	-	-	-	I. 1108	I. 1024	I. 761940
2	-	-	-	I. 1028 II. 1124	I. 999 II. 1079	I. 1758 II. 12994
3	I. 987 II. 1105	I. 946 II. 1040	I. 5064 II. 215860	-	-	-
4	I. 988 II. 1099	I. 949 II. 1038	I. 5861 II. 290680	-	-	-
5	I. 987 II. 1105	I. 949 II. 1040	I. 3243 II. 203050	-	-	-
6	I. 986 II. 1104	I. 947 II. 1041	I. 2173 II. 74867	-	-	-
7	I. 1128	I. 1062	I. 295680			
8	I. 990 II. 1106	I. 962 II. 1041	I. 1880 II. 588350	-	-	-
9	I. 987 II. 1104	I. 947 II. 1042	I. 2374 II. 126680	-	-	-
10	I. 990 II. 1105	I. 954 II. 1042	I. 1995.0 II. 137880	-	-	-
11	I. 986 II. 1106	I. 952 II.1042	I. 3979 II. 329670	-	-	-
12	I. 987 II. 1104	I. 948 II. 1041	I. 9520 II. 546200	-	-	-
13	I. 990 II. 1107	I. 953 II. 1040	I. 8620 II. 644870	-	-	-
14	I. 988 II. 1107	I. 951C II. 1041	I. 9526 II. 745460	-	-	-
23	I. 988 II. 1104	I. 947 II. 1040	I. 3718 II. 181910	-	-	-
24	I. 988 II. 1106	I. 951 II. 1041	I. 4620 II. 354180	-	-	-
25	I. 997 II. 1107	I. 972 II. 1041	I. 2052 II. 1132700	-	-	-
26	I. 989 II. 1101	I. 952 II. 1040	I. 4967 II. 268740	-	-	-
27	I. 986 II. 1107	I. 949 II. 1041	I. 8252.8 II. 410160	-	-	-

28	-	-	-	I. 1122	I. 1040	I. 350990
29	I. 987 II. 1100	I. 946 II. 1043	I. 8734 II. 329080	-	-	-
30	I. 813 II. 985 III. 1102	I. 787 II. 948 III. 1041	I. 3179 II. 4346 III. 208360	-	-	-
31	-	-	-	I. 1117	I. 1040	I. 519490
32	-	-	-	I. 11187	I. 1038	I. 623700
33	I. 986 II. 1115	I. 949 II. 1042	I. 6345 II.701890	-	-	-
34	I. 988 II. 1107	I. 958 II. 1042	I. 3992 II. 1108400	-	-	-

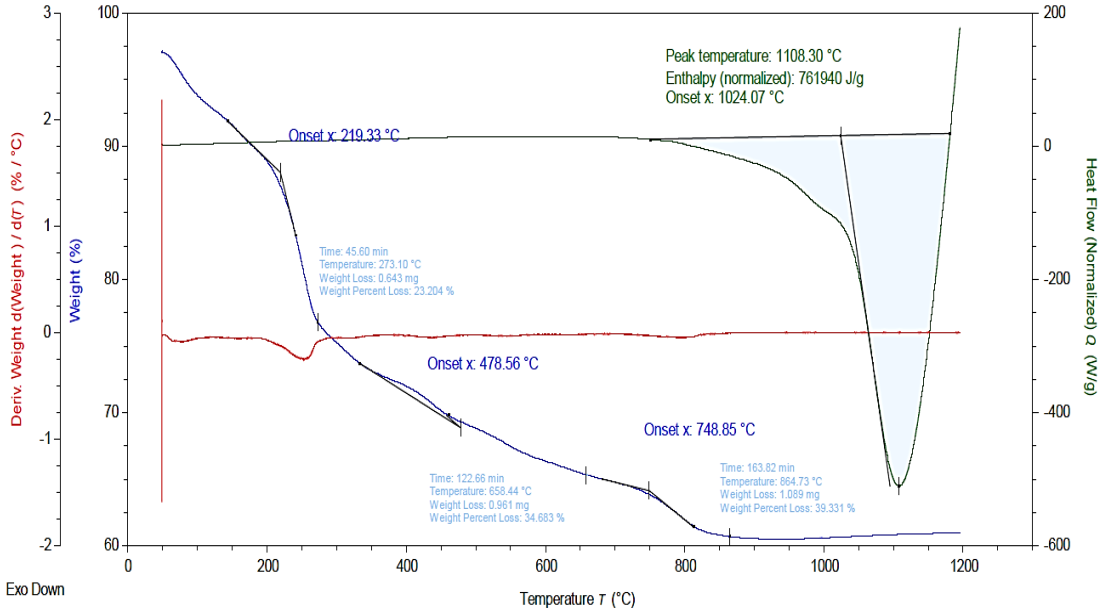

Figure 3.24. Thermal decomposition curve of complex **1** at 5 ^{o}C/min scan rate

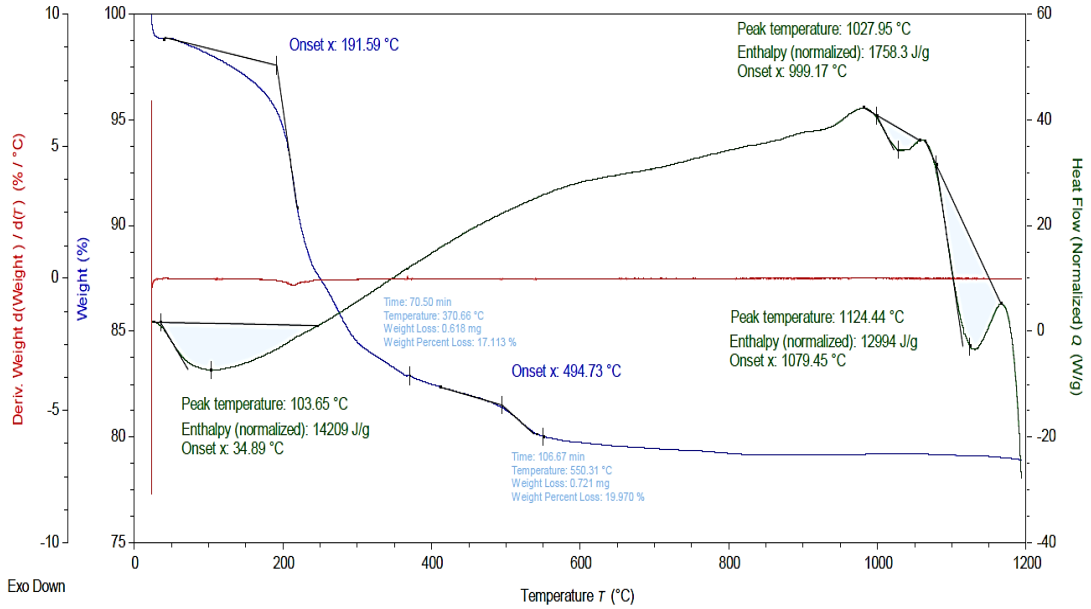

Figure 3.25. Thermal decomposition curve of complex **2** at 5 °C/min scan rate

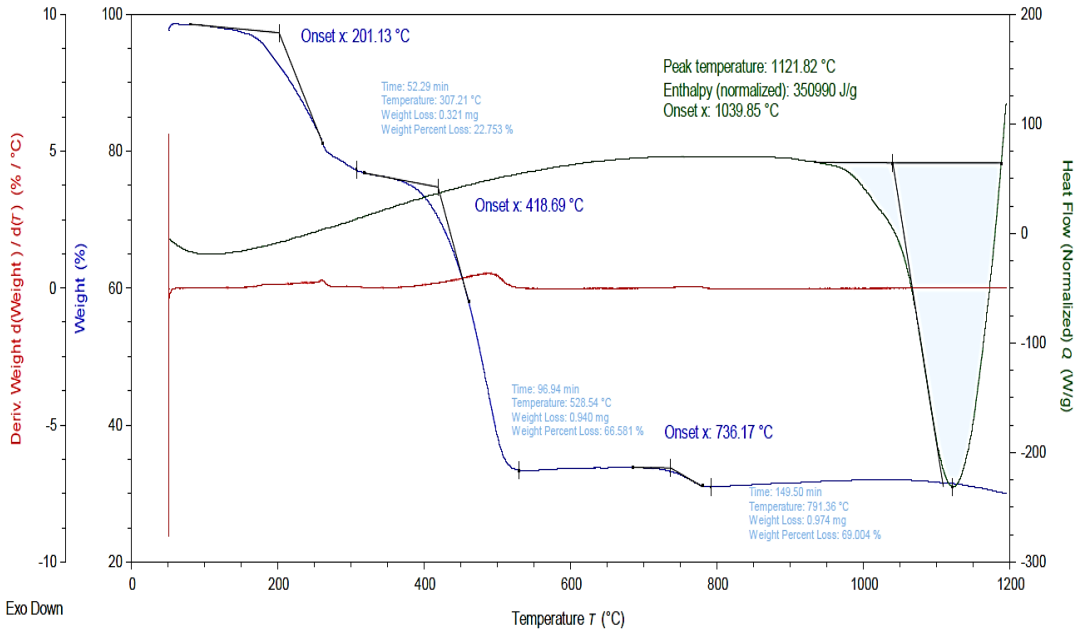

Figure 3.26. Thermal decomposition curve of complex **28** at 5 °C/min scan rate

1, 2, 28, 31 and **32** were subjected for simultaneous TGA-DSC measurements in order to investigate their decompotion kinetics at 2.5, 5, 10, 15 and 20 ^{o}C/min heating rates. However, the obtained thermograms did not include any exothermic peaks surprisingly, except that for **1** and **2**. In these measurements, 2.5 ^{o}C/min scanning rate was detected as too slow to follow the thermal behavior of both complexes since no exothermic peak was observed in their thermograms. On the contrary, the 20 ^{o}C/min scanning rate was too fast to study the kinetic effect since the exothermic peak of **1** was appeared at higher temperature outside of our scale and two exothermic processes of **2** were displayed as just one process at a temperature value obtained between these peak maximas. Because of the scattered temperature data obtained during measurements at different scan rates could not be used in kinetic calculations of **2**, the kinetic parameters were determined only for **1**.

Thermal decomposition kinetics of **1** under non-isothermal conditions were studied using the Kissinger method and the required data were collected from the calorimetric curves given in Figure 3.28. The Kissinger plot of Ln (β/T_p^2) vs 1/RT were displayed in Figures 3.29 was used to determine the apparent activation energy and the pre-exponential factor for **1**.

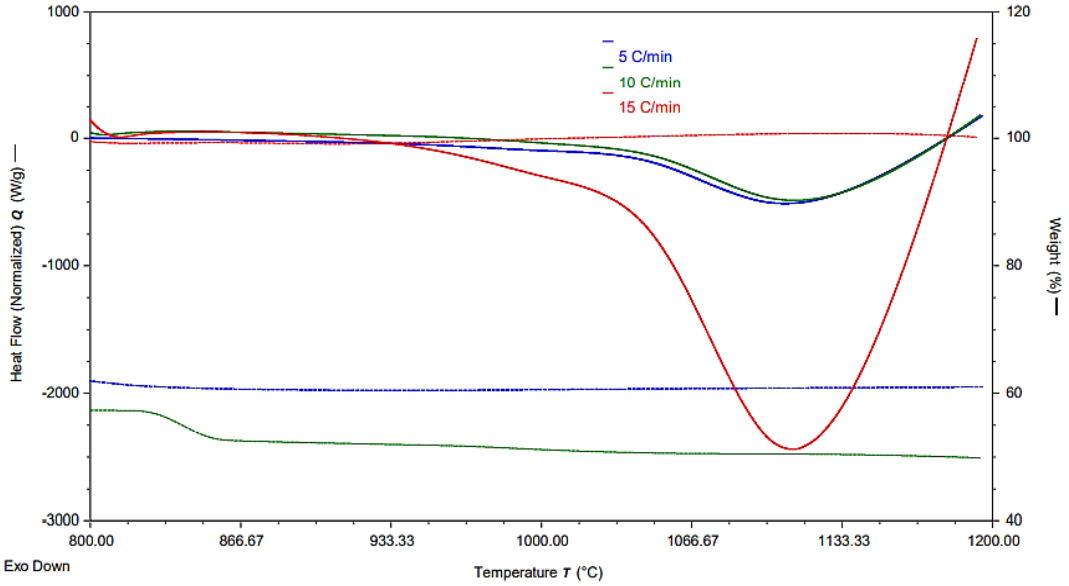

Figure 3.27. Simultaneous TG and DSC profiles of **1** measured 5, 10, and 15 ^{o}C/min heating rates

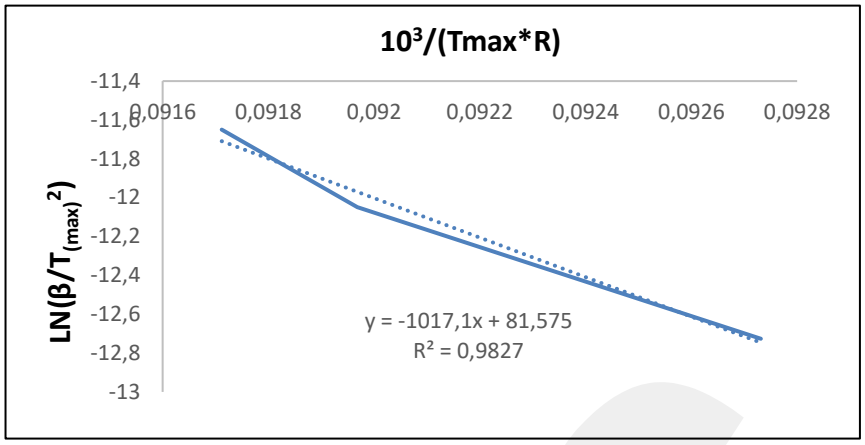

Figure 3.28. Kissinger plot for **1**

DSC profiles can also be used to calculate the self-accelerating decomposition temperature (T_{SADC}), the critical temperature of thermal explosion (T_b) and thermodynamic parameters (ΔH, ΔS, ΔG) of **1**. The results obtained using the equations in section 2.6 are presented in Table 3.14.

Table 3.14. Kinetic and thermodynamic parameters for **1**

	Complex 1
E_a (kJ/mol)	1017
A, dk^{-1}	$2.7x10^{35}$
T_{SADT}, (^oC)	1101.2
T_b, (^oC)	1106.31
ΔH ($kJ.mol^{-1}$)	3083.53
ΔS (kJ/mol.K)	$2.71x10^4$
ΔG (kJ/mol)	$-3.7x10^7$

[Ea]Activation energy; [A] the pre-exponential factor; [TSADT] self-accelerating decomposition temperature; [Tb] critical temperature of thermal explosion and [ΔH, ΔS, ΔG] thermodynamic values at T_b

The logarithm of the calculated pre-exponential factor (A) was obtained as 35.43 for **1**. Similar activation energies (1017 kj/mol) and Log(A) values have been previously reported in the literature [104] to find the minimum energy required to initiate energetic materials. The obtained activation energy and exponential factor value indicated that the complex **1** can be used as an additive in small amounts to change the ballistic properties of composite fuels [34, 37, 104].

3.5. Caloriferic Value, Impact and Friction Tests

Explosive properties of 1 and 2 were examined by caloriferic value, impact and friction tests and the details of these tests were presented in the following section.

3.5.1. Caloriferic Value Measurements

Semi-micro oxygen bomb was used primarily for caloriferic value measurements due to the procurement of low sample amount (approximately 450 mg). This device gives oppourtinity to measurements with 25 mg sample. Because both complexes did not burn in the experiments carried out with this device under nitrogen, the standard bomb calorimeter operating with a large scale was used with the entire remaining sample amount to perform experiment in oxygen environment, where benzoic acid was used as an igniter (spike). As a result of the test, the samples did not undergo a combustion reaction while the wire and benzoic acid burnt. Thus, no calorific value could be obtained for both complexes due to reasons of insufficient sample amounts; the wire used for ignition could not be fully covered by the samples inside the crucibles as shown in Figure 3.30-3.33.

Figure 3.29. Before (left) and after (right) the ignition of **1**

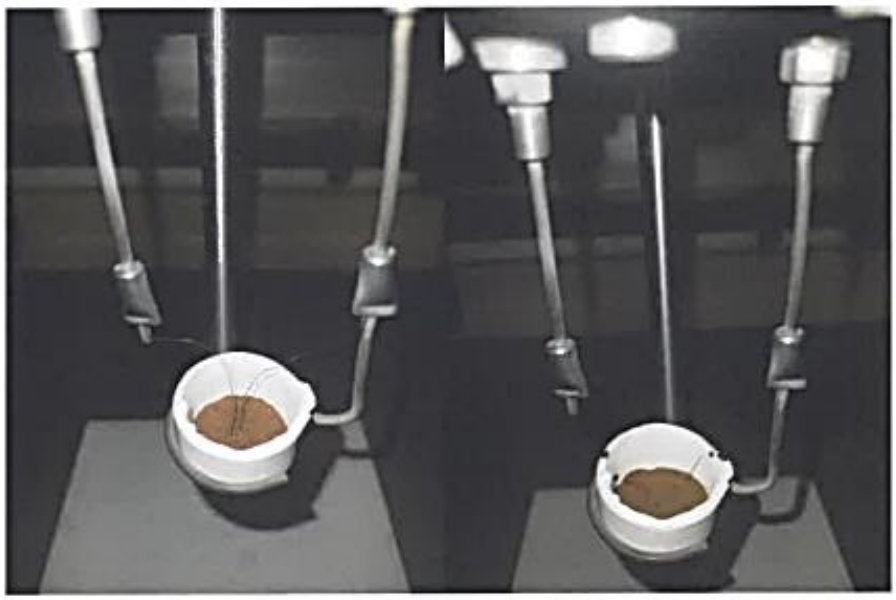

Figure 3.30. Before (left) and after (right) the ignition of **2**

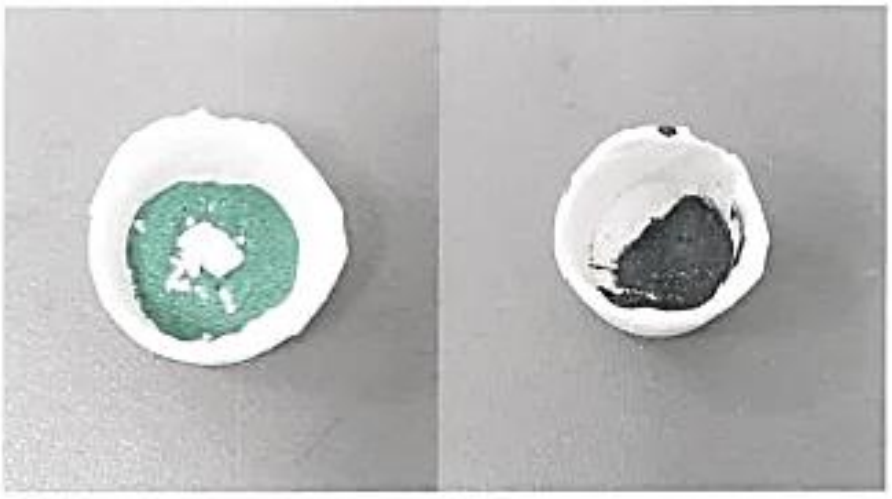

Figure 3.31. Before (left) and after (right) the ignition with spike of **1**

Figure 3.32. Before (left) and after (right) the ignition with spike of **2**

3.5.2. Impact Sensitivity Tests

Impact sensitivity tests followed EN-1361-4 standard methods, and BAM impact sensitivity device was used for this purpose. The tests were initiated with the the highest weight used in the tests, in which 5 kg weight was dropped from 100 cm height. A negative respond was obtained after 6 shots from 5 cm to 100 cm heights with 50 J energy (Figure 3.34-3.37). Since no reaction was observed in the upper energy value, the tests were automatically terminated. As a consequence, both complexes were found to be resistant to impact.

Figure 3.33. Insertion of **1** into the roller

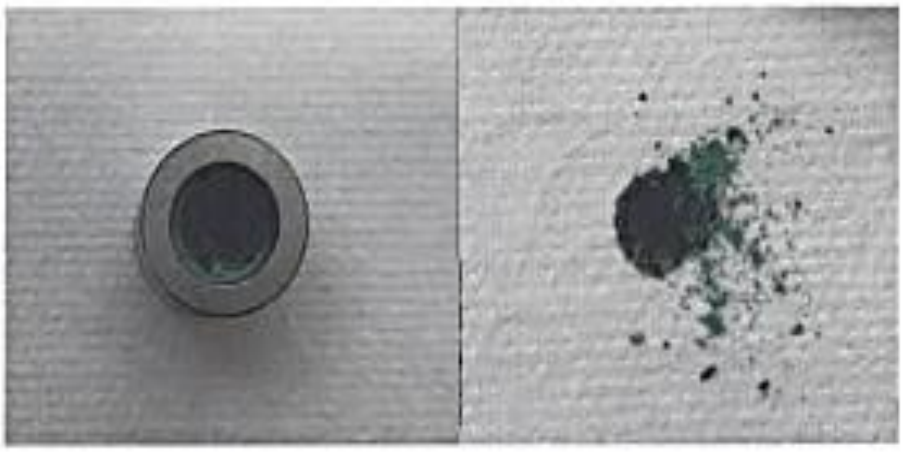

Figure 3.34. Negative reaction of **1** after dropping

Figure 3.35. Insertion of **2** into the roller

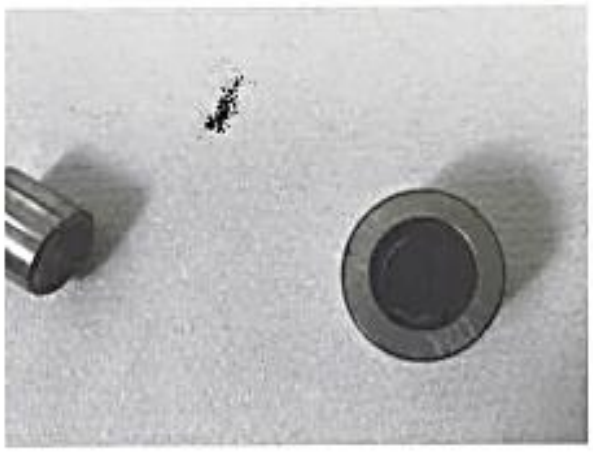

Figure 3.36. Negative reaction of **2** after dropping

3.5.3. Friction Sensitivity Tests

Friction sensitivity tests were carried out using a BAM friction test sensitivity device according to the EN-13631-3 standard procedure. The experiments were achieved firstly applying the highest load value (360 N) on a porcelain plate with a porcelain needle. A negative reaction was obtained for both complexes after 6 trials at 360 N (Figure 3.38 and Figure 3.39). Since no reaction was observed at the maximum load value, the tests were terminated. Consequently, both complexes were reported as insensitive to friction.

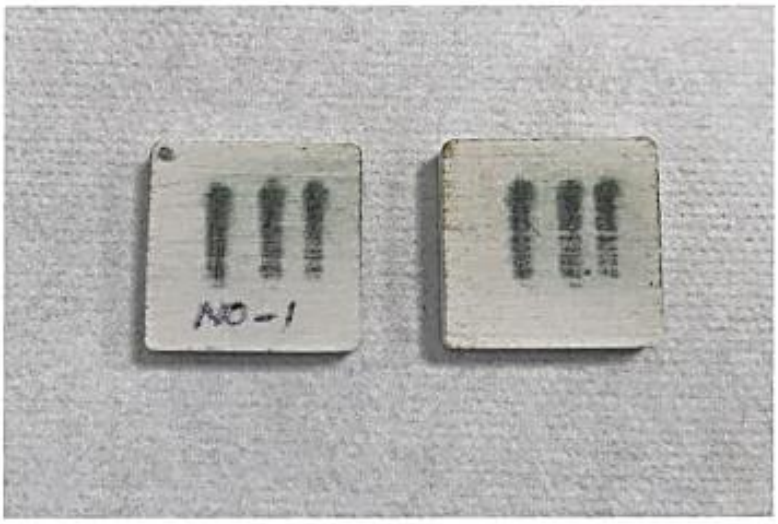

Figure 3.37. The image of **1** on the porcelain plate after the friction test

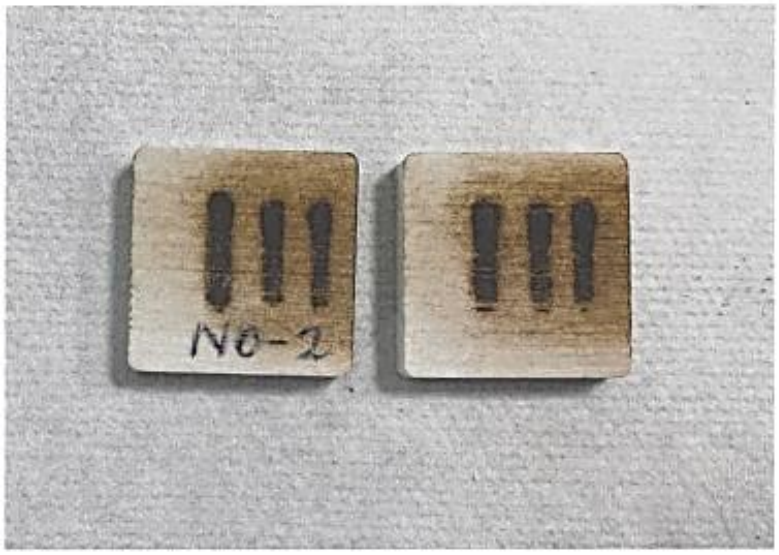

Figure 3.38. The image of **2** on the porcelain plate after the friction test

CHAPTER 4

4. CONCLUSIONS

In this study, nitro-imidazole-based new energetic materials were synthesized, characterized and tested for their thermal properties successfully. In this scope, 5-(chloronitromethyl)-4-nitro-1H-imidazole (HL) molecule and its sodium (NaL) and ammonium (NH_4L) salts were synthesized as a first time. After that, cobalt(II/III), copper(II), iron(II/III) and zinc(II) complexes of L^- having the general formula of $[M(NH_3)_x(L)_y]^n$ [x:0, 2-4; y:1, 2, 4 or 6; n:(+1)-(-4)] were designed and prepared in different geometries by using different counter ions such as Na^+, NH_4^+, PF_6, and CO_3^{2-} to neutralize the structure when needed. The analyses of the synthesized compounds were elucidated using elemental analysis, ESI-MS, IR, ^1H and ^{13}C NMR spectroscopic techniques. The symmetry optimized structures of HL and its derivatives as well as their explosive properties were completed earlier in a research project [1] of our group. As the theoretical calculations revealed that 6 L^- coordinated Co(II/III) and Fe(II/III) were unstable due to the steric effects, those complexes were not synthesized.

Thermal stability of HL, NaL and NH_4L was investigated by simultaneous TG-TA method. An endothermic decomposition process was obtained with a mass loss of 63.5% for HL, 10% for NaL and 42% for NH_4L between 171-239 ^oC. The higher endothermic peak temperature (239 ^oC) and enthalpy value required for the thermal degradation of NH_4L indicated its higher stability compared to HL and NaL. The remaining mass losses were complemented by an energy release at around 873-933 ^oC.

Thermal decomposition of HL and NH_4L were followed at different scan rates and the kinetic partameters were estimated applying the Kissinger method for both compounds. The results demonstrated that substituting NH_4^+ with H^+ ion in the ligand structure slightly decreased its activation energy.

The decomposition and critical explosion temperatures for HL and NH_4L were very close to each other for the exothermic process, while the enthalpy at the explosion temperature was found slightly higher for NH_4L (1169 kJ/mol) than that for HL (1078 kJ/mol). The logarithm of the pre-exponential factors (A) in the exothermic phase was obtained as 47.07 for HL and 51.39 for NH_4L. Similar activation energy and Log(A) values were also reported in the literature for some of the energetic materials [113]. The higher temperature of exothermic decomposition process for our compounds revealed their high stability and their higher potential to be used as additives in small amounts to alter the ballistic properties of composite propellants [104-105].

Based on the theoretically achieved explosive properties, heat of explosion was calculated as 653 kJ/mol (2.92 kJ/g) for HL and 683 kJ/mol (3.16 kJ/g) for NH_4L. The calculated heat of explosion values falls within the recommended range of 2.09 to 6.27 kJ/g for propellants [106]. The most important requirements to generate higher specific impulse are high heat of combustion and low molecular weight compounds. Since the heat of combustion is determined by the heat of formation of the propellant components, positive or low negative heat of formation is highly preferable [107]. In this work, our low molecular weight compounds having positive heat of formation values appropriately satisfy these requirements in line with the literature. Therefore, the new generation nitro-imidazole-based energetic compounds synthesized in this study exhibited a high potential to be used in propellant formulations due to their good explosive characteristics at high temperatures.

From the simultaneous TG-DSC curves, it was observed that all the complexes have similar decomposition properties and mass losses. Most of them are stable in the temperature range of 25-1200 ^oC and the percent mass losses are less than 30%. The most thermally stable compound was one of the Fe(II) complex, **11** as also verified by the results of theoretical calculations [1].

Among the metal complexes, **1, 2, 28, 31** and **32** showed exothermic decomposition behavior. This exothermic characteristic of the Co(II), Fe(II) and Cu(II) complexes is not only associated with the charge but also with the number of coordinated L^- (1 or 2) in their structures.

Additionally, impact and friction sensitivity test results for **1** and **2** suggested that the complexes were very resistant against to impact and insensitive to friction.

As a consiquence, the nitro-based energetic materials invastigated in this study were stable up to high temperatures with high exothermic energy values. Therefore, within the scope of this thesis, it can be said that novel energetic materials with the high detonation property and excellent safety performance have been successfully obtained. Thus, the contradiction between energy and sensitivity was able to bridge effectively. The result of our studies has shown that our compounds have high potential to be applied as propellants in rocket propellants propulsion systems and as additives to modify ballistic properties.

REFERENCES

[1] Tubitak Grant No 117Z391, Lead-Free New Generation Primer Explosive Design, Synthesis and Characterization, 2017-2022.

[2] K. Pomeranz and R. Wong, "China and Europe: 1500-2000 and Beyond: What is Modern". Published by Asia for Educators at Columbia University URL: http://afe. easia. columbia. edu/chinawh, November 29 (2007).

[3] G. Kerr, *A short history of China*. Harpenden, United Kingdom: Oldcastle Books, 2013.

[4] S. A. Takacs and E. H. Cline, *The Ancient World*. New York: Routledge, 2015.

[5] A. Bailey and S. Murray, *Explosives, propellants and pyrotechnics*. London: Brassey's, 1989.

[6] J. P. Agrawal, *High energy materials: propellants, explosives and pyrotechnics*. Weinheim, Germany: John Wiley & Sons, 2010.

[7] K. D. Oyler, "*Green primary explosives*". United Kingdom: John Wiley & Sons, 2014, pp. 103-132.

[8] N. Fischer, T. Klapötke, and J. Stierstorfer, "Calcium 5-Nitriminotetrazolate-A green replacement for lead azide in priming charges". *Journal of Energetic Materials*, vol. 29, pp. 61-74, 2011.

[9] O. Redddy, "Co-Precipitation Studies on Lead Azide with Tetrazole Derivatives-a search for lead azide substitute". *Propellants, Explosives, Pyrotechnics*, vol. 17, pp. 241-248, 1992.

[10] R. C. Ankony, *Lurps: A Ranger's Diary of Tet, Khe Sanh, A Shau, and Quang Tri*. America: Hamilton Books, 2008.

[11] T. L. Davis, *The chemistry of powder and explosives*. Kingston, Jamaica: Pickle Partners Publishing, 2016.

[12] P. W. Cooper, *Explosives engineering*. Toronto, New York: John Wiley & Sons, 2018.

[13] D. R. Gaskell, *Forensic investigation of explosions*. Bota Raton, Florida: CRC Press, 2011.

[14] J. Akhavan, *The chemistry of explosives*. United Kingdom: Royal Society of Chemistry, 2022.

[15] R. Meyer, J. Köhler, and A. Homburg, *Explosives*. Weinheim, Germany: John Wiley & Sons, 2016.

[16] J. Ledgard, *The Preparatory Manual of Explosives-a Laboratory Manual*. Columbus, Ohio: Paranoid Publications Group, 2003, pp. 81-82.

[17] M. Marshall, "Post-blast detection issues," in *Aspects of Explosives Detection*, Jimmie C. Oxley, London, United Kingdom: Elsevier, 2009, pp. 223-243.

[18] J. T. Thurman, *Practical bomb scene investigation*. Bota Raton, Florida: CRC Press, 2017.

[19] G. Baysinger *et al.*, *CRC handbook of chemistry and physics*, Bota Raton, Florida: CRC Press, 2015.

[20] W. Benenson, J. W. Harris, H. Stocker, and H. Lutz, *Handbook of physics*. New York: Springer, 2002.

[21] T. E. Ricks, *Fiasco: the American military adventure in Iraq*. London, United Kingdom: Penguin UK, 2007.

[22] M. A. Cook, *The science of high explosives*. Newyork: Reinhold Publishing Corporation, 1958.

[23] B. T. Fedoroff, *Encyclopedia of explosives and related items*. Dover, New Jersey: Picatinny Arsenal, 1960.

[24] R. Matyáš and J. Pachman, *Primary explosives*. Heidelberg, Germany: Springer, 2013.

[25] T. Urbanski, S. Laverton, W. Ornaf, *Chemistry and technology of explosives*. Oxford: Pergamon press, 1964.

[26] G. Manelis, *Thermal decomposition and combustion of explosives and propellants*. London, United Kingdom: Taylor & Francis, 2003.

[27] P. A. Persson, R. Holmberg, and J. Lee, *Rock blasting and explosives engineering*. Bota Raton, Florida: CRC press, 2018.

[28] N. Kubota, *Propellants and explosives: thermochemical aspects of combustion*. Weinheim, Germany: John Wiley & Sons, 2015.

[29] A. S. Shteinberg, *Fast reactions in energetic materials: high-temperature decomposition of rocket propellants and explosives*. Heidelberg, Germany: Springer Science & Business Media, 2008.

[30] J. P. Agrawal and R. Hodgson, *Organic chemistry of explosives*. Chichester, England and Hoboken, New Jersey: John Wiley & Sons, 2007.

[31] M. W. Beckstead, K. Puduppakkam, P. Thakre, V. Yang, "Modeling of combustion and ignition of solid-propellant ingredients" *Energy combustion Science,* vol. 33, pp. 497-551, 2007.

[32] G. Singh, *Recent advances on energetic materials*. New York: Nova Science Publishers, 2015, pp. 1-411.

[33] A. Mezroua, K. Khimeche, M. H. Lefebvre, M. Benziane, D. Trache, "The influence of porosity of ammonium perchlorate (AP) on the thermomechanical and thermal properties of the AP/polyvinylchloride (PVC) composite propellants". *Journal of Thermal Analysis Calorimetry.* vol. 116, pp. 279-286, 2014.

[34] D. Trache, F. Maggi, I. Palmucci, L. DeLuca, "Thermal behavior and decomposition kinetics of composite solid propellants in the presence of amide burning rate suppressants". *Journal of Thermal Analysis Calorimetry*, vol. 132, pp. 1601-1615, 2018.

[35] A. Dey, A. K. Sikder, M. B. Talawar, and S. Chottopadhyay, "Towards new directions in oxidizers/energetic fillers for composite propellants: an overview". *Central European Journal of Energetic Materials*, vol. 12, pp. 377-399, 2015.

[36] N. Kubota, "Combustion of energetic azide polymers". *Journal of Propulsion and Power*, vol. 11, pp. 677-682, 1995.

[37] D. Badgujar, M. Talawar, S. Asthana, and P. Mahulikar, "Advances in science and technology of modern energetic materials: an overview". *Journal of Hazardous Materials,* vol. 151, pp. 289-305, 2008.

[38] T. Archibald, R. Gilardi, K. Baum, and C. George, "Synthesis and x-ray crystal structure of 1, 3, 3-trinitroazetidine". *Journal of Organic Chemistry,* vol. 55, pp. 2920-2924, 1990.

[39] R. L. McKenney Jr *et al.*, "Synthesis and thermal properties of 1, 3-dinitro-3-(1′, 3′-dinitroazetidin-3′-yl) azetidine (TNDAZ) and its admixtures with 1, 3, 3-trinitroazetidine (TNAZ)". *Journal of Energetic Materials,* vol. 16, pp. 199-235, 1998.

[40] M. A. Hiskey, M. C. Johnson, and D. Chavez, "Preparation of 1-substituted-3, 3-dinitroazetidines". *Journal of Energetic Materials*, vol. 17, pp. 233-252, 1999.

[41] J. Zhang, R. Hu, C. Zhu, G. Feng, and Q. Long, "Thermal behavior of 1, 3, 3-trinitroazetidine". *Thermochimica acta*, vol. 298, pp. 31-35, 1997.

[42] M. Geetha *et al.*, "Studies on CL-20: the most powerful high energy material". *Journal of Thermal Analysis Calorimetry*, vol. 73, pp. 913-922, 2003.

[43] J. A. Conkling and C. J. Mocella, *Chemistry of pyrotechnics: basic principles and theory*. Bota Raton, Florida: CRC press, 2019.

[44] J. Donner, *A Professional's Guide to Pyrotechnics: Understanding and Making Exploding Fireworks*. Colorada, USA: Paladin Press, 1997.

[45] T. M. Klapötke, "2. Classification of Energetic Materials," in *Chemistry of High-Energy Materials*, 5th ed., Berlin, Germany: De Gruyter, 2019, pp. 55-124.

[46] J. Zhang, J. Zhou, F. Bi, and B. Wang, "Energetic materials based on poly furazan and furoxan structures". *Chinese Chemical Letters*, vol. 31, pp. 2375-2394, 2020.

[47] S. Zhang *et al.*, "High-energy metal–organic frameworks (HE-MOFs): Synthesis, structure and energetic performance". *Coordination Chemistry* Reviews, vol. 307, pp. 292-312, 2016.

[48] D. Herweyer, J. L. Brusso, and M. Murugesu, "Modern trends in “Green” primary energetic materials". *New Journal of Chemistry*, vol. 45, pp. 10150-10159, 2021.

[49] P. Yin and M. S. Jean'ne, "Nitrogen-rich azoles as high density energy materials: reviewing the energetic footprints of heterocycles" in *Advances in heterocyclic chemistry*, vol. 121, Eric F.V. Scriven, Christopher A. Ramsden, Elsevier, San Diego, United States: 2017, pp. 89-131.

[50] A. Katritzky, D. Cundy, and J. Chen, "Polyiodoimidazoles and their nitration products". *Journal of energetic materials*, vol. 11, pp. 345-352, 1993.

[51] S. Bulusu *et al.*, "Thermal rearrangement of 1, 4-dinitroimidazole to 2, 4-dinitroimidazole: characterization and investigation of the mechanism by mass spectrometry and isotope labeling". *Journal of Physical Chemistry*, vol. 99, pp. 5009-5015, 1995.

[52] A. J. Bracuti, "Crystal structure of 2, 4-dinitroimidazole (24DNI)". *Journal of chemical crystallography*, vol. 25, pp. 625-627, 1995.

[53] S. G. Cho, Y. G. Cheun, and B. S. Park, "A computational study of imidazole, 4-nitroimidazole, 5-nitroimidazole and 4, 5-dinitroimidazole". *Chemistry of Heterocyclic Compounds*, vol. 432, pp. 41-53, 1998.

[54] S. G. Cho, B. S. Park, and J. R. Cho, Explosives, Pyrotechnics, "Theoretical Studies on the Structure of 1, 2, 4, 5-Tetranitroimidazole". *Propellants, Explosives, Pyrotechnics*, vol. 24, pp. 343-348, 1999.

[55] R. P. Singh, H. Gao, D. T. Meshri, and J. Shreeve, "Nitrogen-rich heterocycles" *High Energy Density Materials*, vol 125, pp. 35-83, 2007.

[56] H. Jadhav, M. Talawar, R. Sivabalan, D. Dhavale, S. Asthana, and V. Krishnamurthy, "Synthesis, characterization and thermolysis studies on new derivatives of 2, 4, 5-trinitroimidazoles: Potential insensitive high energy materials". *Journal of Hazardous Materials*, vol. 143, pp. 192-197, 2007.

[57] P. Yin, J. Zhang, C. He, D. A. Parrish, and J. Shreeve, "Polynitro-substituted pyrazoles and triazoles as potential energetic materials and oxidizers". *Journal of Materials Chemistry A*, vol. 2, pp. 3200-3208, 2014.

[58] D. Cromer and C. Storm, "Structure of the diammonium salt of 4, 4', 5, 5'-tetranitro-2, 2'-biimidazole, $C_6N_8O_8$. $2NH_4$". *Acta Crystallographica Section C-Crystal Structure Communications*, vol. 46, pp. 1959-1960, 1990.

[59] S. Novikov, L. Khmel'nitskii, O. Lebedev, V. Sevast'yanova, and L. Epishina, "Nitration of imidazoles with various nitrating agents". *Chemistry of Heterocyclic Compounds*, vol. 6, pp. 465-469, 1970.

[60] P. Lian, L. Chen, D. Huang, and J. Wang, "Comment on 1-methyl-2, 4, 5-trinitroimidazole (MTNI), a meltcast explosive: synthesis and studies on thermal behavior in presence of explosive ingredients". *Journal of Energetic Materials*, vol. 38, pp. 1-3, 2021.

[61] S. Chaturvedi and P. Dave, "Solid propellants: AP/HTPB composite propellants". *Arabian Journal of Chemistry*, vol. 12, pp. 2061-2068, 2019.

[62] S. Chaturvedi, P. Dave, and N. Shah, "Applications of nano-catalyst in new era". *Journal of Saudi Chemical Society*, vol. 16, pp. 307-325, 2012.

[63] L. Meda, G. Marra, L. Galfetti, F. Severini and L. Luca, "Nano-aluminum as energetic material for rocket propellants". *Materials Science Engineering: C* vol. 27, pp. 1393-1396, 2007.

[64] J. C. Bottaro, P. E. Penwell, and R. Schmitt, "1, 1, 3, 3-Tetraoxo-1, 2, 3-triazapropene anion, a new oxy anion of nitrogen: the dinitramide anion and its salts". *Journal of the American Chemical Society*, vol. 119, pp. 9405-9410, 1997.

[65] P. Dendage, S. Asthana, and H. Singh, "Ecofriendly energetic oxidizer-hydrazinium nitroformate (HNF) and propellants based on HNF". *Journal of the Indian Chemical Society*, vol. 80, pp. 563-568, 2003.

[66] M. Frankel, L. Grant and J. Flanagan, "Historical development of glycidyl azide polymer". *Journal of Propulsion Power*, vol. 8, pp. 560-563, 1992.

[67] L. Galfetti *et al.*, "Pre and post-burning analysis of nano-aluminized solid rocket propellants". *Aerospace Science Technology*, vol. 11, pp. 26-32, 2007.

[68] W. H. Hsieh, A. Peretz, I. T. Huang, and K. Kuo, "Combustion behavior of boron-based BAMO/NMMO fuel-rich solid propellants". *Journal of Propulsion Power*, vol. 7, pp. 497-504, 1991.

[69] T. Miyazaki and N. Kubota, "Energetics of BAMO". *Propellants, explosives, pyrotechnics*, vol. 17, pp. 5-9, 1992.

[70] N. Kubota, K. Katoh, and G. Nakashita, "Combustion mechanism of GAP/AN propellants" in *22nd International Annual Conference on ICT*, Karlsruhe, Germany, 1991, pp. 41-49.

[71] M. A. Talukder and G. Lindsay, "Synthesis and the preliminary analysis of block copolymers of 3, 3′-bis (azidomethyl)-oxetane and 3-nitratomethyl-3′-methyloxetane". *Journal of Polymer Science Part A: Polymer Chemistry*, vol. 28, pp. 2393-2401, 1990.

[72] M. Golfier, H. Graindorge, Y. Longevialle, and H. Mace, "New energetic molecules and their applications in energetic materials", International Annual Conference-Fraunhofer Institut fur Chemische Technologie, Germany, 1998.

[73] L. De Luca *et al.*, "Burning of nano-aluminized composite rocket propellants". *Combustion, Explosion and Shock Waves*, vol. 41, pp. 680-692, 2005.

[74] M. H. V. Huynh, M. D. Coburn, T. J. Meyer, and M. Wetzler, "Green primary explosives: 5-Nitrotetrazolato-N_2-ferrate hierarchies". *Proceedings of the National Academy of Sciences of the United States of America*, vol. 103, pp. 10322-10327, 2006.

[75] S. Cudziło and M. Nita, "Synthesis and explosive properties of copper (II) chlorate (VII) coordination polymer with 4-amino-1, 2, 4-triazole bridging ligand". *Journal of hazardous materials*, vol. 177, pp. 146-149, 2010.

[76] M. A. Ilyushin, I. V. Tselinsky, and I. Shugalei, "Environmentally friendly energetic materials for initiation devices". *Central European Journal of Energetic Materials*, vol. 9, pp. 293-327, 2012.

[77] K. Karaghiosoff *et al.*, "1, 4-Diformyl-2, 3, 5, 6-Tetranitratopiperazine: A New Primary Explosive Based on Glyoxal". *Propellants, Explosives, Pyrotechnics*, vol. 28, pp. 1-6, 2003.

[78] D. Gidlow, "Lead toxicity". *Occupational medicine*, vol. 54, pp. 76-81, 2004.

[79] J. J. Sabatini and K. Oyler, "Recent advances in the synthesis of high explosive materials". *Crystals*, vol. 6, pp. 5, 2015.

[80] T. M. Klapötke, B. Krumm, and M. Scherr, "The binary silver nitrogen anion $[Ag(N_3)_2]$". *Journal of the American Chemical Society*, vol. 131, pp. 72-74, 2009.

[81] C. Hogstrand and C. Wood "Toward a better understanding of the bioavailability, physiology, and toxicity of silver in fish: implications for water quality criteria". *Environmental Toxicology and Chemistry*, vol. 17, pp. 547-561, 1998.

[82] D. Fischer, T. M. Klapötke, D. G. Piercey and J. Stierstorfer, "Copper salts of halo tetrazoles: Laser-ignitable primary explosives". *Journal of Energetic Materials*, vol. 30, pp. 40-54, 2012.

[83] M. H. V. Huynh, M. A. Hiskey, T. J. Meyer, and M. Wetzler, "Green primaries: Environmentally friendly energetic complexes". *Proceedings of the National Academy of Sciences of the United States of America*, vol. 103, pp. 5409-5412, 2006.

[84] J. W. Fronabarger, M. D. Williams, W. B. Sanborn, J. G. Bragg, D. A. Parrish, and M. J. P. Bichay, explosives, pyrotechnics, "DBX-1–A Lead Free Replacement for Lead Azide". *Propellants, Explosives, Pyrotechnics*, vol. 36, pp. 541-550, 2011.

[85] J. W. Fronabarger, J. B. Pattison and M. Williams, "Alternatives to Existing Primary Explosives". *International Journal of Energetic Materials Chemical Propulsion*, vol. 20, pp. 65-79, 2021.

[86] T. M. Klapötke *et al.*, "Preparation of High Purity Sodium 5-Nitrotetrazolate (NaNT): An Essential Precursor to the Environmentally Acceptable Primary Explosive, DBX-1". *Zeitschrift für anorganische und allgemeine Chemie*, vol. 639, pp. 681-688, 2013.

[87] D. Sundaram, V. Yang and R. Yetter, "Metal-based nanoenergetic materials: synthesis, properties, and applications". *Progress in Energy and Combustion Science*, vol. 61, pp. 293-365, 2017.

[88] S. Sinha, "Coordination compounds as potential explosives". *Advanced Scientific Research*, vol. 3, pp 8-10, 2018

[89] Q. Zhang *et al.*, "Access to green primary explosives via constructing coordination polymers based on bis-tetrazole oxide and non-lead metals". *Green Chemistry*, vol. 21, pp. 1947-1955, 2019.

[90] M. H. Wurzenberger, M. S. Gruhne, M. Lommel, and J. Stierstorfer, "1-Amino-5-methyltetrazole in Energetic 3d Transition Metal Complexes–Ligand Design for Future Primary Explosives". *Propellants, Explosives, Pyrotechnics* vol. 46, pp. 207-213, 2021.

[91] D. L. Naud, M. A. Hiskey, and H. Harry, "Synthesis and Explosive Properties of 5, 5′-Dinitro-3, 3′-azo-1 H-1, 2, 4-triazole (DNAT)". *Journal of Energetic Materials*, vol. 21, pp. 57-62, 2003.

[92] J. R. Cho, K. J. Kim, S. G. Cho, and J. Kim, "Synthesis and characterization of 1-methyl-2, 4, 5-trinitroimidazole (MTNI)". *Journal of Heterocyclic Chemistry*, vol. 39, pp. 141-147, 2002.

[93] J. Suwiński and K. Świerczek, "Synthesis and mass spectra of labelled 4 (5)-nitro-1H-imidazole-5 (4)-carbonitriles". *Journal of Labelled Compounds Radiopharmaceuticals*, vol. 45, pp. 795-801, 2002.

[94] O. Bortolini, S. Campestrini, F. Di Furia, G. Modena, and G. Valle, "Metal catalysis in oxidation by peroxides. 27. Anionic molybdenum-picolinate N-oxido-peroxo complex: an effective oxidant of primary and secondary alcohols in nonpolar solvents". *The Journal of Organic Chemistry*, vol. 52, pp. 5467-5469, 1987.

[95] R. M. Silverstein, G. C. Bassler and T. C. Morrill, *Spectrometric identification of organic compounds*. New York: Wiley, 1991, pp 1-430.

[96] D. A. Skoog, F. J. Holler, and S. R. Crouch, *Principles of instrumental analysis*. Belmont, USA: Cengage learning, 2017.

[97] R. S. Drago, *Physical methods in inorganic chemistry*. New York: Reinhold Publishing Corporation, 1966.

[98] H. Kissinger, "Variation of peak temperature with heating rate in differential thermal analysis". *Journal of Research of the National Bureau of Standards*, vol. 57, pp. 217-221, 1956.

[99] R. J. O. Drago, *Physical Methods for Chemists*. Philadelphia: Saunders College Publishing, 1992.

[100] M. D. Walter, M. Schultz, and R. Andersen, "Weak paramagnetism in compounds of the type Cp′ 2 Yb (bipy)". *New Journal of Chemistry*, vol. 30, pp. 238-246, 2006.

[101] I. Bertini and C. Luchinat, *NMR of paramagnetic substances*. Amsterdam: Elsevier, 1997

[102] L. Banci, I. Bertini and C. Luchinat, *Nuclear and electron relaxation. The magnetic nucleus-unpaired electron coupling in solution*. Weinheim: Elsevier, 1993.

[103] H. E. Gottlieb, V. Kotlyar, and A. Nudelman, "NMR chemical shifts of common laboratory solvents as trace impurities". *Journal of Organic Chemistry*, vol. 62, pp. 7512-7515, 1997.

[104] Z. He, Z. Xia, J. Hu, L. Ma and Y. Li, "Thermal decomposition and kinetics of electrically controlled solid propellant through thermogravimetric analysis". *Journal of Thermal Analysis and Calorimetry*, vol. 139, pp. 2187-2195, 2020.

[105] A. Pivkina, D. Meerov, K. Monogarov, Y. V. Frolov and N. Muravyev "Prospects of Using Boron Powders As Fuel. II. Influence of Aluminum and Magnesium Additives and Their Compounds on the Thermal Behavior of Boron Oxide". *Combustion Explosion and Shock Waves*, vol. 56, pp. 148-155, 2020.

[106] R. A. Meyers, *Encyclopedia of physical science and technology*. San Diago: Academic Press, 2002.

[107] S. Jain, "Solid propellant binders". *Journal of Scientific & Industrial Research*, vol 11, pp. 899-911, 2002.

APPENDICES

Appendix 1. ESI-MS Analysis Results

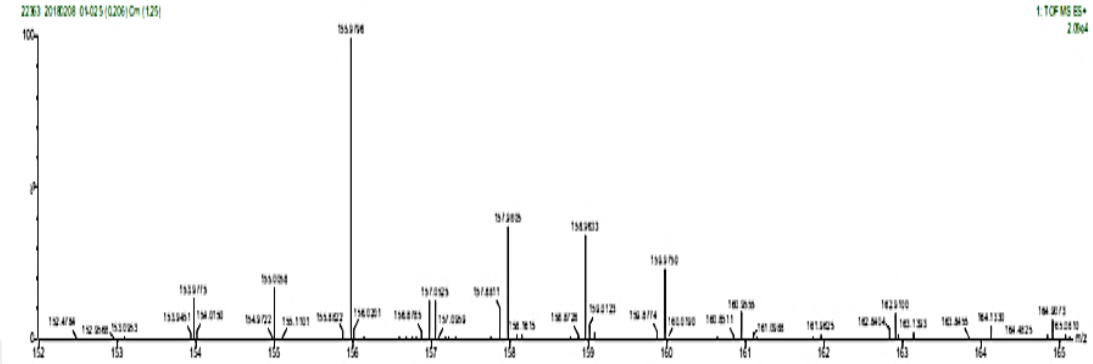

Figure A1.1. Mass spectrum of 1,4-Dinitro-1H-imidazole

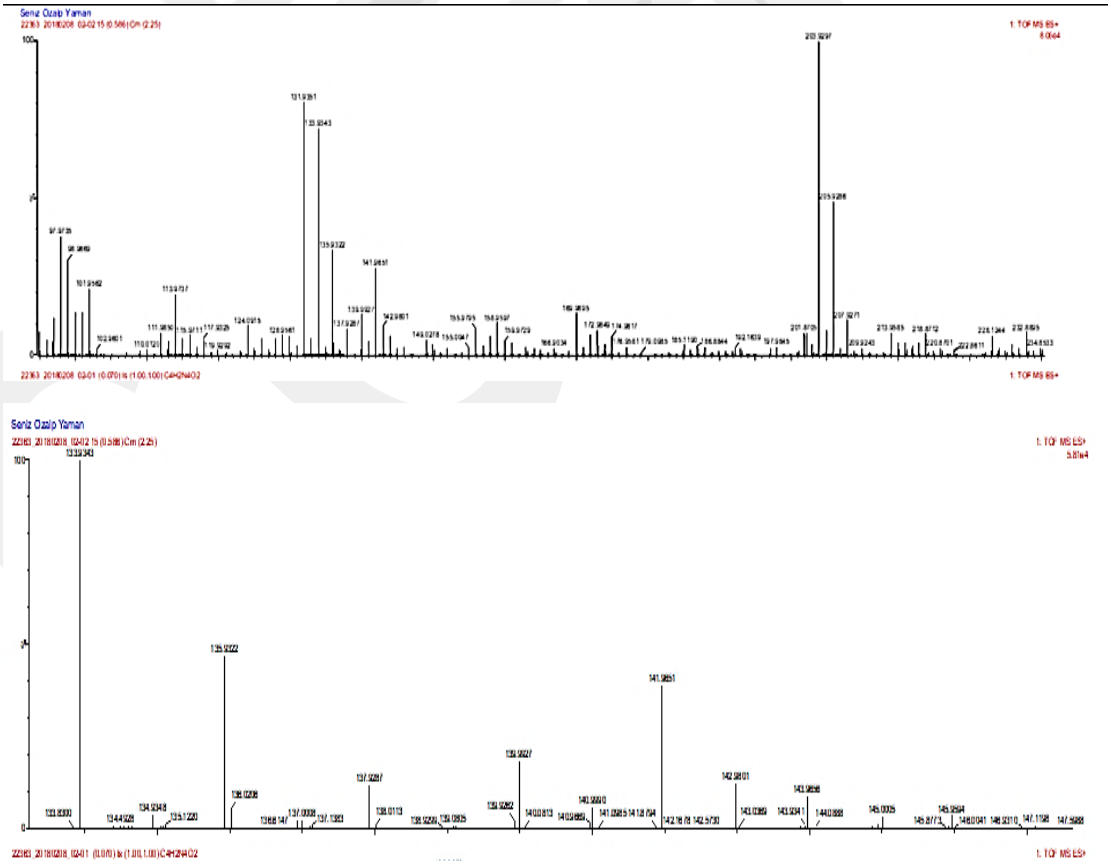

Figure A1.2. Mass spectrum of 2,4-dinitro-1H-imidazole-5-carbonitrile

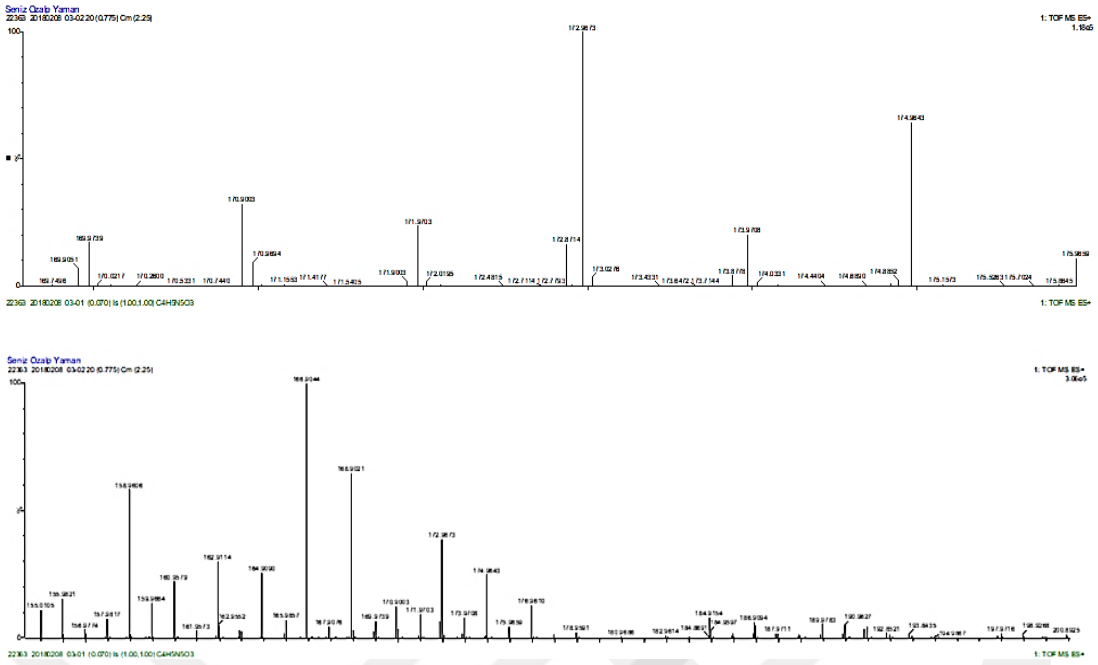

Figure A1.3. Mass spectrum of N'-hydroxy-4-nitro-1H-imidazole-5 carboxamidine

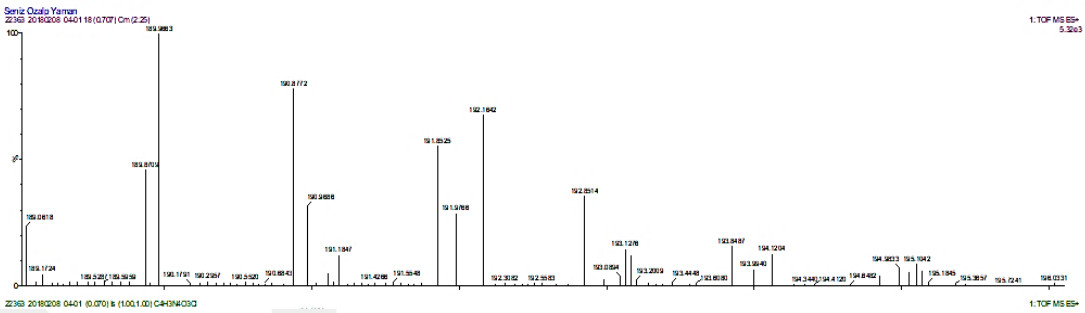

Figure A1.4. Mass spectrum of 4-nitro-1H-imidazole-5-carbonyl chloride

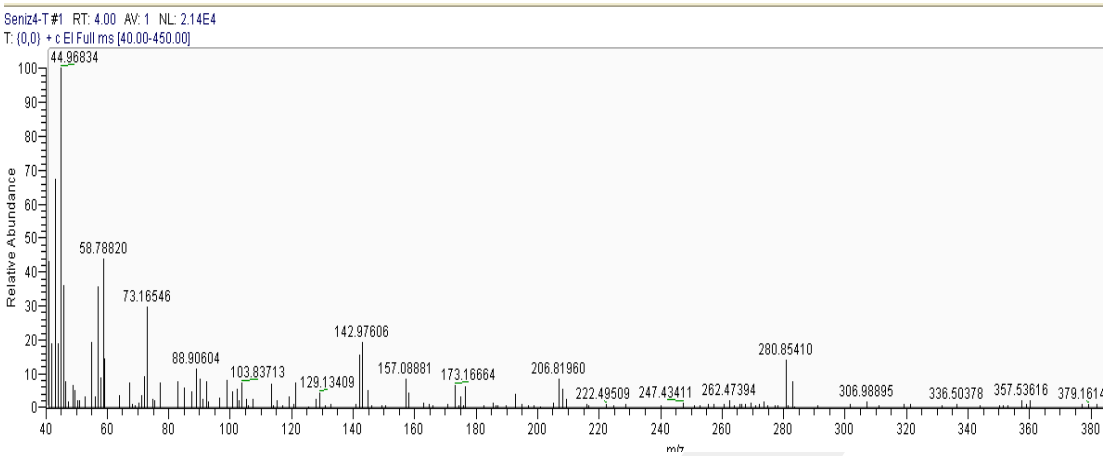

Figure A1.5. Mass spectrum of 5-(chloronitromethyl)-4-nitro-1H-imidazole

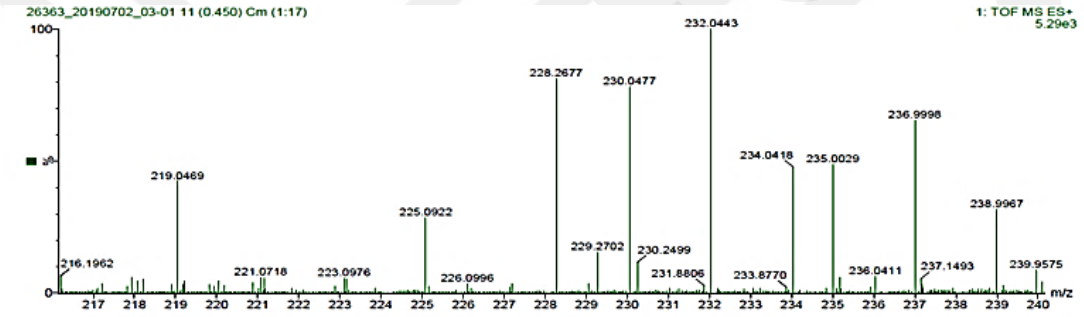

Figure A1.6. Mass spectrum of ammonium salt of 5-(chloronitromethyl)-4-nitro-1H-imidazole

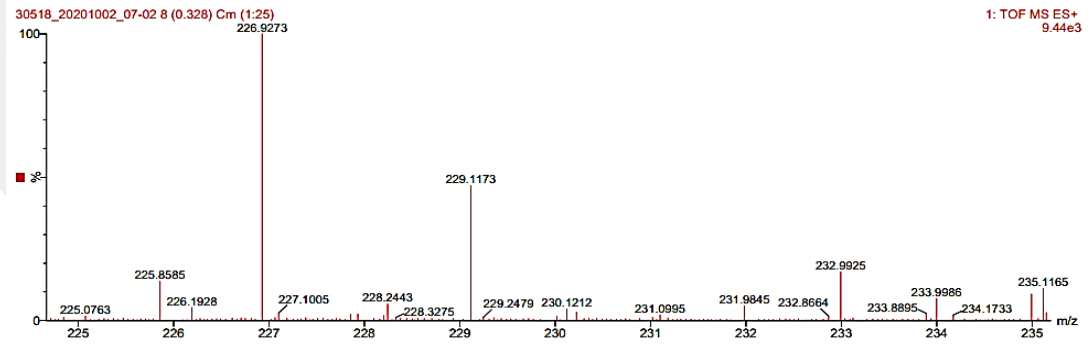

Figure A1.7. Mass spectrum of sodium salt 5-(chloronitromethyl)-4-nitro-1H imidazole

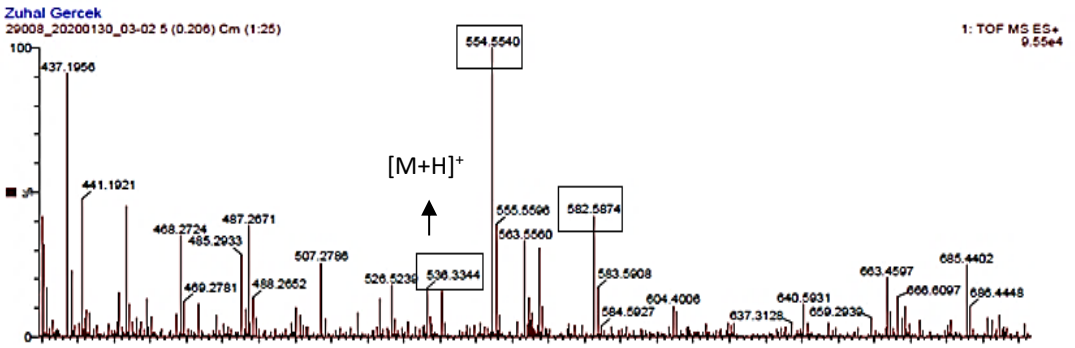

Figure A1.8. Mass spectrum of complex **2**

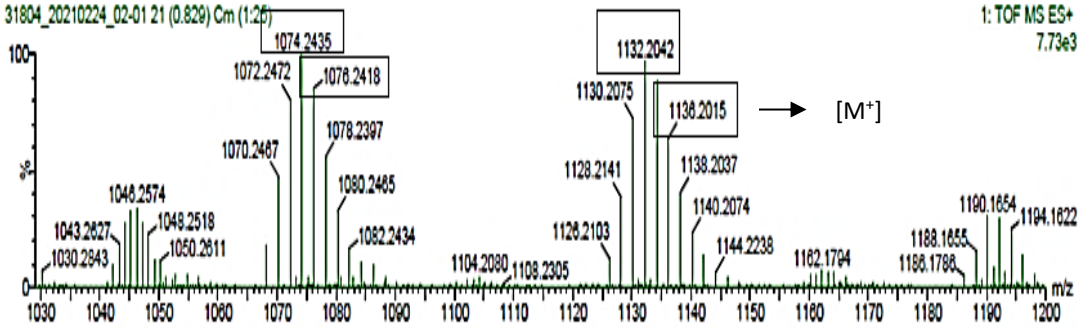

Figure A1.9. Mass spectrum of complex **4**

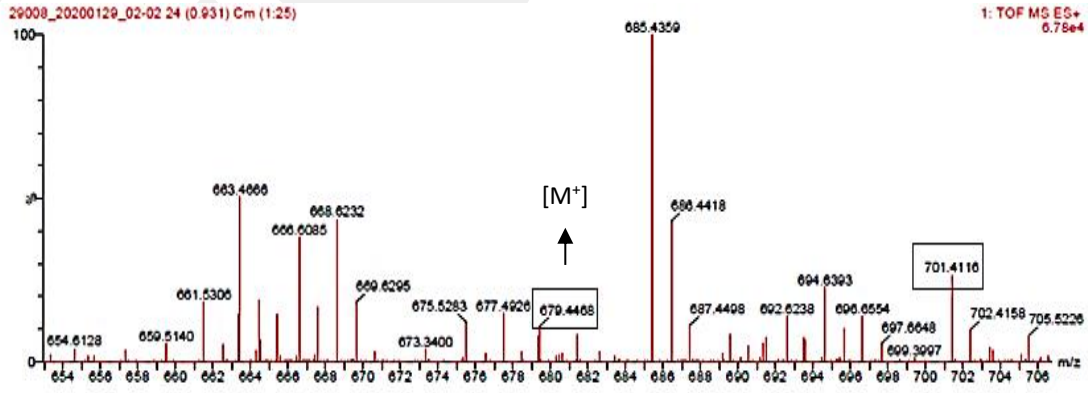

Figure A1.10. Mass spectrum of complex **5**

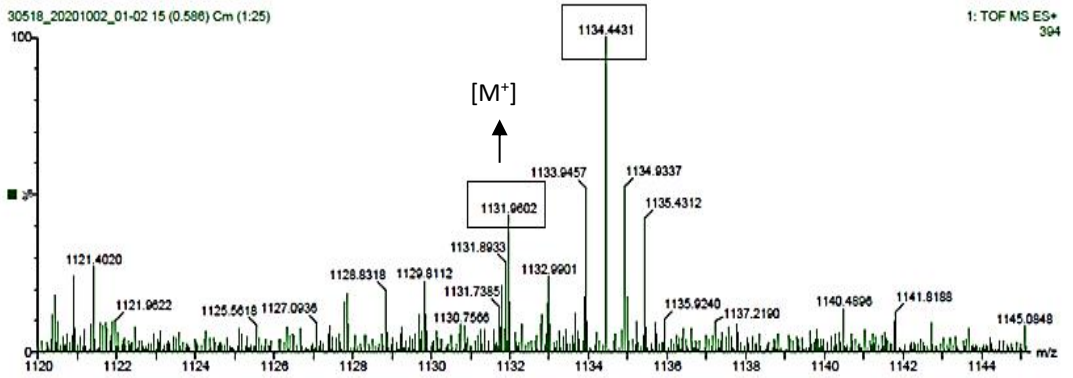

Figure A1.11. Mass spectrum of complex **6**

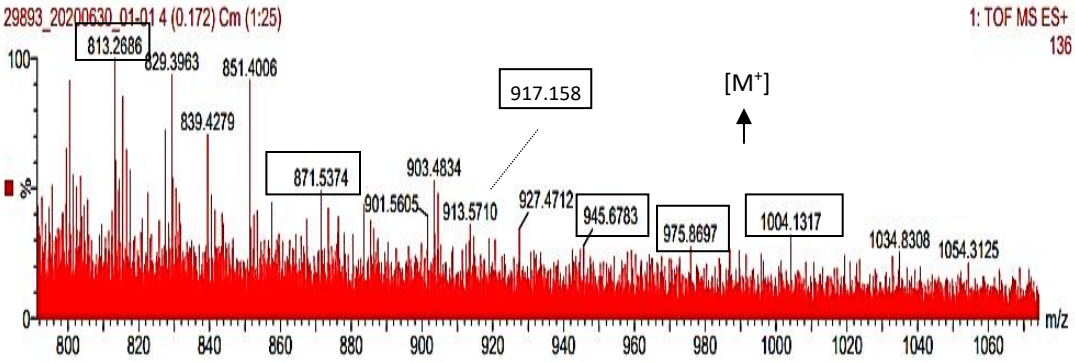

Figure A1.12. Mass spectrum of complex **7**

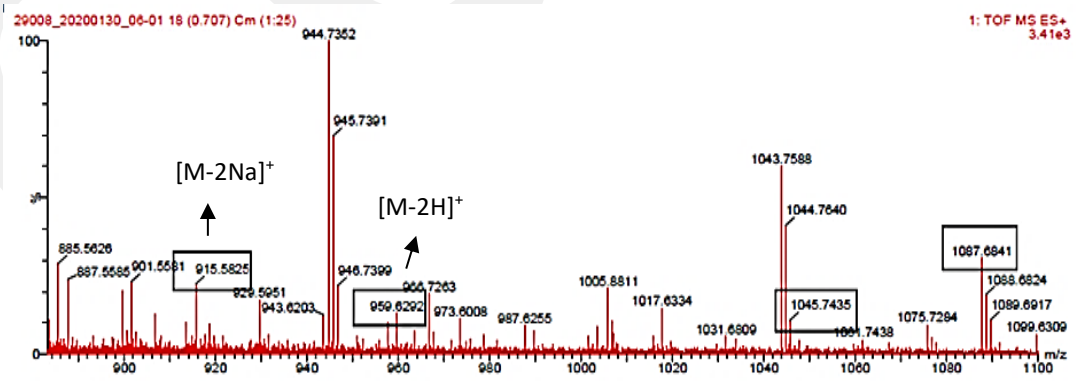

Figure A1.13. Mass spectrum of complex **8**

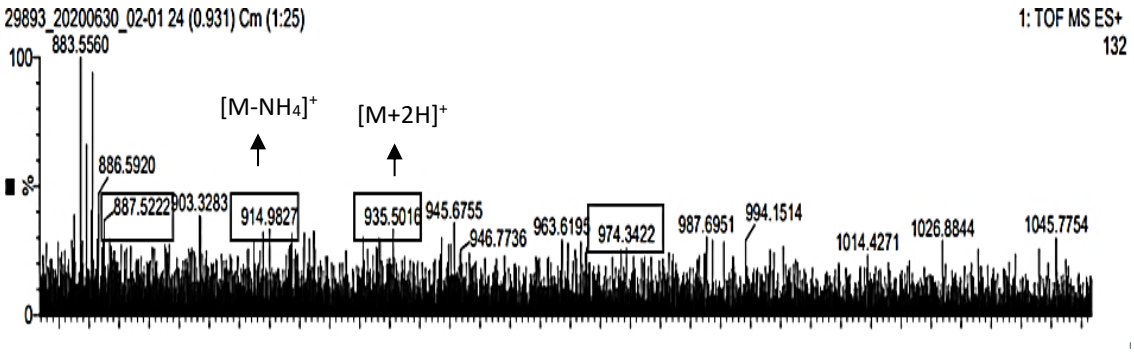

Figure A1.14. Mass spectrum of complex **9**

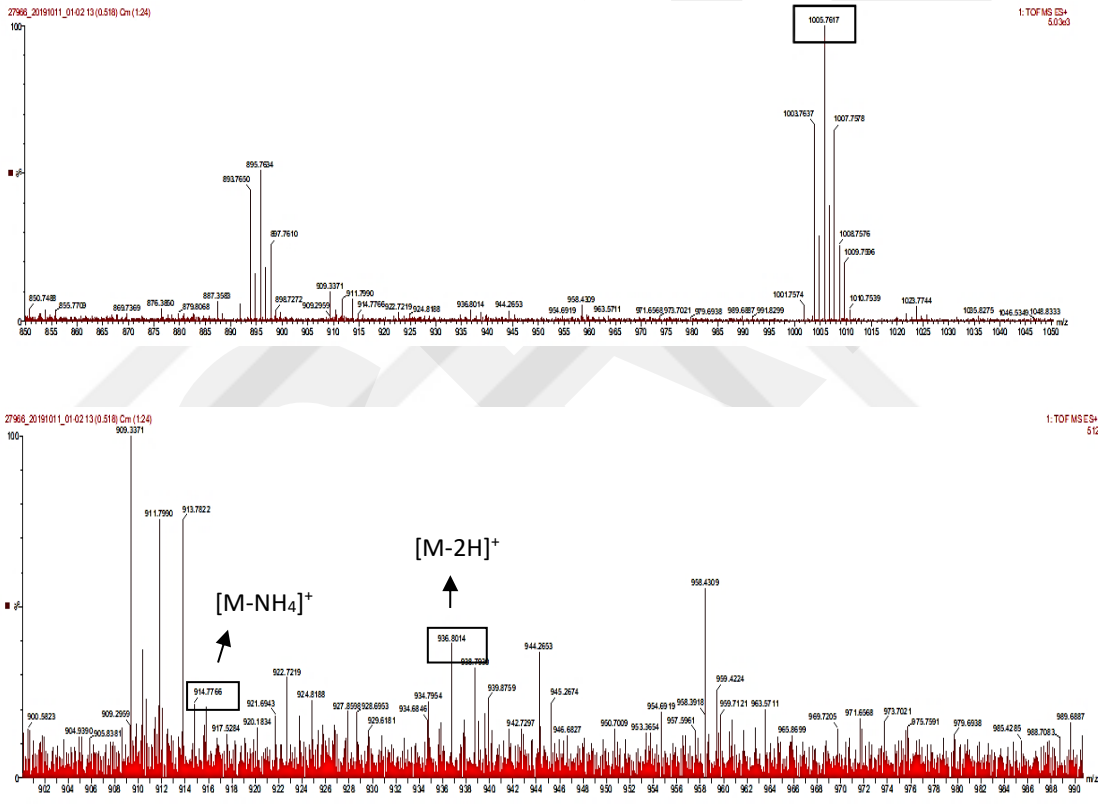

Figure A1.15. Mass spectrum of complex **10**

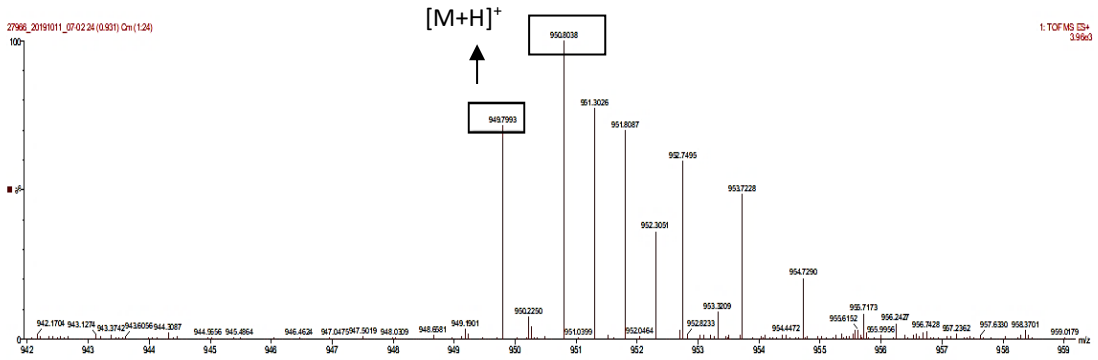

Figure A1.16. Mass spectrum of complex **11**

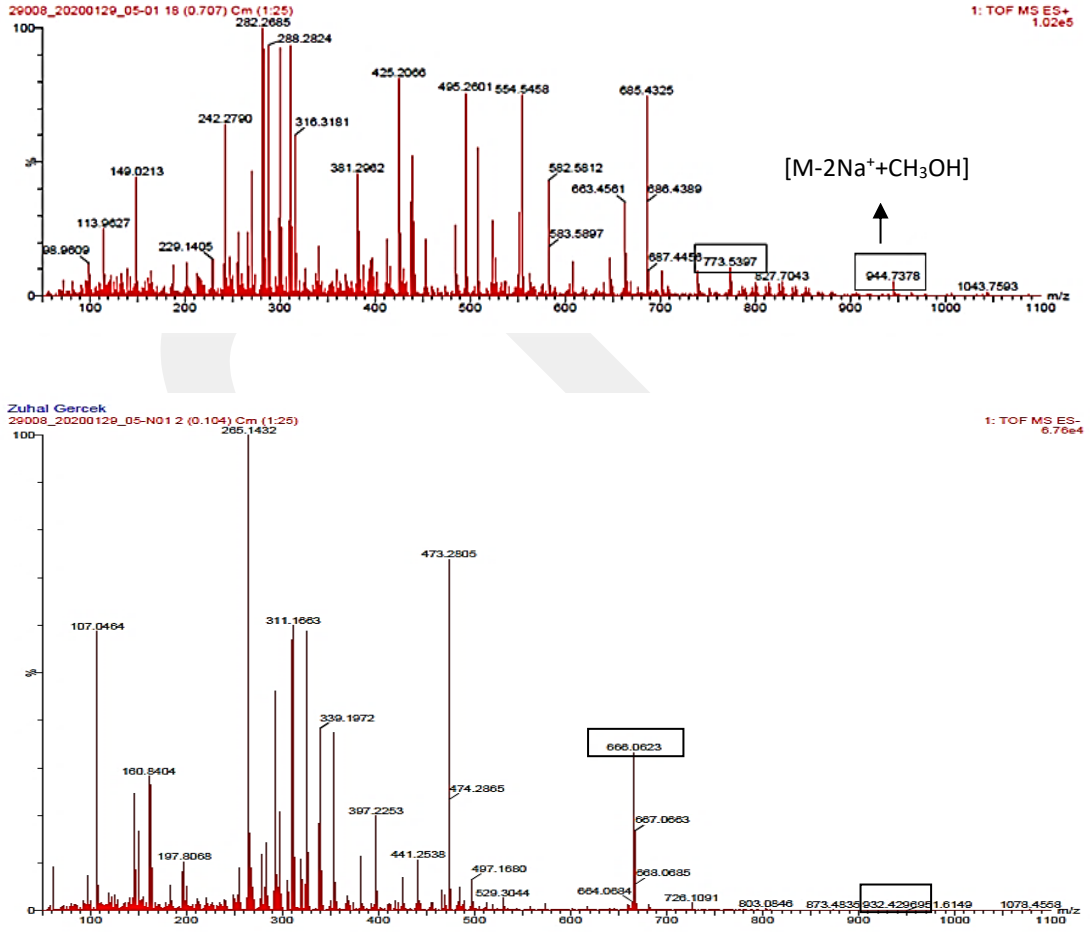

Figure A1.17. Mass spectrum of complex **12**

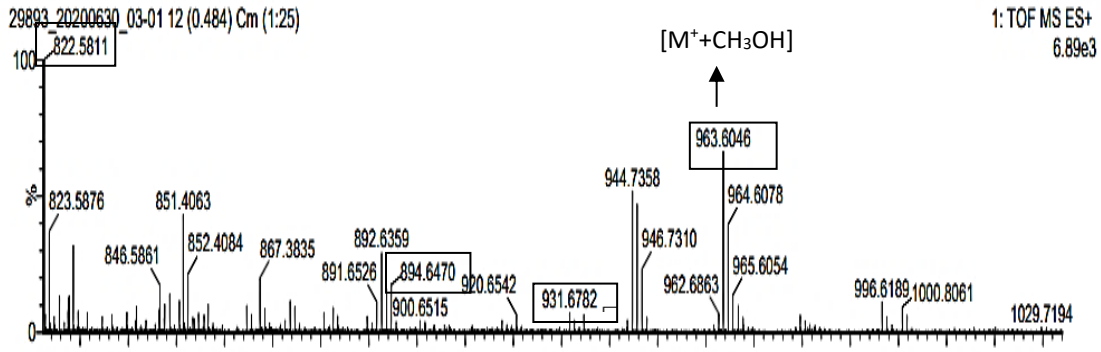

Figure A1.18. Mass spectrum of complex **13**

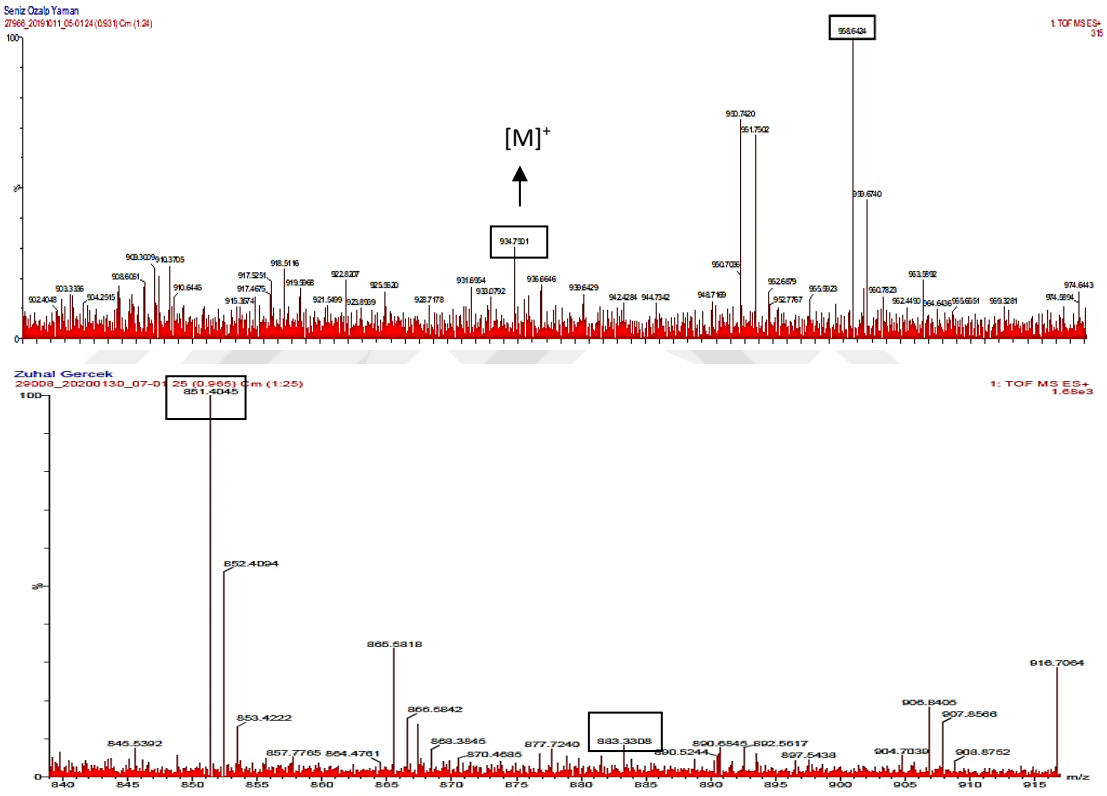

Figure A1.19. Mass spectrum of complex **14**

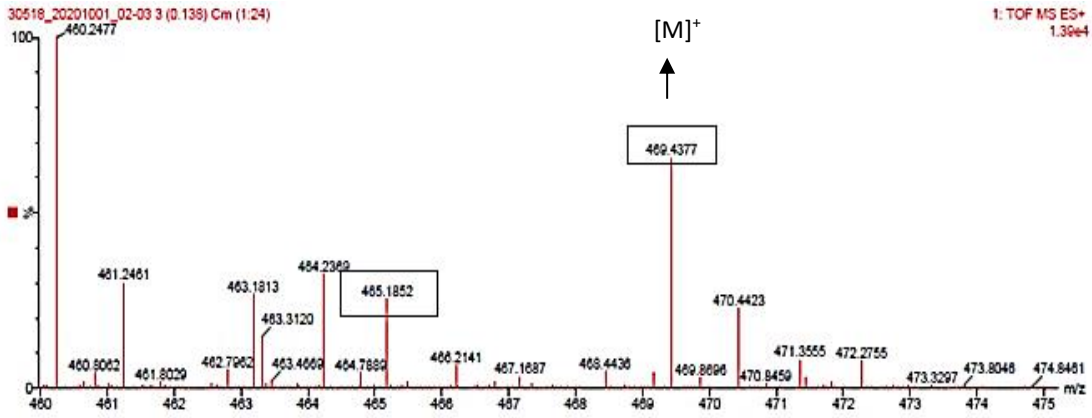

Figure A1.20. Mass spectrum of complex **23**

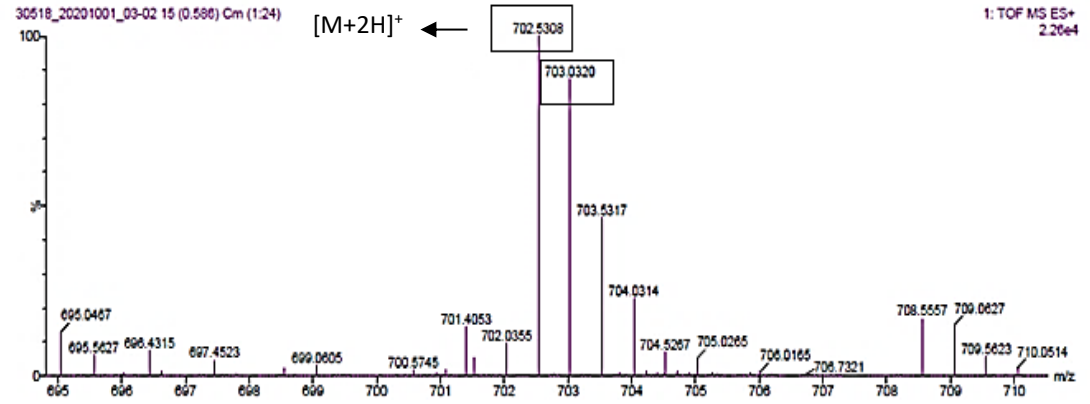

Figure A1.21. Mass spectrum of complex of **24**

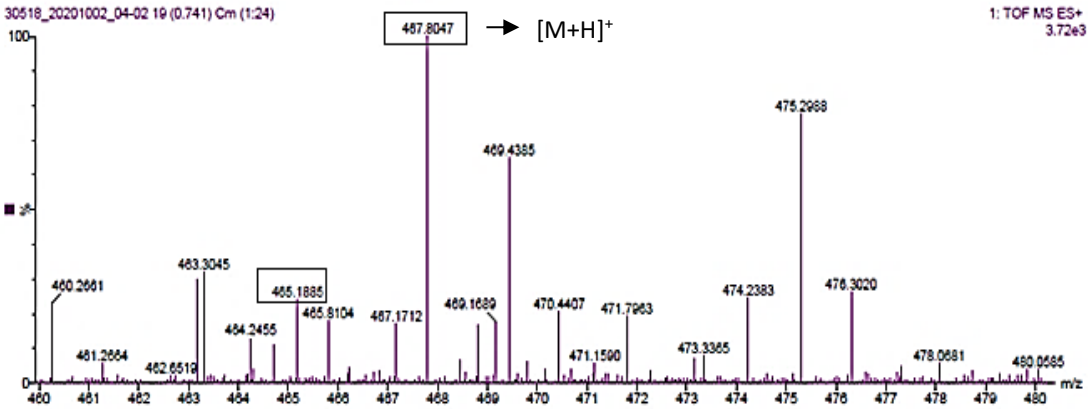

Figure A1.22. Mass spectrum of complex **25**

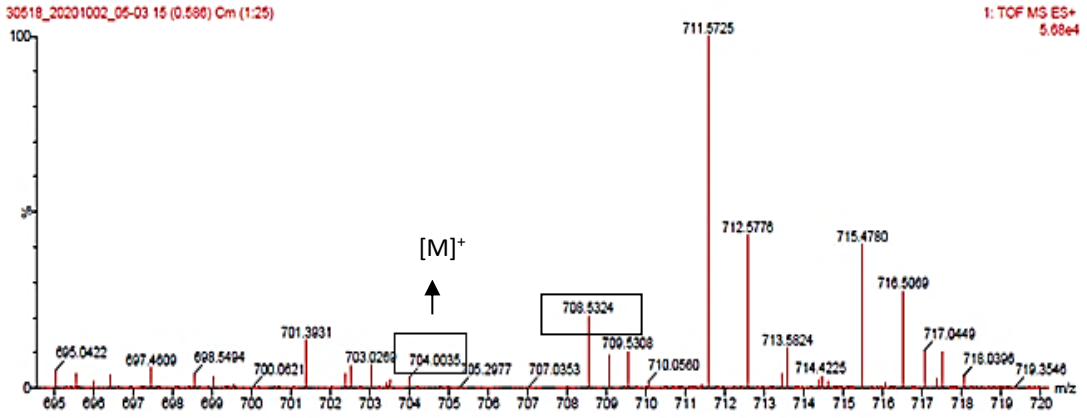

Figure A1.23. Mass spectrum of complex **26**

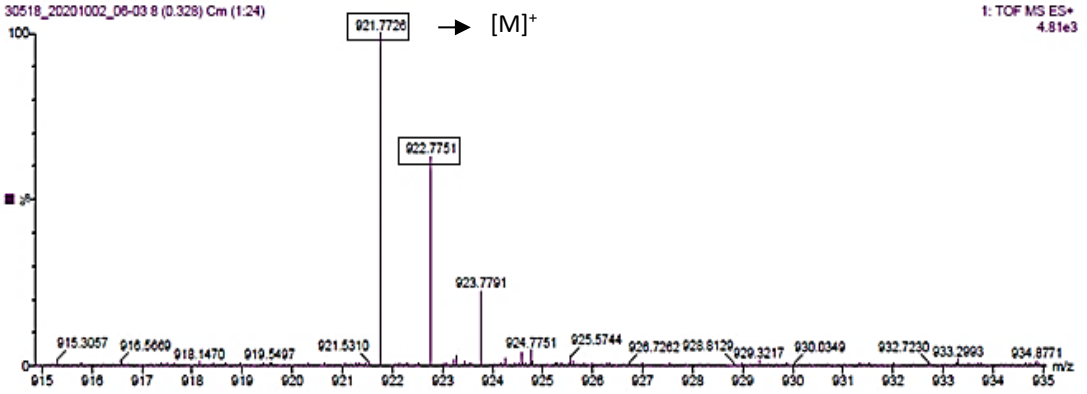

Figure A1.24. Mass spectrum of complex **27**

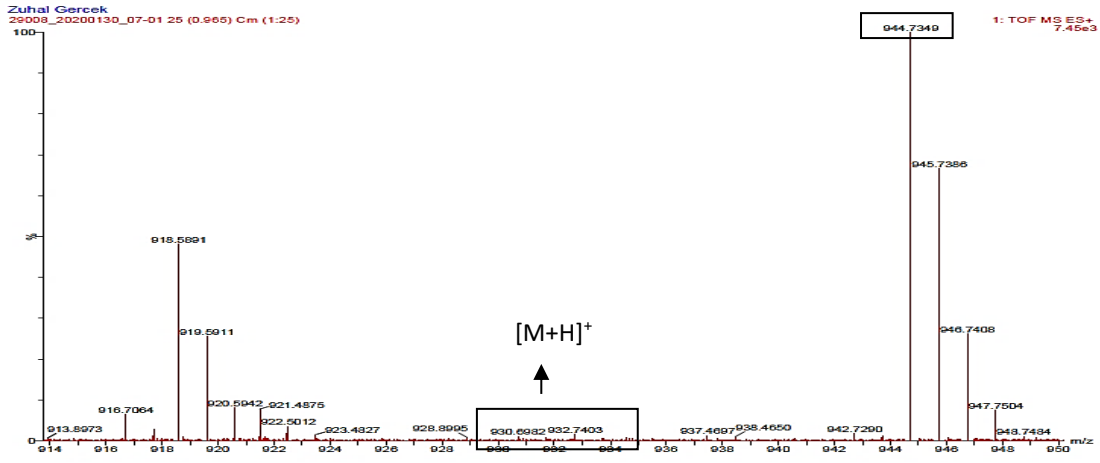

Figure A1.25. Mass spectrum of complex **28**

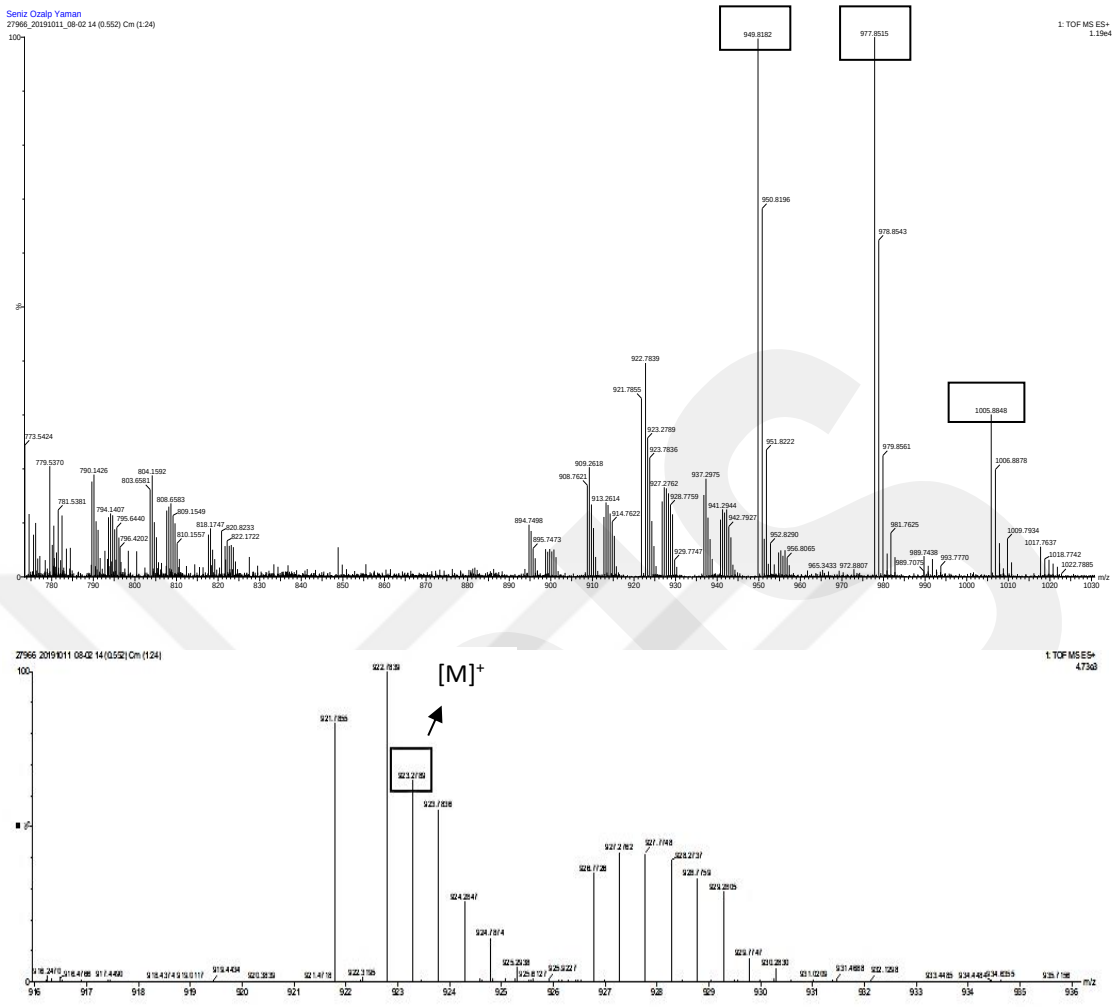

Figure A1.26. Mass spectrum of complex **29**

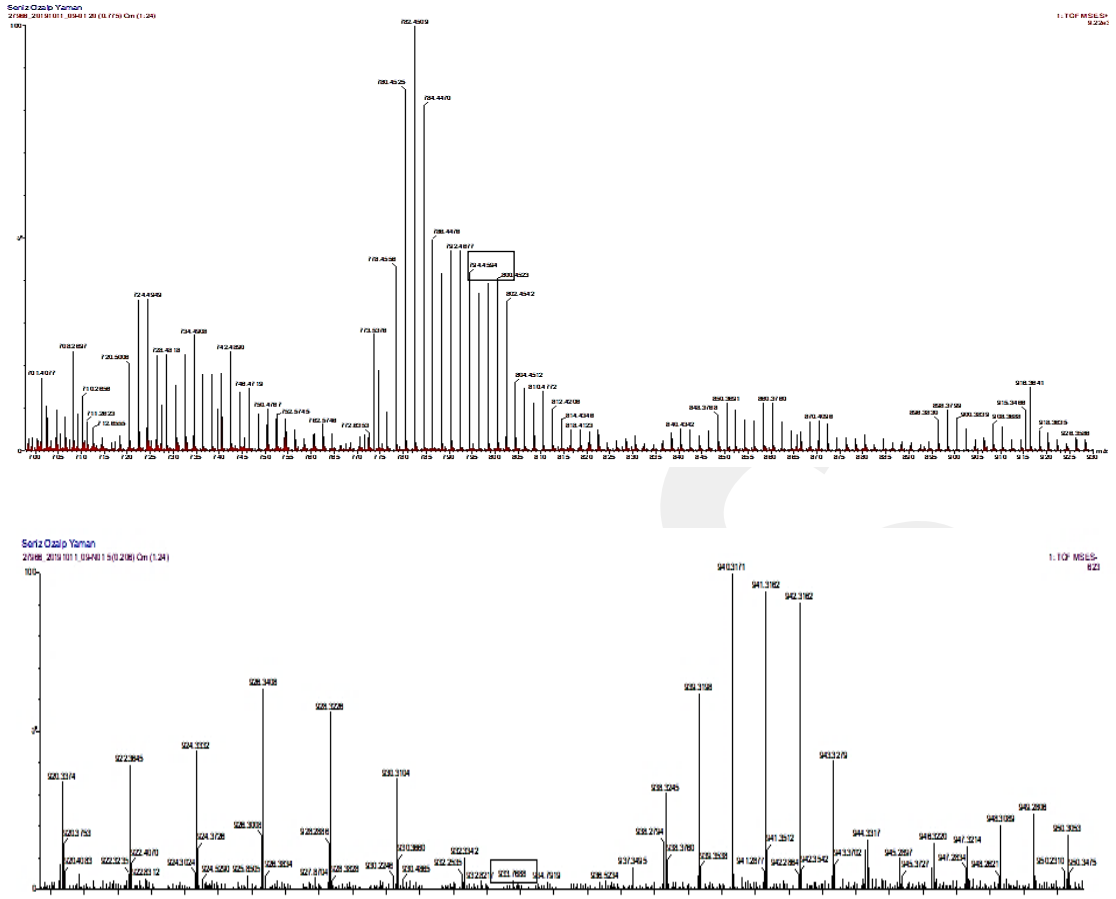

Figure A1.27. Mass spectrum of complex **30**

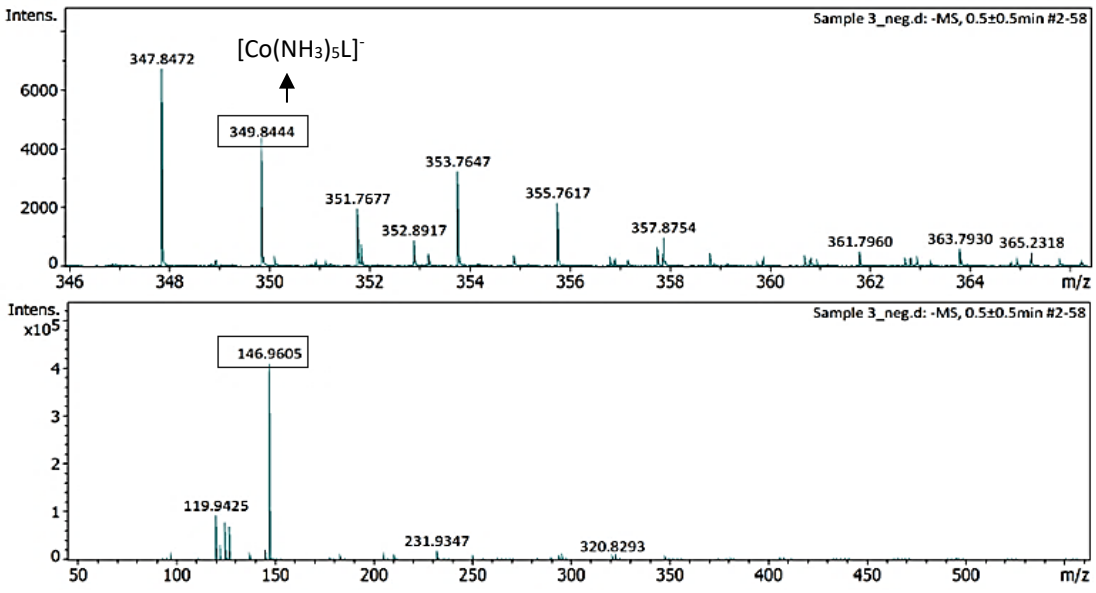

Figure A1.28. Mass spectrum of complex **31**

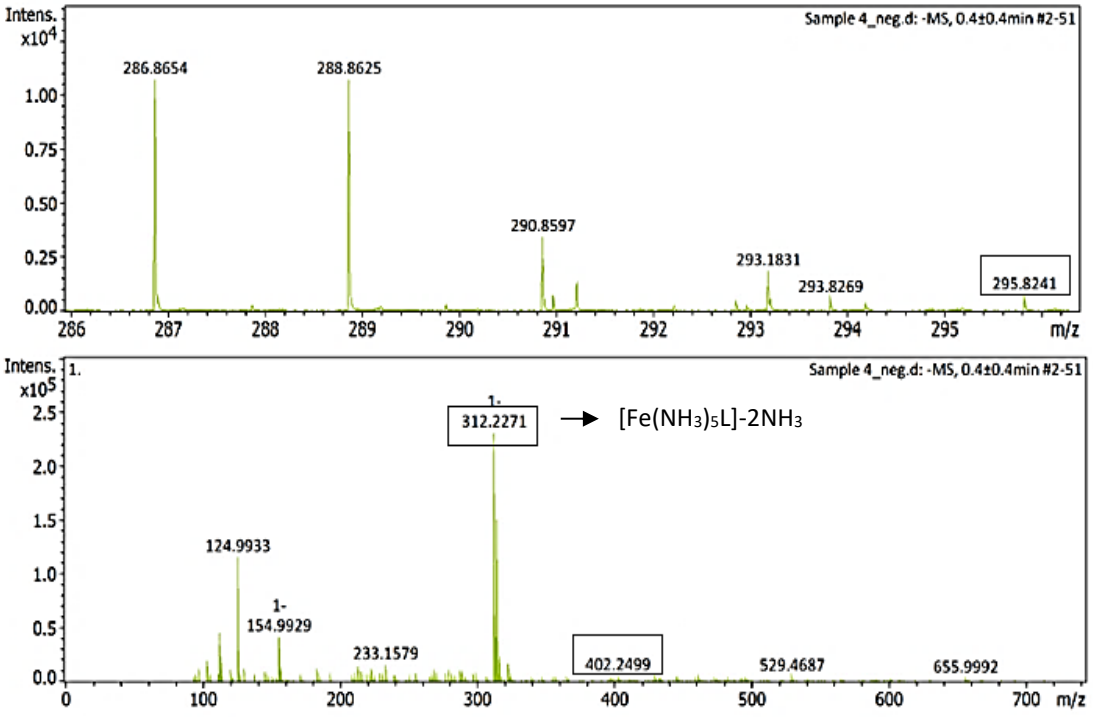

Figure A1.29. Mass spectrum of complex **32**

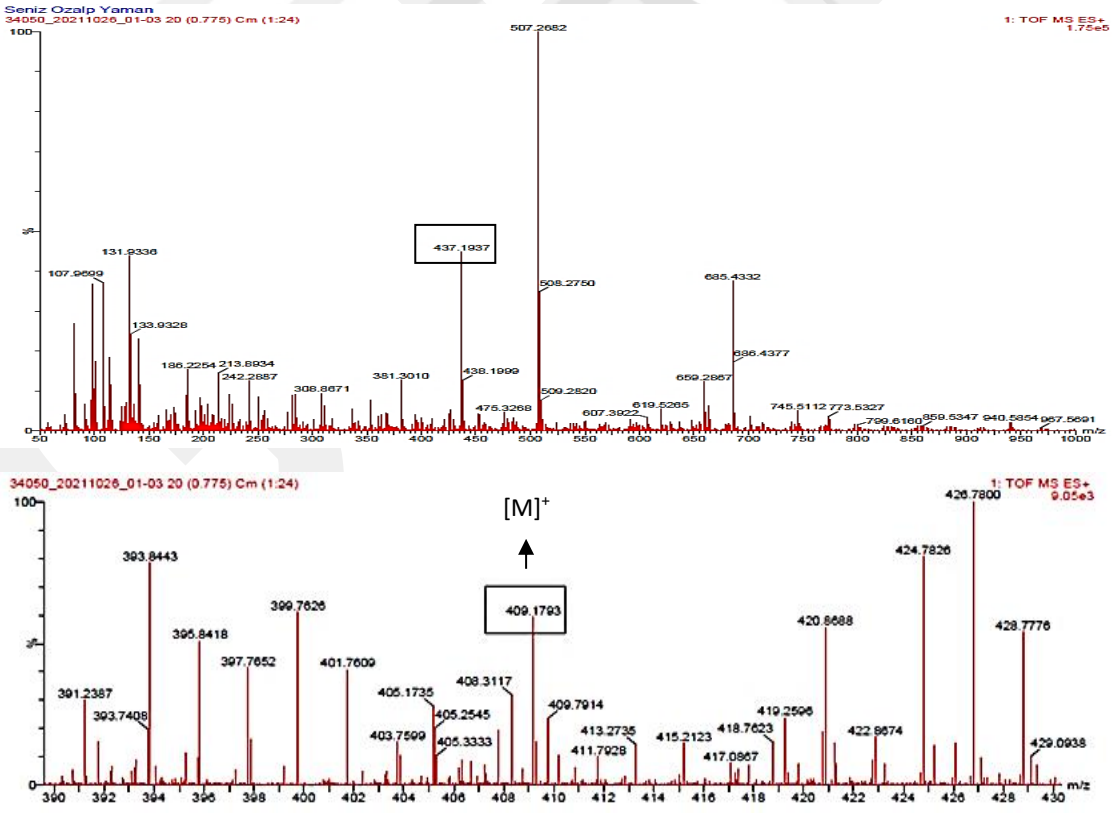

Figure A1.30. Mass spectrum of complex **33**

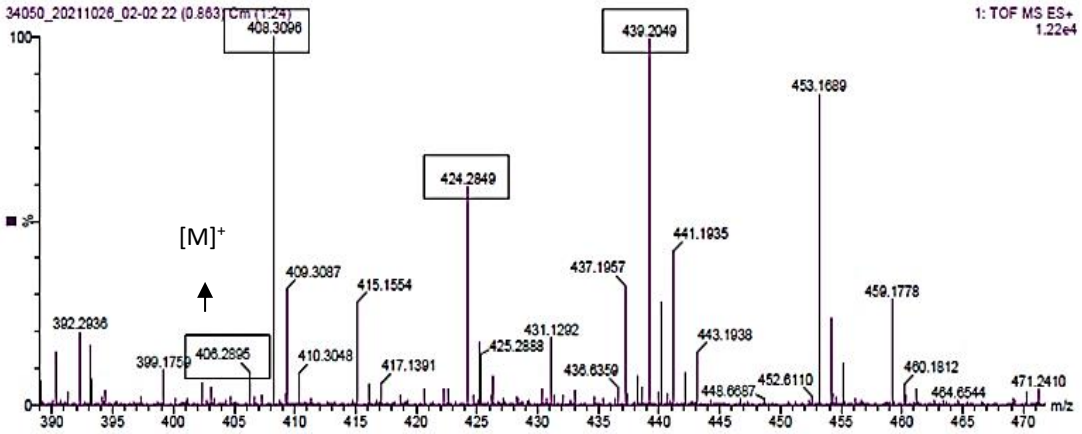

Figure A1.31. Mass spectrum of complex **34**

Appendix 2. FTIR Analysis Results

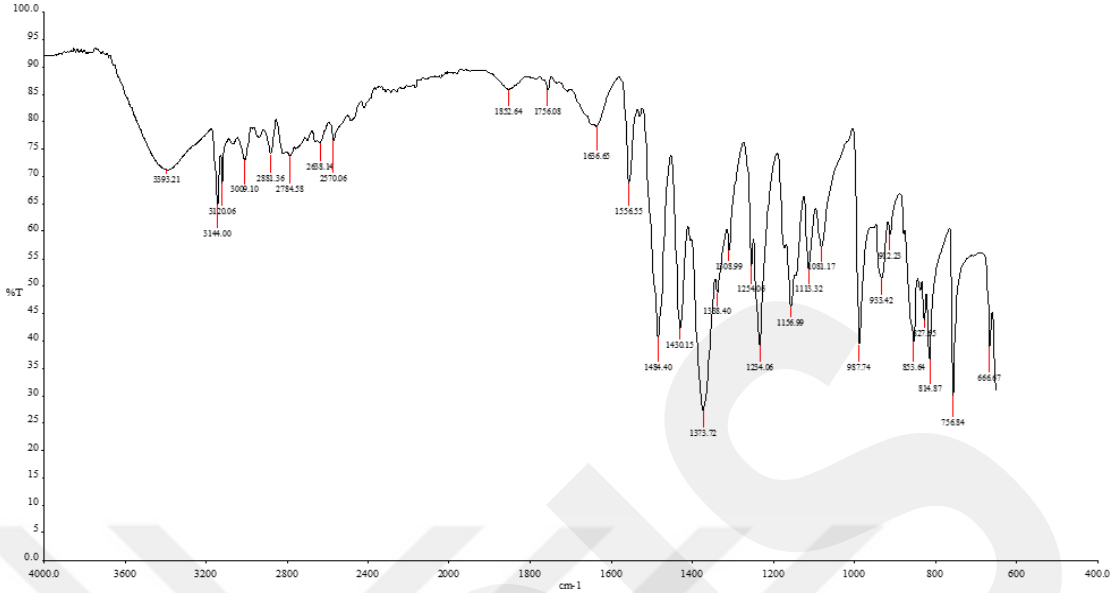

Figure A2.1. FTIR spectrum of N'-hydroxy-4-nitro-1H-imidazole-5 carboxamidine

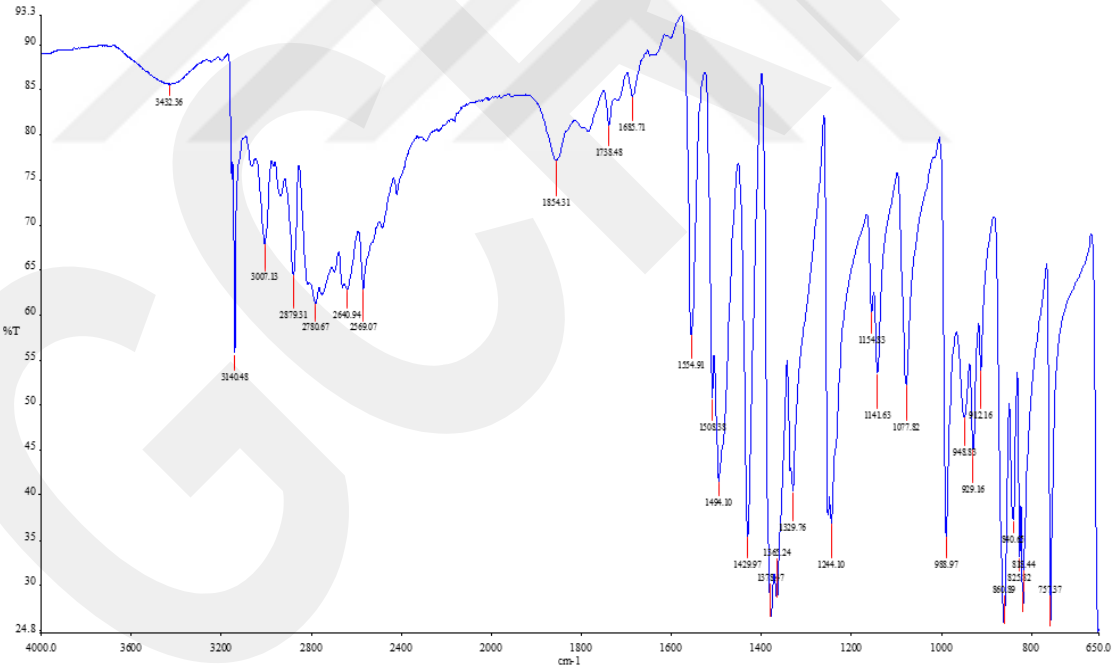

Figure A2.2. FTIR spectrum of 4-nitro-1H-imidazole-5-carbonyl chloride

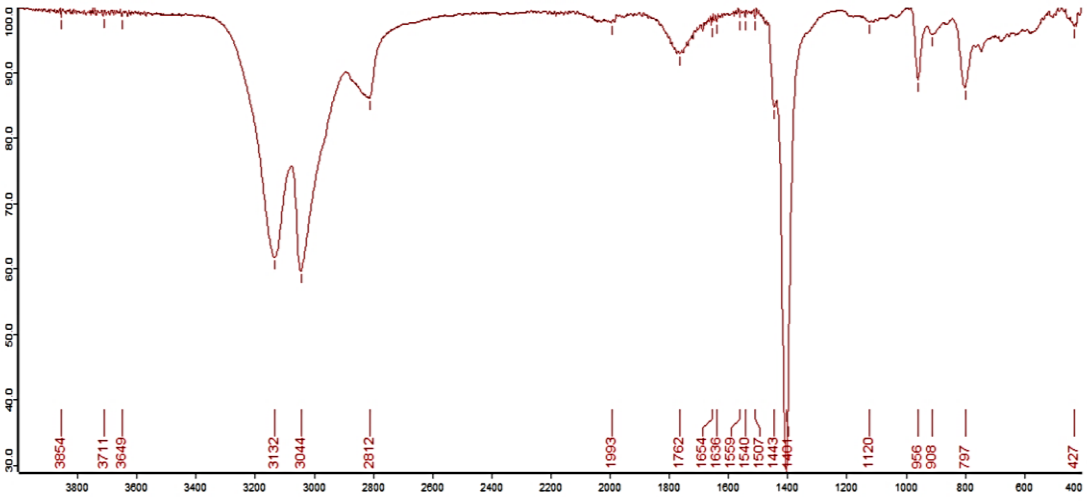

Figure A2.3. FTIR spectrum of ammonium salt of 5-(chloronitromethyl)-4-nitro-1H-imidazole

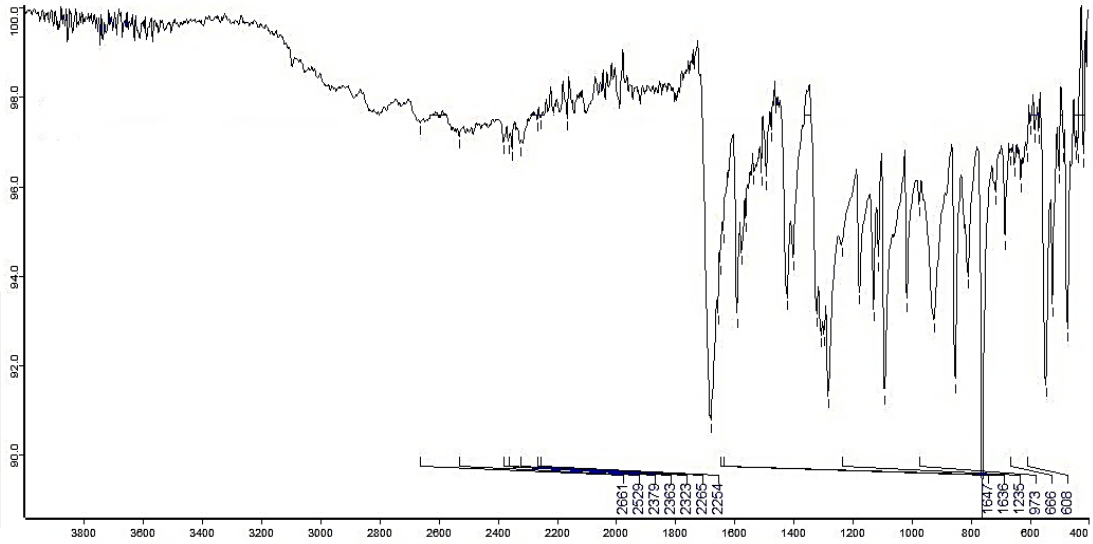

Figure A2.4. FTIR spectrum of sodium salt of 5-(chloronitromethyl)-4-nitro-1H-imidazole

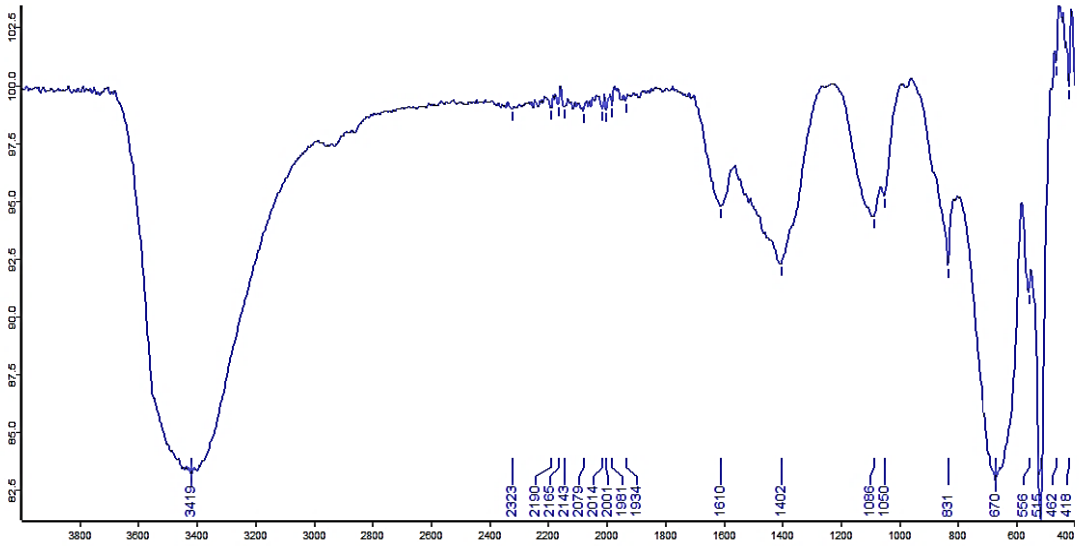

Figure A2.5. FTIR spectrum of complex **1**

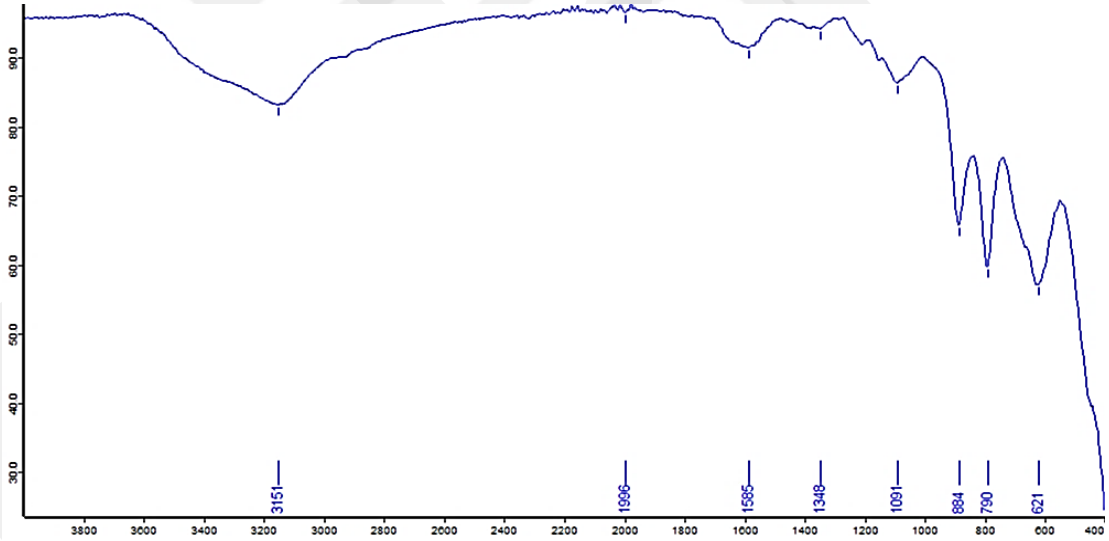

Figure A2.6. FTIR spectrum of complex **2**

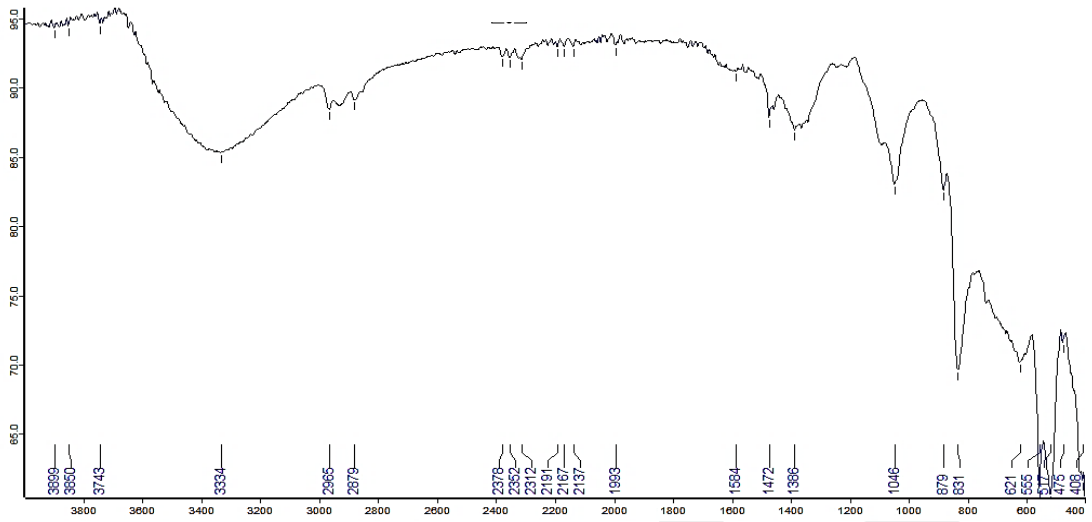

Figure A2.7. FTIR spectrum of complex **3**

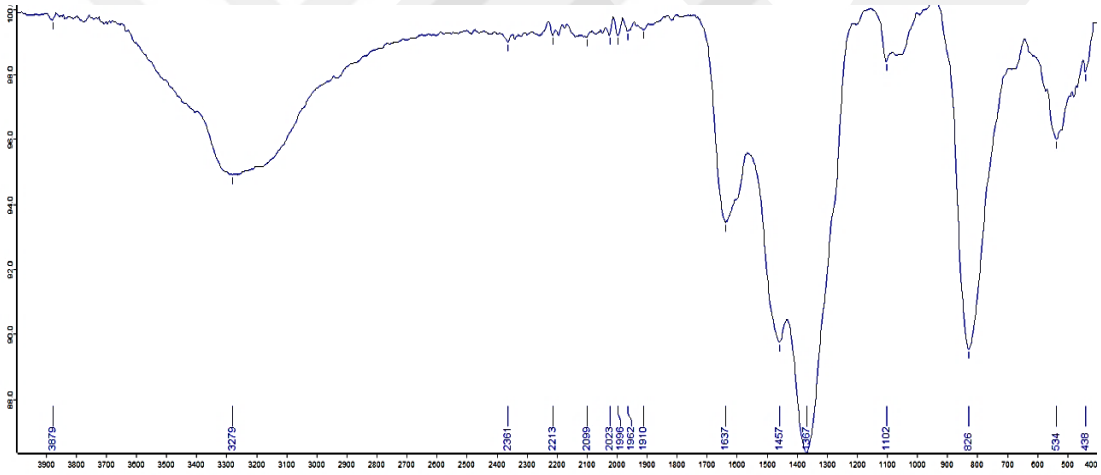

Figure A2.8. FTIR spectrum of complex **4**

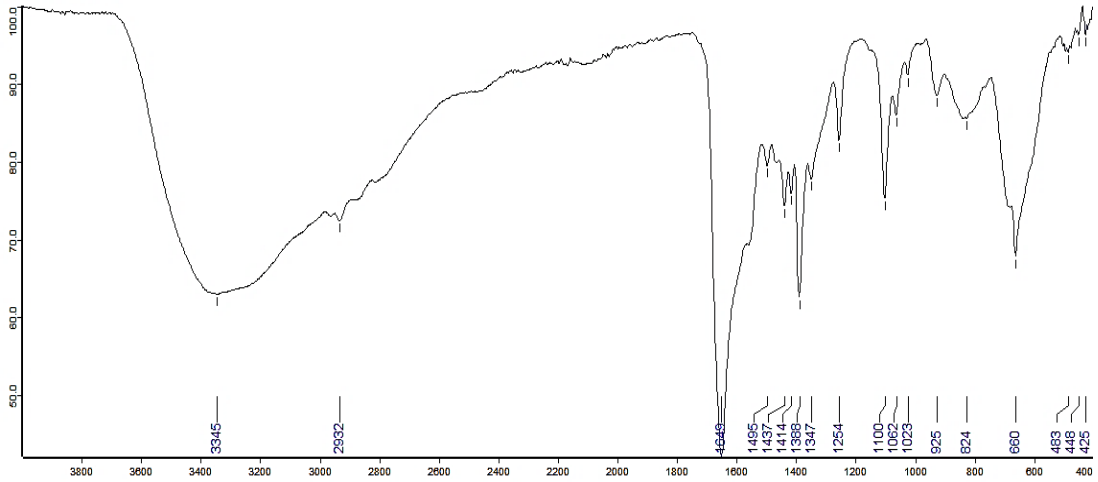

Figure A2.9. FTIR spectrum of complex 6

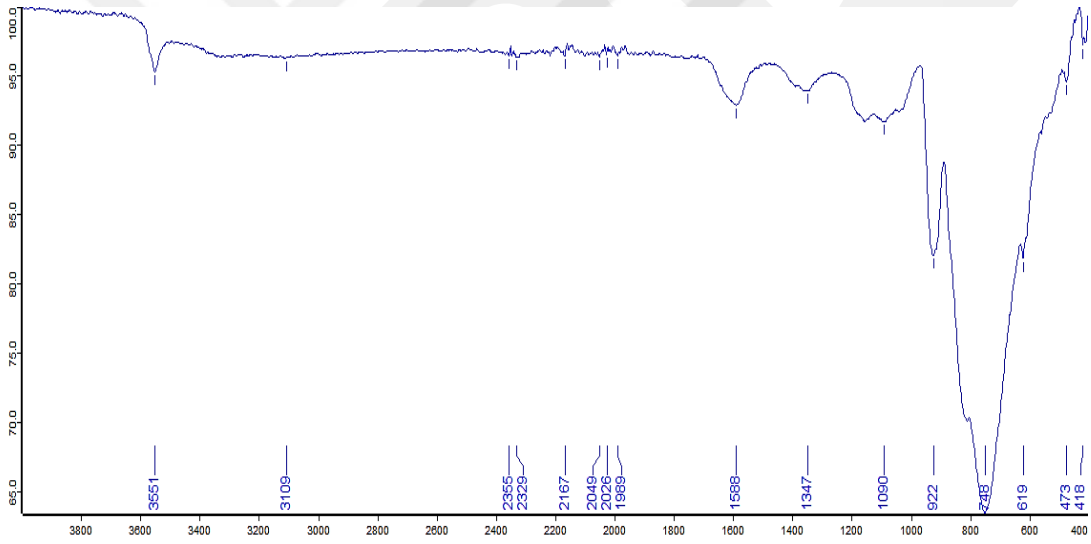

Figure A2.10. FTIR spectrum of complex **7**

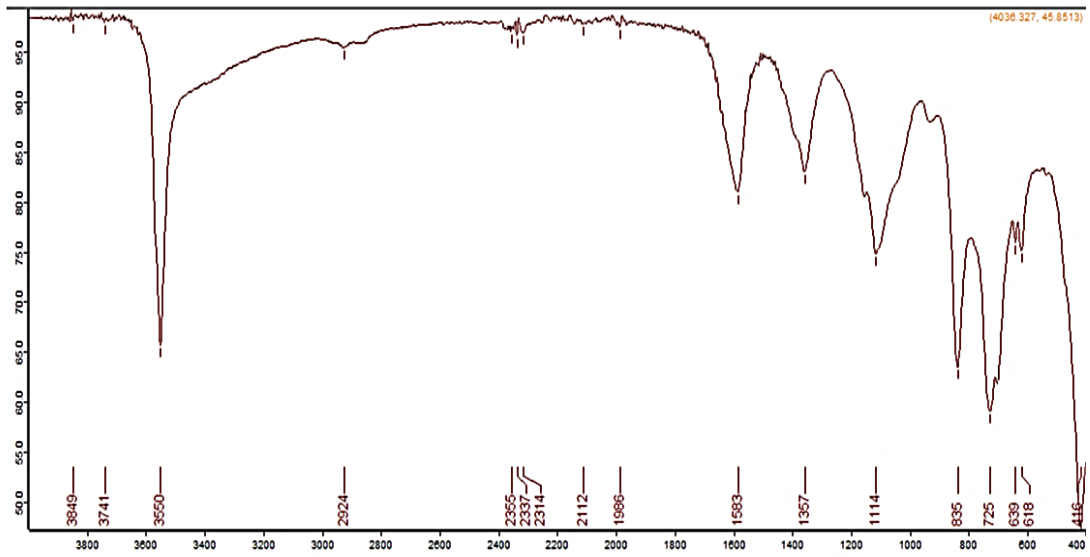

Figure A2.11. FTIR spectrum of complex **8**

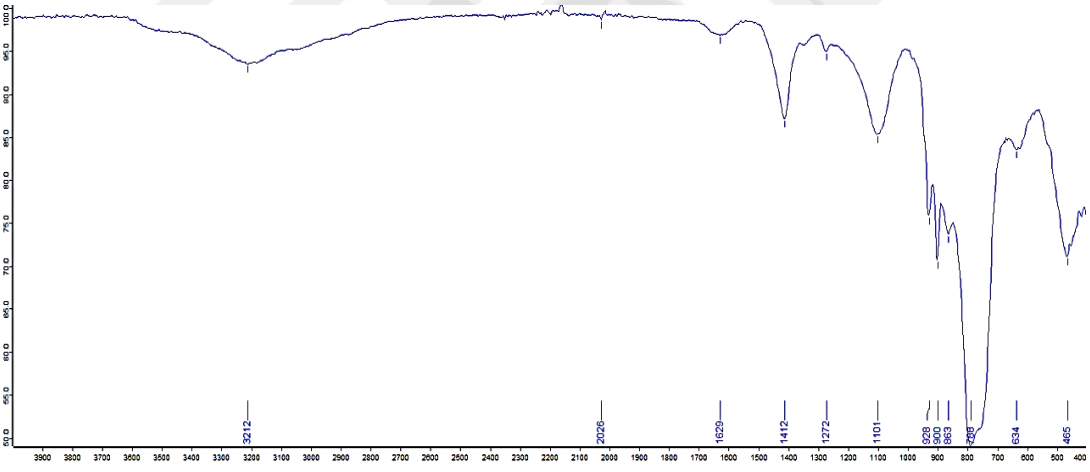

Figure A2.12. FTIR spectrum of complex **9**

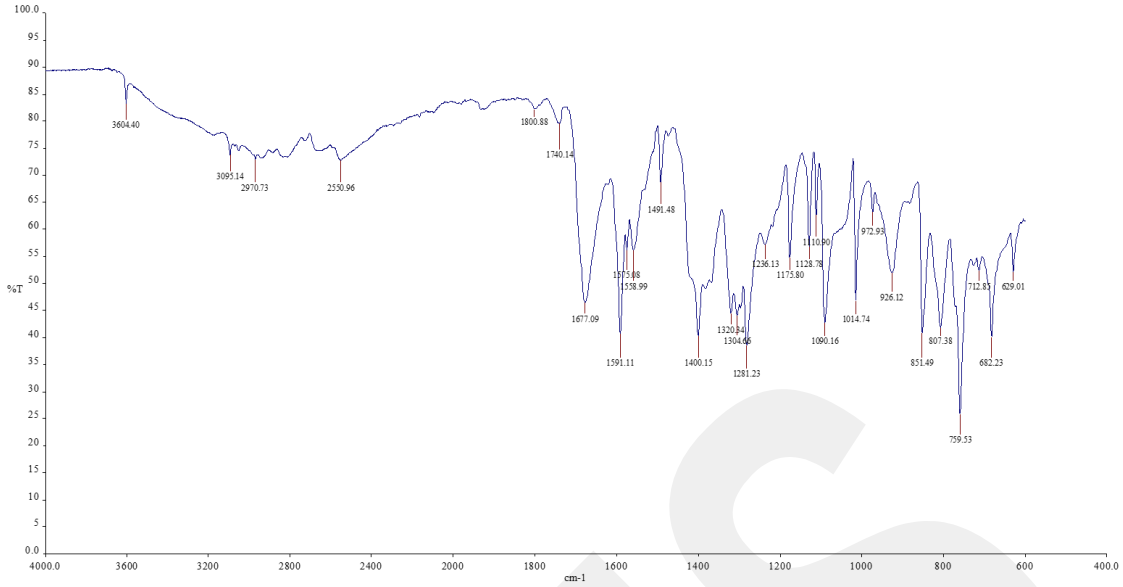

Figure A2.13. FTIR spectrum of complex **10**

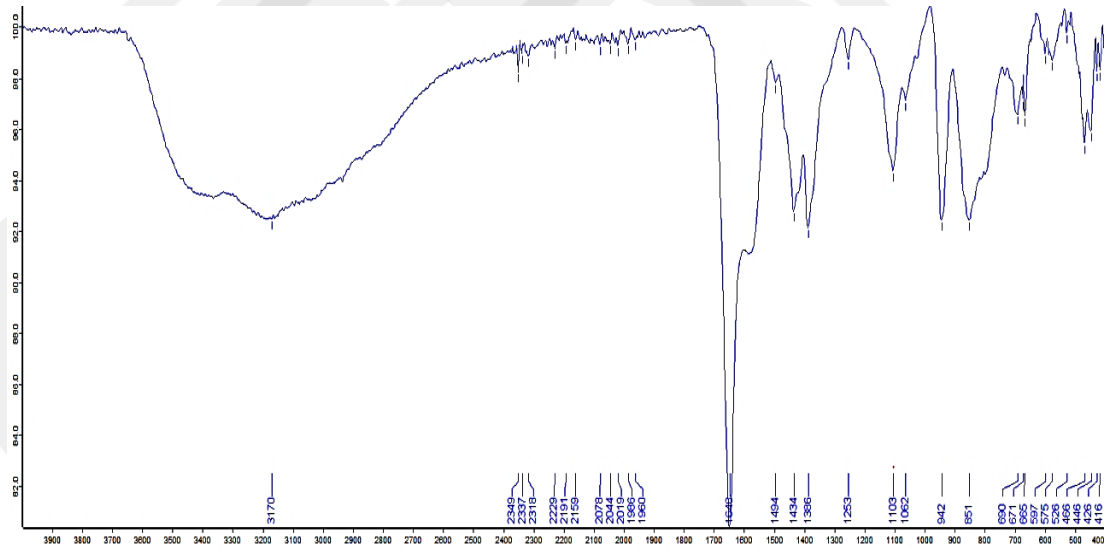

Figure A2.14. FTIR spectrum of complex **11**

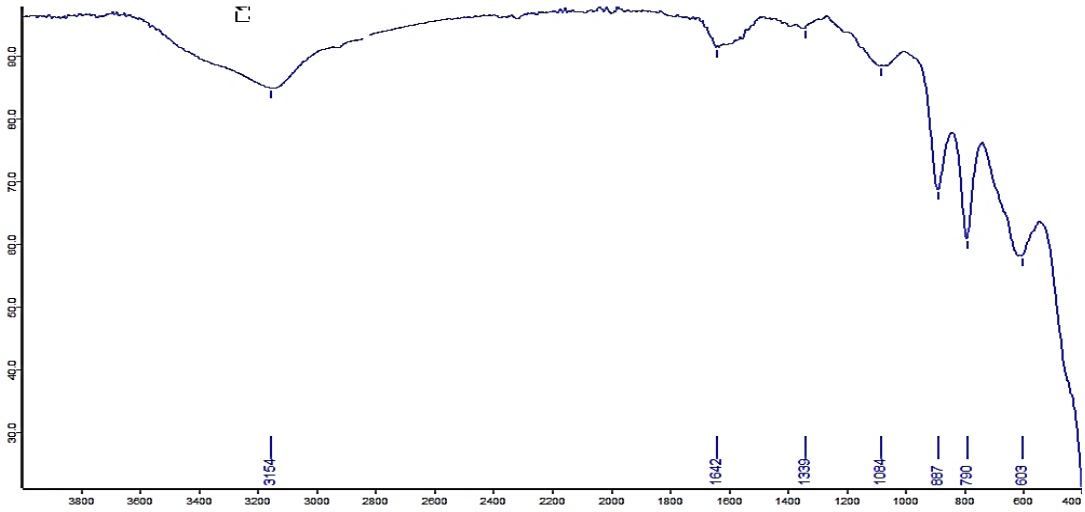

Figure A2.15. FTIR spectrum of complex **12**

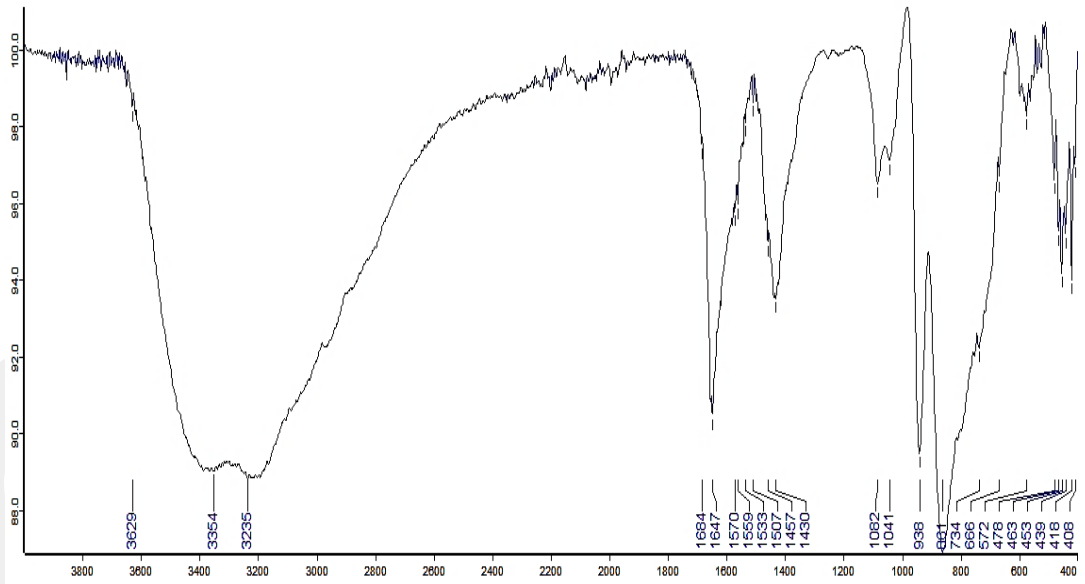

Figure A2.16. FTIR spectrum of complex **13**

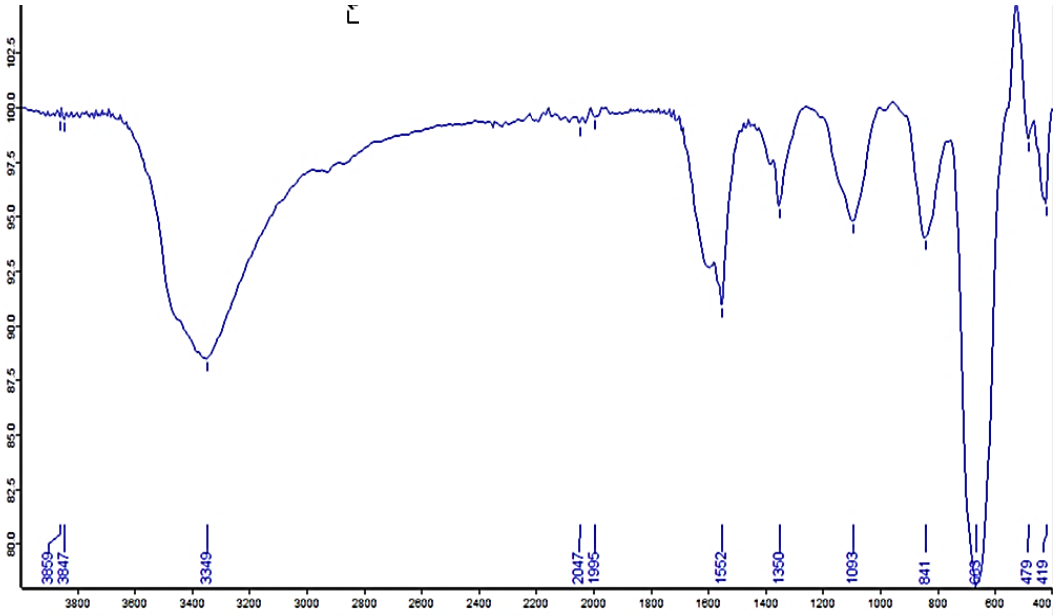

Figure A2.17. FTIR spectrum of complex **14**

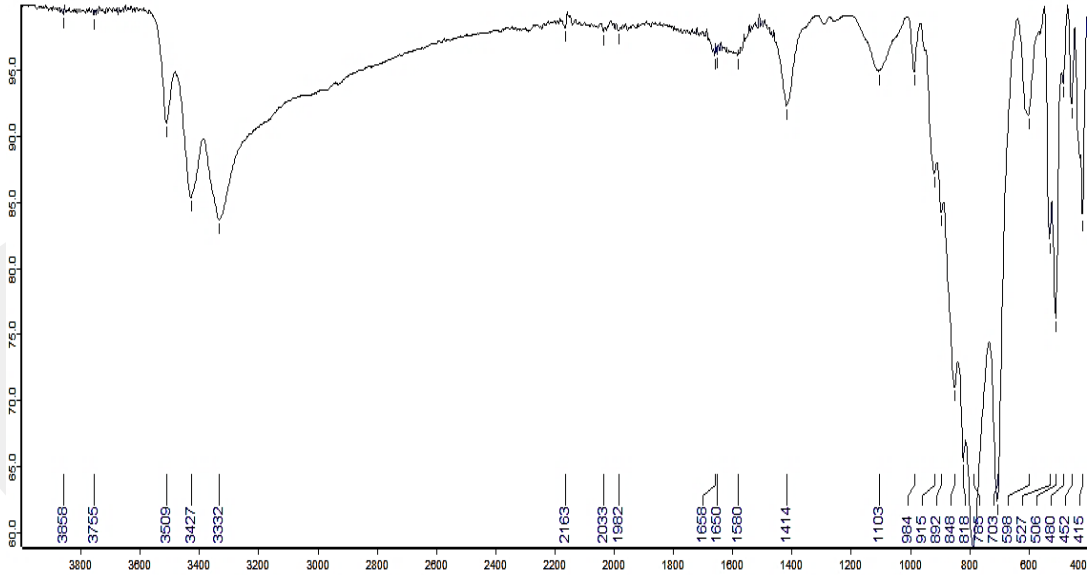

Figure A2.18. FTIR spectrum of complex **23**

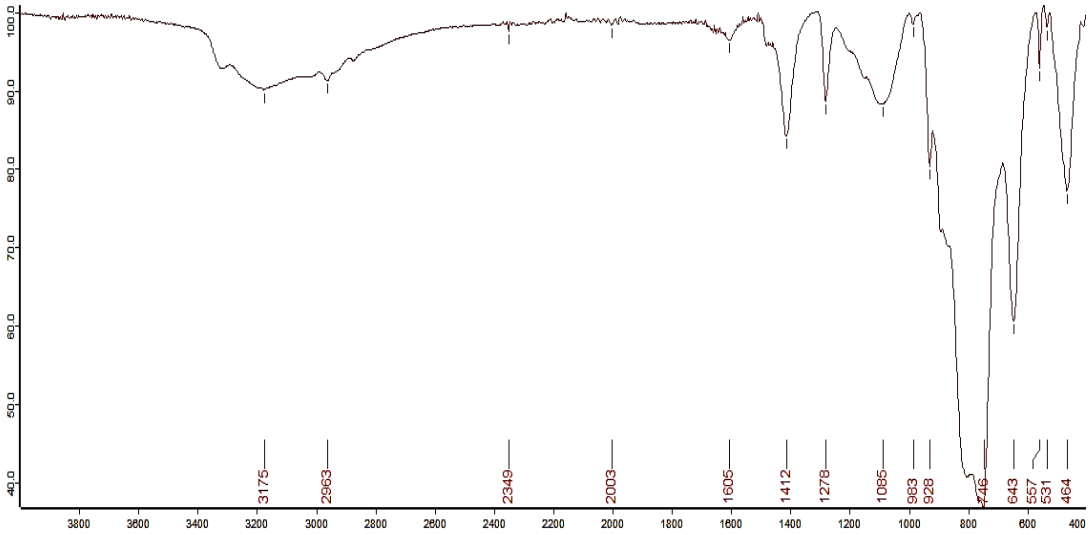

Figure A2.19. FTIR spectrum of complex **25**

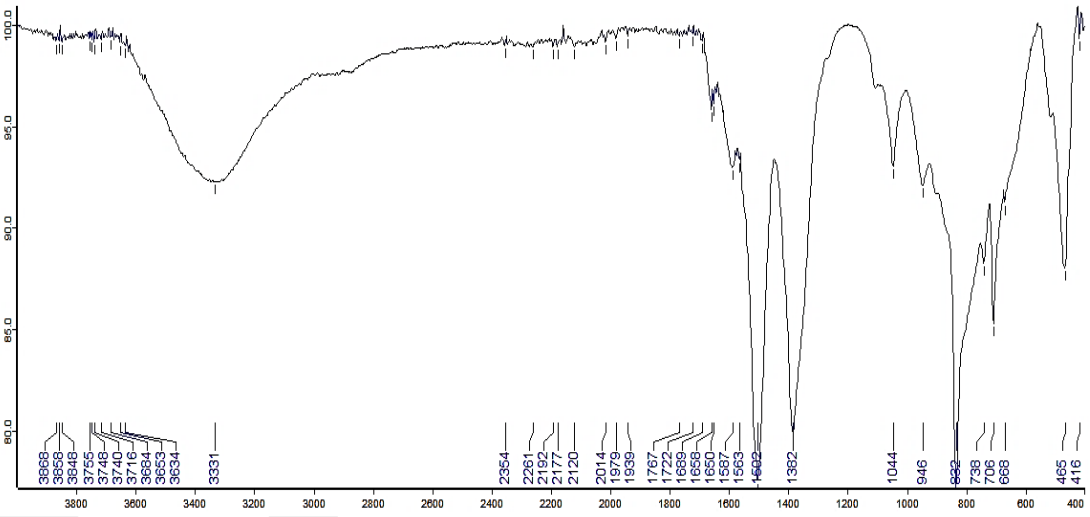

Figure A2.20. FTIR spectrum of complex **26**

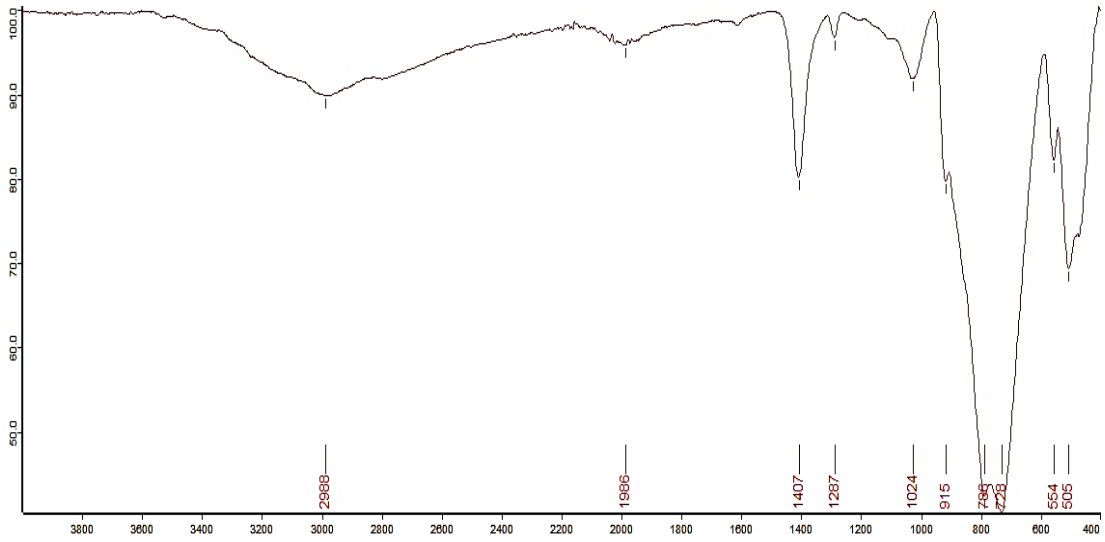

Figure A2.21. FTIR spectrum of complex **27**

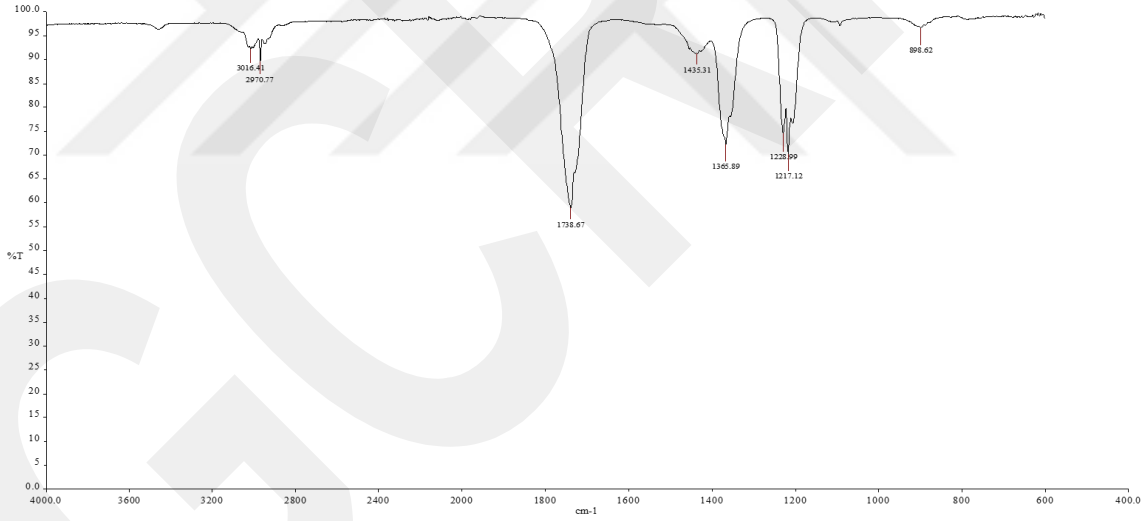

Figure A2.22. FTIR spectrum of complex **28**

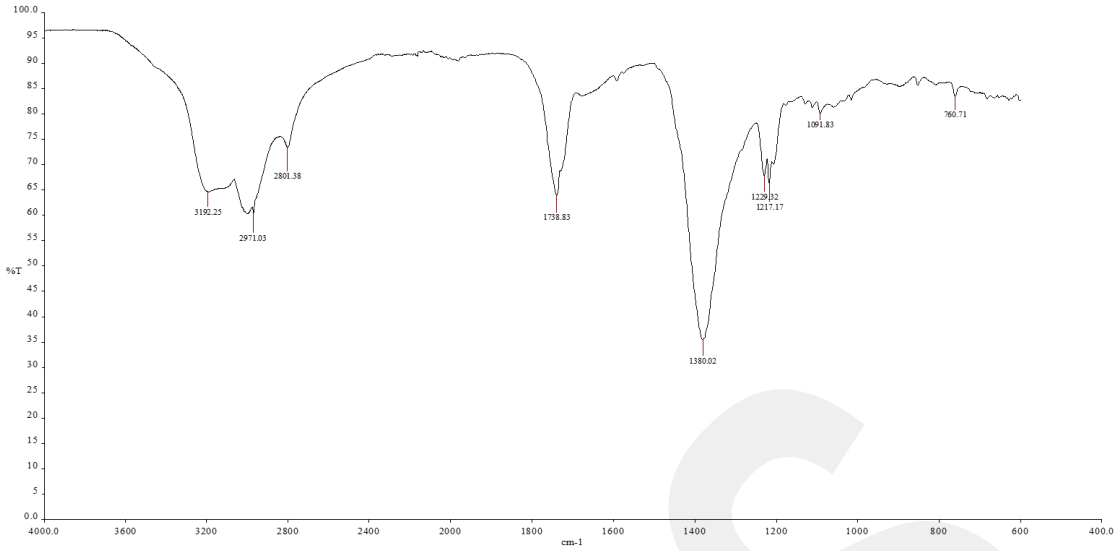

Figure A2.23. FTIR spectrum of complex **29**

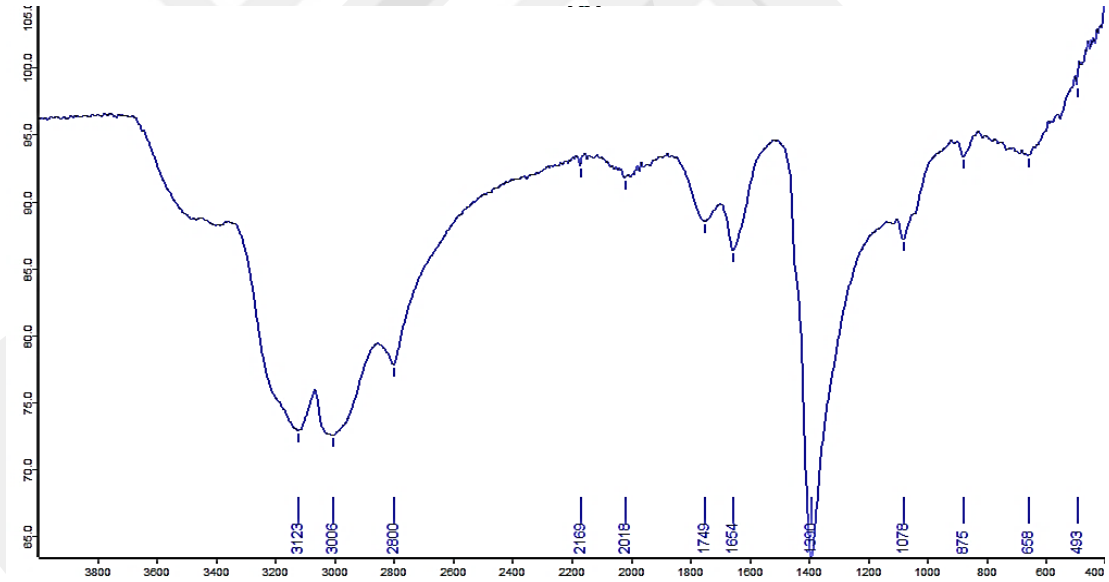

Figure A2.24. FTIR spectrum of complex **30**

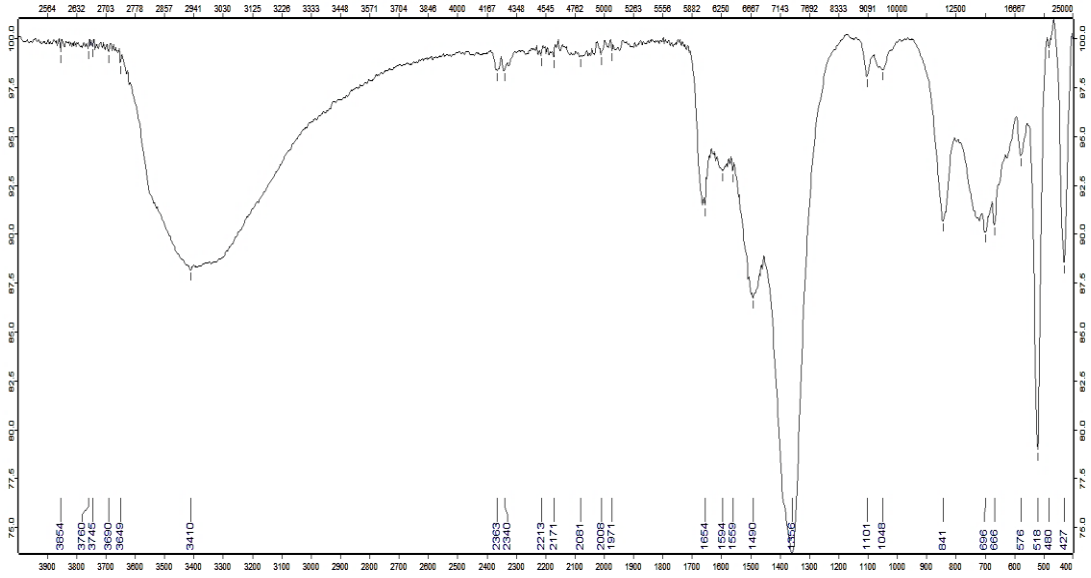

Figure A2.25. FTIR spectrum of complex **31**

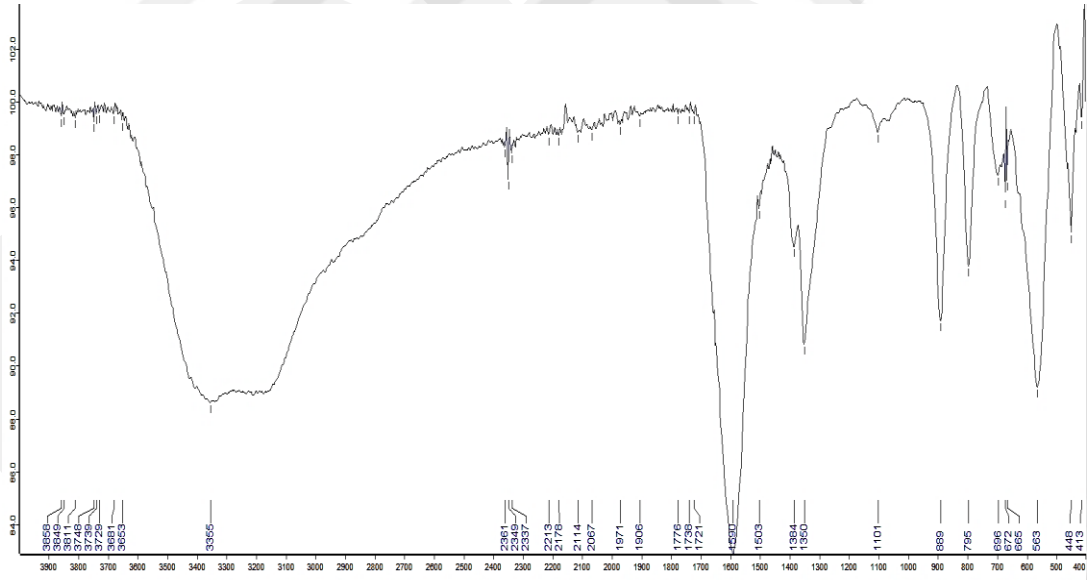

Figure A2.26. FTIR spectrum of complex **32**

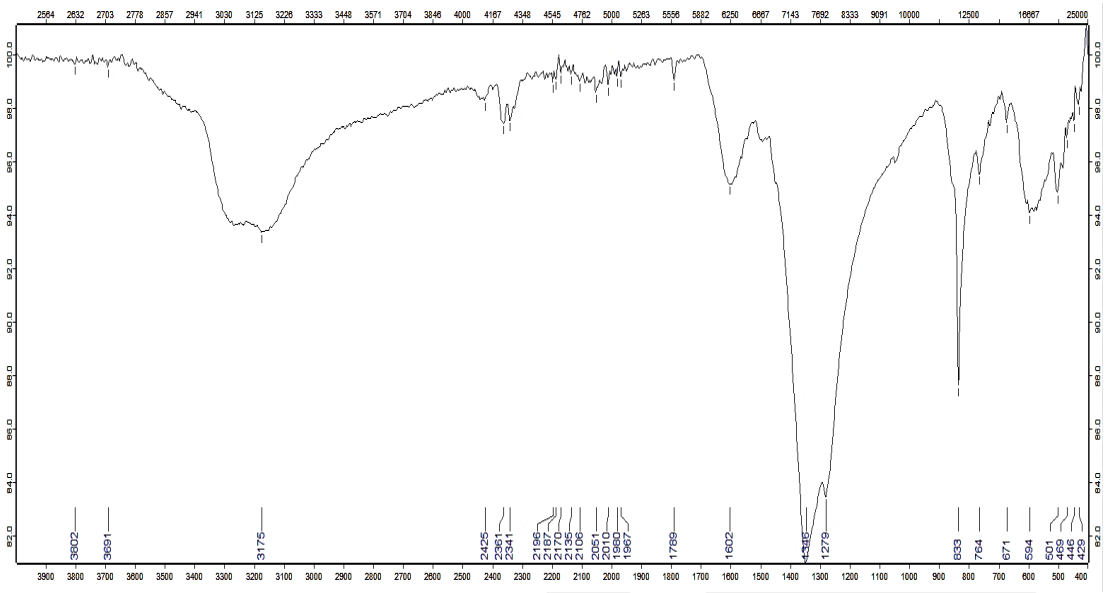

Figure A2.27. FTIR spectrum of complex **33**

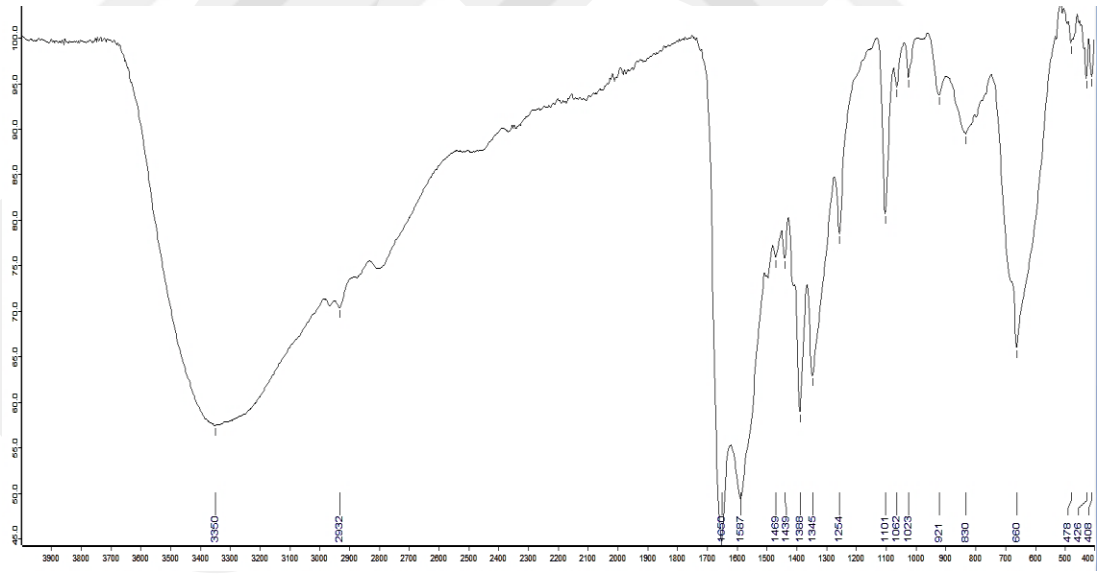

Figure A2.28. FTIR spectrum of complex **34**

Appendix 3. ^{1}H-NMR Analysis Results

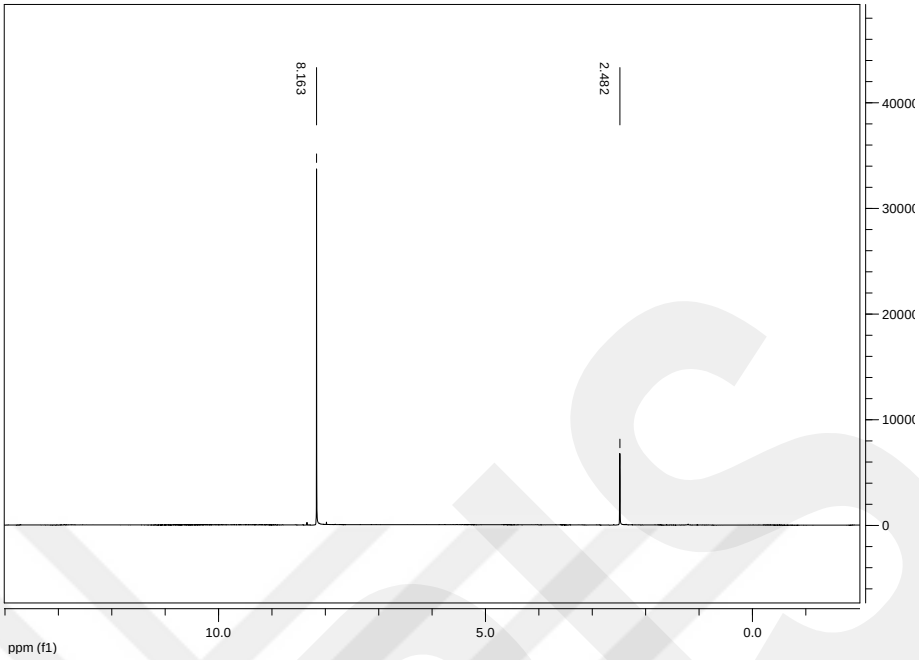

Figure A3.1. ^{1}H-NMR spectrum of 2,4-dinitro-1H-imidazole-5-carbonitrile

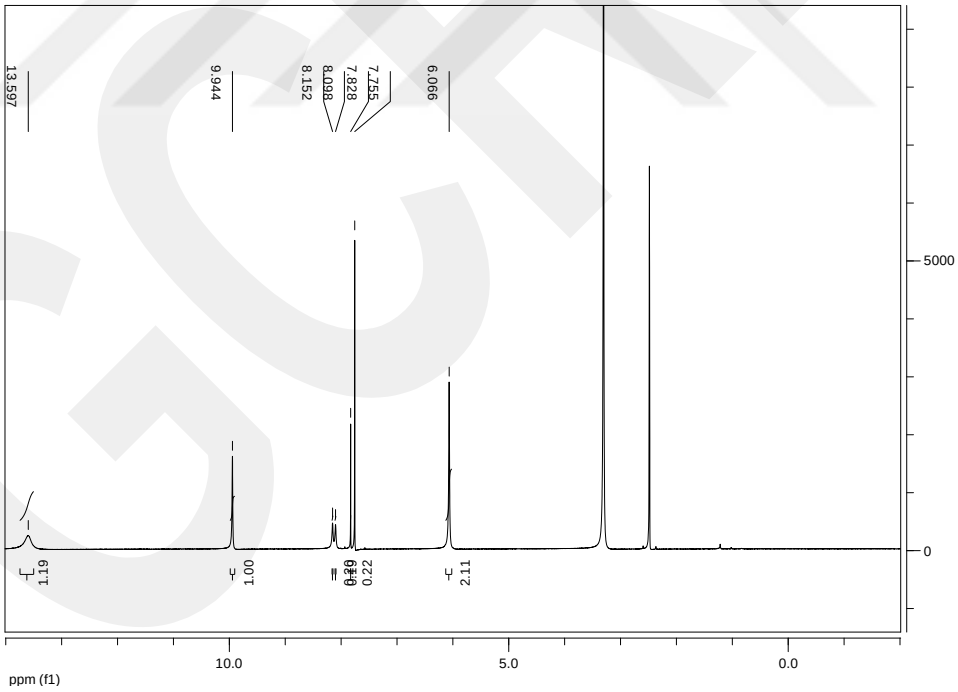

Figure A3.2. ^{1}H-NMR spectrum of N'-hydroxy-4-nitro-1H-imidazole-5 carboxamidine

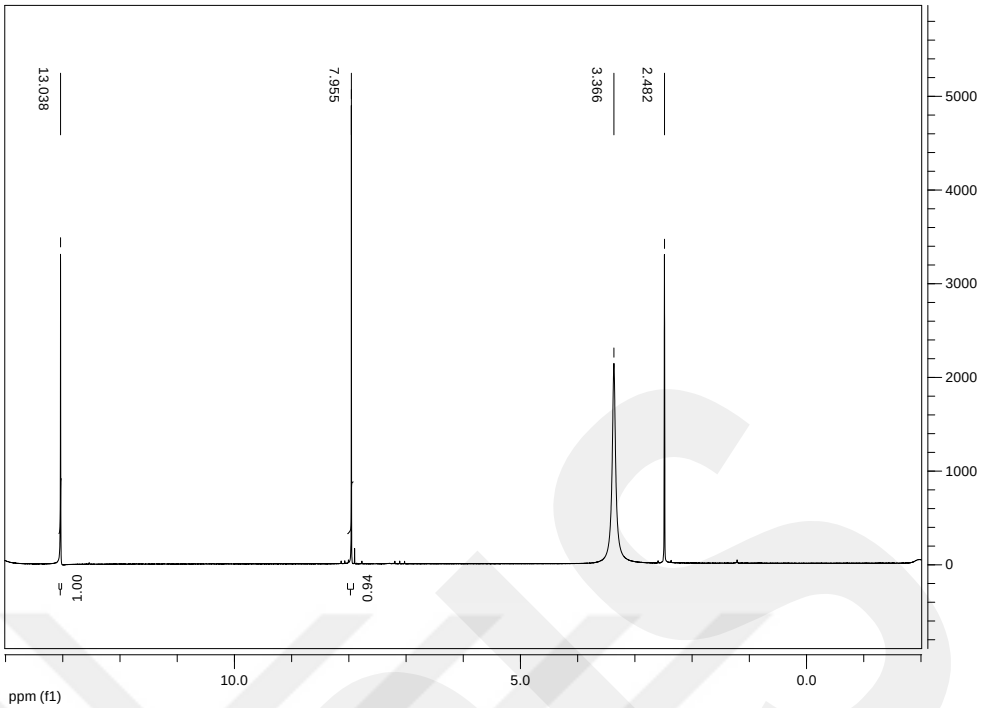

Figure A3.3. ^{1}H-NMR spectrum of 4-nitro-1H-imidazole-5-carbonyl chloride

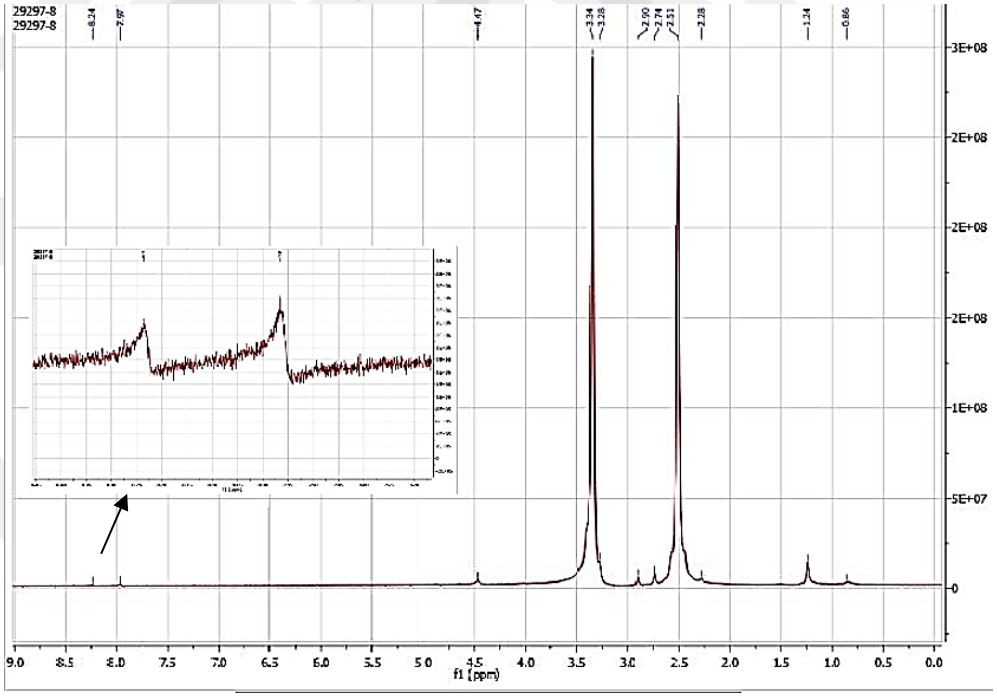

Figure A3.4. ^{1}H-NMR spectrum of **5**

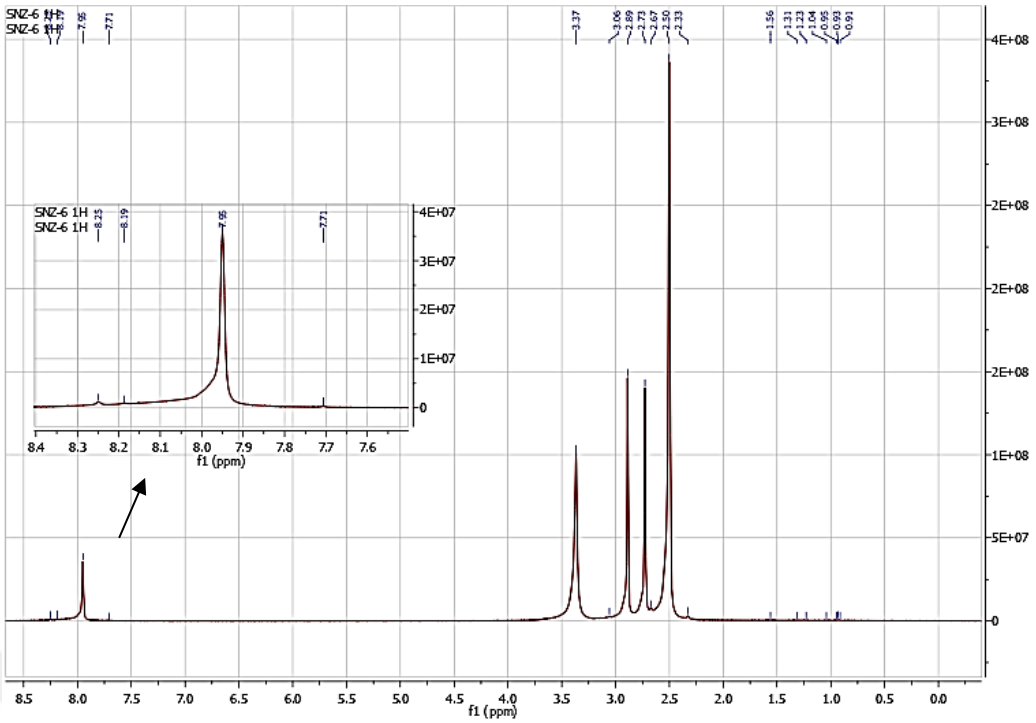

Figure A3.5. ^{1}H-NMR spectrum of **6**

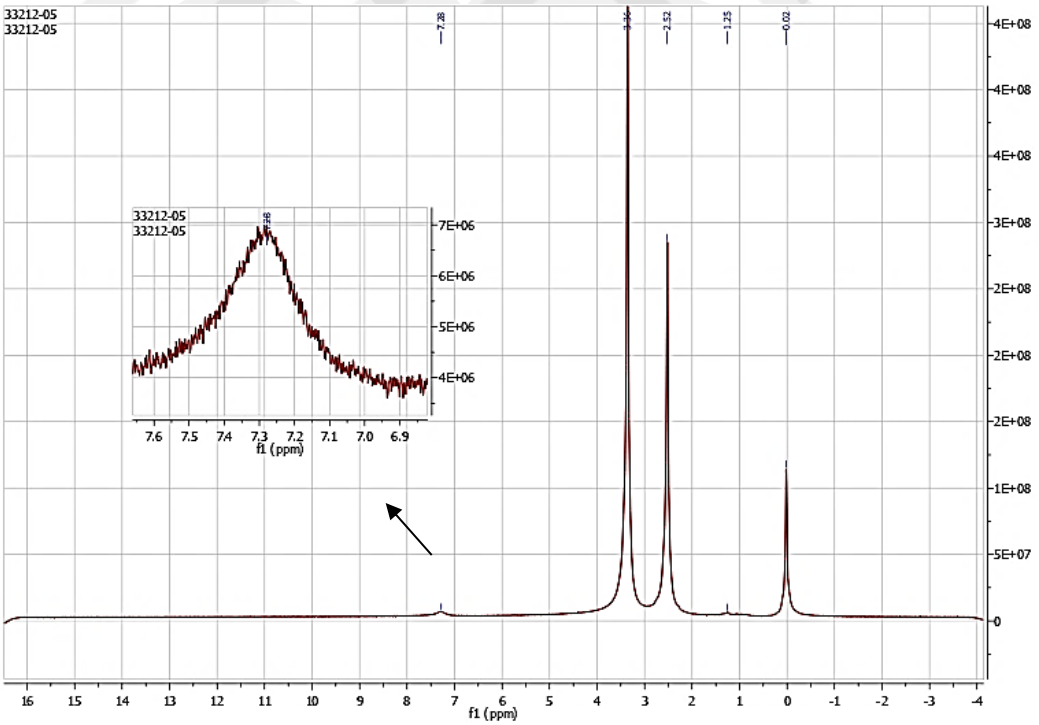

Figure A3.6. ^{1}H-NMR spectrum of **7**

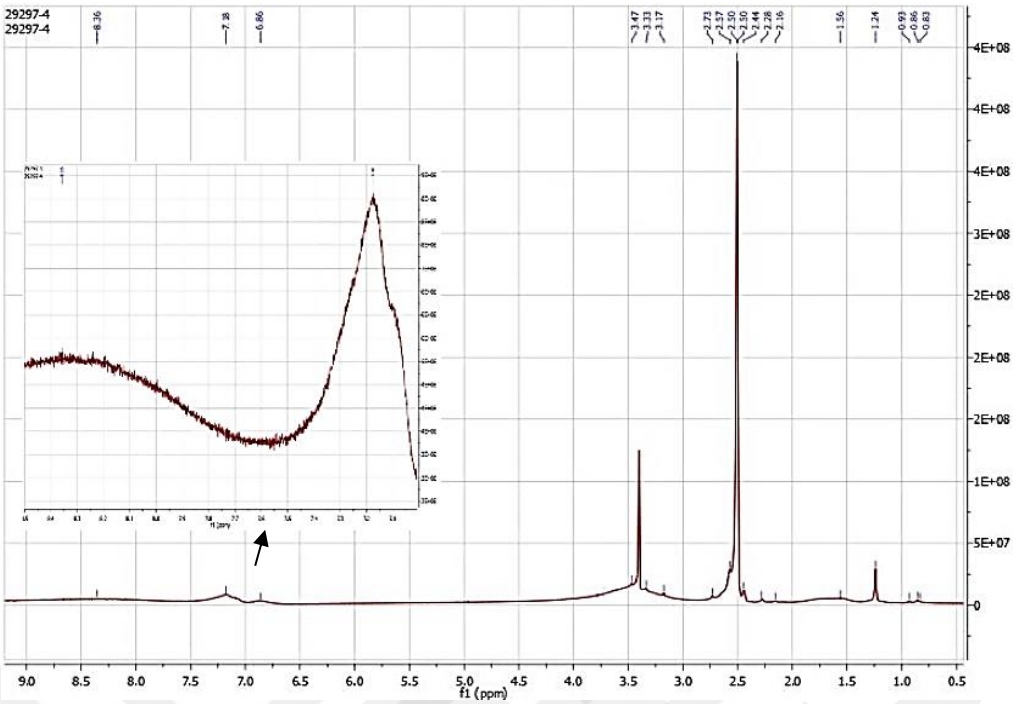

Figure A3.7. ^{1}H-NMR spectrum of **10**

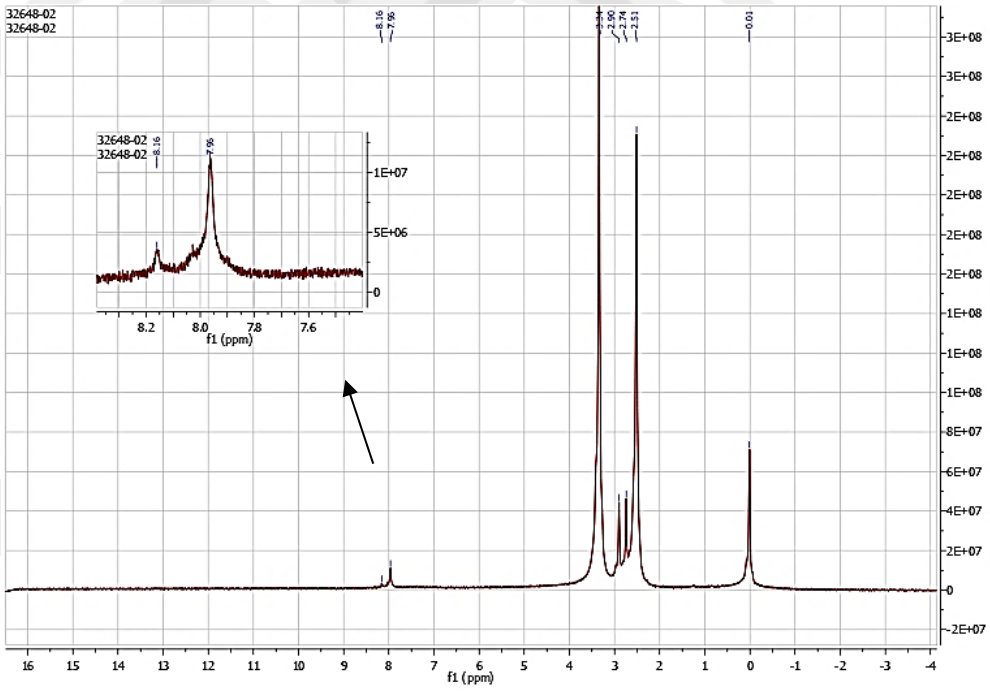

Figure A3.8. ^{1}H-NMR spectrum of **11**

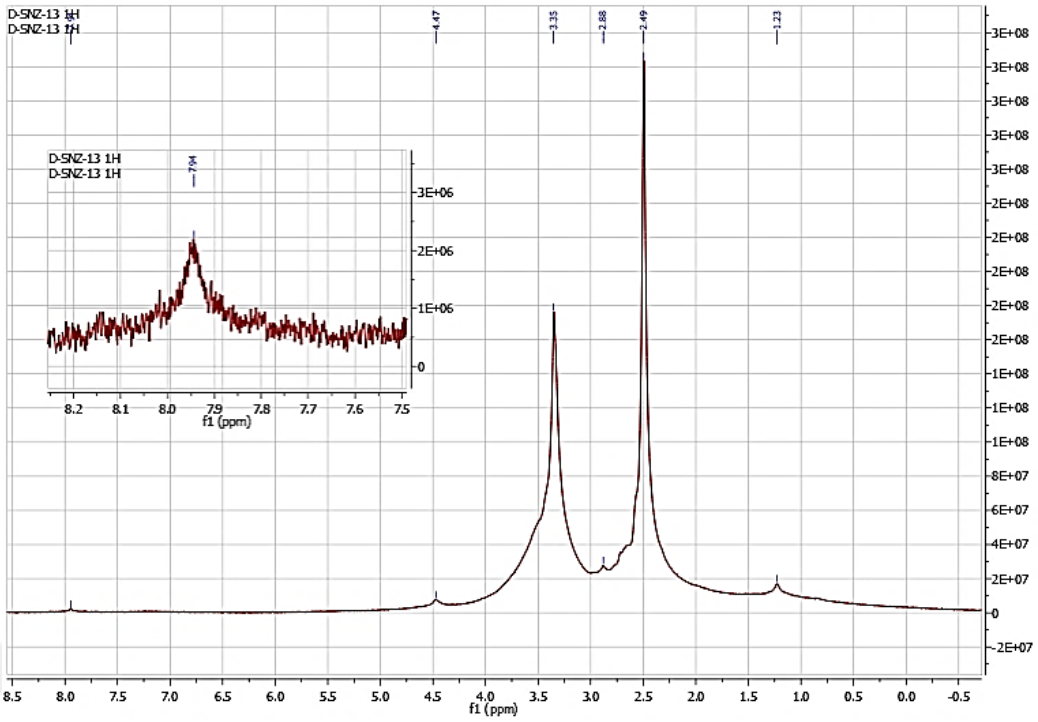

Figure A3.9. ^{1}H-NMR spectrum of **13**

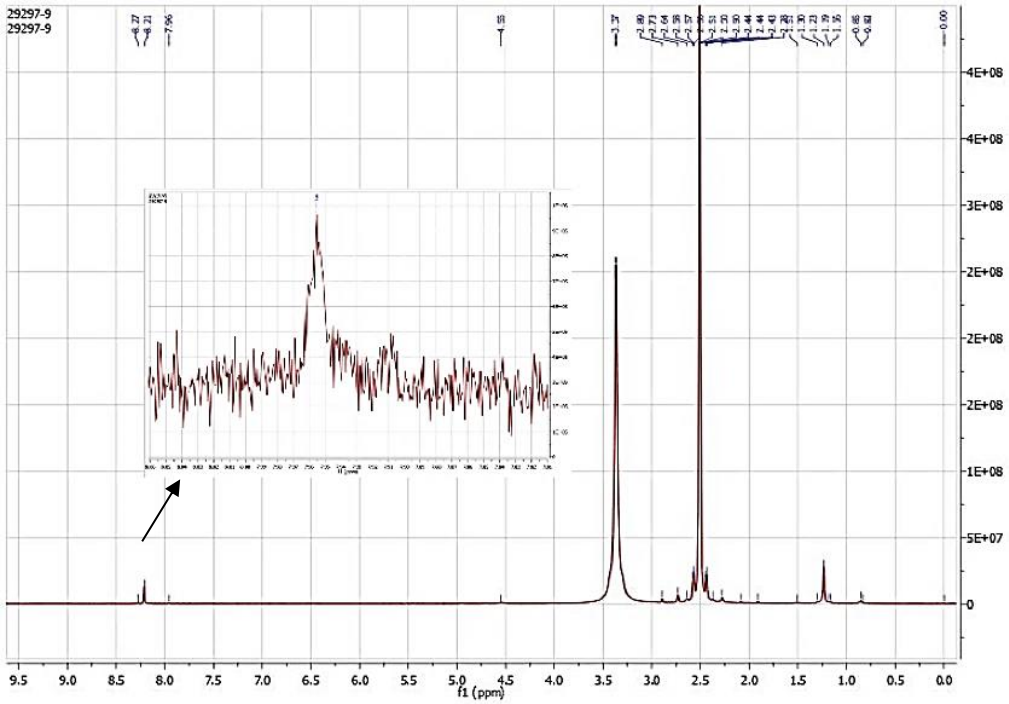

Figure A3.10. ^{1}H-NMR spectrum of **14**

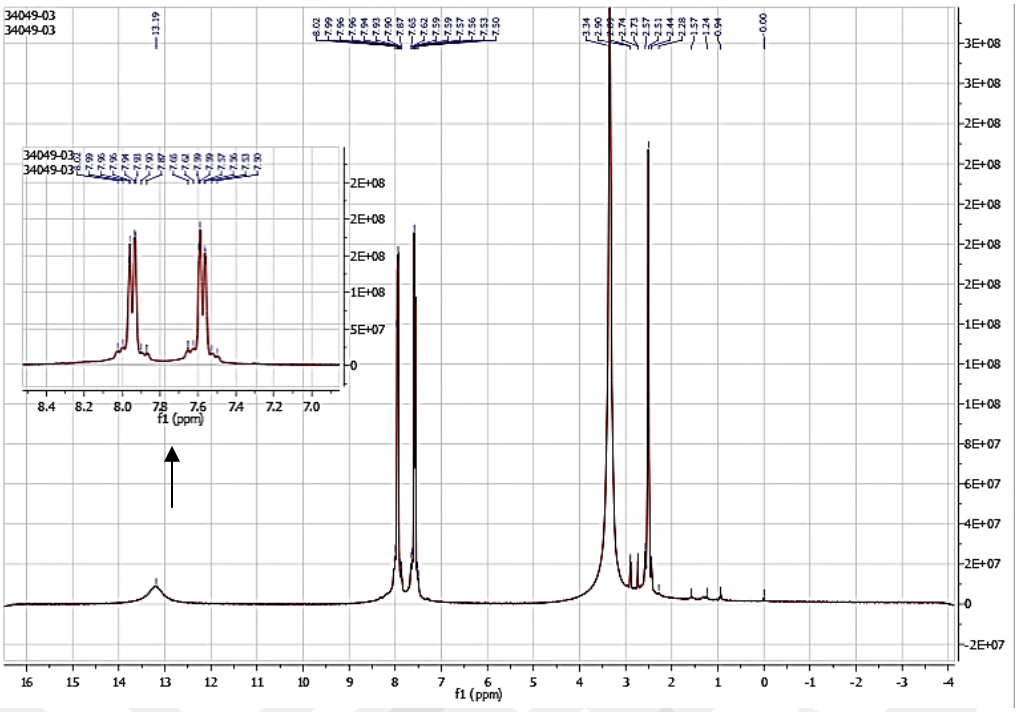

Figure A3.11. ^{1}H-NMR spectrum of **25**

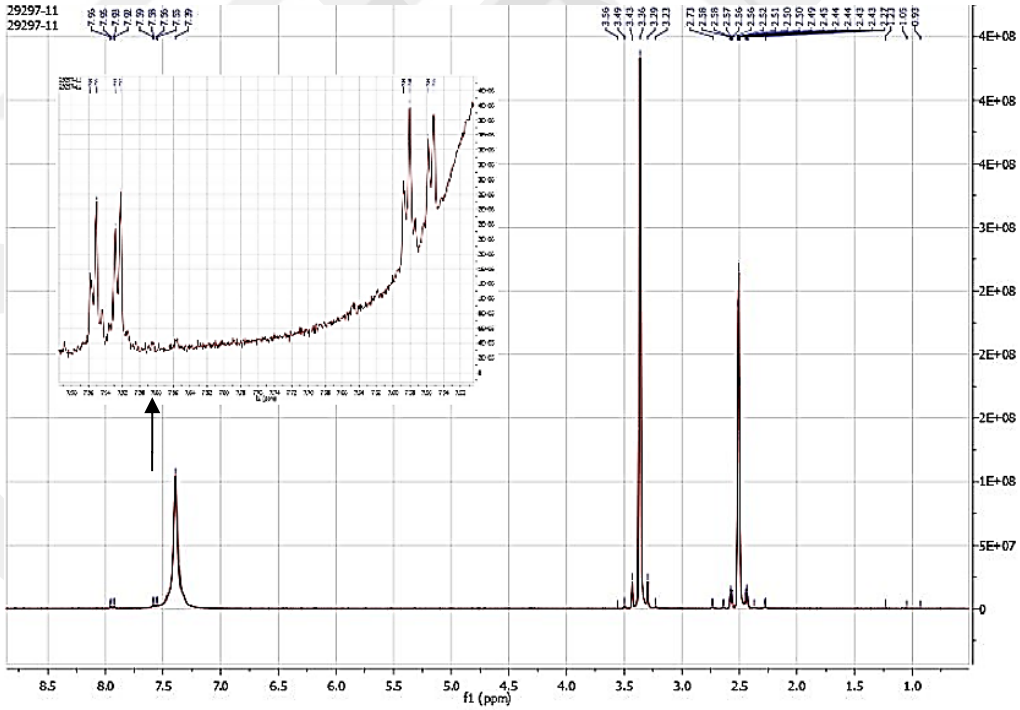

Figure A3.12. ^{1}H-NMR spectrum of **29**

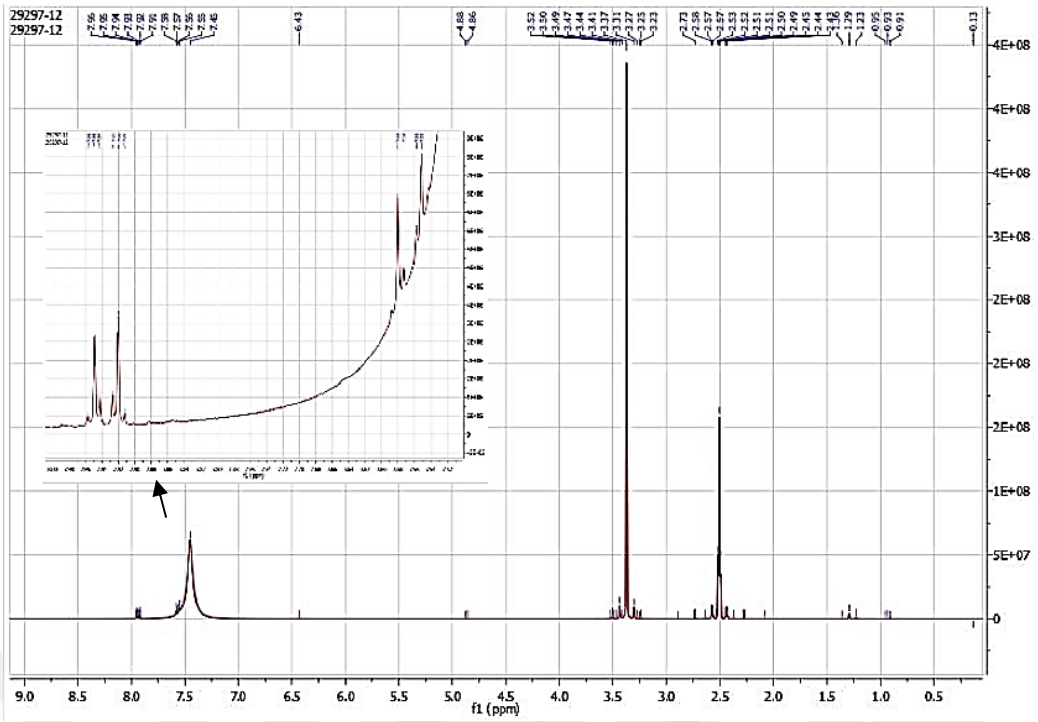

Figure A3.13. ^{1}H-NMR spectrum of **30**

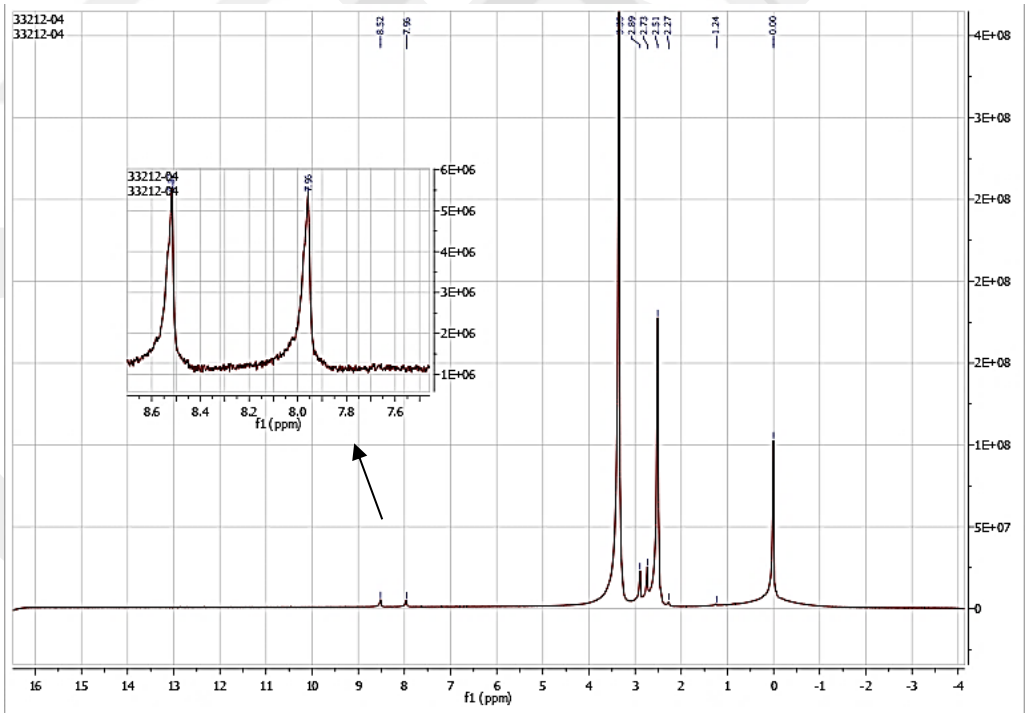

Figure A3.14. ^{1}H-NMR spectrum of **32**

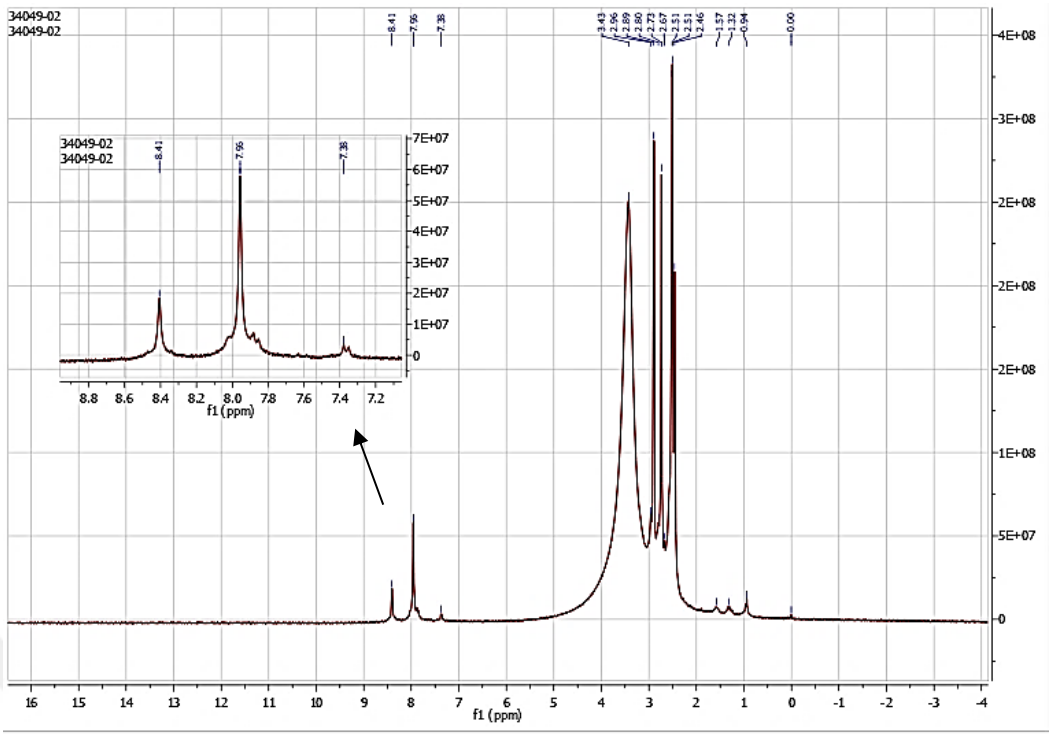

Figure A3.15. ^{1}H-NMR spectrum of **34**

Appendix 4. TGA-DSC Analysis Results

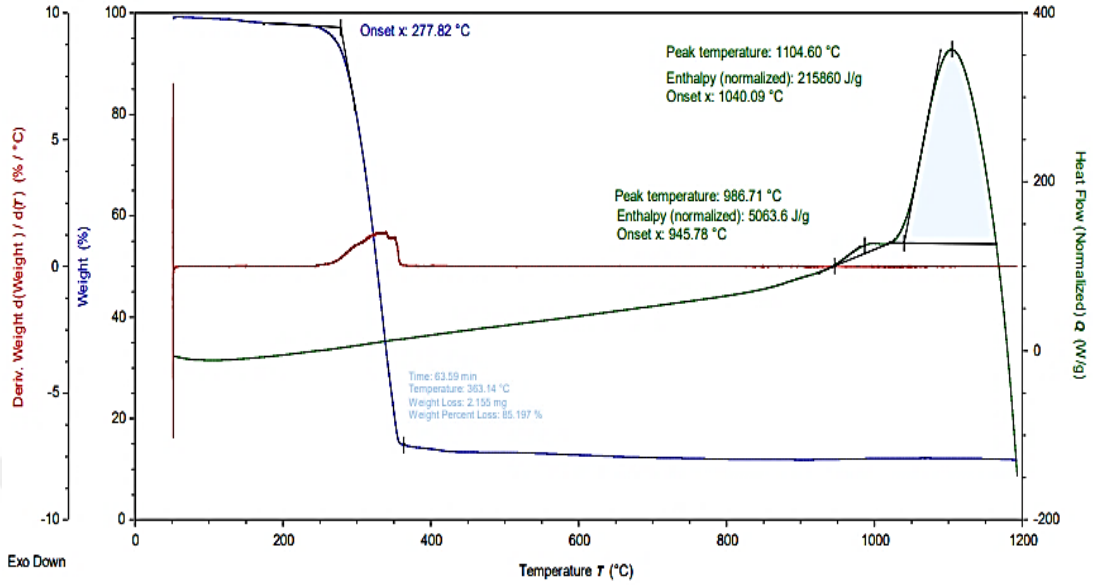

Figure A4.1. TGA-DSC spectrum of complex **3**

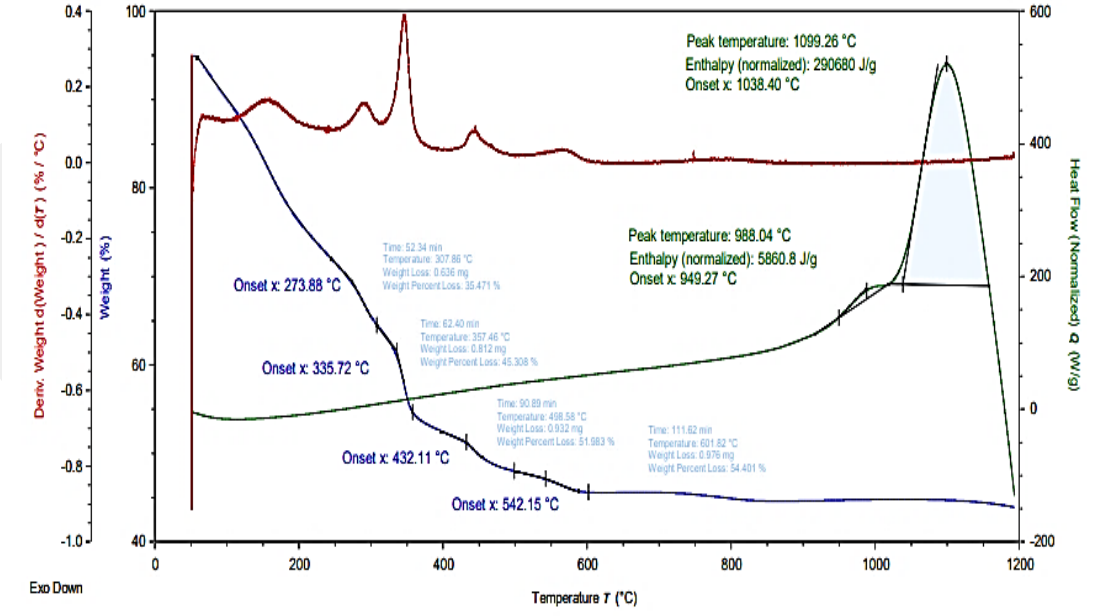

Figure A4.2. TGA-DSC spectrum of complex **4**

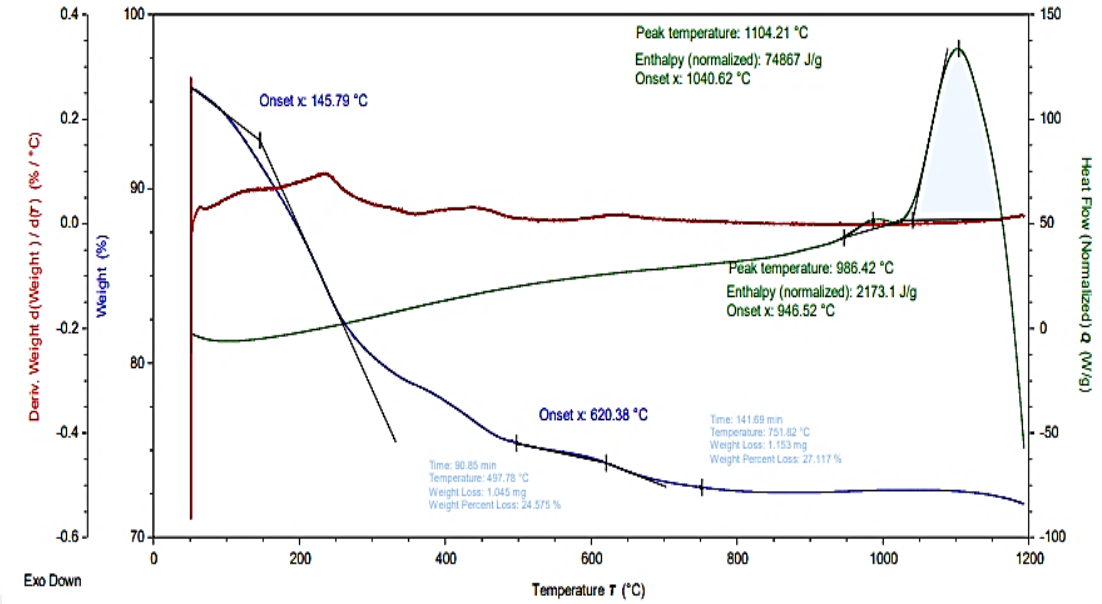

(a)

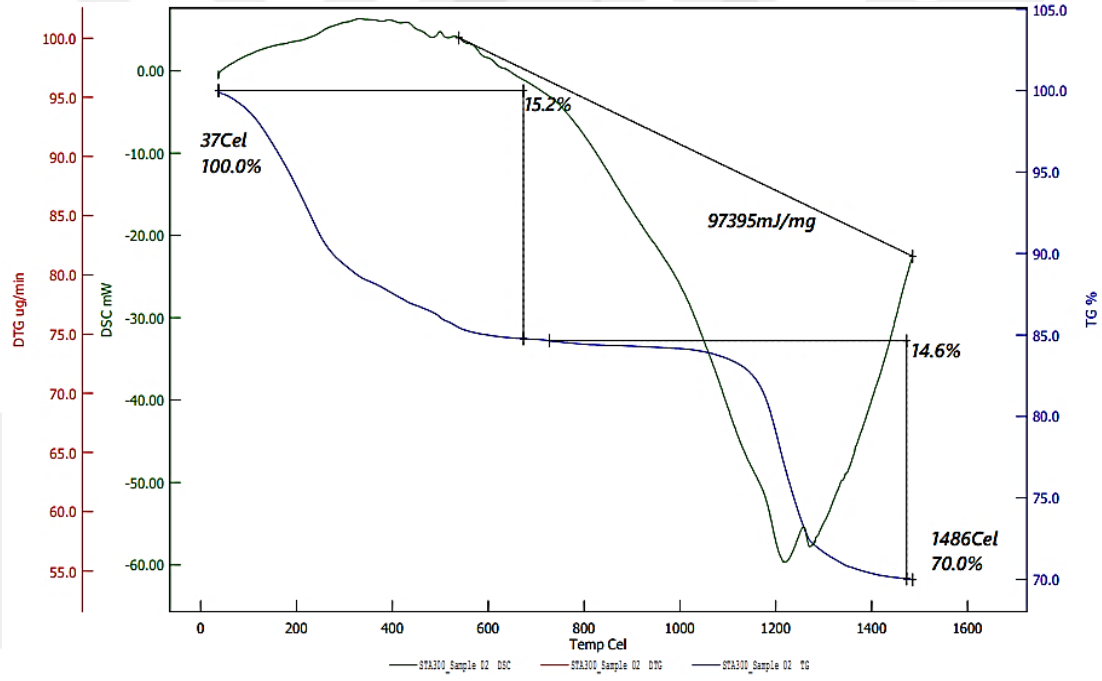

(b)

Figure A4.3. TGA-DSC spectrum of complex **6** in the range of (a) 50-1200 ^{o}C and (b) 50-2000 ^{o}C

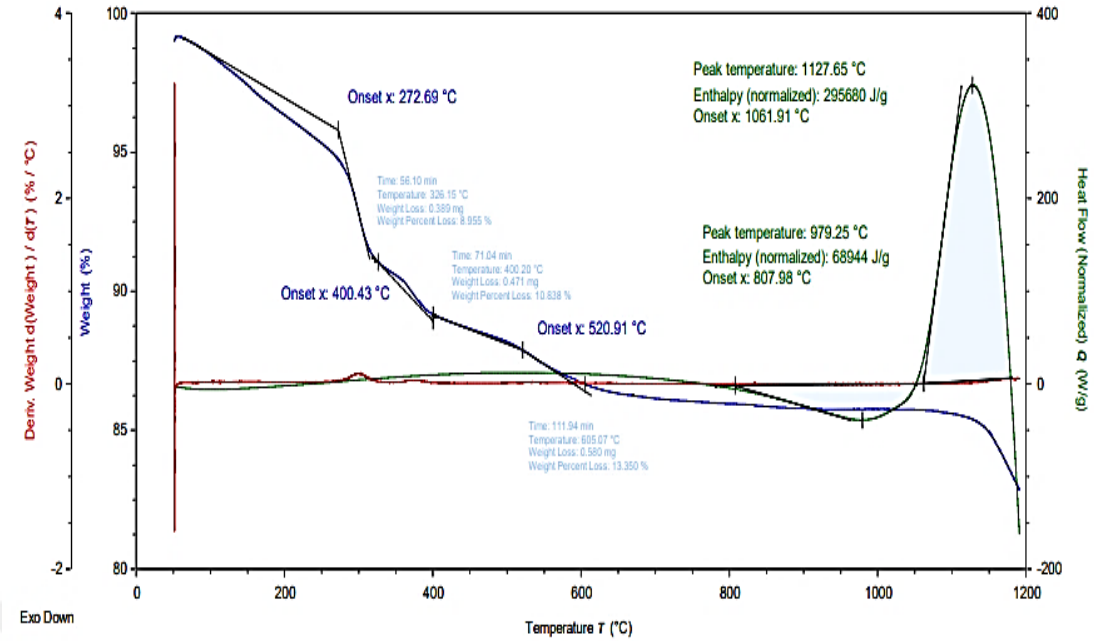

(a)

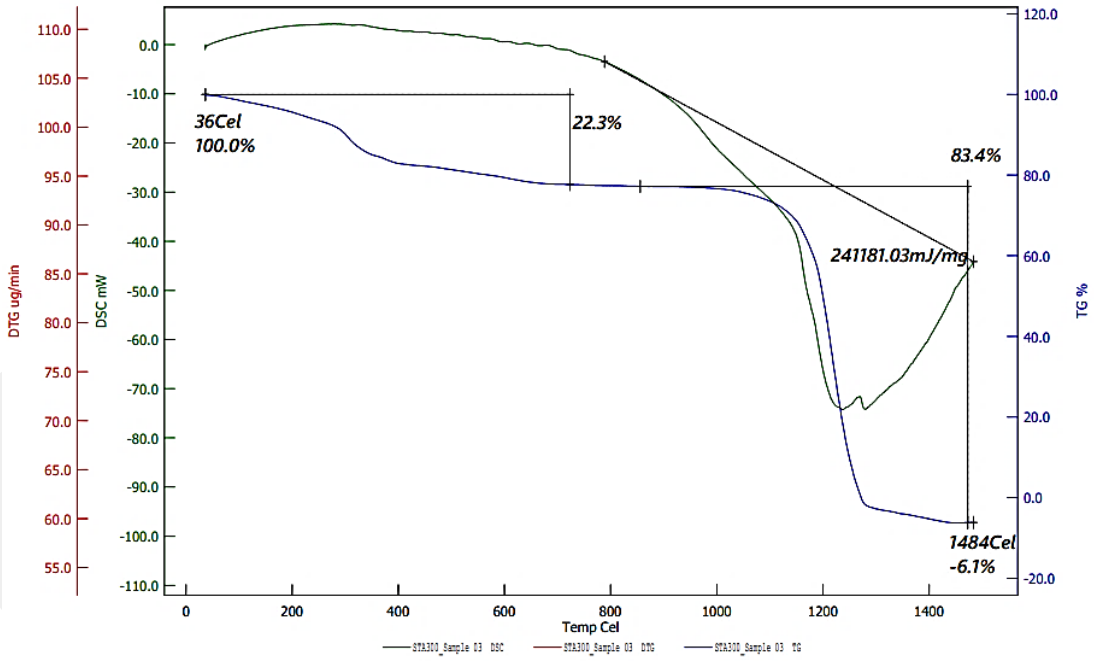

(b)

Figure A4.4. TGA-DSC spectrum of complex **7** in the range of (a) 50-1200 ^{o}C and (b) 50-2000 ^{o}C

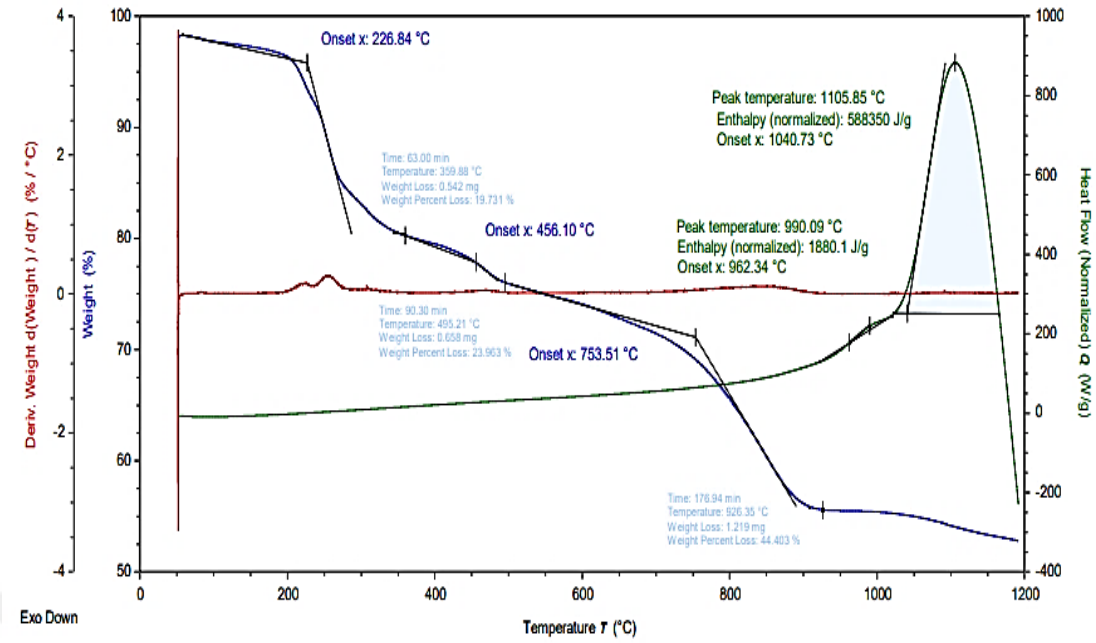

Figure A4.5. TGA-DSC spectrum of complex **8**

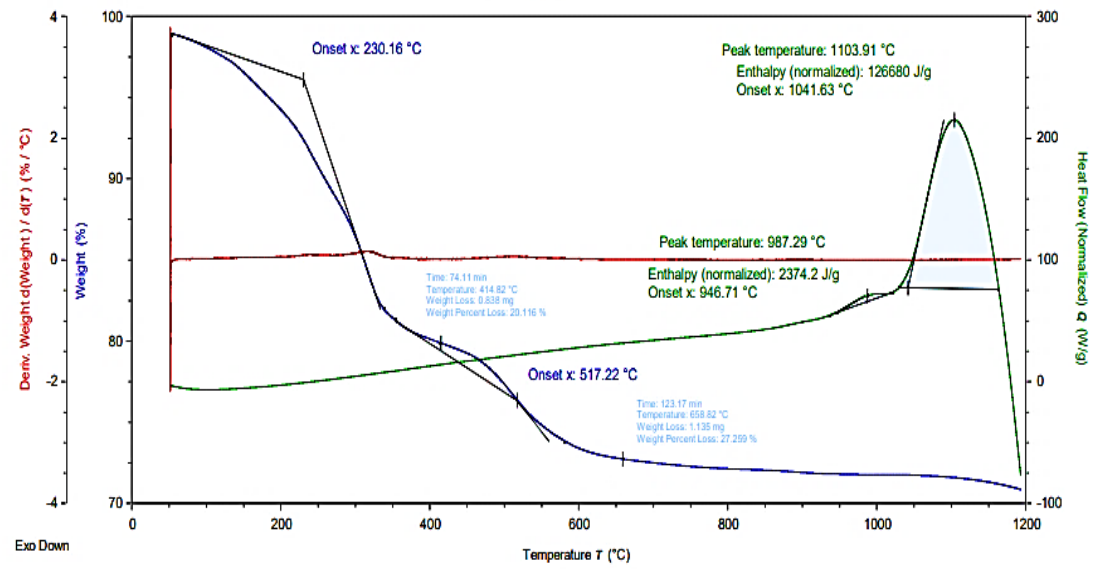

(a)

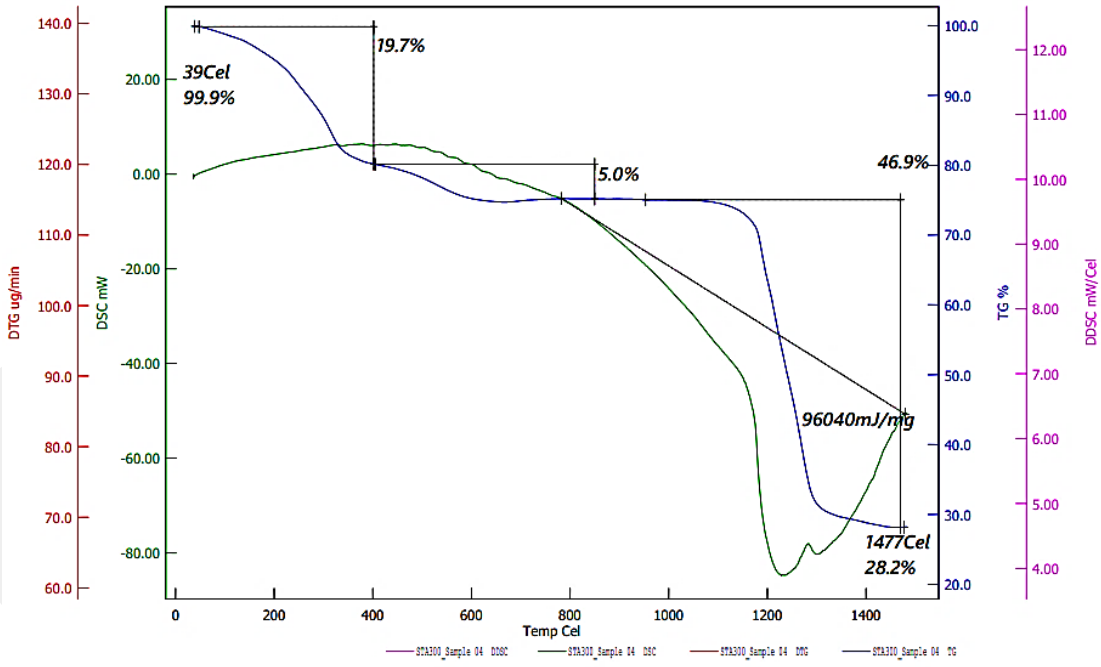

(b)

Figure A4.6. TGA-DSC spectrum of complex **9** in the range of (a) 50-1200 ^{o}C and (b) 50-2000 ^{o}C

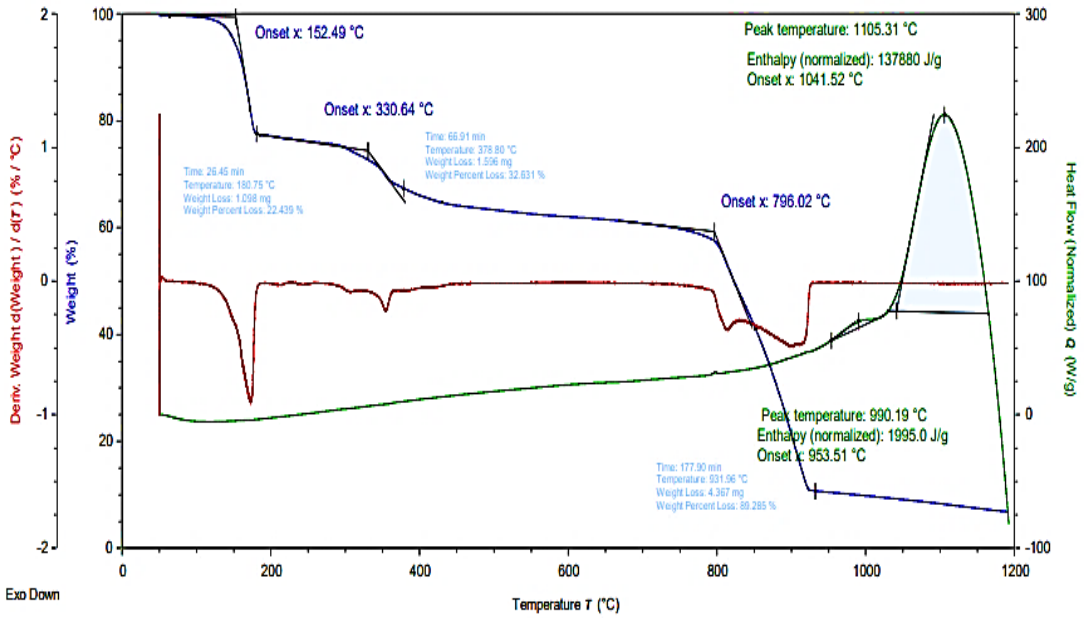

Figure A4.7. TGA-DSC spectrum of complex **10**

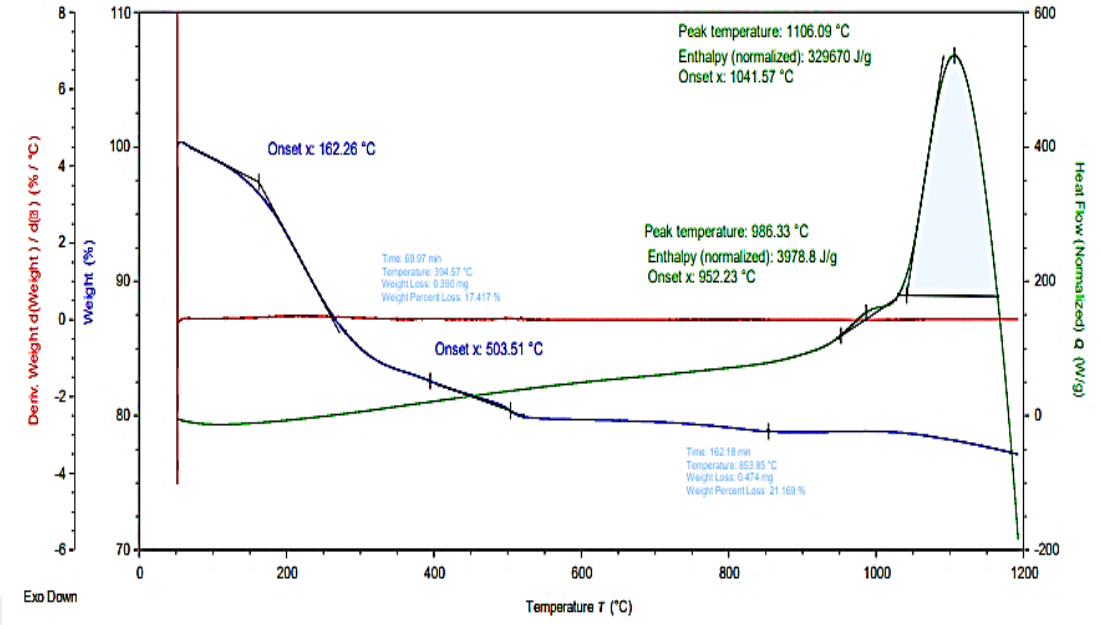

(a)

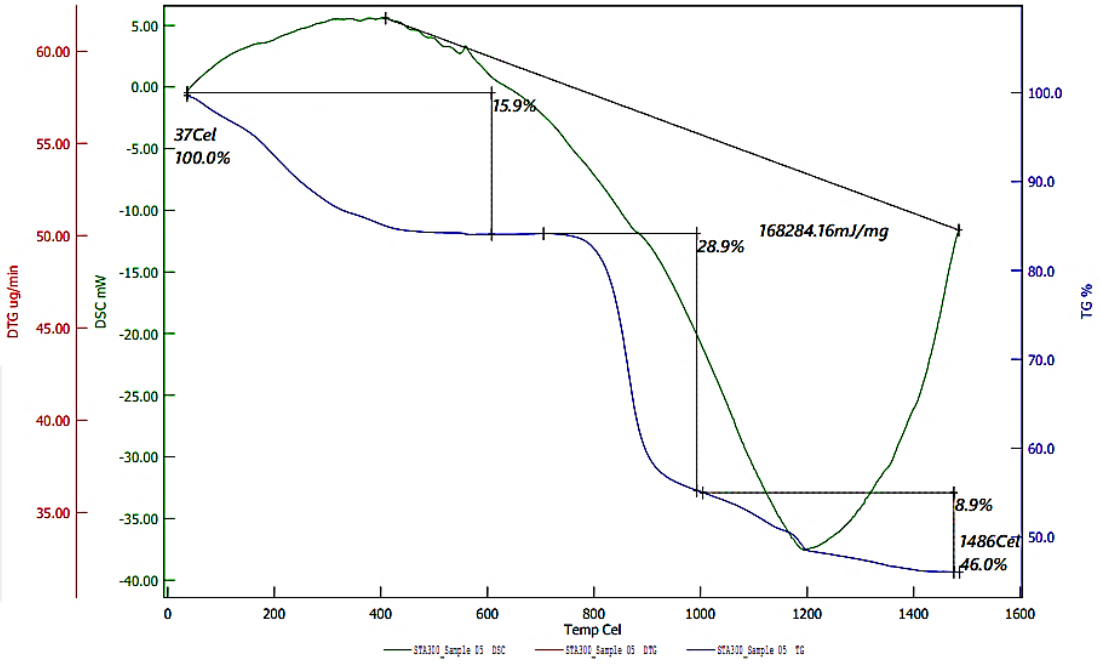

(b)

Figure A4.8. TGA-DSC spectrum of complex **11** in the range of (a) 50-1200 °C and (b) 50-2000 °C

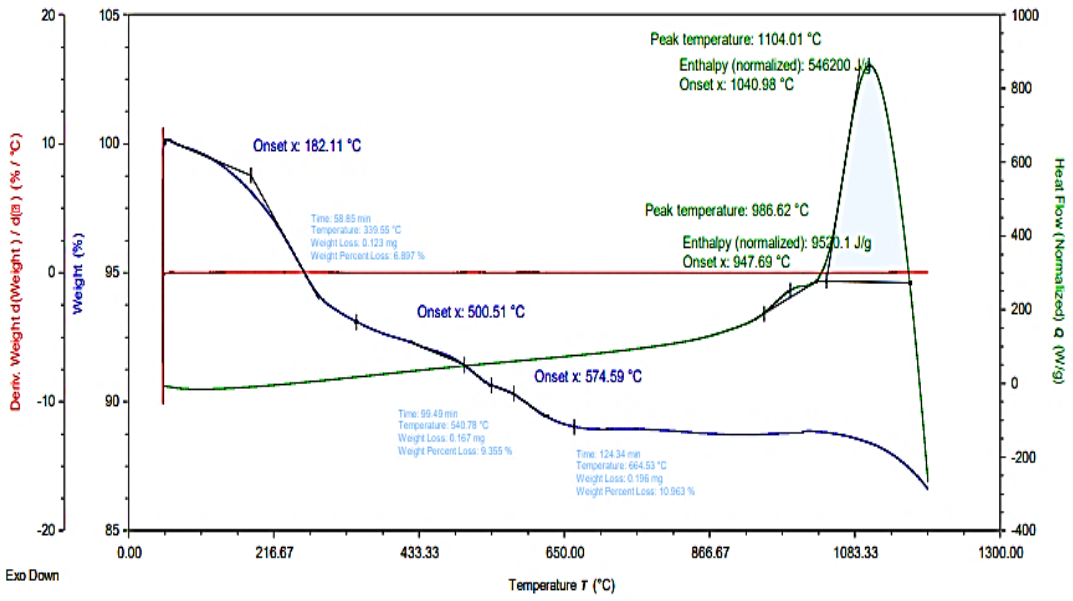

(a)

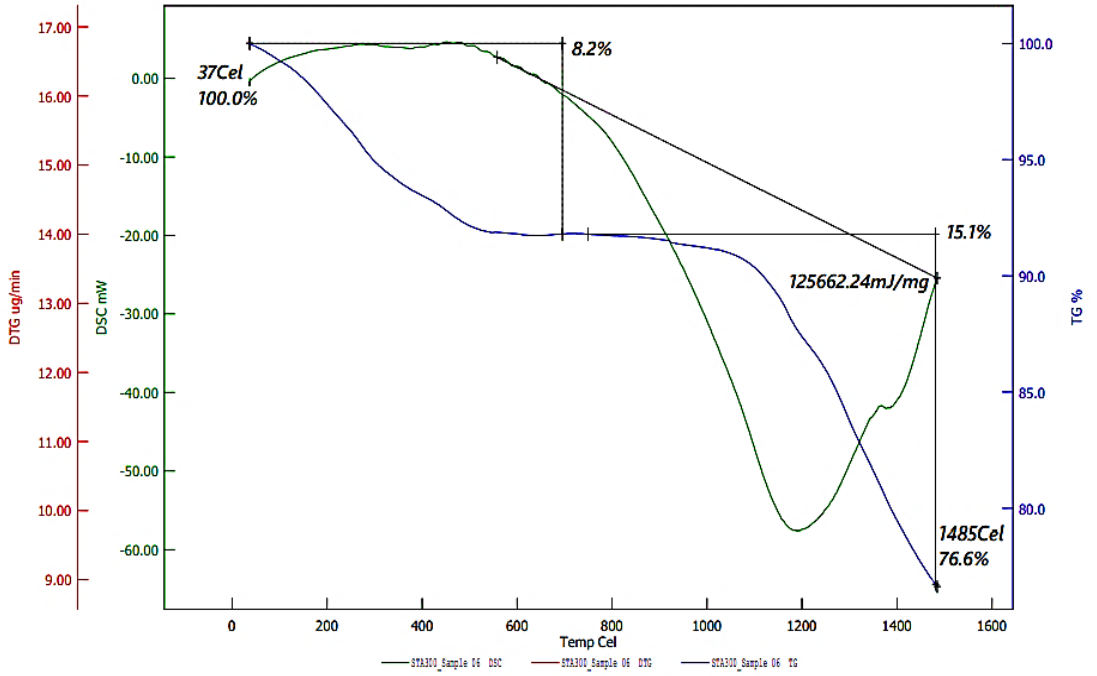

(b)

Figure A4.9. TGA-DSC spectrum of complex **12** in the range of (a) 50-1200 ^{o}C and (b) 50-2000 ^{o}C

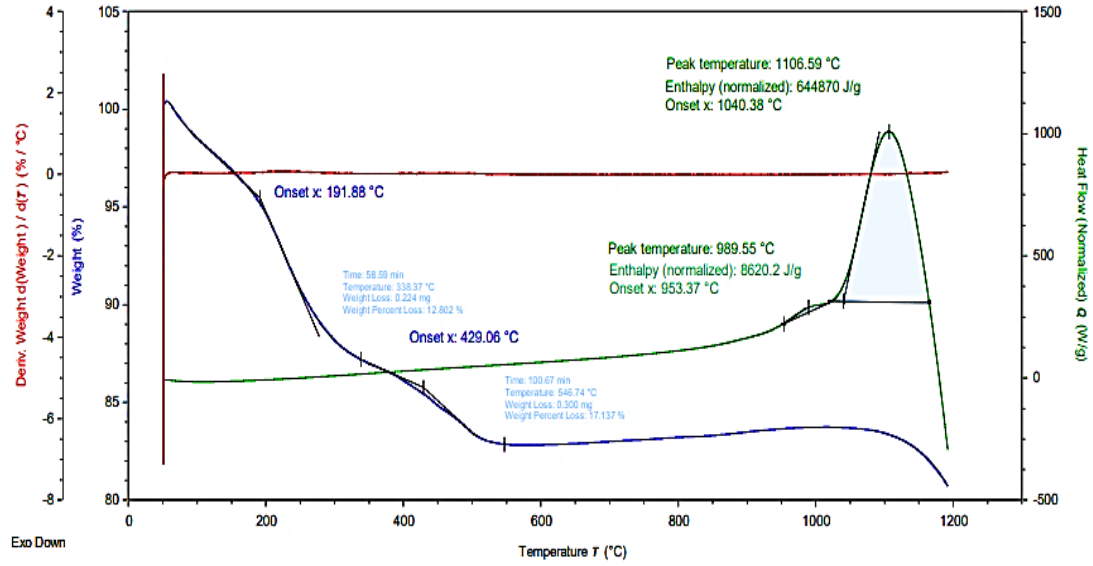

(a)

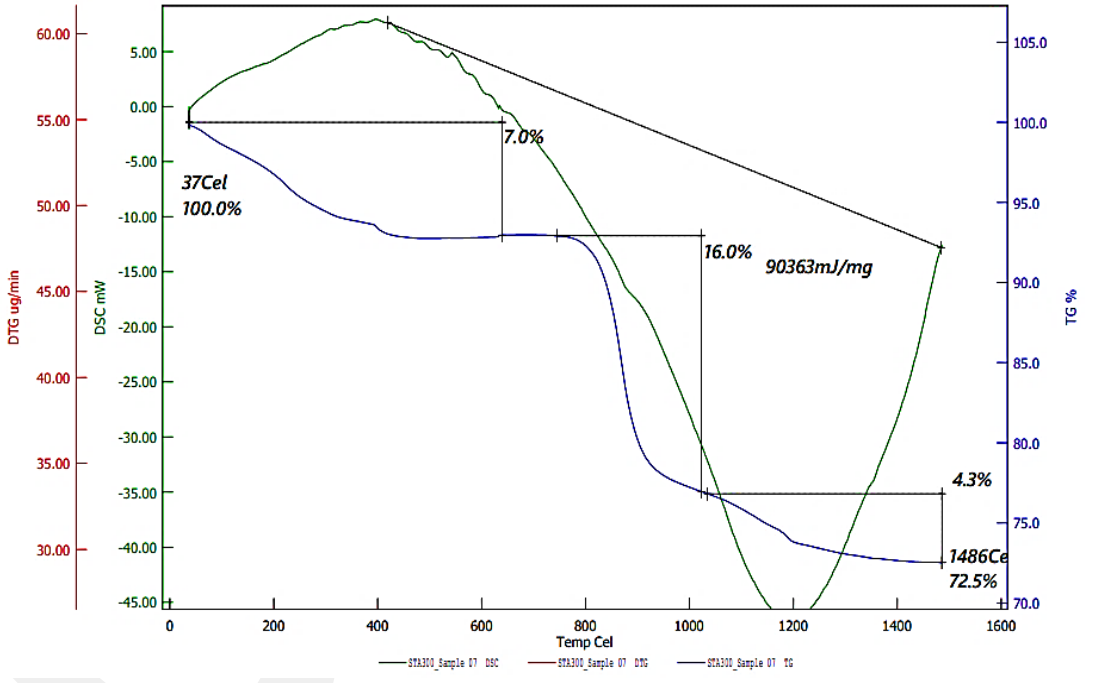

(b)

Figure A4.10. TGA-DSC spectrum of complex **13** in the range of (a) 50-1200 ^{o}C and (b) 50-2000 ^{o}C

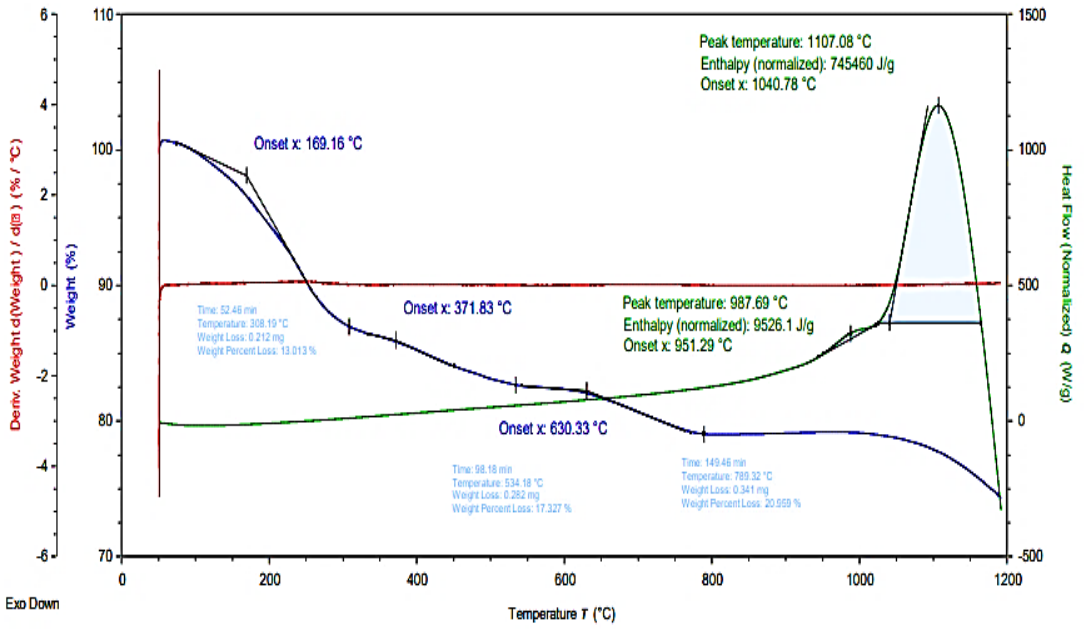

Figure A4.11. TGA-DSC spectrum of complex **14**

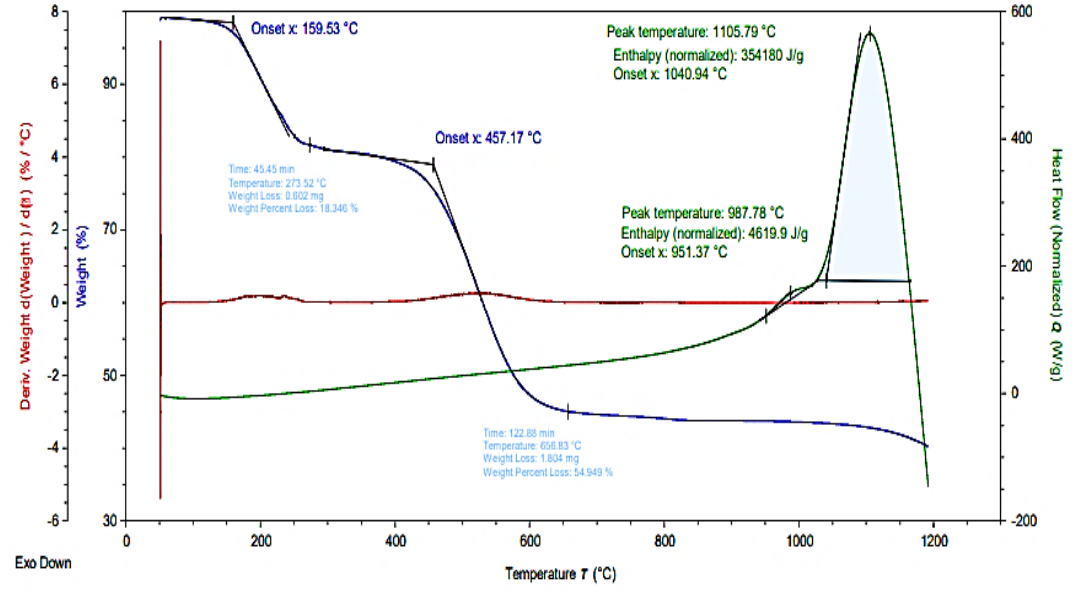

Figure A4.12. TGA-DSC spectrum of complex **24**

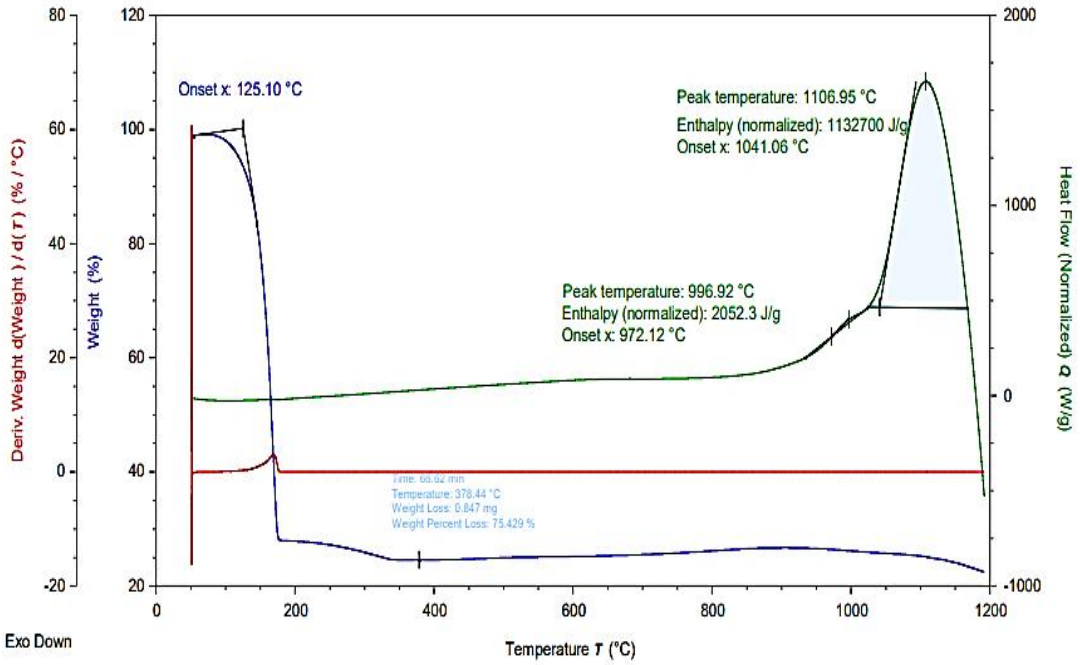

Figure A4.13. TGA-DSC spectrum of complex **25**

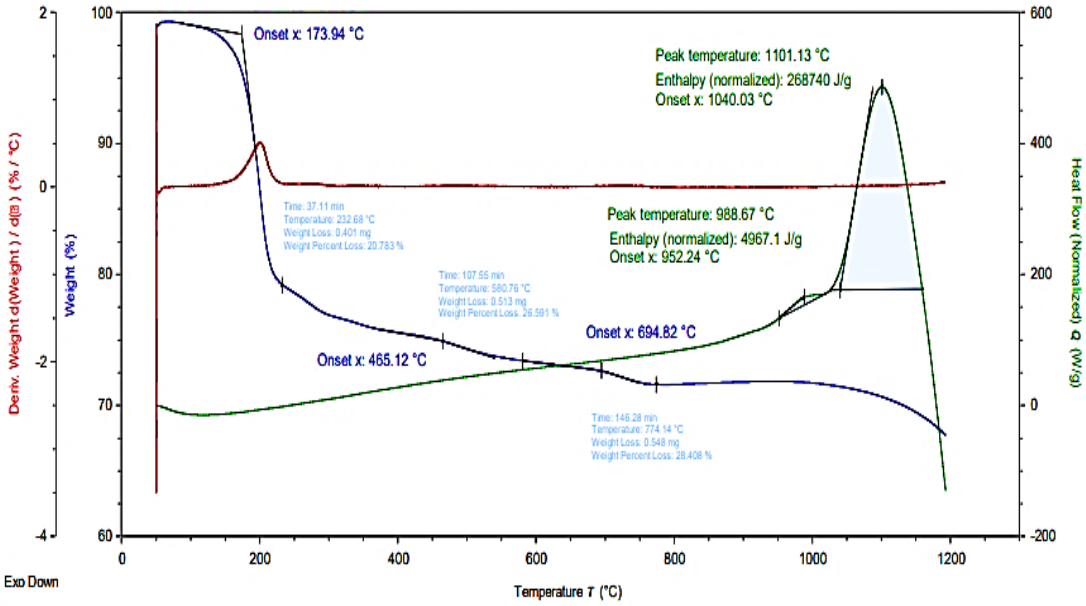

Figure A4.14. TGA-DSC spectrum of complex **26**

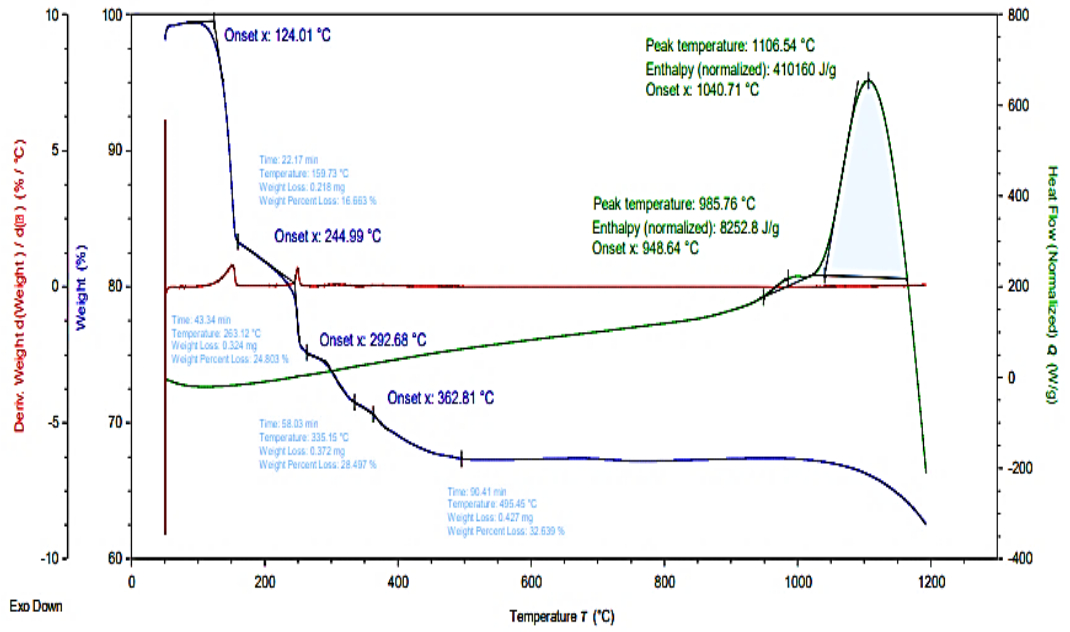

Figure A4.15. TGA-DSC spectrum of complex **27**

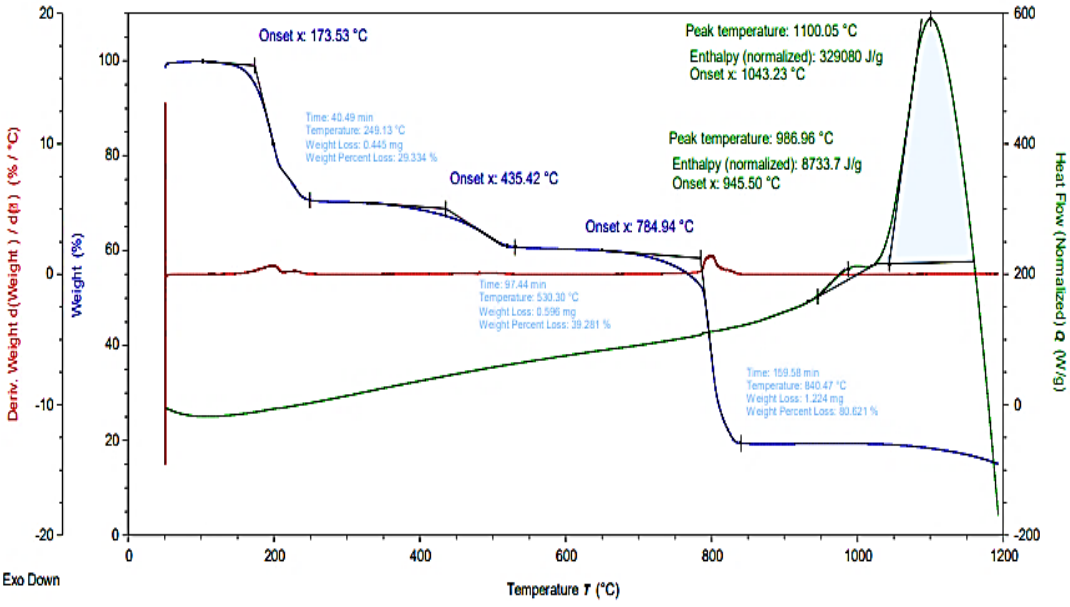

Figure A4.16. TGA-DSC spectrum of complex **29**

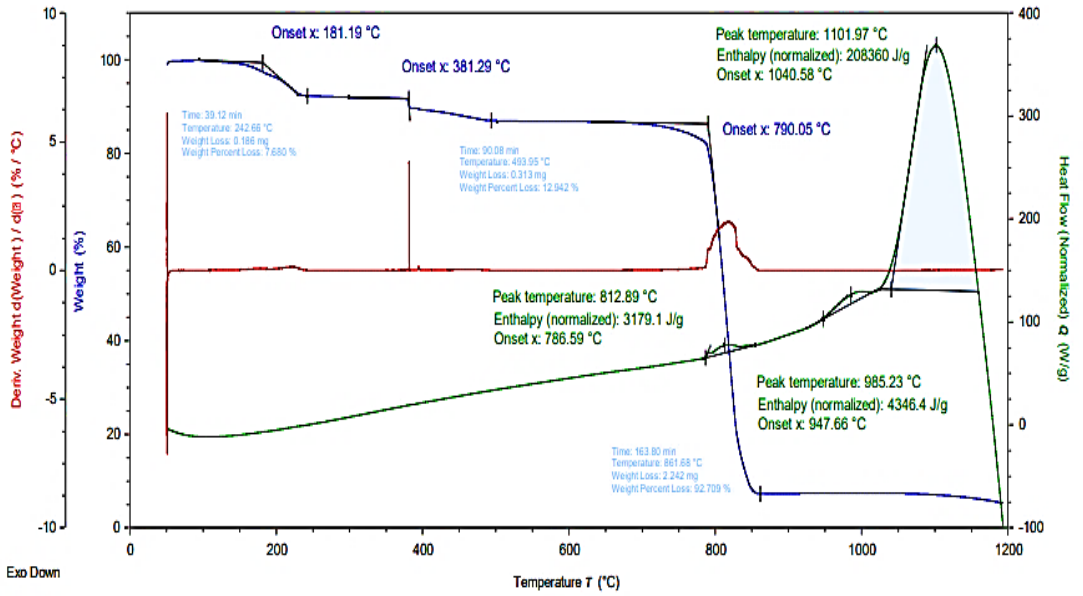

Figure A4.17. TGA-DSC spectrum of complex **30**

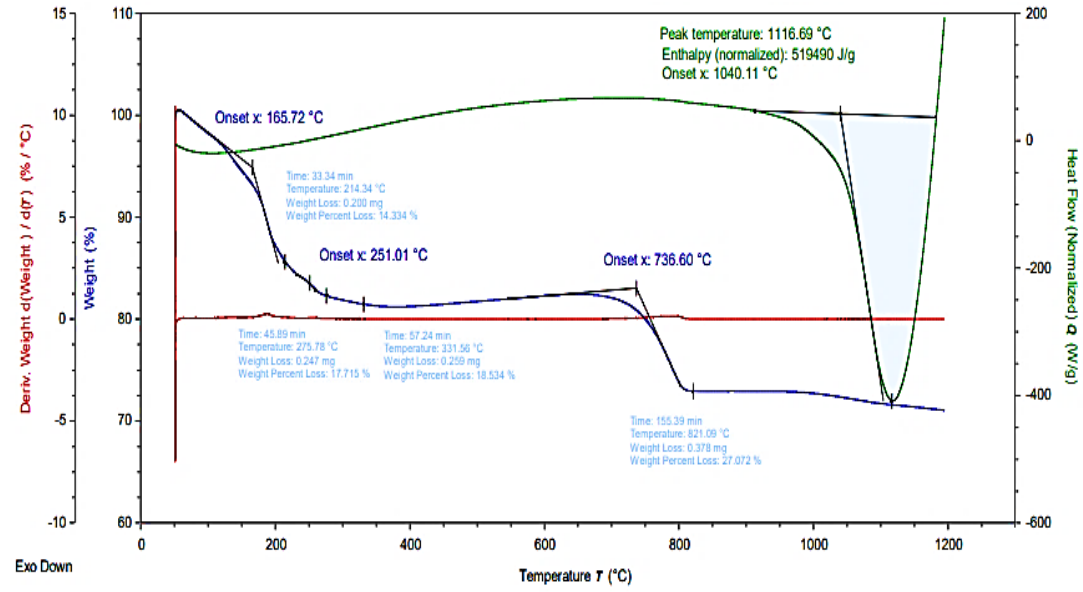

Figure A4.18. TGA-DSC spectrum of complex **31**

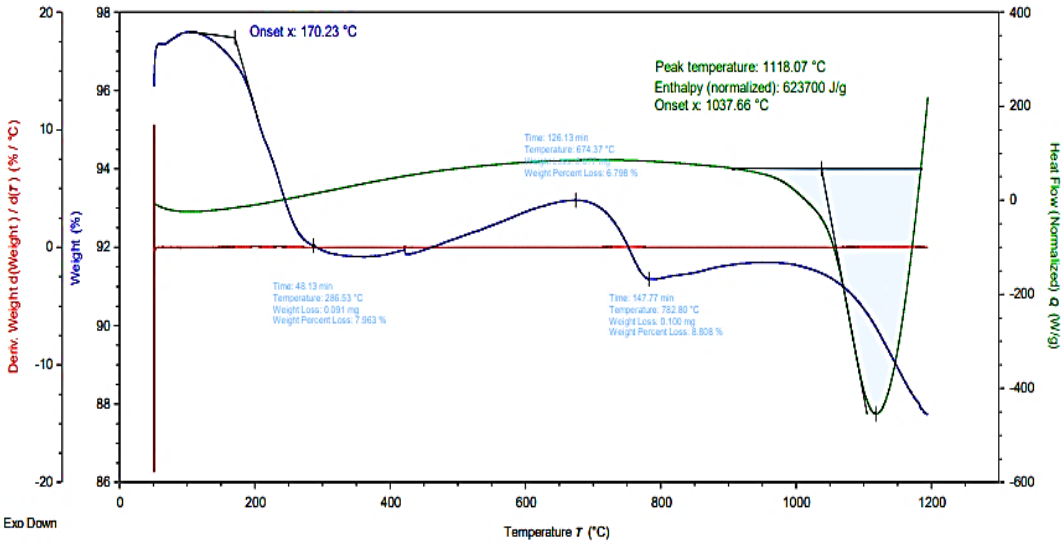

Figure A4.19. TGA-DSC spectrum of complex **32**

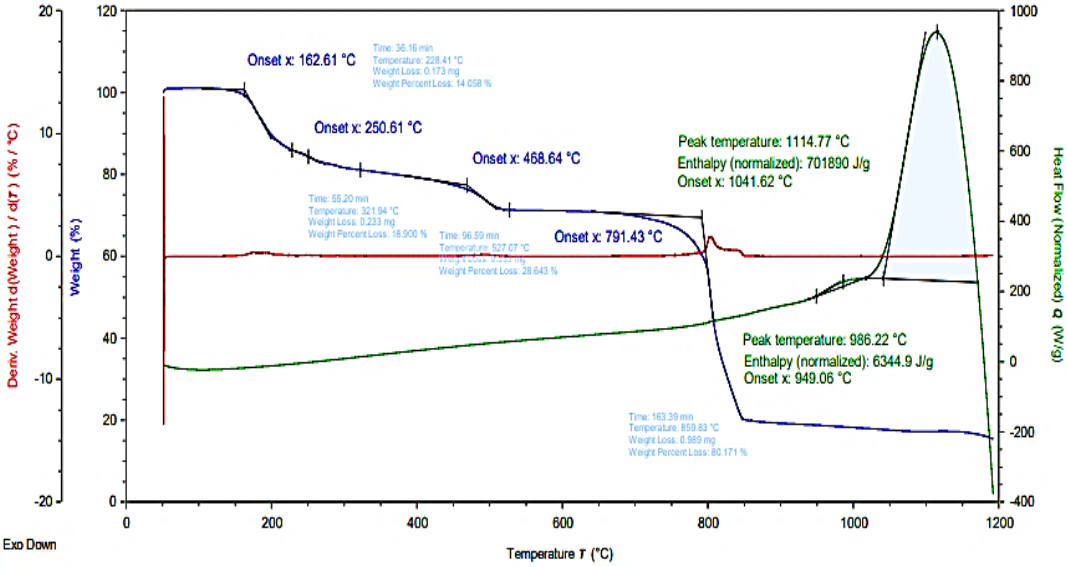

Figure A4.20. TGA-DSC spectrum of complex **33**

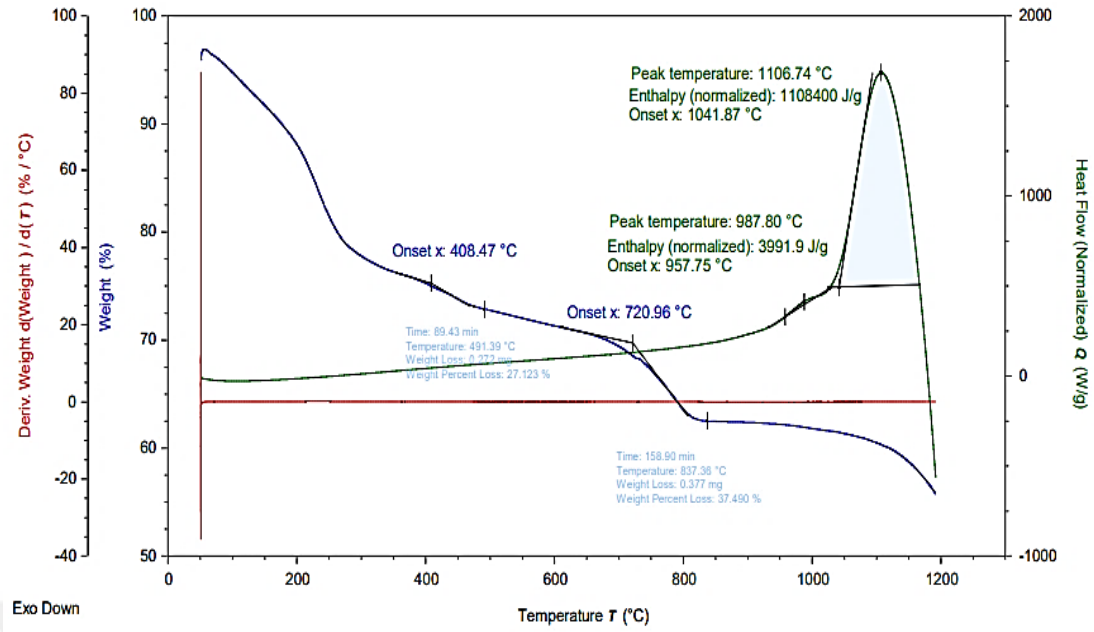

Figure A4.21. TGA-DSC spectrum of complex **34**

Appendix 5. Suggested thermolysis products of complexes in the range of 50-1200 °C

Complex 2:

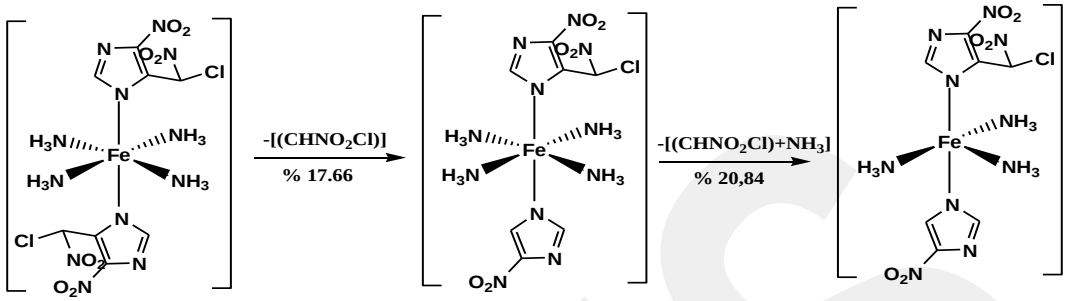

Complex 3:

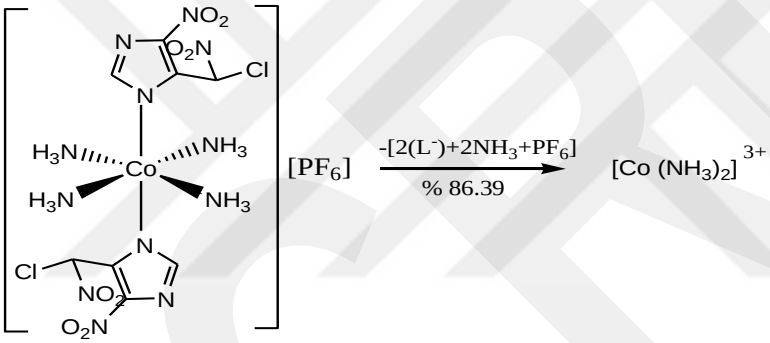

Complex 4:

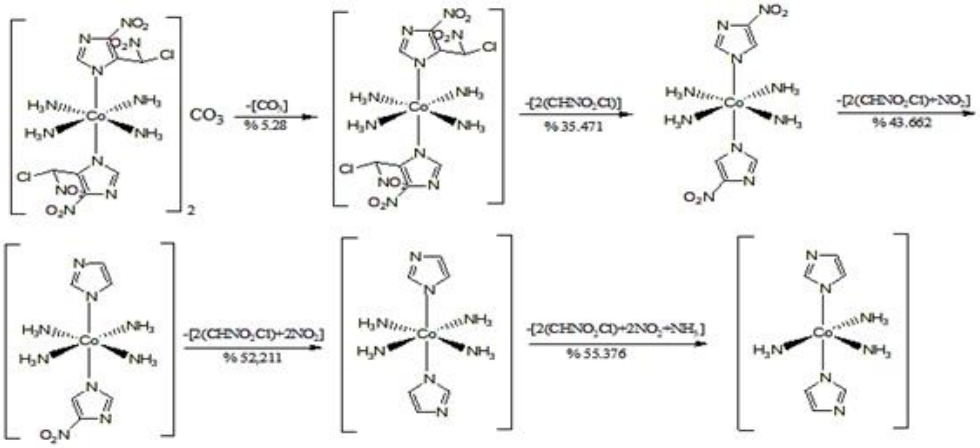

Complex 5:

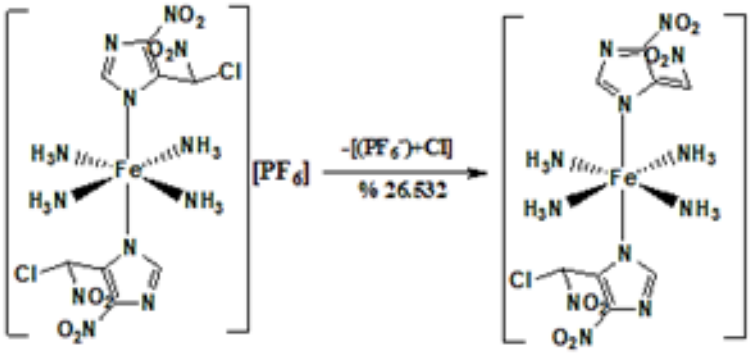

Complex 6:

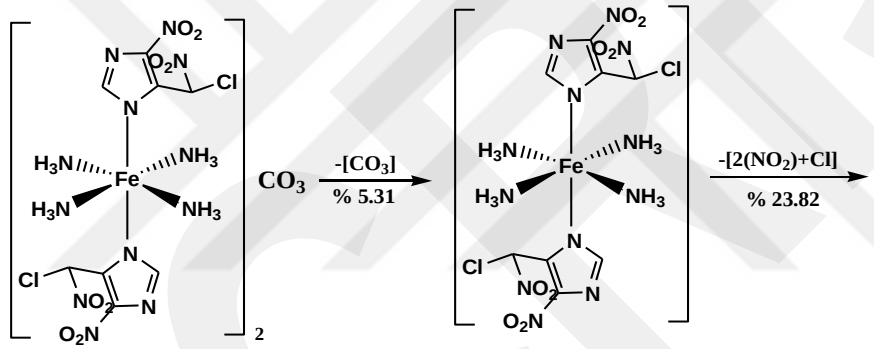

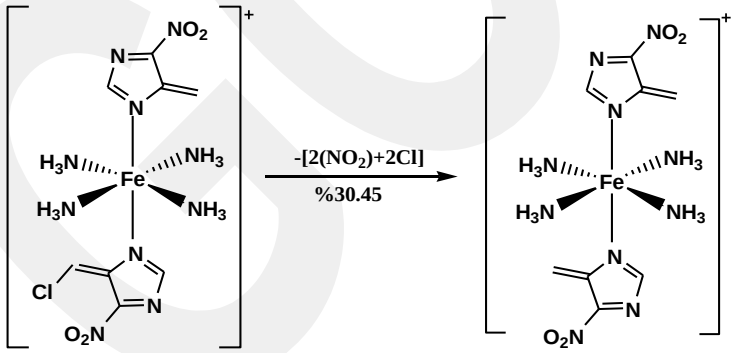

Complex 7:

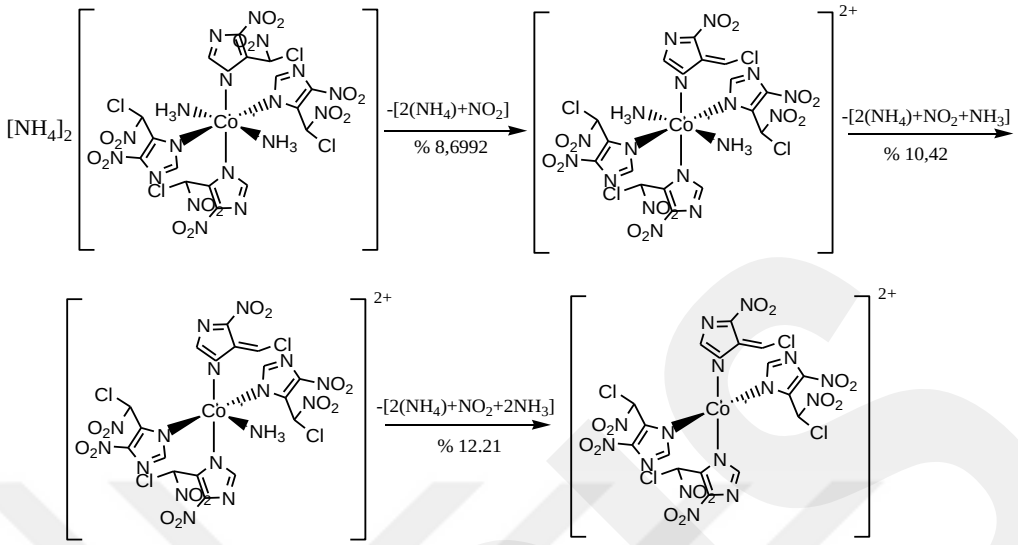

Complex 8:

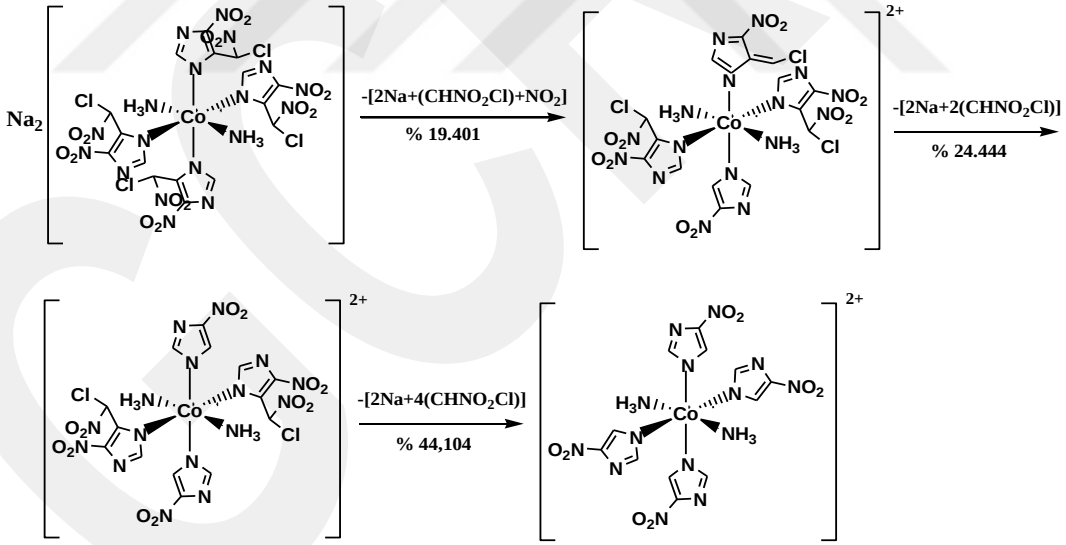

Complex 9:

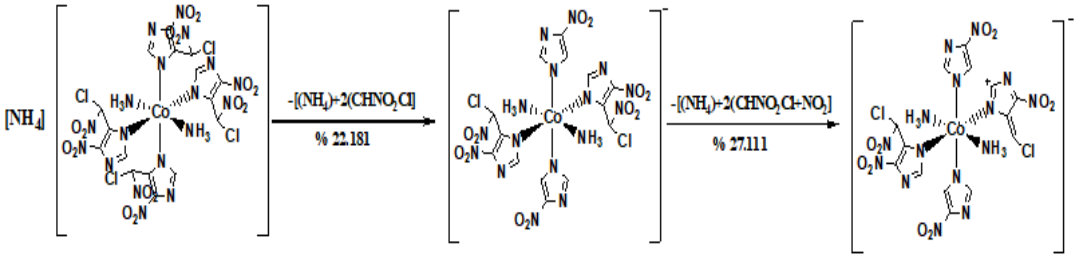

Complex 11:

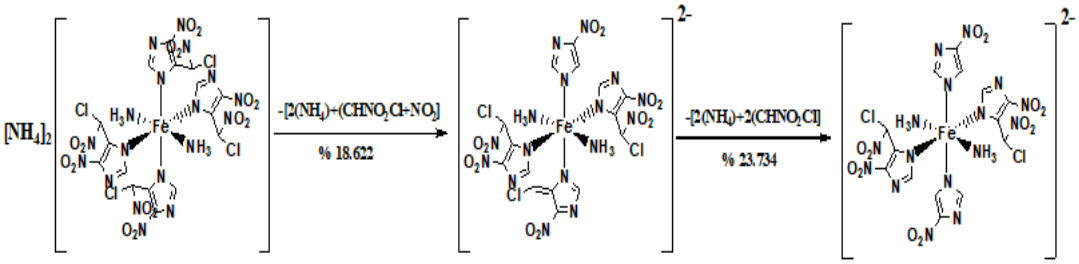

Complex 12:

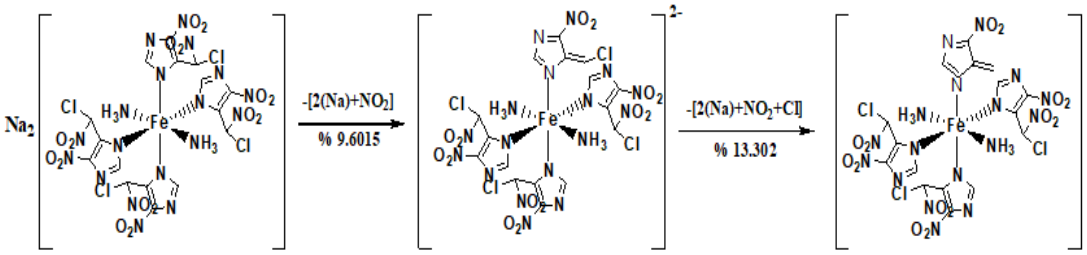

Complex 13:

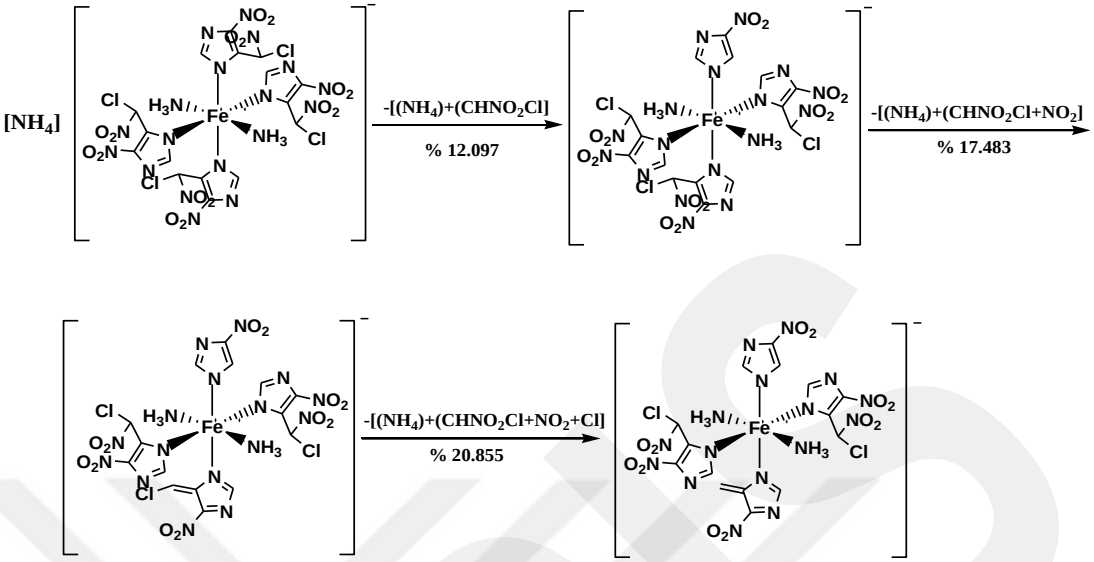

Complex 14:

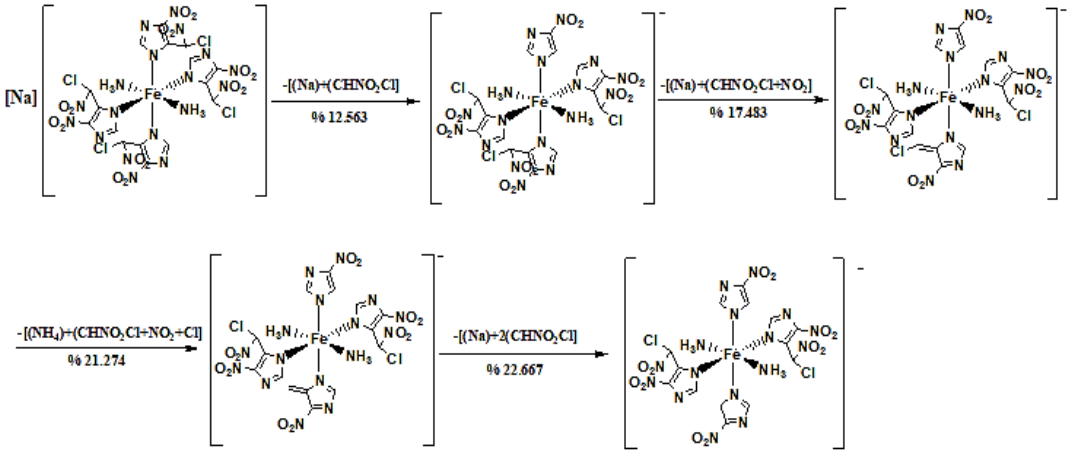

Complex 23:

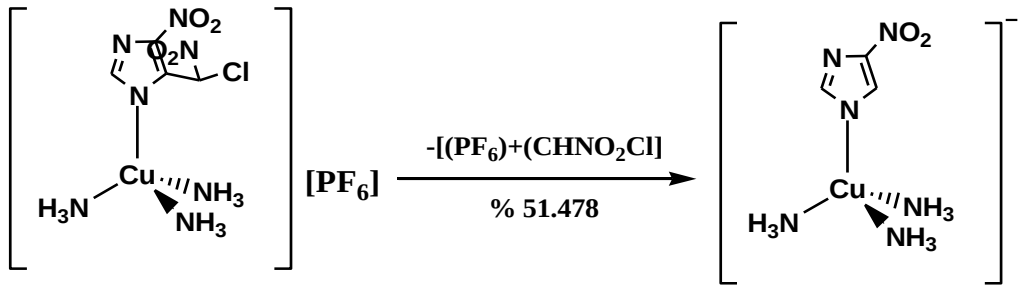

Complex 24:

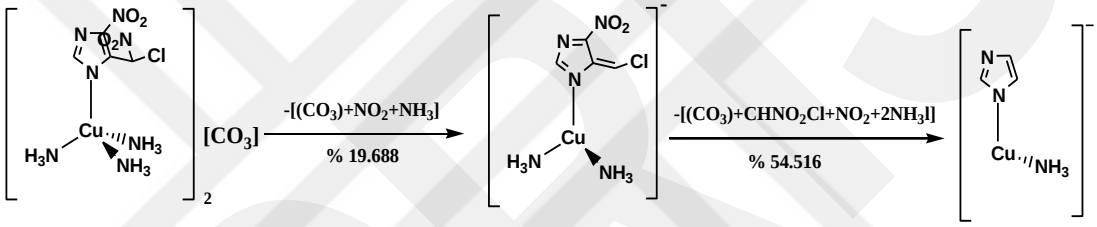

Complex 25:

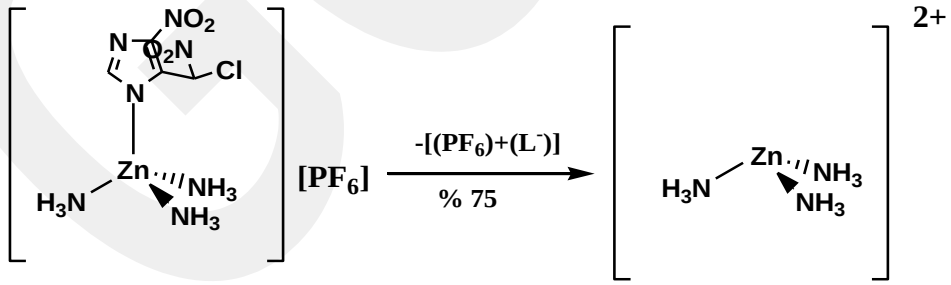

Complex 26:

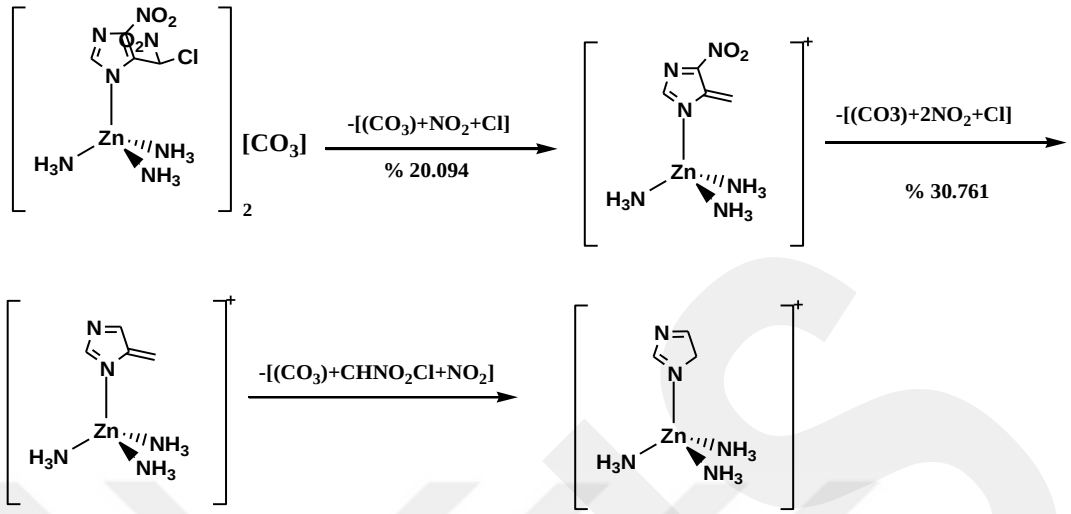

Complex 27:

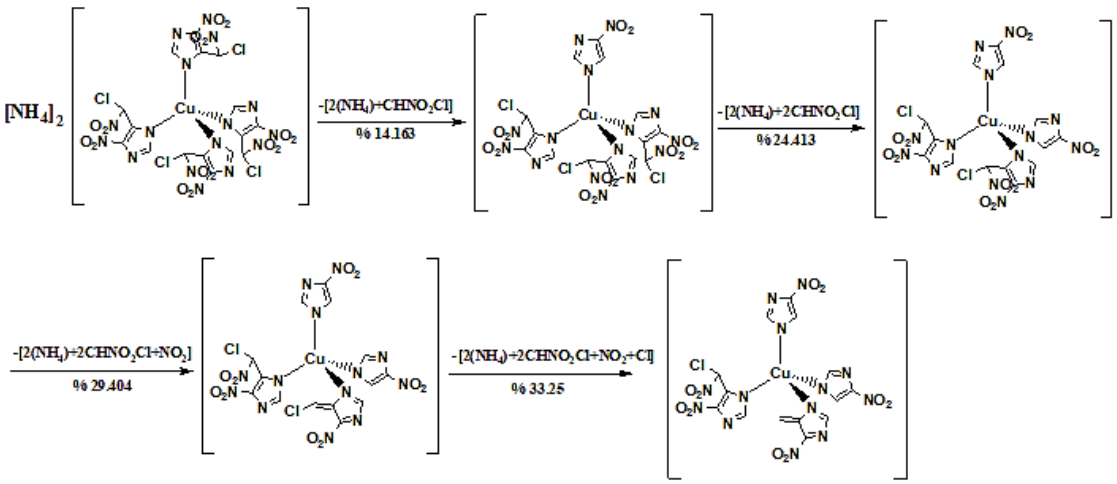

Complex 28:

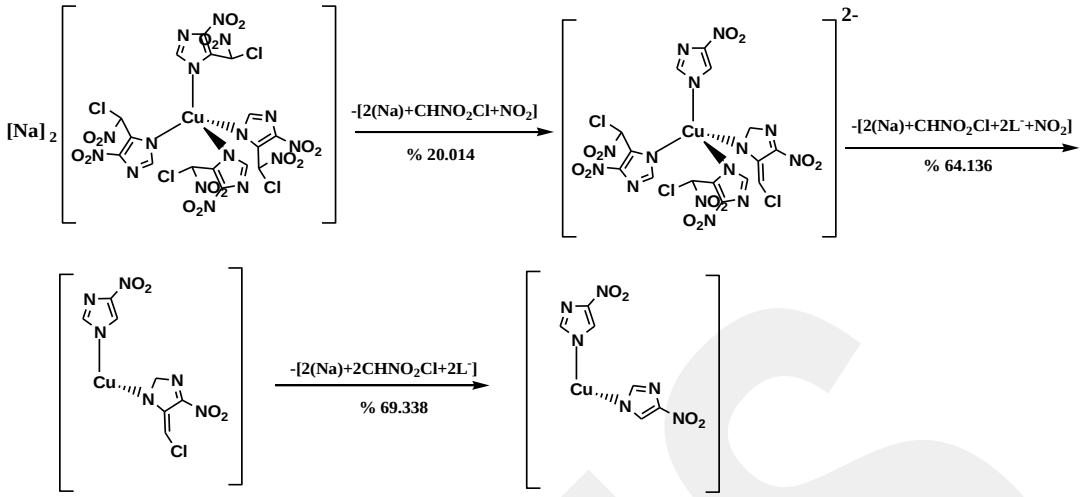

Complex 29:

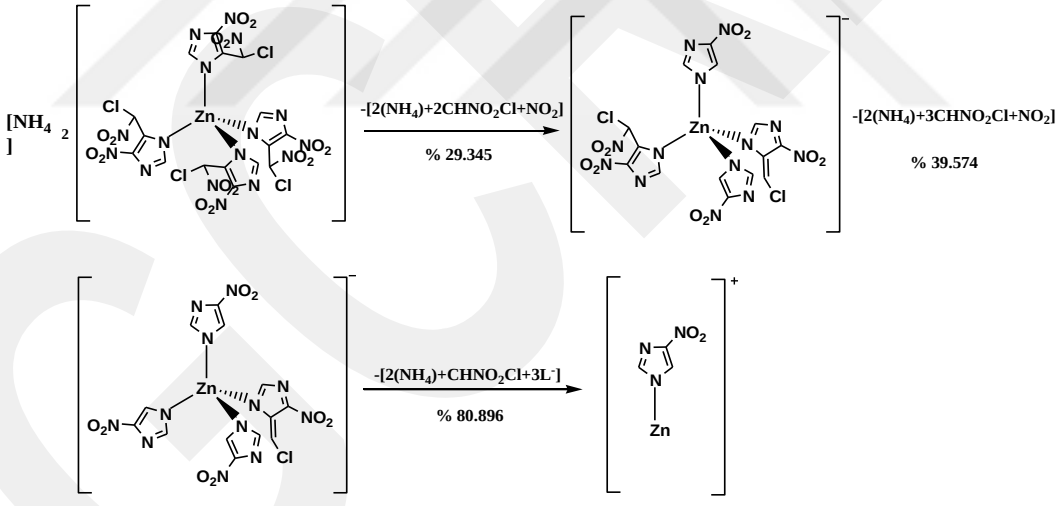

Complex 30:

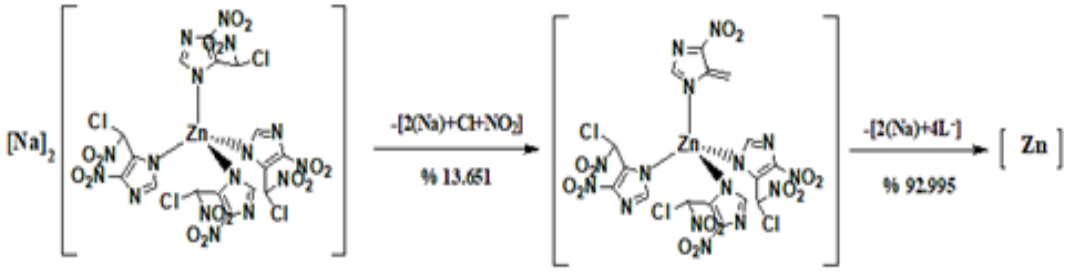

Complex 31:

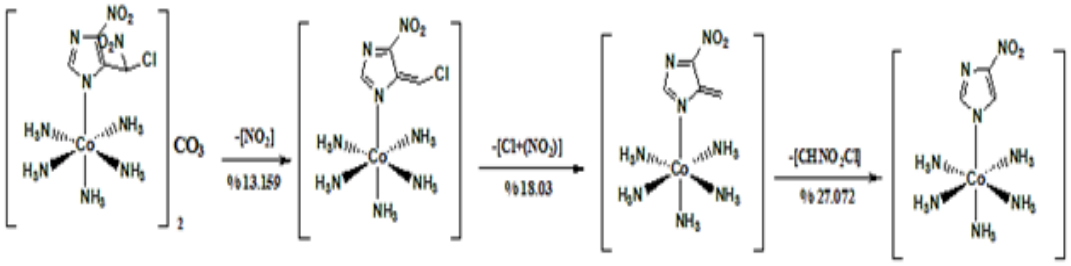

Complex 32:

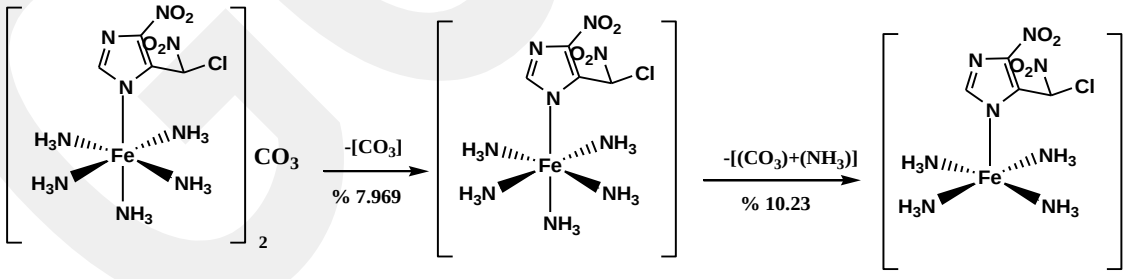

Complex 33:

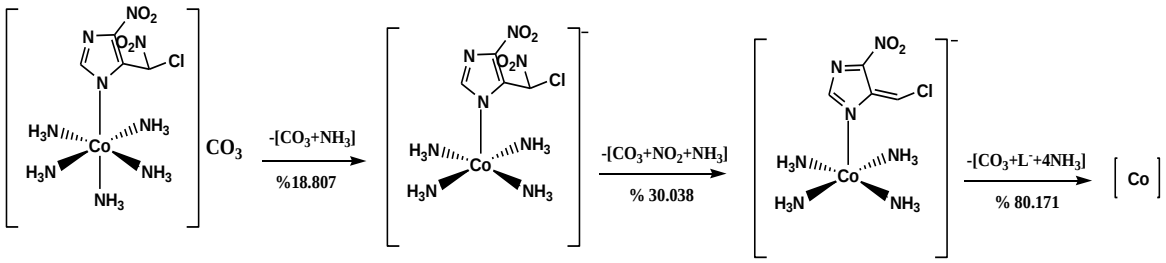

Complex 34: